An Analysis of the Phreatic Surface of Primary Flood Defences

Master Thesis

D.A. de Loor

Technische Universiteit Delft & IV-Groep

TU Delft

Iv-Groep

An Analysis of the Phreatic Surface of Primary Flood Defences

Master Thesis

by

D.A. de Loor

to obtain the degree of Master of Science
at the Delft University of Technology,
to be defended publicly on Friday February 16, 2018 at 15:00 AM.

Student number:	4018206	
Project duration:	June 1, 2017 – February 16, 2018	
Thesis committee:	Prof. dr. ir. M. Kok,	TU Delft, chairman
	Dr. A. Askarinejad,	TU Delft
	Ir. K. J. Reinders,	TU Delft, supervisor
	Ir. T. Sikkema,	IV-Groep, supervisor

An electronic version of this thesis is available at `http://repository.tudelft.nl/`.

TU Delft

Iv-Groep

Preface

This thesis is the product of my graduation research to obtain a Master of Science degree at the Civil Engineering faculty at the Delft University of Technology. It is the final assignment of the Hydraulic Engineering master in the field of Flood Risk. The research is conducted on behalf of IV-Infra bv. part of the IV-Groep holding. The hydraulic engineering branch of IV-Infra is interested in a better understanding of the phreatic surface and factors influencing its position. This report is the product of those eight months of work and presents the methodology, results, and conclusions.

I would like to thank my graduation committee for their support the past couple of months. Chairman Prof. Dr. Ir. Matthijs Kok, daily supervisor Ir. Kristina Reinders, independent supervisor Dr. Amin Askarinejad, and company supervisor Ir. Tom Sikkema all guided me throughout the process with enthusiasm and constructive feedback.

I would also like to express my sincere gratitude to all my colleagues at the hydraulic engineering team of IV-Infra. They deserve my thanks for their help and support during my time at the company.

The other people who directly aided in quality of product laying before you are Dr. Mieke Wattel, Merel Toussaint BSc., Ivo Smink, Hans Brouwer, and Jeffrey Huang BSc. As these friends did (part of) the proofreading; pointing out typos, grammar mistakes, and incomprehensible sentences.

Finally I thank all who supported me throughout my entire studies and helped me get through with a permanent smile and positive attitude; my family, my fellow students from the Civil Engineering faculty, and my swimming and waterpolo-playing friends from DSZ WAVE and DWT.

David A. de Loor
Delft, February 2018

Summary

Every water retaining structure consisting of soil has a water level inside its body. This hidden water level is called the phreatic surface. It is the point where the water pressure between the soil particles is equal or higher than the atmospheric pressure. Below the phreatic surface, the pores between the grains are saturated and pore water pressures are higher than the the atmospheric pressure. Above the surface the pore water pressure is either smaller than the atmospheric pressure due to suction or equal to atmospheric pressure, as air enters the pores. This phreatic surface, in turn, influences the probability of failure for inward macro-stability. A phreatic surface high in the dike increases the likelihood the inner slope will slide away.

This thesis aims to extend the existing knowledge on the influence of hydraulic loads on the phreatic surface in dikes. The current methods used in the estimation of the surface are deterministic and based on two possible scenarios with little probabilistic input: one with extreme rainfall and a mean high water in the river, the other with the design water level with no rainfall. Probabilities of occurrence are ignored for rainfall and design water levels are not calculated in a fully probabilistic way. Furthermore, influences of overtopping are not included in the estimation of the phreatic surface at all. This thesis aims to aid in the upgrading of the deterministic method to a more probabilistic approach by answering the following research question.

How do water levels, precipitation, overtopping, and soil properties influence the inward macro-stability through the shape and level of phreatic surface in river dikes?

In order to investigate the influence of these variables on the phreatic surface, a case study of a primary flood defence is used. A dike section near Groot-Ammers at the Dutch Lek-river is chosen. Its geometry is uploaded in a Finite Element Method-model. The subsoil, mean river levels and part of the soil parameters are based on measurements of this location. For the dike itself, three main types are investigated; a homogeneous clay dike, a clay dike with soil structure deterioration and a sand dike with a clay cover layer with soil structure deterioration. Soil structure deterioration is the decreasing of the permeability of the top clay layer caused by dug holes or cracking. For the dikes with soil structure deterioration, three different hydraulic conductivities (levels of deterioration) for the top layer are tested. At the beginning of each simulation, the starting position of the phreatic surface is reached by applying rainfall to the dike and then wait until it is equal to the level measured in the field.

For each of the dikes, the individual loads of a high water wave, precipitation and overtopping are considered. Furthermore, for precipitation three shapes are applied; uniform, a one-peaked shape, and a two-peaked shape. For the overtopping some adjustments to the loading file were necessary, while the precipitation and water level loads remain close to reality. First, the 1/100,000 loads are applied to each of the three dike types.

However, in none of the simulations the phreatic surface rise was of such severity that it could actually cause failure of the flood defence. So in the chosen case study, with the given dike geometry, soil characteristics, dike types, and soil layer build-up, the influence of water levels, precipitation and overtopping on the phreatic surface and the subsequent macro-stability is too small to be of any significant influence. This is especially true for individual events in clay dikes. A sequence of smaller regular events lifts the phreatic surface in clay dikes more than an extreme event. Thus a wet season or even a wet decade is more dangerous for the stability of the dikes than a rainy week or a single flood wave.

Another important finding of this study is the necessity of a weathered top layer of the soil. The soil structure deterioration allows water to infiltrate in the top layer quickly and thus acts as a buffer basin. Then, the water infiltrated in this top layer can infiltrate the less permeable deeper parts over a longer time. Experiments with no soil structure deterioration, showed no reaction of the phreatic surface at all, as the water applied to the surface barely infiltrates.

There seems to exist an optimal permeability to achieve the highest infiltration into the core. This permeability is dependent on the load intensity. The optimal value ensures that almost all the water can infiltrate in the top layer with little surface run-off, while at the same time the smallest amount of water can flow sidewards inside the top layer, thus inducing more infiltration into the dike core. Furthermore, this study shows that the uniform rain shape ensures the most water infiltrates into the dike, as other shapes lose relatively more water to run-off.

Comparing the results to the current deterministic methods; based on the findings of this thesis, it seems that some methods are too safe. Firstly, the method to estimate the phreatic surface in an extreme precipitation event; from this research it can be concluded that both in sand and especially in clay dikes, the addition of 0.8 meters to the measured phreatic surface as the consequence of a single extreme event is unnecessary. Secondly, the method to estimate the phreatic surface in clay dikes cannot be applied for some primary dikes, as the phreatic surface caused by regular precipitation is already higher than the design high water level. Therefore, this thesis makes a suggestion to expand this rule of thumb.

The results of this research furthermore suggest that within clay dikes, the current assumption that the pore water pressure has a hydrostatic distribution below the phreatic surface is on the safe side. The simulations show that the pore water pressure distribution below the surface cannot be considered hydrostatic in clay dikes, but significantly less. However, more experiments are needed to back-up this claim, as differences are larger than can now be explained.

This study supports the choice not to incorporate overtopping as a phreatic surface lifting load, as this is a load with a very small probability of occurrence and can only be seen as an individual event. Therefore, it will not influence the phreatic surface notably. Also, the existing methods to estimate the position of the surface for sand dikes largely coincide with the results of this thesis.

Contents

1 Introduction

The Netherlands is a country containing the river delta of two main European rivers, the Rhine and the Meuse. Especially the former is fuelled by a basin which stretches throughout Germany, Luxembourg, France, all the way up to Switzerland and Austria. As a consequence, much of the country is only slightly above or even below sea level. Over the centuries the Dutch developed themselves into masters of flood containment and flood risk management. First by trial and error, later through research and science. As a result of developments in soil mechanics and fluid dynamics as well as the improvement of data collection and statistics, dikes and embankments can now be designed to reach a certain level of safety. To a large extent the demands with respect to outer dimensions and material properties follow from developed theory and empirical testing. Nowadays, dikes are no longer designed only to withstand previous flood levels, but rather according to established theory.

However, theory cannot predict every future behaviour of the dike, as there are still many practical factors which are not yet accounted for in calculations. For example, uncertainties in the calculations made to estimate return periods of water levels as well as the inherent uncertainty of a future prediction itself. Furthermore, the behaviour of the soil and unknown layer build-up are difficult to assess precisely during the design phase; at least without extremely high sounding, boring, and lab-testing costs.

To address these uncertainties, several processes which play a role in and around embankments are still ripe for further research. A better understanding of the governing mechanisms will contribute to an improved design for dikes. This may reduce the costs of constructing and upgrading embankments or ensure they are safer. This thesis will assess one such mechanism called the phreatic surface.

Every water retaining structure consisting of soil has a water level inside its body. This hidden water level is called the phreatic surface. By definition, this is the line where the water pressure between the soil particles is equal or higher than the atmospheric pressure. Below the phreatic surface, the pores between the grains are saturated and pore water pressures are higher than the the atmospheric pressure. Above the surface the pore water pressure is either smaller than the atmospheric pressure due to suction or equal to atmospheric pressure as air enters the pores. Water levels on both sides of the structure (dike, levee or embankment) and precipitation influence the location of phreatic surface in dikes. In extreme circumstances, overtopping and overflowing water also have an effect on the phreatic surface in the dike. This surface, in turn, greatly influences the macro stability of the dike, and can result in the collapse of a large part of the slope. These processes are thus the loading factors for the phreatic surface and therefore the dike.

The dike should be constructed in such a way that it will not collapse. Different variables play a role in this resistance, such as the type(s) of soil the dike is made of, soil characteristics, geometry, and the presence of 'hard' structures (e.g. sheet piles or dams). The soil type and characteristics influence the location of the surface as dikes consisting of soil with a large hydraulic conductivity (sand dikes with a clay cover or sandy dikes) absorb new water quickly. After the load is gone, however, the phreatic surface also adjusts quickly to normal levels. Dikes consisting of soil with a small hydraulic conductivity (peat and clay) absorb water less quickly during an event. However, once the load is gone the levels inside the dikes take longer to get back to their old levels.

When testing dikes for their macro-stability, the position of the phreatic surface is an important variable, but the current methods of indicating the surface are questionable and rather deterministic. In 2017, the new WBI was implemented and thus the ways to cope with failure probabilities of dikes and dike rings were

updated. The method of assessing the location of the phreatic surface is, however, still based on two possible scenarios with little probabilistic input: one with extreme rainfall and a mean high water in the river, the other with the design water level with no rainfall. Probabilities of occurrence are ignored for rainfall and, since mean and design high water are just calculated values, the methodology is deterministic. Influences of overtopping are not included in the estimation of the phreatic surface, while at design circumstances it may be of importance for the macro-stability of the dike, acting like a kind of extreme heavy but short 'rain' events.

It is practice to look at an extreme event as a single scenario which is reasonable for easily drained soil structures. However, when looking at dikes which hold the water for a longer period of time it would make sense to look at a series of events. Currently, precipitation is not taken into account during Design High Water (DHW) but the likelihood that it rained the week prior to a high river discharge, already soaking the soil before the high water wave arrives downstream, may be substantial. This could induce a higher phreatic surface at the beginning of the extreme event, weakening the dike.

Nowadays, with the help of computers, the design methods are shifting from a deterministic or safety factor approach towards more probabilistic methods. A full probabilistic approach to obtain the probability distribution of the phreatic surface would be an ambitious goal. This would mean, however, that dikes could be better optimized and be designed more efficiently at lower costs. The current methods are, as usual, rather conservative and extreme high phreatic surfaces need to be taken into account without any probability of occurrence attached to it.

The first and foremost reason for the difficulties with respect to assessing the surface is the uncertainty in soil build up and soil parameters. Secondly the full probability space of the loads is hard to simulate due to many mechanisms and their dependencies. This thesis aims to unfold a part of those loads and resistance mechanisms and their influence on the phreatic surface and consequently inward macro-stability. It mainly aims to get more insight about the upper limit of the phreatic surface in a more probabilistic manner. This is done by the construction of several scenarios and assigning them probabilities.

The rest of the report starts with a more elaborate problem description in Chapter 2. Also the formal research question and methodology to answering the question are presented. Then Chapter 3 describes the literature and the current methods of dealing with macro-stability and the phreatic surface. Chapter 4 deals with the more theoretical background of several mechanisms and processes around the dike. It also describes the statistical background for the hydraulic loads, subsurface flow, and the finite element model used for this thesis, PLAXIS. Chapter 5 describes the PLAXIS-model, the translation from theory to model input, and the scenarios that are calculated. Chapter 6 describes the results from these simulations and interprets them. Chapter 7 handles the results of some extra simulations, based on the conclusions in Chapter 6. Then, finally Chapter 8 presents the conclusions and points of discussion for this research. It also gives some recommendations for further research. Some special attention is needed for Appendix D, as an important part of PLAXIS settings and result interpretation is presented there. Also some different parameter settings for soils are tested in this last Appendix.

2

Problem

2.1. Problem description and motivation

In 2017 the new WBI was launched by the Dutch government to keep the Dutch delta reasonably safe for the years to come. It describes demands for dunes and other primary flood defences for the coming decades. The WBI2017 has a lot of new views and demands for all type of defences. All the primary flood defences in the Netherlands need to be reviewed and tested to check if the new standards are met.

One of the failure mechanisms primary defenses need to be tested for is macro-instability. This is the sliding of a part of the inner or outer slope of a dike. Both processes are influenced to a large extend by the phreatic surface. This thesis only focuses on macro-instability due to sliding of the inner slope, see Figure 2.1.

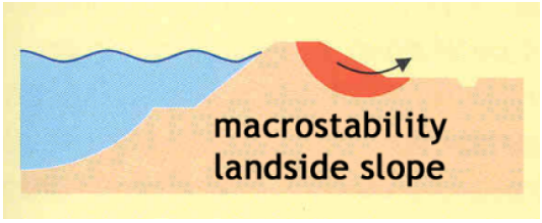

(a) Theoretical slide plane

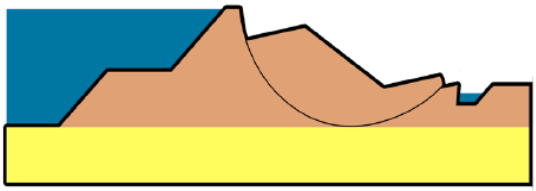

(b) Theoretical slide

(c) Slide in practice

(d) Subsequent dike breach

Figure 2.1: Theoretical inner slope sliding and an example; Breitenhagen, Elbe river, June 2013. Source: Flood Defences Lecture Notes, [7].

The WBI2017 describes a method on how to calculate the failure probability of this kind. One of the important input variables is the location of the phreatic surface in the dike. Right now the location for this phreatic surface and thus the input for the failure computation is simulated with the computer tool Waternet. According to the current WBI the results of the Waternet tool are entered in a deterministic way in Ringtoets (as of 2019, right now BM-Macrostabiliteit is used) which calculates the probability of failure due to inward macro-instability via a semi-probabilistic or full probabilistic method.

The parameters used for the phreatic surface as computed by Waternet are mainly based on methods and theory coming from TAW[2004], [11]. It uses a dike type (four available), water level in the polder, water

level outside, leakage length, intrusion length and the initial phreatic surface. It then produces the phreatic surface, pressure height in the aquifer and pressure distribution dependant on depth. See Chapter 3 for a more elaborate review of the current methods.

This also shows some clear shortcomings. Influences of rainfall and wave overtopping are not or deterministically included in the computation. Also the four homogeneous dike types may severely hamper the applicability of the tool.

This thesis gives a broader look on the variables leading to the phreatic surface. It considers more hydraulic loads than the TAW[2004] and it tries doing so in a more probabilistic way. From research it is known that both precipitation and overtopping influence the phreatic surface and with that, the macro-stability of the slope. When one would take a look at Figure 2.2 it is imaginable that the overtopping mechanism could have a significant influence on the water level inside the dike body.

Figure 2.2: Photo of the overtopping of a sea dike at Hartepool, UK. Source: Flood Defences Lecture Notes, [7].

From the picture however, it is also evident that the largest part of the overtopping water stays on the surface of the dike and runs off without infiltrating the soil. This is the reason almost all research regarding overtopping is focused on inner slope erosion. For sea dikes this is a logical choice. Due to the high crest height the phreatic surface in the dike is relatively low. Secondly, individual waves can be huge causing high overtopping volumes. This makes slope erosion a more likely failure mechanism than instability due to a high phreatic surface.

For river dikes the opposite is the case, although much less research has been conducted on this topic. Macro-instability due to a high phreatic surface is more likely to occur than erosion of the inner slope for two reasons. Since waves on rivers are significantly lower than at sea, the crest of the dike is relatively lower to the design water level, leading to a relatively high phreatic surface in the dike. Secondly due to the smaller waves, the overtopping volume of individual waves is lower and thus the erosion force on the inner slope is also less. Though several small overtopping waves may have the potential of wetting the dike. By intrusion, the waves could induce (temporary) over-pressures in the already saturated dike, triggering its final collapse.

Precipitation events also influence the phreatic surface in a dike. Much research indicates that due to global warming processes the rain events in the future will become more extreme. As a consequence it might play a more important role in the phreatic surface level. In clay dikes, long rain duration let the surface rise

over a course of days. Short intense rain falls have less effect since most of the water runs off. The thesis will address the macro-stability failure mechanism for primary flood defenses of rivers related to the phreatic surface rise in the dike due to overtopping, precipitation and high water levels.

This can't be done without regarding the influence of soil permeability and thus it will be included in this study. The TAW[2004] uses four dike types of which I will use two; A clay dike on an impermeable subsoil and a dike with a sand core on an impermeable subsoil. For the top layer, consisting out of clay, several gradations of cracking, weathering, and holes are applied. The calculated phreatic surface influences more than only the macro-instability. Also settlement, piping and other mechanisms are influenced by its position; these processes however are not considered.

2.2. General description of the phreatic surface and loads

Macro-stability is influenced by several uncertain factors. These will be elaborated in the WBI literature study. As mentioned above, one of these uncertainties is the position of the phreatic surface. If one were to conduct a full probabilistic approach in order to determine the location of the phreatic surface, the result would be a distribution of the location rather than a deterministic location.

This uncertain location is the result of aleatory and epistemic uncertainties. The former is the natural randomness of a variable and is thus mostly applicable on the loads influencing the surface. The latter is caused by lack of knowledge on a variable, inherent to in situ soil and thus stretches of dikes. Both types of uncertainty however are present in the loading as well as the resisting part. So, the surface location is uncertain mainly because the soil parameters and the build-up of the soil in the dike is uncertain (epistemic). Even with controlled hydraulic boundary conditions, the precise surface location remains unknown and is a distribution as depicted in Figure 2.3a.

On the other hand, a theoretical dike consisting out of perfect homogeneous soil subjected to varying loads also has an uncertain phreatic surface (aleatory). Hydraulic conditions, of course, vary over time. Extreme water levels, precipitation, waves or a combination, lead to loads with a certain probability of occurrence per year and play an important role in designing flood defences. Polder level, overtopping due to (wind)waves, precipitation and river discharge all influence this probability and all are correlated one way or another see Figure 2.3b.

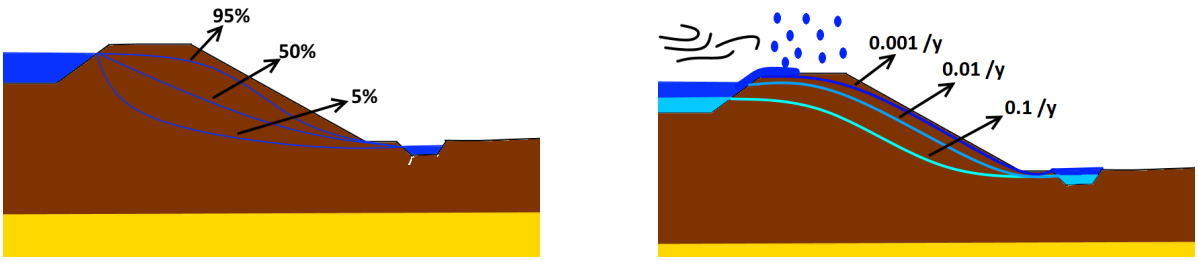

(a) Probability of phreatic lines due to uncertainties of soil (epistemic).

(b) Chance of occurrence per year of phreatic lines dependent on load combinations (aleatory).

Figure 2.3: Uncertainty due to strength and load. (Conceptual image, not actual results)

In an ideal world with all information available one would be able to create the full probability curve of the phreatic surface, constructing the perfect input for a full probabilistic calculation of the dike macro-instability. Such a curve would look something like the two drawn in Figure 2.4 but then for every vertical slice along the profile of the dike. These two example locations are picked for illustration purposes. On the vertical axis the probability of the level z as the maximum location of the phreatic surface for a year is depicted while on the horizontal axis the value of z_{max} is depicted.

At the dike toe, the probability per year that the maximum phreatic level reaches surface level ($z_{max} = 0$) is rather high since water seeps out of the dike here with small water level elevations or normal precipitation. At the inner crest the phreatic surface only reaches the surface when the dike is entirely saturated, something that will occur almost never. The graph however continues further down the z-axis as lower maximum yearly levels are possible.

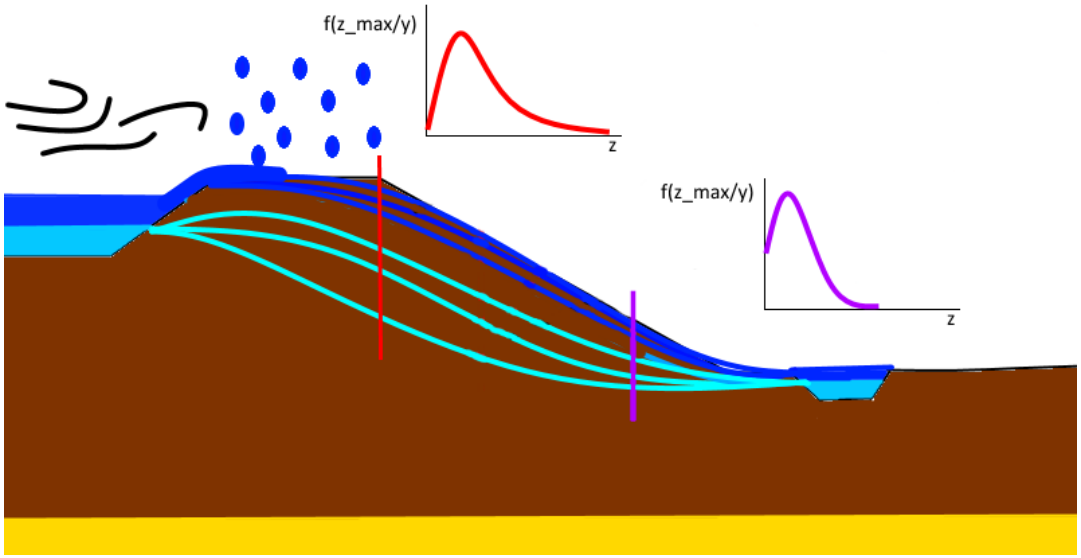

Figure 2.4: Both hydraulic (load) and soil (strength) uncertainty producing the total chance of occurrence per year for every possible surface. (Conceptual image, not actual results)

However, one does not have all the information on soil parameters although in theory they could be acquired. Furthermore one certainly cannot acquire future data of the hydraulic loads so these are by definition uncertain. The best one can do is get an as good as possible insight in probabilities of occurrence of meteorological events and correlations and dependencies between loads.

In order to illustrate the load side of the phreatic surface in a dike Figure 2.5 helps. The complexity of the dependency structure is rather high. The blue variables are available by measurements including some of their green characteristics. Some analytical translations can be made to simplify the process illustrated by the red trapeziums. The orange blocks are the ones relevant for the calculation of the phreatic surface.

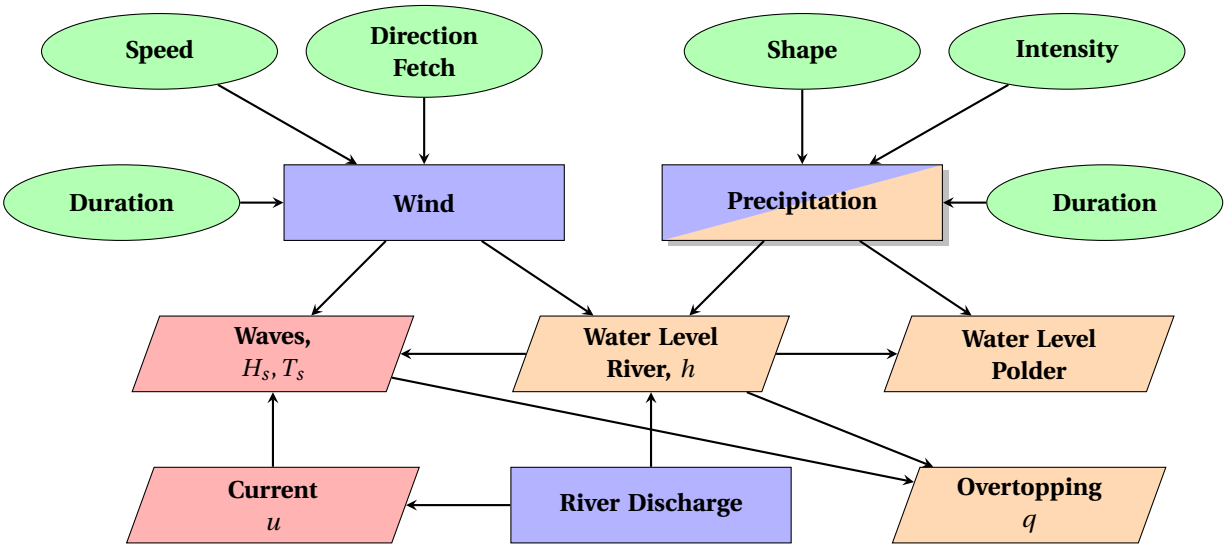

Figure 2.5: Dependencies hydraulic loads. Orange blocks are the direct loads on the dike.

A large part of these loads and their return periods are available through Hydra-NL. This program, made available by Rijkswaterstaat, calculates return periods for wind speed, wind direction, water levels, overtopping, run-up and a combination of these loads. This means that local precipitation and its characteristics are not included in the calculations. Information about this load is available through the KNMI and the STOWA 2015 report, [4].

Second point of interest for the phreatic surface is time. Due to (low) permeability filling and emptying the dike body with water takes time. Therefore a period of rain before a flood wave may cause earlier collapse

than when a period of relative drought precedes the same flood. Also a quick emerging flood wave might induce less phreatic level based trouble than a slow one. The duration of an event, everything that occurs during that time, and the order of these occurrences are of influence for the position of the phreatic surface.

Furthermore the location where the load is exerted and where the surface rises are of importance. Phreatic surface rise is more dangerous at the inner crest of the dike than at the outer crest. This also highly depends on the geometry of the dike. The final large problem for executing a full probabilistic simulation is the large output of scenarios. When looking for the 0.001/y load for an individual variable gives a value, a point. The 0.001/y load for two parameters gives a line or curve. For example, the IDF curves from the KNMI giving the joint probability of rainfall duration and intensity, see Figure 2.6. Three variables gives a surface etc. Although etcetera in this case would mean multi-dimensional figures which are impossible to visualize.

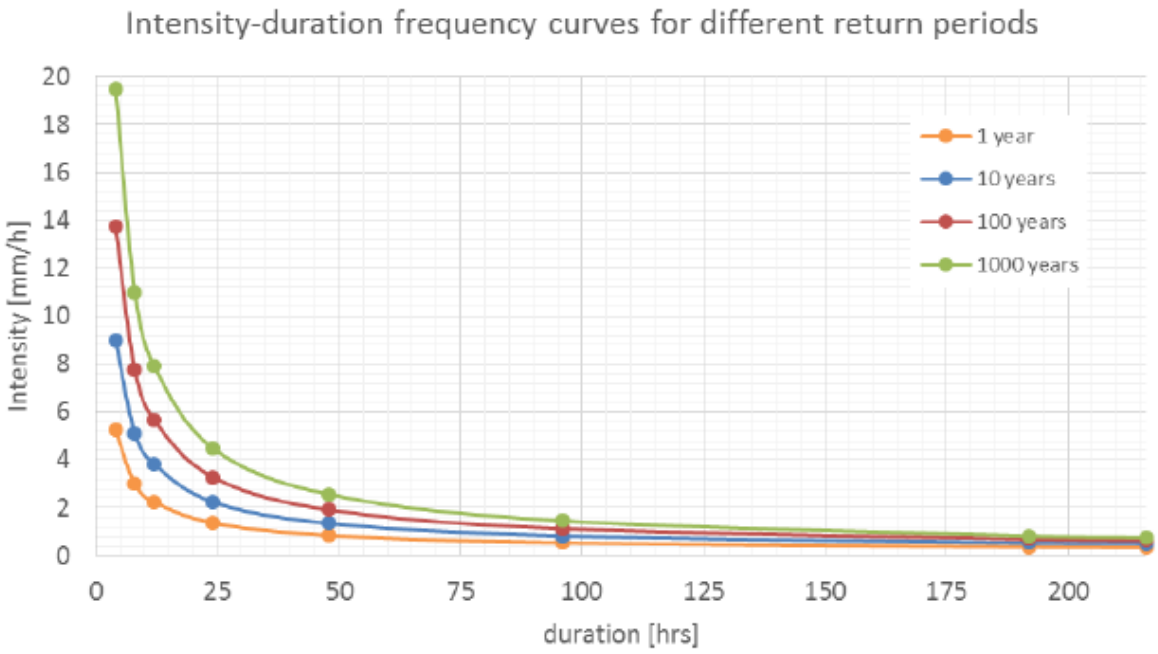

Figure 2.6: Example of return period curves dependent on 2 variables. Source: Thesis Ten Bokkel Huinink, [12].

From Figure 2.5 it is clear that 6 different parameters are of importance plus their occurrence in time.

- Precipitation shape
- Precipitation intensity
- Precipitation duration
- Water level river
- Water level polder
- Overtopping discharge
- All of the above connected in time

On the resisting side the hydraulic conductivity of the soil needs to be regarded as an important variable. From previous research it is known that this parameter has a large influence on the location of the phreatic surface and therefore can not be ignored. Furthermore the behaviour of the soil above the phreatic surface, in the vadose zone is of importance for the phreatic surface. How quickly can infiltrated water reach the surface and how much water is retained in the soil after an event. These characteristics are different per soil type and are also uncertain. Final uncertainty of the soil which is regarded is the presence of cracks and macro pores in the top layer, severely enlarging the permeability of the soil.

With super computers and a lot of time it might become possible to do a full Monte Carlo simulation to construct the probability surface of the phreatic surface. For now, however, this approach is unreachable due

to lack of computer power and time. Therefore the subject of research is narrowed down and only certain parts of the probability surface of the phreatic surface are considered.

Now that the problem on a larger scale is addressed, choices have to be made, since only a part of that puzzle can be solved within the scope of this thesis. All suggestions aim to get a better understanding of the reaction of the phreatic line. Naturally extreme water levels in the river are taken into account as this is the main load for the macro-stability of dikes. Overtopping is probably most innovative as it is totally disregarded for river dikes at the moment. Its influence on the phreatic surface, although likely to be similar to precipitation, and probability of occurrence in combination with high water levels might lead to interesting results. The precipitation is also regarded as it is known from previous research that it can have a significant influence on the phreatic surface. For precipitation only the intensity and shape are varied, while duration is kept constant to reduce the number of scenarios.

The placement in time is also of importance: Precipitation at the beginning of a flood wave have a less severe impact on the stability than near the end of a flood wave. Discarded as research topic is the influence of polder levels since these are kept mostly constant and vary little.

2.3. Research question

All the problems stated lead to the research question of this thesis:

How do water levels, precipitation, overtopping and soil properties influence the inward macro-stability through the shape and level of phreatic surface in river dikes?

2.4. Methodology

As stated before it is impossible to do a full probabilistic approach on the level of the phreatic surface due to various dependencies and correlations and thus a complicated probability space build-up, load and strength wise.

The type of research this thesis handles can be qualified as an uncertainty study or reliability analysis. The thesis of A. Rippi, [9], gives a general description of these study types in Chapter 3 which will be applied on this case. The variable of interest to be studied is the phreatic surface and the consecutive macro-instability. The question is how several input variables influence the variable of interest. For these input variables data and/or expert judgement are available. A Finite Element Method (FEM) model in turn takes these input variables and calculates the target variable based on the given input variables and their values.

The goal of the uncertainty study is to obtain information about the probability distribution of the variable of interest. To get an idea about this distribution the researcher can use several ways to assess its properties:

- Quantiles: assess the value of the variable which exceeds a predetermined probability.
- Central dispersion: tries to obtain characteristics of the distribution, mean and variance.
- Treshold exceedence: tries to determine the probability that the value of the variable is exceeded.

For this research the first option is used. As the distribution of the target variable is likely to be an asymmetric one, the second method gives a wrong idea. The third method starts with a certain value for the target variable and aims to seek the probability of the loads accompanying that phreatic surface level, but as the surface level is the output of the model this method is rather cumbersome.

Then the input variables and their uncertainties need to be quantified. The univariate (marginal) distributions of all the input variables need to be estimated and modeled. Both for load and resistance input. Then also the correlations between these input variables need to be assessed in order to obtain a joint probability function. The next thing to do is to translate the uncertainties of the input variables onto the target variable. This can be achieved by an approximation or a sampling method.

Finally it can be of interest to do a sensitivity analysis of the input variables to get a better understanding of the contribution to the uncertainty in the target variable. If the sensitivity analysis shows that some input variables are insignificant it can be smart to discard them in order to enhance computational time.

The input variables need to limited beforehand because not all can be assessed within the amount of time given. First, as stated above, mainly the hydraulic load part is varied. Soil characteristics with exemption of the hydraulic conductivity and soil layer build up are considered constant in time and space. All the different load combinations, dike types, and soil parameters are put into a FEM-model which calculates a maximum

phreatic surface in a more sophisticated way. Then, this phreatic surface is used as input for a macro-stability test checking the influence on the failure probability of the dike.

The flow chart in Figure 2.7 illustrates the process towards completion. First data is gathered from the KNMI (STOWA report) and Hydra-NL to generate realistic input for the model. Based on this data, several scenarios are constructed to investigate the influence of loads on the phreatic surface. The FEM-model is used to check which circumstances bring about a high phreatic surface. This phreatic surface, in turn, is entered in D-Geo stability to assess the influence on the failure probability of the dike. The outcome of the model is also used to obtain a more probabilistic view of the phreatic surface. In order to obtain input for the FEM-model a clever sampling or approximation method needs to be chosen and applied to construct the scenarios in an efficient way.

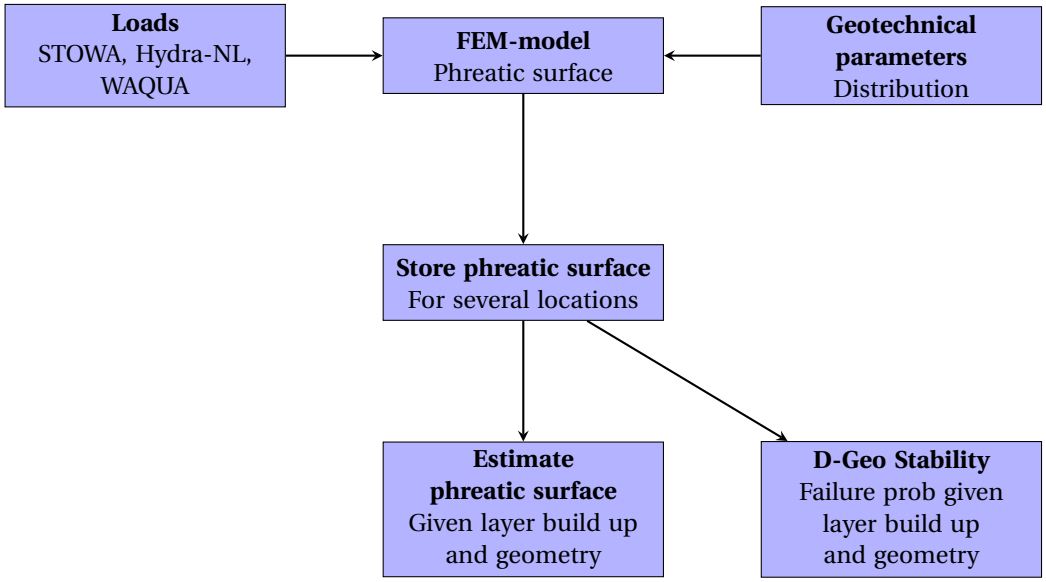

Figure 2.7: Global plan of approach

In order to check the influence of several hydraulic loads, first the heaviest ones are applied. If these significantly influence the surface, less severe loads are applied etc. Up to the minimal loads with a return period of once every 10 years. Once a certain load or load combination does not influence the surface significantly, the less severe loads are not simulated, reducing the total number of runs needed. Then finally the findings will be compared to the methods currently used in practice in order to contribute to the current knowledge of this uncertainty in embankment design.

3

Literature

This chapter presents the literature research and its conclusions. As stated in the problem description this thesis aims to get a better grasp of phenomena causing the phreatic surface rise. Therefore it is evident to describe the current methods applied in practice today. The first part of the literature study therefore focuses on the WBI2017 macro stability guidelines [1] and the technical report behind it for internal processes around the phreatic surface the, TAW [2004], [11], as these reports describe the current methods.

Then the thesis of ten Bokkel Huinink, [12] is being treated. His thesis research is about precipitation influences on the phreatic surface in regional river dikes. With respect to overtopping, a paper about the influence of soil structure deterioration and macro pores in the top clay layer is treated, [19].

3.1. WBI 2017 and TAW [2004]

This thesis puts its result next to that of the method proposed by the WBI 2017. The WBI is implemented since 2017 and is a Dutch abbreviation and stands for Wettelijk Beoordelings Instrumentarium. It means that it can only be used for the assessment of current dikes and not as a design guide for new ones. The WBI 2017 is only applicable on primary flood defences as is the subject of this study. It is thus a logical step to first describe and analyze the methodology proposed by the WBI 2017.

A large part of the assumptions regarding the phreatic surface are based on TAW [2004]. Since this thesis mainly focuses on the influence and modelling of the phreatic surface, information from both reports is described with that in mind.

The WBI is different from previous guidelines in the way the safety of dikes is calculated. No longer a design value with a return period is used but rather the failure of probability of an entire dike section (dijktraject). This automatically entails a more probabilistic approach. Furthermore this way of calculation allows a straight forward way to include length effects and the consequences of a flood in the assessment.

Safety levels of areas protected by these primary flood defences need to meet two safety standards:

1. A basis level of safety indicated with LIR (Local Individual Risk). For everybody in the Netherlands this level has been set to 10^{-5} per year. It is calculated as:

$$LIR = P_f \cdot M \cdot (1 - EF) \tag{3.1}$$

where

P_f = Probability of flooding dike section
M = Mortality rate given a flooding event
EF = Evacuation fraction of people that can be evacuated before flooding

2. Some regions get a higher level of safety than the basic LIR. This safety level is based on the concept group risk and a Social Cost Benefit Analysis (MKBA). For the completeness both are explained shortly:

   - Group risk gives the probability of a flooding with many casualties expressed in an FN-curve, which gives the probability of exceedance of N fatalities.

- In the MKBA the financial consequences of a flood are compared to the costs of lowering the flood probability.

The probability of flooding of dike section is off coarse dependent on the probability of failure of the dike stretches in that particular section. In order to assess the probability of failure of the dikes in the dike sections the WBI 2017 applies three types of tests. The scheme which decides which tests need to be conducted in which situation is shown in Figure 3.1.

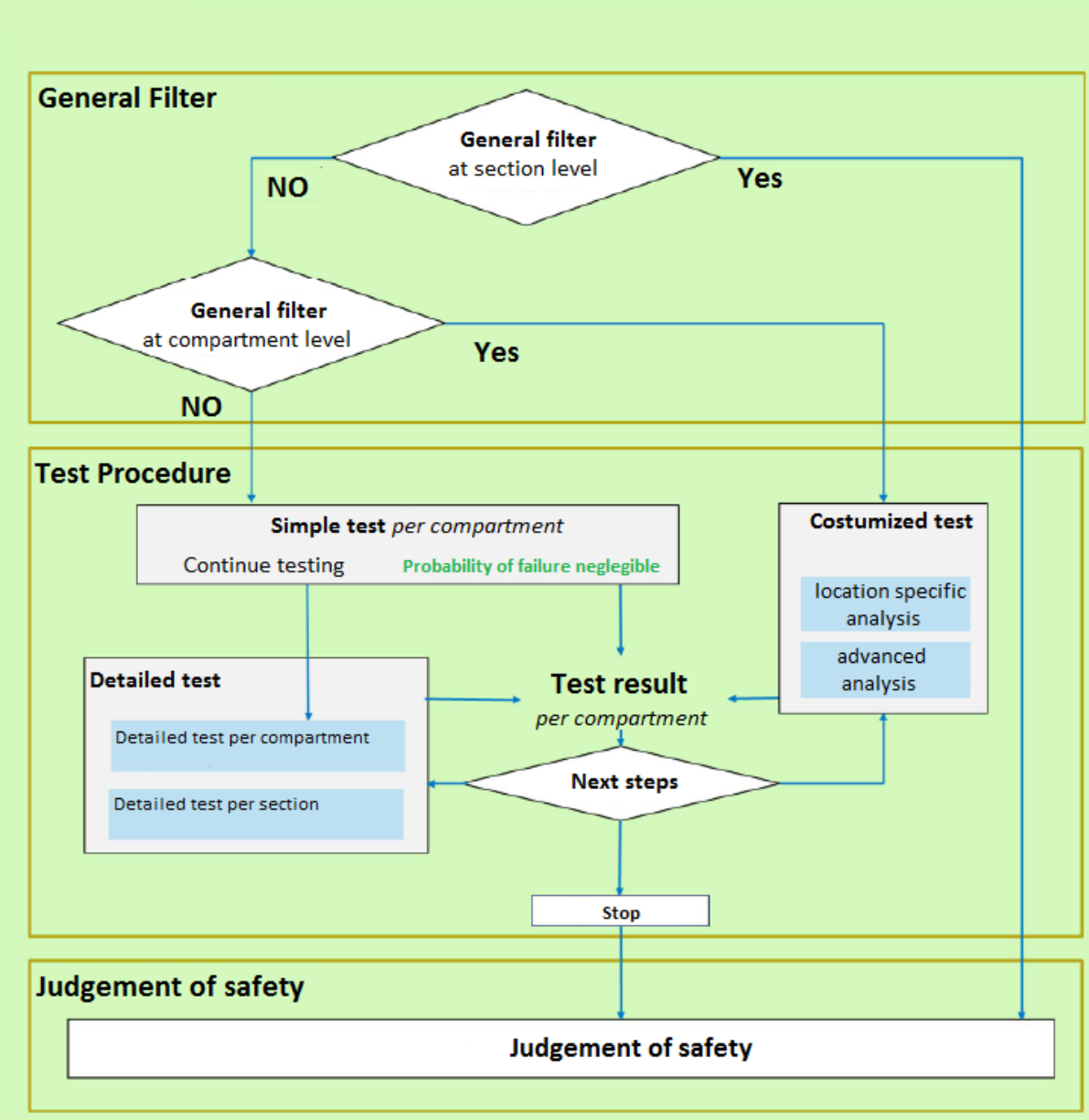

Figure 3.1: System of tests according to WBI 2017. Source: WBI 2017, [2].

First, a general filter decides whether an entire dike section needs testing. If it does not, the entire section is approved. If it does, a general filter per dike compartment is applied. If for that dike compartment still no general filter can be applied, the testing procedure starts.

Then, there are three existing test levels: the first test is a simple test for inherent safe dikes e.g. a wide crest or for more gentle slopes. The second test is a more detailed test which can be done semi-probabilistic per dike compartment (dijkvak) or a probabilistic test per dike section. These tests use more input parameters and information for the assessment of the stability. If the dike still fails, a customized test (toets op maat)

could be conducted. In this type of test the engineer get some more freedom, but it is an elaborate and labor intensive process. If also this last test indicated that the dike does not have the right requirements, it has to be redesigned or upgraded so that it will meet the safety standards. This procedure is followed per failure mechanism, and thus also for macro-stability.

3.1.1. WBI 2017 macro-stability

The test procedures as shown in Figure 3.1 for the macro-stability track if further described in the corresponding guidelines, [1]. It also covers any assumptions made for the detailed tests. In general as with every civil engineering problem there are always loads and resistances. Both have uncertainties in them and the loads should not overcome the resistance because then the structure fails. For its tests and schematizations the WBI indicates several types of loads important for inwards macro-instability of the dike. The list is adapted to primary flood defences in the river areas (WBI also regards sea dikes).

- Permanent loads:
  - Own weight
  - Soil subsidence
- Variable loads:
  - Hydraulic loads:
    - The regular water levels.
    - Design water levels.
    - Water level development in time (waterstandsverlooplijn).
    - Wave heights, wave periods, wave direction (generated by wind and ships) in relation to overtopping discharge.
    - Tide (lower river area).
  - Polder level
  - Traffic loads (for repair during high water)
  - Other loads:
    - Wind (not applicable)
    - Ship collision
    - Nature induced degrading (digging animals and roots)
    - Weather induced degrading (cracking of clay by drought)

Notice that precipitation is not mentioned as a (variable) load, while water levels and overtopping are. With respect to the pore water pressures and (sub)soil relevant around the dike these are the mentioned factors of influence:

- Geometry of the dike.
- The buildup of the subsoil.
- The buildup of the soil layers in the dike.
- Water level in the polder.
- Location of the phreatic surface
- Piezometric head in the aquifer.
- Piezometric head in the aquitard.
- Parameters of the soil layers.

This is the first time the phreatic surface is mentioned in the WBI. It is of significant importance but together with subsoil and dike soil layer buildup and parameters the most uncertain. According to the WBI The Waternet Creator tool should be used to simulate the phreatic surface and water pressures in the soil conform TAW [2004]. Therefore the literature study will now zoom in on this Technical Report.

3.1.2. TAW [2004]

The TAW [2004] is used as basis for everything in the WBI 2017 related to pore water pressures and water pressures inside and around dikes. It divides the pore water pressures in three different types:

- Ground water flow induced pressures (e.g. water levels and precipitation).
- Soil stress depended pore water pressures (e.g. consolidation and creep).
- Pore water pressures induced by deformation (e.g. elasto-plastic deformations).

Both the TAW [2004] and this research will focus on the first type of load. While the others are neglected or supposed to be constant. Separated by water system, the report distinguishes four types of dikes:

- Rivers upstream
- Rivers downstream
- Lake
- Polder buffer area (regional dikes)

The research is applied to the first type of water system. As a consequence high water levels due to river discharge give the main boundary conditions for the problem.

In the Netherlands a dike is mostly constructed on a semi-permeable top layer (Holocene) which in turn rests on a incompressible but permeable sand layer (Pleistocene). Changes in river water levels are usually instantaneously noticeable in the Pleistocene layer and only after some time in the dike itself.

When more water enters the dike it gets stored in the soil through phreatic storage, in extra pore space developed during consolidation and/or compaction of the Pleistocene layer. Naturally the first is of interests in this case.

Figure 3.2 shows the most important types of flow around a typical Dutch dike.

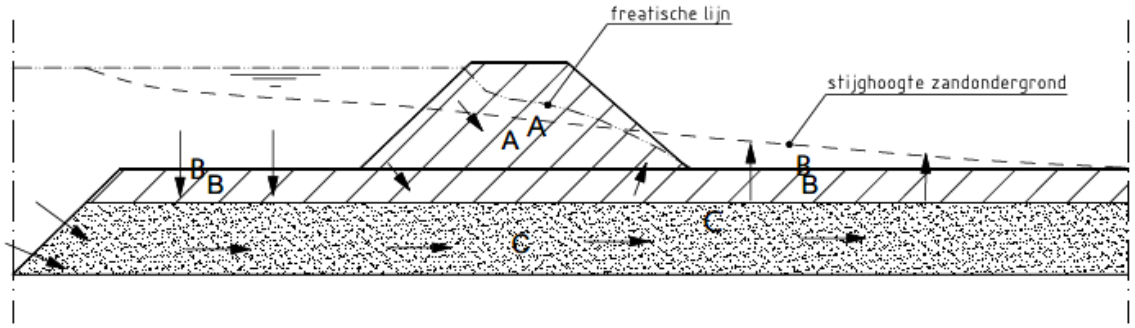

Figure 3.2: Types of flow in a standard Dutch dike. A: Flow through the dike. B: Vertical flow through the Holocene layer. C: Horizontal flow trough the Pleistocene layer. Source: TAW [2004], [11].

Pore water pressures altered by external influences are always modelled compared to an equilibrium situation. This equilibrium is usually the average water level in the river and the average level in the polder. In the equilibrium state there thus is a stationary flow. Especially in regional dikes the water flows through the dike from the canal into the polder. For primary flood defences this is not always the case. Especially with respect the outer dike (winter dikes) the equilibrium surface may be below the dike entirely. All other effects affecting the pore water pressures are modelled with respect to this equilibrium stage. For regional embankments the equilibrium has a more constant character as both the canal and the polder level are managed and only in extreme cases these will differ. With primary defences, however, this equilibrium can change throughout the year and differs per season or over the years due to climate change.

Another effect needs to be specified for this research: Phreatic vs elastic water storage in the soil. Phreatic storage occurs when the phreatic surface rises and the pores above are getting filled with water. The porosity of the soil is thus an important parameter although the effective phreatic storage is lower since only a part of the pores actually gets filled.

Elastic storage is when the water pressures change but the total soils stresses are constant. As a result the space in the pores which can be filled by water changes. Also present air or other gases as methane in

the water can compress allowing more water storage in the water itself. This storage coefficient related to the consolidation coefficient can be calculated for different types of soils. Phreatic storage however is several orders larger than elastic storage.

Flow inside the soil can be either stationary (constant velocity in time) or non-stationary (accelerating or decelerating). In the first case the soil stresses and water pressures remain constant while in the latter these change in time. This can have severe consequences for stability of the dike. Dependent on the permeability of the soil the flow can mainly be considered stationary. This permeability can best be expressed in a hydrodynamic period compared to the duration of the load.

Flow and its modelling can be regarded in a 3D or 2D sense. It is common to approach the problems in a 2D manner unless structure or other type of disturbances are of influence. This research focuses on a straight stretch of dike with no structures, sand wells or bends. Making a 2D approach of the system a logical simplification of the problem.

Influence of precipitation and overtopping
Both precipitation and overtopping can raise the phreatic surface as well as the water pressures in the dike. The influence of these two phenomena depends on several factors:

- Permeability of the soil layers.
- Storage capacity of water.
- Amount of 'hard' surface.
- Slope angle.
- Vegetation.
- Roads and especially road sides and cunets.
- Sewage systems in urban areas.
- In clay tunnel structures due to animals and roots can be present.
- In clay also smaller less continuous system of cracks can be present above the phreatic surface.
- Atmospheric circumstances; which part of the absorbed water actually sinks into the body to the core and which part evaporates.

These factors all influence the amount of water that infiltrates the dikes and which part just flows along the dike slope into the polder. Then there are some special aspect which need to be acknowledged to get a more complete understanding of the soil and hydrodynamics.

- Capillary rise. Due to capillary suction the soil above the phreatic surface (defined as the hypothetical line where the water pressure equals the atmospheric pressure) can still be saturated. This suction also creates a negative water pressure leading to higher effective soil stresses and thus soil strength. However in some cases a large capillary zone with a high saturation can cause an extra danger, because only little infiltration water can cause the extra strength to dissipate quickly. Especially if the zone reaches all the way to the surface. This is why the effect is not taken into account in practice unless the surface of the dike is impermeable for sure.
- Phreatic bulging in rainy periods lead to a high phreatic surface at the center of the dike while the surface flows away trough the sides of the dike. In older relative more impermeable dikes the bulging comes slowly but also takes a long time to disappear again. Therefore quite often a high phreatic surface is found.
- Intrusion length, L, is the height for which water pressure variations in the aquifer penetrate into the aquitard. It plays an important role in sand dikes but also for macro-instability of a covering peat or clay layer and its inward macro-stability. Intrusion length increases with the square root of the time. The intrusion length influences the water pressures in the Holocene layer by either compression or swell.
- Leakage factor is the resistance of the aquitard compared to the permeability of the aquifer.
- An-isotropic permeability often plays an important role. In sand the horizontal permeability can be 1.5 times larger that the vertical one. In clay and peat this difference can become as high as 3 times.

- Relaxation of the phreatic surface after an extreme event can take some time. The build up storage of water slowly relaxes over time. This can be important if two or more loads follow up on each other rather quick.
- The hydrodynamic period, T_c, is the consolidation period of a layer and depends on the layer thickness and the consolidation coefficient through: $T_c = 2d^2/c_v$. Where 2 is a factor for 99% consolidation. The consolidation coefficient, c_v, depends on the hydraulic conductivity, compressibilities of the water and soil, and the porosity. A high value induces a short consolidation time and the other way around.

In these current guidelines several load combinations are regarded and for each of these loading scenarios a safe schematization for the ground water flow needs to be made first. Measured water pressures are needed to verify and calibrate the numerical models. This can not be done for design circumstances and thus a extrapolation of loads is needed. This extrapolation might be tricky as other (strength) parameters might also be behaving differently.

In practice three different piezometric head lines are of interest for the civil engineer. The phreatic surface, so the piezometric head line in the dike. The phreatic height in the Holocene semi-permeable layer just about the intrusion length from the Pleistocene layer. Last the piezometric head in the Pleistocene layer itself. This thesis will clearly be about the first one, hard to predict and subjected to a lot of different processes. The others, however, are also of importance for macro-stability of the dike.

For the modelling of the phreatic surface roughly two types of dikes and two types of subsoil, divided by soil characteristics, are distinguished by the TAW [2004]. The phreatic surface in an impermeable dike or in a permeable one build on a sandy subsoil or on a clay/peat subsoil:

- Impermeable body, see Figure 3.3. Difficulties of modelling the phreatic surface in these type of dikes is due to the large uncertainties about the top clay soil. Formed cracks and the saturation in the clay are of large importance and unknown beforehand. The permeability depends greatly on these factors and is thus a uncertain factor in itself. It can also differ greatly over the length of the dike. Due to inhomogeneous properties water could unexpectedly infiltrate in the body. Water pressures could rise in random place inside the dike, like an old buried road of some sand fill. In TAW [2004] this type of dike build on clay/peat is known as type 1A and build on sand it is known as type 1B.
- Permeable body. If the body is permeable the cover layer needs to be impermeable. To reduce the water pressure inside the dike this layer is usually positioned on the outer slope. Furthermore, the dike can be build upon a permeable or impermeable subsoil. Build on a impermeable subsoil the phreatic surface will decrease steep in the cover layer and continue on the same level as during normal circumstances, see Figure 3.4. Build on a permeable layer the water can simply infiltrate from below resulting in a high phreatic surface in the dike, see Figure 3.5. Also in these types of dikes phreatic surfaces can make unexpected jumps due to lack of homogeneity. In TAW [2004] this type of dike build on clay/peat is known as type 2A and build on sand it is known as type 2B.

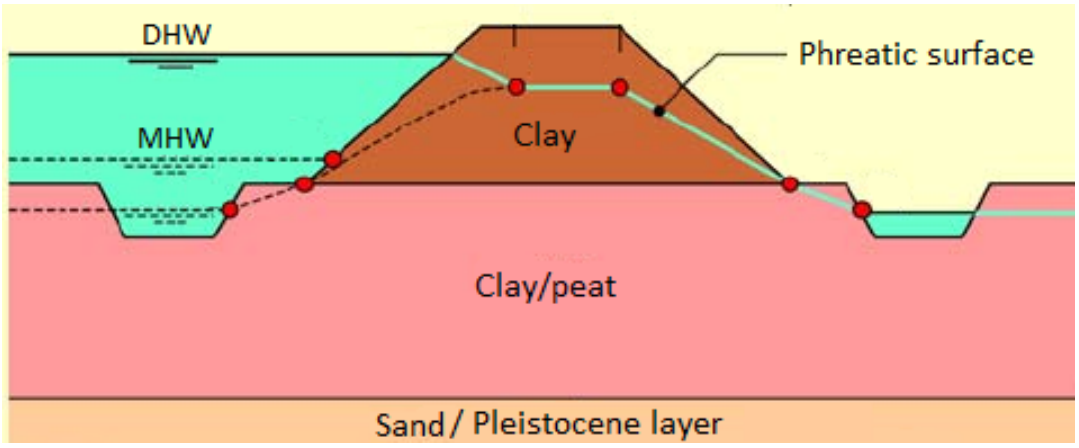

Figure 3.3: Clay dike and peat/clay as subsoil. Phreatic surface during DHW. Dotted line gives phreatic surface during normal conditions. Source: TAW [2004], [11].

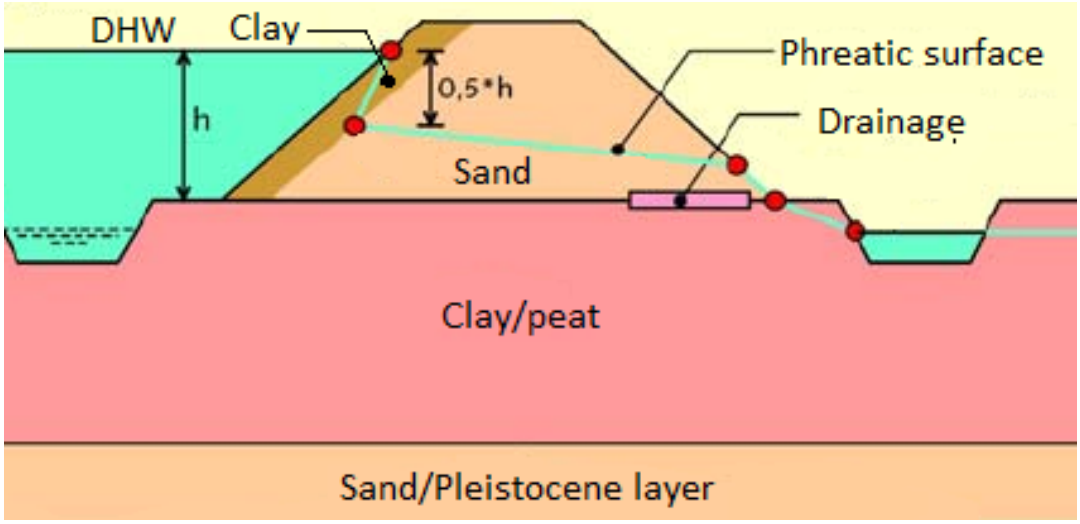

Figure 3.4: Sand dike with impermeable cover (clay) and peat/clay as subsoil. Phreatic surface during DHW. Source: TAW [2004], [11].

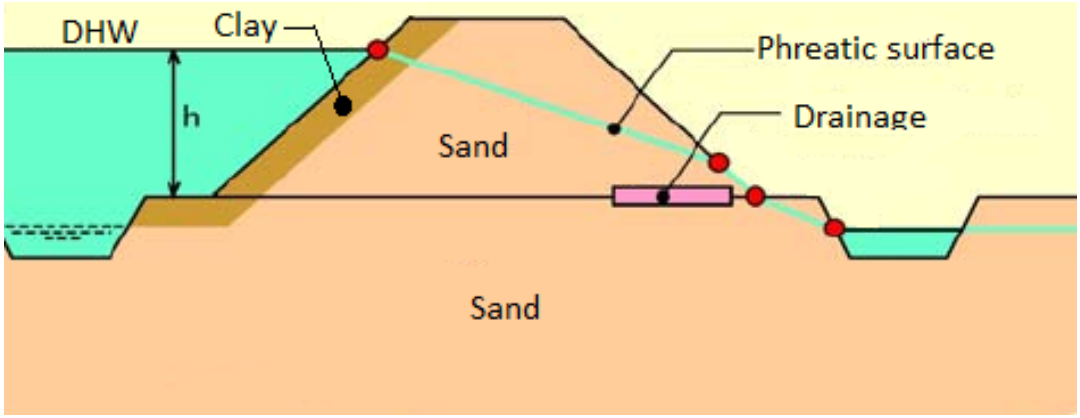

Figure 3.5: Sand dike with impermeable cover (clay) and sand as subsoil. Phreatic surface during DHW. Source: TAW [2004], [11].

In the past some tests with the first dike type have been conducted to find a connection between precipitation and phreatic level rise. However, the differences between test locations were to large to draw clear conclusions. Still the TAW gives a guideline how to incorporate an extreme rainfall event.

For the extreme precipitation scenario the assumptions in TAW [2004] are:

- Mean high water.
- Phreatic line at inner slope rises with 0.5 to 1.0 meters.
- Ground water level in the polder is up to surface level.
- Precipitation does not influence piezometric level subsoil.

For the design river discharge scenario the assumptions in TAW [2004] are:

- Design high water.
- No rise phreatic line at inner slope.
- Ground water level in the polder is at normal level.
- Traffic needs to be taken into account.

This means another situation occurs during extreme rainfall than during Design High Water when no rainfall is taken into account. The scenarios are completely separated. See Figures 3.6 and 3.7 respectively. For the DHW-scenario also traffic on the dike needs to be taken into account for macro-instability.

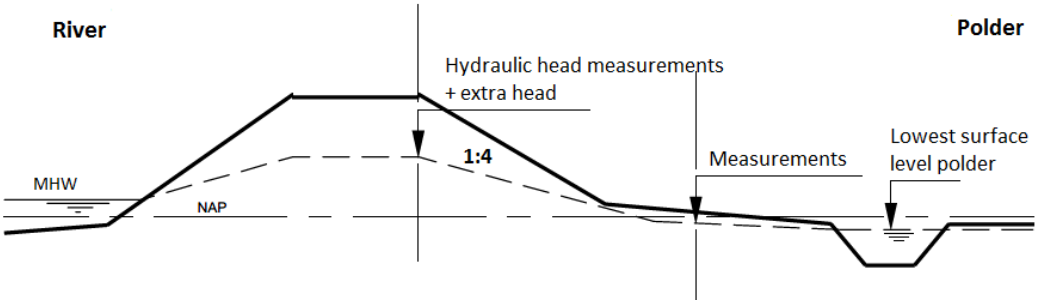

Figure 3.6: Design scenario with extreme precipitation and Mean High Water. Source: TAW [2004], [11].

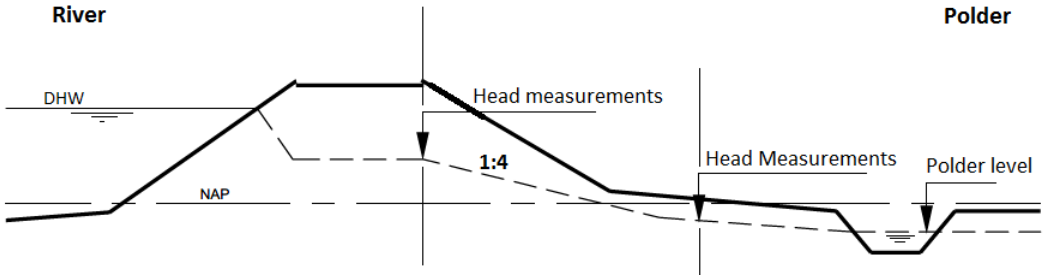

Figure 3.7: Design scenario without precipitation and Design High Water. Source: TAW [2004], [11].

In TAW [2004] it is assumed that overtopping has no influence on the phreatic surface due to lack of validated models at the time of writing. Due to demands in height it is assumed that overtopping is less than 0.1 m/l/s and that this is not enough to properly infiltrate the dike to influence the phreatic surface.

Using Figure 3.8 the phreatic surface for an impermeable dike on an impermeable subsoil (case 1A) in the DHW case without any numerical modelling needs to be calculated as follows (so no precipitation or overtopping influence):

$$A = \min(C + \frac{L}{X}, \quad D + \frac{L}{X}, \quad h_{crest} - 0.3) \tag{3.2}$$

where

$$X => \quad \text{if} \quad d < 4.0m \qquad X = 10$$
$$\text{if} \quad d > 4.0m \qquad X = 8$$

For C and D one of the suggested values need to be picked depending on what the average water level is. L is then the distance between C and D. In this thesis the distance C2 to D1 is used as a starting position which would this mean that L2 should be used as L in the formula above.

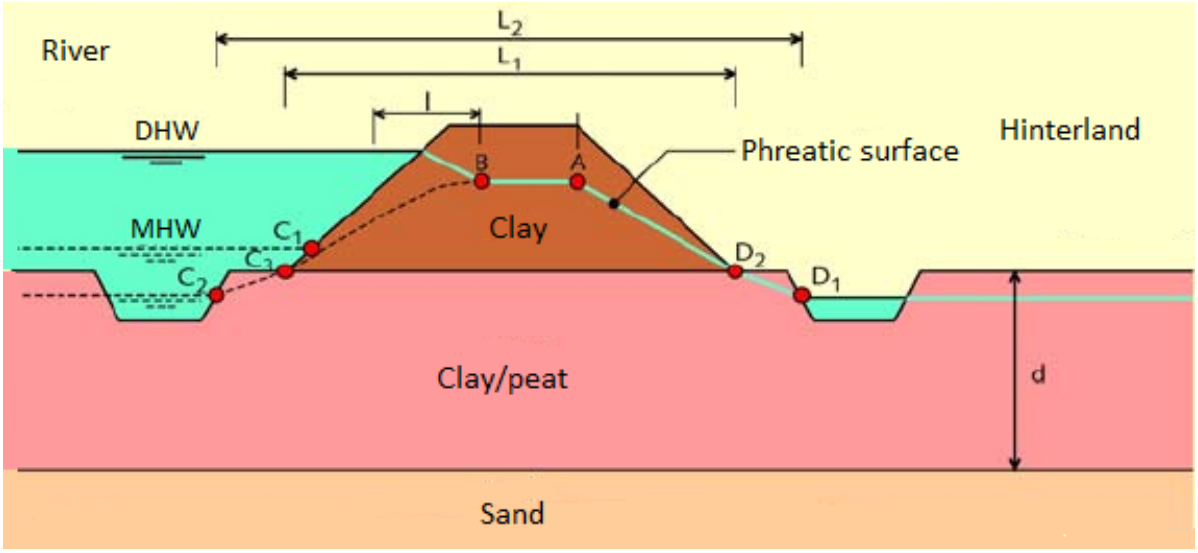

Figure 3.8: Clay dike and peat/caly as subsoil. Phreatic surface during DHW. Dotted line gives phreatic surface during normal conditions. Source: TAW [2004], [11].

The horizontal location of point B is given by the horizontal intrusion length as seen from the point where Mean High Water (MHW) touches the dike, see Figure 3.9. This is a time dependent process as can be seen in both the formula and the Figure. The intrusion length can be calculated with:

$$I = \sqrt{\frac{2 * k_z * h_0 * t}{n_z}} \tag{3.3}$$

where

k_z = Hydraulic conductivity dike material $[m/s]$
h_0 = Water depth w.r.t. Holocene layer $[m]$
t = Duration high discharge causing MHW $[s]$
n = porosity dike material $[-]$

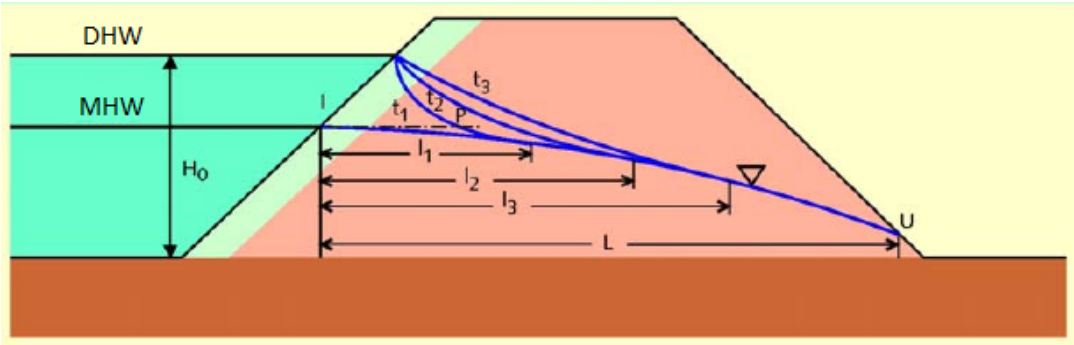

Figure 3.9: Infiltration development in time. Source: TAW [2004], [11]

Thus the TAW [2004] considers two scenarios:

- One with extreme precipitation and mean high water. First the equilibrium surface is calculated based on the mean high water outside and a higher polder level. Then 0.5 meters is added below the crest for extreme precipitation. A traffic load could be added.
- The other is calculating the surface with design water levels but with normal precipitation (and traffic load).

The statistical argumentation behind these scenarios is rather small and only the water level in the river is based on a data analysis. In summary; the Waternet creator used for computing the phreatic surface the input of:

- Dike type (one of the four mentioned above)
- Water level in the polder
- Water level in the river
- Leakage length
- Intrusion length
- Initial phreatic surface

The results of the Creator are:

- Phreatic surface
- Piezometric head in the Holocene layer
- Piezometric head as a function of depth.

Also several sub-scenarios can be created:

- With and without a water tight layer on the foreshore.
- Drainage in the inner toe or not.
- With or without and old clay core.
- Presence of a old permeable road foundation.
- Higher polder level due to extreme rain or seepage.

The WBI 2017 advises in the first place to base the initial phreatic surface on measurements. If these are not available the estimation based on the TAW [2004] methods are recommended. If these still give extreme (high failure probability) results, a ground water flow model can be developed. It also mentioned the analytical formulas of Dupuit and Hooghoudt for a more detailed assessment of the initial phreatic surface.

After the phreatic surface is established the test for macro-instability is conducted with the computer tool Ringtoets (BM-Macrostabiliteit up to 2019). But first some more geo-parameters need to be implemented. The buildup of the subsoil needs to be extracted from SOS or Stochastic subsoil schematization (Stochastische ondergrond schematisatie), a large database constructed by Deltaris and TNO for the Dutch subsoil. Although this does not account for the subsoil directly under the dike which often differs due to compaction. Then the soil parameters and their distributions are inserted in D-Soil Model. These in turn are also implemented in Ringtoets which does the actual macro-instability calculations.

Also for each dike stretch the most unfavourable cross section needs to be determined for each load case. In case of instability induced by a high phreatic surface a small crest width and a low relative crest height. Then Ringtoets calculates the resulting failure probabilities according to the LiftVan or Spencer method. For now, during this research Ringtoets is not available yet. Therefore BM-Macrostabiliteit is used.

This concludes the entire methodology as prescribed by the WBI 2017 for the macro-stability track. Next, more literature about the influence of rain and overtopping on the phreatic surface is treated.

3.2. Precipitation and overtopping research

3.2.1. Rain

In the thesis study of Ten Bokkel Huinink, [12], numerical modelling is used to compute several phreatic surfaces in regional water defences. Although it entails only precipitation, his methodology and conclusions are helpful for this research.

The thesis varies in and accounts for:

- Rainfall duration.
- Rainfall intensity.
- Non-hydrostatic pressures due to downward flow.

- Distinction between saturated and unsaturated soil permeabilities.
- Relation to failure due to macro-instability through D-Geo Stability.
- Relation to computations as suggested by TAW [2004], [11].
- Regional flood defenses only.
- Three different homogeneous dikes: peat, clay and sand.
- Only phreatic surfaces occurring less than once a year are considered.
- Actual failure probability computed with D-Geo.

He does not consider:

- Shape of rainfall.
- Water levels i.c.m. rainfall and their correlations.
- Overtopping.
- Dikes consisting out of different soil types.
- Exceedance frequencies higher than 1/1000 years.
- Capillary suction.
- Outer slope macro-instability.
- Stochastic soil parameters.
- Verification with a case and measured phreatic surfaces.

He concludes that:

- Rainfall influences the phreatic surface significantly in clay and peat dikes.
- Permeable soil types react stronger to intense and short events while less permeable soil types react to long events.
- Due to non-hydrostatic pressures the pore pressure lower in the dike is actually lower than the WBI and TAW [2004] suggests. This difference is largest in the area where slip circles form and is thus an important factor.
- Both for clay and peat a permeability of $k = 2.8 * 10^{-7} m/s$ generated the highest phreatic surface.
- Crest width and difference between water level and crest height influence the starting position of the phreatic surface and therefore the saturation levels of the surface level at the crest and inner slope. This in turn influences the permeability of the top soil.
- In contradiction to the TAW [2004] there is a response of the surface in sand with a low permeability with a rise up to 0.7m.
- In contradiction to the TAW [2004] the phreatic surface can rise to crest level in peat and clay dikes.
- Location of the phreatic surface depend on both the saturated (determines maximum phreatic layer) as well as the unsaturated permeability (determines infiltration speed of precipitation) of the soil (layers).

3.2.2. Overtopping

Research on consequences of overtopping are thus far mainly limited to erosion of the inner slope (e.g. Bijlard [5], van der Meer et al. [17], Jonkman et al. [7], Ponsioen [8], and many others) and little on infiltration and the influence on the phreatic surface.

For sea dikes some research has been conducted in the recent years which will be treated here. Van der Meer is the first to consider wave overtopping rather than overflow and its influence on dike failure in [15] and [16]. With the wave overtopping simulator they simulate overtopping for sea dikes but also for a river dike. They remark that overtopping load for river dikes is of a different nature than for sea dikes. Where sea dike have a high relative crest height i.c.m. high wave attack the river dike is subjected to a small relative crest height a small wave attack. However at river dikes the same relative overtopping discharges can be found ranging from 0.1 l/s/m up to 125 l/s/m. Figures 3.10 and 3.11 show the results for the overtopping simulations from [16].

Characteristic values depending on mean overtopping discharge. Background: H_s = 0.75 m for 0.1;1 and 10 l/s per m and H_s = 1 m for other; s_{op} = 0.04, outer slope 1:3 and storm duration 2 hours

Mean overtopping discharge (l/s per m)	*0,1*	*1*	*10*	*30*	*50*	*75*	*100*	*125*
Crest freeboard (m)	1.91	1.36	0.82	0.89	0.73	0.6	0.51	0.44
Percentage of overtopping waves (%)	1.1	10.1	44	58	69	78	84	88
Number of overtopping waves	32	295	1263	1450	1733	1952	2091	2188
Maximum overtopping volume (l/m)	98	208	659	1765	2543	3460	4317	5185

Figure 3.10: Artificially simulated values of overtopping waves for river dikes. Source: Van Hoven et. al. (2010), [19].

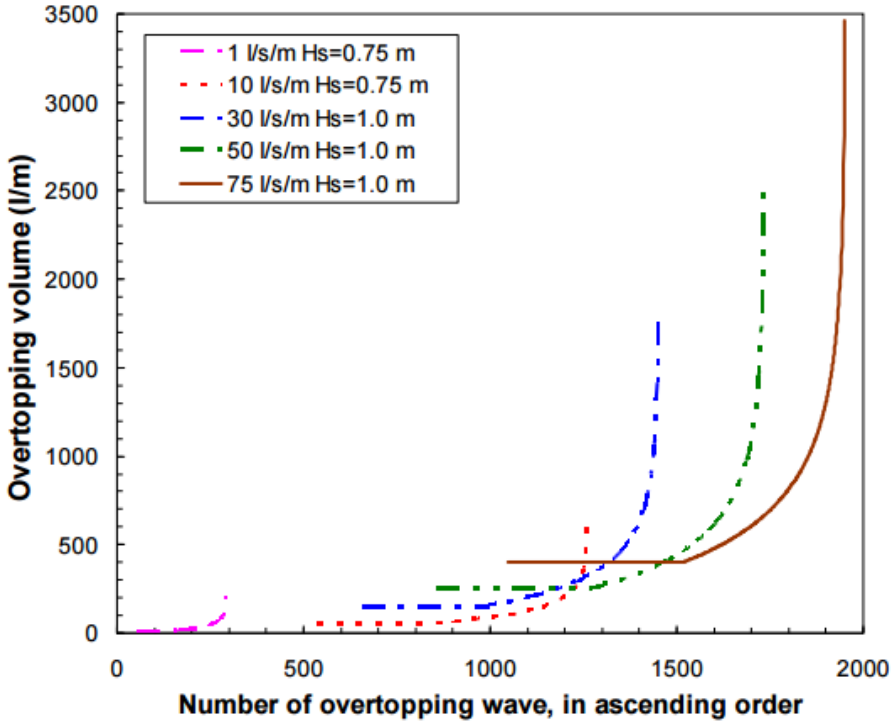

Figure 3.11: Artificially simulated distribution of overtopping waves for river dikes and various mean overtopping discharges. Source: Van Hoven et. al. (2010), [19].

These values are simulated and are not based on any probability analysis.

Van Hoven et al. [19], are then the first to look at the consequences of overtopping inside the dike and sliding induced failure. They look at sliding of the top layer of the inner slope and therefore consider how pore pressures are affected by overtopping. They also stress the importance of soil structure deterioration in clay dikes. Due to roots, animals, and drying in the sun the top 1-2 meters of the clay layer becomes more permeable in an an-isotropic way. Only the vertical permeability increases considerably. The influence of this soil structure deterioration is shown in Figure 3.12. It can also influence the shear strength of the soil. Large parts of the clay soil assumptions are based on the findings and recommendations of TAW[1996], [10]. In case of wave overtopping the large structures will be saturated in a short notice, while some parts will to some extend still have negative pore water pressures inside due to capillary suction.

Depth (m)	Aggregates description	Macro pores
0-0,05	Very small, very loose, kept together by roots	>30%
0,05 -0,2	0,1 – 3 cm, Loosely packed	20-30%
0,2-0,4	3-6 cm, loose fit	5-20%
0,4-0,8	5-15 cm elongated, tight fit.	2-5%
>0,8	Vertical fissures	<2%

Figure 3.12: General soil structure deterioration levels of clay cover layer. Source: TAW [1996], [10].

Van Hoven, [18], compares large tri-axial tests with a saturation procedure similar to a wave overtopping situation. The standard tri-axial tests seem to suggest standard tests will not underestimate the shear strength of the clay with soil structure deterioration. The results are however not generally conclusive.

Van Hoven et al. [19], assume that sliding will not occur if the overtopping is less than 0.1 l/s/m or if the slope is less than 1 : 4. They apply a three step method to determine pore pressure build up in the dike due to wave overtopping for sea dikes:

1. Infiltration time $[s]$. The time when there is actual water on the crest and inner slope. On average 30 seconds per overtopping is mentioned, but it clearly depends on the slope. They use Monte Carlo simulation to get an amount of time there is actual water on the dike. The wetting period per overtopping wave, however, is set to 30 seconds deterministically.

2. Infiltration capacity of the soil $[m^3/s/m^2]$. That is the amount of water that can infiltrate in the soil. For clay with clay structure the value is estimated to be between 10^{-5} and $10^{-4}[m^3/s/m^2]$. Based on 21 field tests they find that the infiltration capacity of sand dikes has the same order of magnitude as clay dikes and sand dikes with clay cover.

3. Determine potential pore pressure build up. This depends on the infiltration volume (multiplication of step 1 and 2), the dike structure and the dike geometry. Pressure build up only occurs if the infiltrated water reaches a less permeable layer or the phreatic surface. Here Van Hoven et al. [19] make a difference between:

    - Sand dikes (with a clay cover). The core is as permeable as the cover layer with soil structure deterioration. Thus the infiltrated water flows directly to the phreatic surface, following the path of the least resistance. The rise is simply equal to the infiltrated volume divided by the effective pore space.
    - Clay dikes. For clay dikes the story is slightly more complicated. The dike can be divided in a cover layer with the aforementioned soil structure deterioration and a much less permeable clay core. Water will infiltrate down until the core where pressure builds up. At a certain moment the pressure get high enough and starts flowing parallel to the surface. In order to reach this state the cover layer needs to become saturated. Using the numbers in Figure 3.12 it can be calculated this happens after 60 - 125 $[l/m^2]$. The unfavourable situation is low macro pores and a thick cover layer (quick saturation over a large depth).

They find that their three-step-method is a bit too safe and with field measurements the predicted pore pressures are not reach. They attribute this to 3D effects and thus internal horizontal flow outward of the test area.

Final paper which investigates the influence of overtopping on the phreatic surface is De Raadt et al, [6]. They apply it on the Afsluitdijk and thus again only in sea-like conditions. Now a fully saturated dike needs to be assumed during storm conditions due to the uncertain influence of overtopping and in order to lower the phreatic line they conducted the research. Just like [12] and [19] they use the finite element program, PLAXIS, to model the phreatic surface. They use measured phreatic surface, soil parameters, geometry and layer build up as input to calibrate the model and then apply a storm scenario. Unfortunately, it is not clear how they implemented the overtopping load in PLAXIS. They get positive results in phreatic surface reduction.

4

Theoretical model

The research will mainly be executed by a finite element program. Before using the finite element program several processes need a proper explanation and elaboration. These are the current theories on the physics behind some important phenomena which should be addressed and understood before any finite element program and its hydraulic input can be used and interpret in a correct way. The chapter starts with the external influences and works its way to the essence of the research, so in this section order: Hydraulic loads construction methods, run-up and overtopping, subsurface flow, and finally macro stability.

4.1. Hydraulic loads

4.1.1. Hydra-NL and flood waves

The Hydra-NL program, published by Rijkswaterstaat, uses wind, sea and discharge data to calculate return periods of water levels, overtopping discharges, and wave characteristics. The only thing it does not consider is precipitation, which needs to be implemented in another way. In order to get a better understanding of the return periods of certain phreatic levels, a statistical analysis of the loads is necessary. The return period of water levels and overtopping discharges is a rather cumbersome challenge, but is to a large extend solved by the Hydra-NL program.

Inputs for the program are the location for a primary defense structure to assess and its cross section profile on the water side. Also the roughness factor and orientation of the profile need to be inserted. The program has three modes, Basic (programmed to handle input as prescribed by the WBI), Climate (several future scenarios can be implemented), and Test (freedom for the user but more complicated). Since the program is used to produce water levels and hydraulic load levels only, the Basic mode is used.

The user defines a characteristic he/she wants to know the value of for certain return periods which he/she can also define. The program then searches for each wind direction (16 in total) a combination of loads which have a probability per winter semester to occur. These probabilities need to add up such that they reach the desired return period. Figure 4.1 shows and example of the output for a location at the Lek river for the 1/5,000 year overtopping discharge. Upper table are the statistics for an opened Europoort storm barrier and the lower table for a closed Europoort barrier.

```
Locatie                      = LE_1_16-3_dk_00351 (115259,437251)
Berekeningstype              = Overslagdebiet-berekening bij aanwezige dijkhoogte van  6.12 (m+NAP)
Overslagdebiet               =     0.16 (l/s/m)
Terugkeertijd                =     5000 (jaar)
Overschrijdingsfrequentie    = 2.00E-04 (per jaar)

Geopende Europoortkering

  r      | zeews.   | q Rijn   |      -- | windsn.  | h,teen   | Hm0,teen| Tm-1,0,t| golfr    | ov. freq    | ov. freq
         | m+NAP    | m³/s     |      -- | m/s      | m+NAP    | m       | s       | graden   | *0.001/whj  | %
---------+----------+----------+---------+----------+----------+---------+---------+----------+-------------+---------
  NNO    |     1.36 |    13000 |      -- |     26.0 |     3.24 |    1.08 |    3.23 |     22.5 |       0.000 |     0.0
  NO     |       -- |       -- |      -- |       -- |       -- |      -- |      -- |       -- |       0.000 |     0.0
  ONO    |       -- |       -- |      -- |       -- |       -- |      -- |      -- |       -- |       0.000 |     0.0
  O      |       -- |       -- |      -- |       -- |       -- |      -- |      -- |       -- |       0.000 |     0.0
  OZO    |       -- |       -- |      -- |       -- |       -- |      -- |      -- |       -- |       0.000 |     0.0
  ZO     |       -- |       -- |      -- |       -- |       -- |      -- |      -- |       -- |       0.000 |     0.0
  ZZO    |       -- |       -- |      -- |       -- |       -- |      -- |      -- |       -- |       0.000 |     0.0
  Z      |       -- |       -- |      -- |       -- |       -- |      -- |      -- |       -- |       0.000 |     0.0
  ZZW    |       -- |       -- |      -- |       -- |       -- |      -- |      -- |       -- |       0.000 |     0.0
  ZW     |       -- |       -- |      -- |       -- |       -- |      -- |      -- |       -- |       0.000 |     0.0
  WZW    |     2.77 |     2400 |      -- |     30.5 |     3.36 |    1.12 |    3.26 |    247.5 |       0.008 |     3.8
  W      |     2.98 |     2200 |      -- |     28.0 |     3.51 |    0.92 |    3.27 |    270.0 |       0.031 |    15.4
  WNW    |     2.97 |     2600 |      -- |     24.0 |     3.31 |    0.97 |    3.03 |    292.5 |       0.023 |    11.7
  NW     |     4.14 |     2350 |      -- |     26.3 |     3.87 |    0.73 |    2.85 |    315.0 |       0.003 |     1.4
  NNW    |     4.46 |     2550 |      -- |     28.1 |     3.93 |    0.73 |    2.82 |    337.5 |       0.000 |     0.2
  N      |     3.23 |     3400 |      -- |     27.0 |     3.10 |    1.04 |    3.15 |    360.0 |       0.000 |     0.1
---------+----------+----------+---------+----------+----------+---------+---------+----------+-------------+---------
  som    |                                                                                     |       0.065 |    32.5
Gesloten Europoortkering

  r      | zeews.   | q Rijn   |      -- | windsn.  | h,teen   | Hm0,teen| Tm-1,0,t| golfr    | ov. freq    | ov. freq
         | m+NAP    | m³/s     |      -- | m/s      | m+NAP    | m       | s       | graden   | *0.001/whj  | %
---------+----------+----------+---------+----------+----------+---------+---------+----------+-------------+---------
  NNO    |       -- |       -- |      -- |       -- |       -- |      -- |      -- |       -- |       0.000 |     0.0
  NO     |       -- |       -- |      -- |       -- |       -- |      -- |      -- |       -- |       0.000 |     0.0
  ONO    |       -- |       -- |      -- |       -- |       -- |      -- |      -- |       -- |       0.000 |     0.0
  O      |       -- |       -- |      -- |       -- |       -- |      -- |      -- |       -- |       0.000 |     0.0
  OZO    |       -- |       -- |      -- |       -- |       -- |      -- |      -- |       -- |       0.000 |     0.0
  ZO     |       -- |       -- |      -- |       -- |       -- |      -- |      -- |       -- |       0.000 |     0.0
  ZZO    |       -- |       -- |      -- |       -- |       -- |      -- |      -- |       -- |       0.000 |     0.0
  Z      |       -- |       -- |      -- |       -- |       -- |      -- |      -- |       -- |       0.000 |     0.0
  ZZW    |       -- |       -- |      -- |       -- |       -- |      -- |      -- |       -- |       0.000 |     0.0
  ZW     |       -- |       -- |      -- |       -- |       -- |      -- |      -- |       -- |       0.000 |     0.0
  WZW    |     3.44 |     3150 |      -- |     36.6 |     3.49 |    1.06 |    3.49 |    247.5 |       0.008 |     4.1
  W      |     3.64 |     2550 |      -- |     32.1 |     3.17 |    1.00 |    3.43 |    270.0 |       0.058 |    29.1
  WNW    |     4.24 |     2350 |      -- |     32.1 |     3.22 |    1.03 |    3.01 |    292.5 |       0.062 |    31.2
  NW     |     5.14 |     2550 |      -- |     32.8 |     3.15 |    0.89 |    3.12 |    315.0 |       0.006 |     2.8
  NNW    |     4.74 |     3950 |      -- |     31.8 |     3.16 |    1.00 |    2.96 |    337.5 |       0.000 |     0.1
  N      |     3.90 |     4000 |      -- |     30.9 |     3.05 |    0.97 |    3.35 |    360.0 |       0.000 |     0.1
---------+----------+----------+---------+----------+----------+---------+---------+----------+-------------+---------
  som    |                                                                                     |       0.135 |    67.5
```

Figure 4.1: Example of Hydra-NL overtopping load with a return period of 5000 years.

As can be seen the opened and closed Europort scenario frequency of exceedance add up to $2 \cdot 10^{-4}$ per year. For every wind direction the combination of loads that leads to an overtopping of $0.16[l/s/m]$ are shown with their accompanying frequency of exceedance. Herein also lies a problem with respect to implementation in the FEM-model for this research. The same overtopping load with the accompanying return period can be caused by several different water level-wave climate combinations with each having a higher return period. To reduce the number of runs the wind direction with the highest probability of occurrence (often responsible for 30% to 40% of the total probability) is used as input. For the example above in Figure 4.1 the input for the 1/5000 year overtopping would be; Water level of 3.22m, H_{m0} of 1.03m, and a $T_{m-1,0}$ of 3.01m. And while the used overtopping discharge is indeed the 1/5,000 year one, the corresponding water level with that discharge occurs only 0.312/5,000 year.

Another feature of the used Basic mode is that uncertainties as a result of the model or used formulas are incorporated in the results. A point of attention is that for return periods higher than 20,000 years the input needs to be extrapolated to such extends that the results become less reliable. This research however ignores this warning.

Hydra-NL only gives one value maximum value for the water level for a certain return period. However, in reality around this maximum value a water level rise and drop occur in time. This flood wave has a certain duration and shape. The WAQUA Deltares report, [3], describes these waves. Figure 4.2 shows the distribution of shapes at the entry point of the Rhine river in the Netherlands at Lobith.

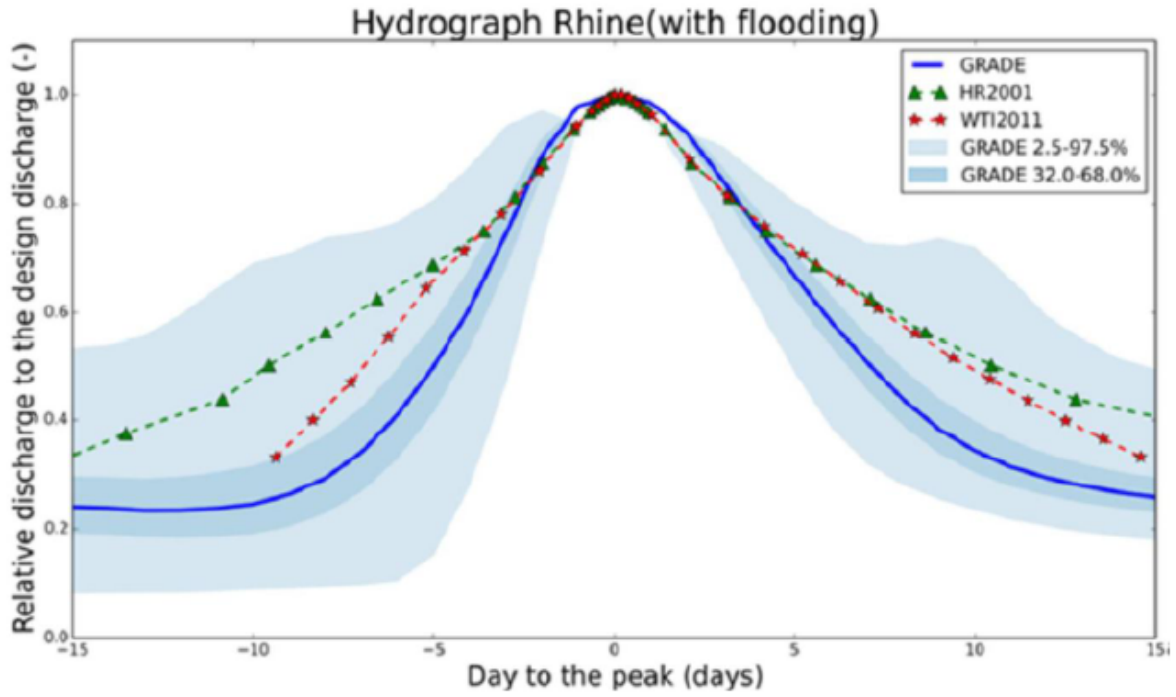

Figure 4.2: Normalized shape of flood wave for the Rhine river at Lobith. Source: Deltares WAQUA report, [3].

Due to bifurcations and hydraulic structures several non-linear transformations occur for downstream locations. The WAQUA report constructed these altered flood waves for different discharges and downstream locations.

4.1.2. Run-up and overtopping

Hydra-NL also only gives one value for the hydraulic load with respect to overtopping. However, to implement this load in the FEM-program it has to be analyzed in more detail. In order to do so the EurOtop Manual 2016, [17], is used as a guidance. All formulas and Figures, and theory used in this section come from that report.

For modelling purposes the dike is divided into three zones. Outer slope, crest, and inner slope and hinterland. These zones are numbered 3, 4, and 5 respectively in Figure 4.3.

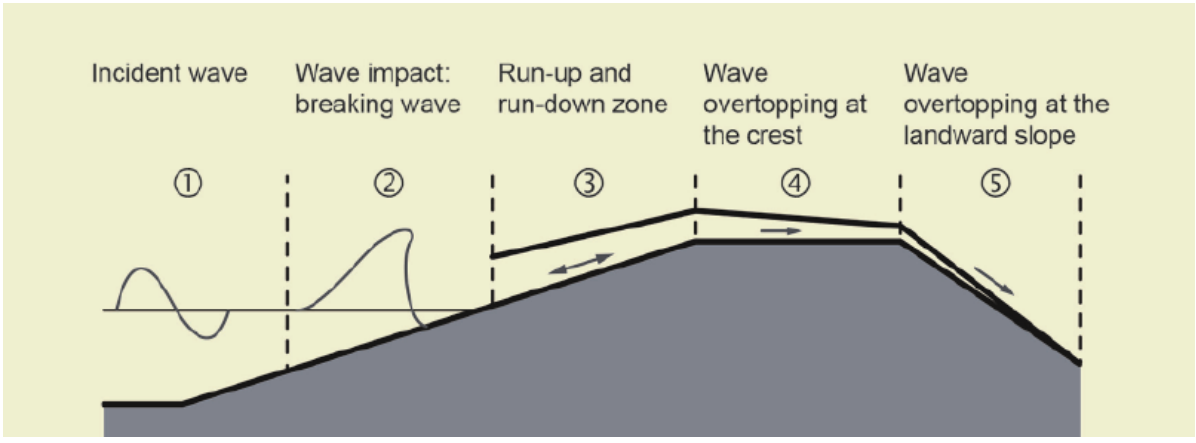

Figure 4.3: Phases of run-up and overtopping. Source: EurOtop Manual 2016, [17].

Run-up is defined as all the water coming up the dike in phase 3. For run-up the water tongue is thicker than 2 cm and it is measured compared to still water level (SWL). So almost every wave no matter how big generates run-up. An important characteristic for run-up quantification is the run-up height. $z_{2\%}$, for example, is the vertical height compared to SWL for which 2% of the incoming waves surpasses this value.

Overtopping is defined as the average volume of overtopping water per meter dike per second at the outer crest in l/m/s. So the amount of water that surpasses phase 3 and enters phase 4. A wave will overtop if the run-up is higher than the crest level. Run-up follows a Rayleigh distribution, thus:

$$P_{ov} = 1 - \Pr(\underline{R_u} < z_c) = \exp\left[-\left(\sqrt{-\ln(0.02)} \cdot \frac{z_c}{z_{2\%}}\right)^2\right] \tag{4.1}$$

where $z_{2\%}$ is the characteristic run-up level. The total number of overtopping wave during a storm event can now be calculated with

$$N_{ov} = P_{ov} \cdot N_w = P_{ov} \cdot \frac{T_{storm}}{T_m} \tag{4.2}$$

where

$$\begin{aligned} N_{ov} &= \text{Number of overtopping waves } [-] \\ N_w &= \text{Number of wave in the storm } [-] \\ T_{storm} &= \text{Storm duration } [s] \\ T_m &= \text{Mean wave period } [s] \end{aligned}$$

The storm duration is a uncertainty in itself an could as be implemented as a distribution. For this thesis it is set deterministically to 48 hours. Naturally that is a really long time for a storm, and its peak winds last shorter. A slow moving strong depression could last for quite some time however and the period of 48 hours is also often used for storms at see.

For water infiltrating the dike only the pressure of the water on the dike at the surface is of interest. But a wave overtopping the embankment is of course a very turbulent mass over propagating water. So in order to make the translation from this phenomenon to a pressure value some basics need to be considered. Bernoulli states the following balance equation.

$$H = h + \frac{u^2}{2g} = z + \frac{p}{\rho_w g} + \frac{u^2}{2g} \tag{4.3}$$

Wave overtopping threatens the dike in two ways: by wetting the dike, thus supplying infiltrating water which elevates the phreatic surface. And by erosion caused by the flow velocity of the overtopping water. The second phenomenon is not regarded as it is not of interest for the phreatic surface.

So, only the piezometric head, h, is of interest for this research rather than u. While a lot of the EurOtop Manual focuses on the erosion and thus the velocity part some empirical conclusions presented of the overtopping and running up waves are about flow thickness rather than velocity. This flow thickness translates to the pressure p as is clear from the Bernoulli formula.

What values for head need to be imposed in which phase and for what duration? Van der Meer (2011), [14], states the the thickness of the wave run-up flow is a translation using

$$h_{c,rep} = c_h * (R_u - z_{c,rep}) \tag{4.4}$$

Where c_h differs per run-up height and is calculated through

$$c_{h,x} = c_{h,2\%} \frac{\sqrt{-\ln(P(R_{u,x} < R_{u2\%}))}}{\sqrt{-\ln(0.02)}} \quad \text{with,} \quad c_{h,2\%} = 0.20 \tag{4.5}$$

Combining these two equations gives a flow thickness for a corresponding run-up height and the relation between the two is clearly non-linear.

This flow thickness is the maximum flow thickness for a run-up event. However, the head generated by the incoming wave upon the subsoil peaks first and then diminishes over time. This pattern of diminishing flow thickness is shown in Figure 4.4.

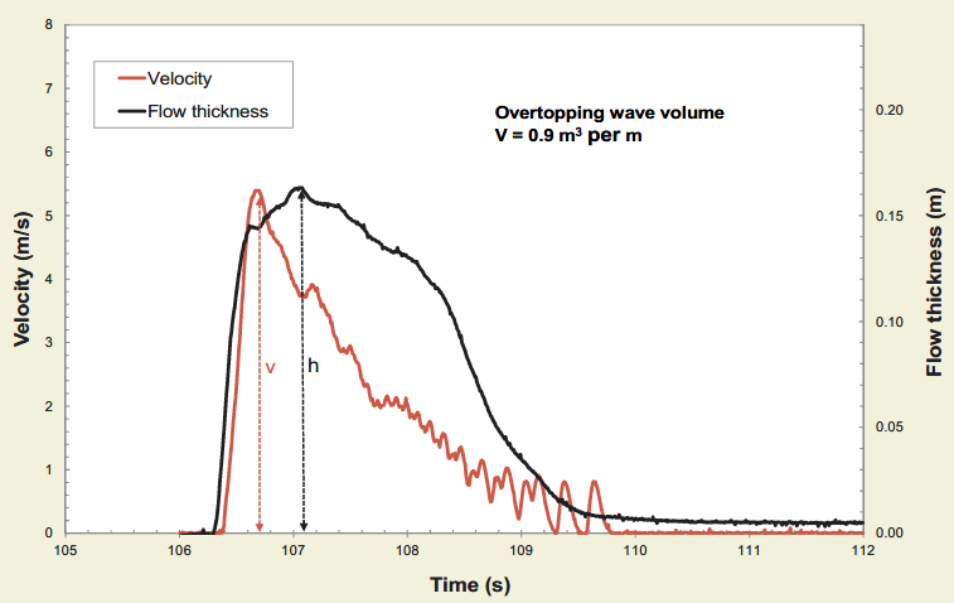

Figure 4.4: Example of flow thickness and velocity distributed in time at the crest of the dike. Source: EurOtop Manual 2016, [17].

This graph is made for the crest of the dike. Since both run-up boundaries have an angle, the water will run-off much faster, especially the last few millimeters, compared to a horizontal boundary.

According to the EurOtop Manual if a wave reaches the crest, the flow thickness is reduced by $1/3^{th}$ compared to is thickness at the top of the outer slope and then stays pretty much the same for the entire crest, only decreasing slightly.

For the landward slope again mainly the velocity induced slope erosion is the main focus of the manual. Some definitions for the calculation of this flow are given in Figure 4.5.

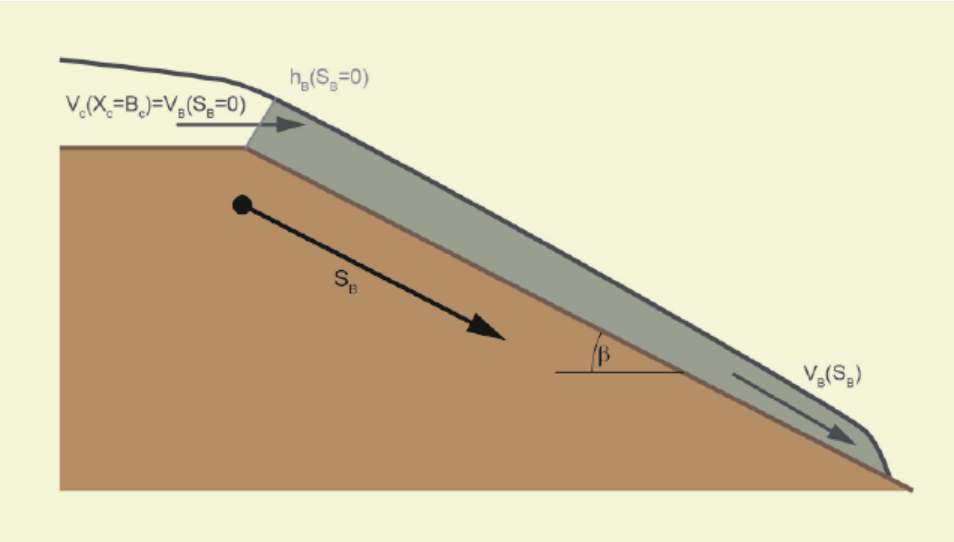

Figure 4.5: Definitions of some parameters for the flow on the inward part of the dike. Source: EurOtop Manual 2016, [17].

The flow velocity and flow thickness for the inner slope need to be determined iteratively with the following formulas.

$$v_b = \frac{v_{b,0} + \frac{k_1 h_b}{f} \tanh\left(\frac{k_1 t}{2}\right)}{1 + \frac{f v_{b,0}}{k_1 h_b} \tanh\left(\frac{k_1 t}{2}\right)}$$

with

$$t \approx -\frac{v_{b,0}}{g \sin\beta} + \sqrt{\frac{v_b^2}{g^2 \sin^2\beta} + \frac{2 s_b}{g sin\beta}} \tag{4.6}$$

$$k_1 = \sqrt{\frac{2 f g \sin\beta}{h_b}}$$

Where s_b is the location and f the friction of the inward slope and is found to be around 0.01 for grass covers. For the first step of the iteration h_b can be replaced by:

$$h_b = \frac{v_{b,0} h_{b,0}}{v_b} \tag{4.7}$$

The value for $v_{b,0}$ can be calculated from the formula

$$\begin{aligned} v_{2\%}(x_C) &= v_{2\%}(x_C = 0) \cdot \exp\left(\frac{-1.4 x_C 2\pi}{g T_{m-1,0}^2}\right) \\ v_{2\%}(7.7) &= v_{2\%}(x_C = 0) \cdot \exp\left(\frac{-1.4 \cdot 7.7 \cdot 2\pi}{g T_{m-1,0}^2}\right) \end{aligned} \tag{4.8}$$

in which

$$v_{2\%}(x_C = 0) = c_{v2\%} \sqrt{g \cdot (R_{u2\%} - z_A)} = 1.4 \cdot \sqrt{9.81 \cdot (R_{u2\%} - z_c)} \tag{4.9}$$

.

This concludes the overtopping section as all information to model the head loads on the dike is mentioned. It should be mentioned that most of the EurOtop manual is written with sea waves in mind. Friction of grass covers for example is generally ignored, while for river waves this might be of influence. Furthermore, almost all research is of empirical nature and thus bears a lot of uncertainty in the used formulas. This uncertainties are ignored for now but the reader should be aware of it.

4.1.3. STOWA and precipitation

The STOWA 2015 report, [4], about the actualized meteorological data for the Netherlands, gives information about rainfall events and their probabilities for several climate scenarios. Historical data is analyzed and gives some indication in the amount of precipitation during a certain amount of time for a certain return period. Their methodology to obtain these values from a historical time series is as follows.

- Homogenize the data series. This entails corrections for object in the surroundings of the measurement equipment, type of equipment and measurement methods.
- Then the series is detrended for the 2014 climate. This means that historical data is altered in such a way that it represents values as if all measured in the current climate. This is done for both precipitation as well as evaporation.
- The series is then translated from the Bilt location to other areas in the Netherlands.
- Fit a Generalized Extreme Value distribution on the data (not detrended) with time dependent parameters and extend this to higher return periods.
- The detrended series are used for the estimation of several climate scenarios.

The report gives precipitation extremes for several raining durations and return periods. They supply these for the Bilt location and for several climate scenarios. The also split the results in the winter and summer semester.

For an analysis of precipitation distribution within an event an older STOWA report from 2004, [13], is used. For an 8-day precipitation event a uniform distribution of the rain over these 8 days is not very likely. Rather, it consists out of peaks and maybe even periods of drought.

The most common distribution of precipitation during these events are presented and analyzed in the report and are used in this thesis to make the input more realistic. Although with respect to infiltration in the dike the uniform distribution of rain would be the worst case so any other pattern is more profitable in terms of phreatic surface rise.

As the report mentions it would be ideal to obtain a design pattern but due to very large variability among distributions this is not possible. Instead they construct several patterns each with a certain probability of occurrence. The precipitation events are presented as cumulative precipitation volume graphs. These are defined as the maximum of 1 hour, then the maximum of 2 contiguous hours, then three etc. Below in Figure 4.6 an example is given.

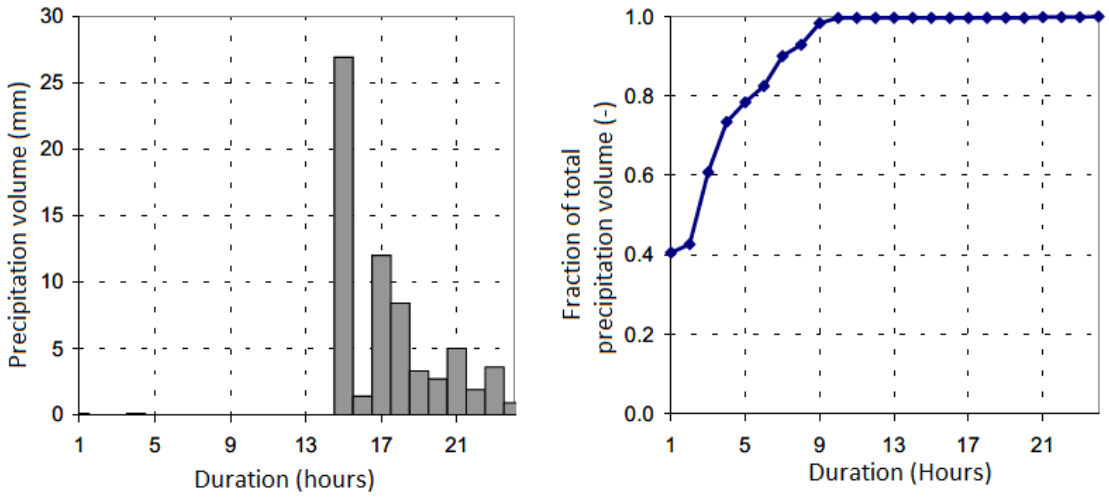

Figure 4.6: Example of cumulative precipitation volume. Left: The 24-hour rain event. Right: The cumulative graph to characterize the event. Source: STOWA 2004, [13].

By constructing these for several extreme events selected with a Peak over Threshold-method (P.o.T.) different precipitation fractions for different percentiles and durations are constructed.

It is also investigated whether the patterns depend on return period, event duration and season. From their analysis it appears that the former has no influence on the pattern while the latter two do. For longer event durations more uniform patterns are signaled as is the case for the winter semester November-February.

In order to construct design patterns the report distinguishes 1 peak, 2 peak, and uniform events. The two peak event is divided into pattern with a long duration between two peaks and a short duration. They also define four different patterns for the 1 peak scenario leading to 7 different shapes in total, each with a probability of occurrence.

4.2. Subsurface flow

Subsurface flow can be divided into two kinds of flow: flow in the saturated zone and flow in the unsaturated zone.

4.2.1. Saturated flow

At the basis of all models for ground water flow are two principles, Darcy and conservation of mass. The FEM-model defines flow in a porous medium via Darcy as:

$$\underline{q} = \frac{\underline{\underline{k}}}{\rho_w g}(\underline{\nabla} p_w + \rho_w \underline{g}) \tag{4.10}$$

where

$$\underline{q} = \text{specific discharge } [m/s]$$
$$\underline{\underline{k}} = \text{permeability tensor } [m/s]$$
$$\underline{\nabla} = \begin{bmatrix} \frac{\partial}{\partial x} \\ \frac{\partial}{\partial y} \\ \frac{\partial}{\partial z} \end{bmatrix}$$
$$\rho_w = \text{water density } [kg/m^3]$$
$$\underline{g} = \begin{bmatrix} 0 \\ 0 \\ -g \end{bmatrix} [m/s^2]$$

Notice that the flow in the z direction has an extra term. This term is to make sure the flow is not effected by pore water pressure differences in the z-direction as hydrostatic conditions are assumed.

The second law is the continuity equation of mass conservation: when there is (quasi-)stationary flow the equation can be written as:

$$\nabla' \cdot \left[\frac{k_{rel}}{\rho_w g} \underline{\underline{k}}^{sat} (\underline{\nabla} p_w + \rho_w \underline{g}) \right] = -\frac{\partial}{\partial t} (\rho_w n S). \tag{4.11}$$

Where n and S are the porosity and saturation (1 for saturated flow) respectively. By assuming the absence of no deformations of the soil particles and water density gradients the equation simplifies. Furthermore, when it is assumed that no solid particles move, which is the case, the equation becomes:

$$\nabla' \cdot \left[\frac{k_{rel}}{\rho_w g} \underline{\underline{k}}^{sat} (\underline{\nabla} p_w + \rho_w \underline{g}) \right] = n \left(\frac{S}{K_w} - \frac{\partial S}{\partial p_w} \right) \frac{\partial p_w}{\partial t}. \tag{4.12}$$

with K_w being the bulk modulus of the pore water.

It is important to stress that the hydraulic conductivity is one of the most important and complex parameters in ground water modelling. It influences the phreatic surface and the reaction of the phreatic surface to certain loads to a large extend, while lots of complex problems arise:

- Large value range
- Varying randomly through space
- Differs per direction (anisotropic)
- Can be scale dependant
- Non-linear dependency with on water content (see next section)

Lots of these properties will be ignored for this research. To give the reader without prior knowledge some indication of common values for different hydraulic conductivities Table 4.1 is helpful.

Soil	k-min [m/day]	k-max [m/day]
Gravel	86	8,600
Sand	0.086	86
Silt	0.00086	0.086
Clay	0.0000086	0.00086

Table 4.1: Hydraulic conductivities by soil type as given in Verruijt, [20].

The subsequent infiltration depends on this k-value and a pressure gradient as described above. However the maximum k-value for clay of just below $1mm/day$ suggest that it will take a long time to infiltrate the soil properly. Therefore the influence of the macro pores as described in Chapter 3 is investigated, see Section 4.3.

4.2.2. Unsaturated flow

Water does not exclusively flow in the fully saturated zone. Especially with precipitation and overtopping, but also water level rise, a part of the flowing water goes through the unsaturated zone. This zone is situated above the phreatic surface and its behaviour can be described by two important curves: the Water Retention Curve (WRC) and the Hydraulic Conductivity Function (HCF).

The WRC describes the capacity of the soil to keep water in its structure for different stress levels. These stresses are always negative and can thus be seen as suction which is defined as pore air pressure minus pore water pressure.

A widely used model to simulate the WRC is the Van Genuchten model (1980). After a simple and commonly made assumption that one of the variables can be expressed in terms of another, the resulting model is a two-parameter function reads:

$$S(\psi_p) = S_{res} + \frac{S_{sat} - S_{res}}{\left[1 + (g_a|\psi_p|)^{g_n}\right]^{1-(1/g_n)}} \tag{4.13}$$

in which

$$\psi_p = -\frac{p_w}{g \cdot \rho_w} \tag{4.14}$$

where

p_w = Suction pore stress
ρ_w = Density of water
S_{res} = Residual saturation which describes the amount of water which will always remain in the soil
S_{sat} = The saturation degree below the phreatic surface. In practice air bubbles are trapped in the groundwater causing a somewhat lower saturation even below the phreatic line. However, it is assumed here that it is always equal to 1.0
g_a = A fitting parameter related to the inverse of air entry suction. It is a material property.
g_n = A fitting parameter related to the rate of water extraction from the soil. This is also a property of the material.

The relation provides credible results for low and intermediate suctions while for high suctions the limit of residual saturation is reached.

The flow in the unsaturated zone is in the end dictated by the hydraulic conductivity or permeability. These characteristics are related to the saturation through the effective saturation defined as:

$$S_{eff} = \frac{S - S_{res}}{S_{sat} - S_{res}} \tag{4.15}$$

The relative permeability by Van Genuchten is now defined as:

$$k_r(S) = \max\left[(S_{eff})^{g_l}\left(1 - \left[1 - S_e^{\left(\frac{g_n}{g_n-1}\right)}\right]^{\left(\frac{g_n-1}{g_n}\right)}\right)^2, 10^{-4}\right] \tag{4.16}$$

where g_l is a fitting parameter that is again a property of the material. The relative permeability in turn is defined as

$$k_r = \frac{k_{unsat}}{k_{sat}} \tag{4.17}$$

4.3. Cracks, macro pores, and porosity

In theory the clay used in river dikes is very close to impermeable. Usual k-values of 2cm to 0.01mm per day are no exception for this soil type and thus even lower unsaturated permeabilities. Given that high water waves last a matter of days, overtopping events 2 days max and precipitation events up to 8 days a problem becomes clear.

In practice however, the clay layer is not perfectly intact. It always exhibits soil structure deterioration. Macro pores, crack and holes give way for the water to immediately infiltrate into the top layer dike. The holes can for example be dug by rats. Smaller macro pores are caused by smaller animals like worms and roots of plants. Cracks are a consequence of weathering of the clay; expanding and shrinking by temperature and alternating saturation degrees. The nature differs much and also determines where the location of these larger structures is.

The manner in which these macro pores are incorporated into the model is based on two main sources. The paper of van Hoven et al.(2010) [19], and the findings from an analyses of IV-Infra b.v. on the dike Capelle-Moordrecht excecuted in 2016. Although the report itself is not public some of its conclusions and recommendations are used in the modeling of the macro pores.

While weathering of the outer clay layer occurs over the entire dike, the cracks and holes created by larger animals only occur on the crest and inner slope. The size distribution of the crack found by IV-Infra is presented in Figure 4.7.

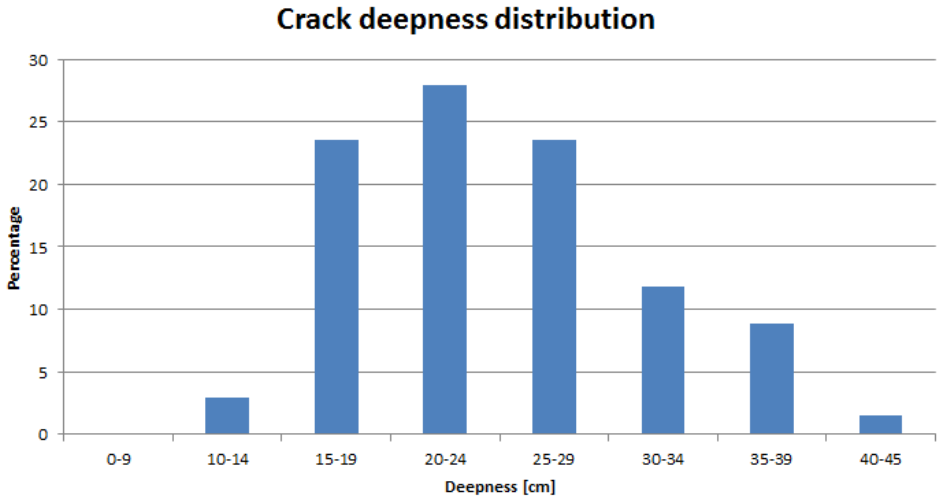

Figure 4.7: Distribution of crack deepness. Source: IV-Infra report.

Of all these crack the width at surface level varied from 4-10 centimeter. Based on this report the choice is made to divide the crest and inner slope in two layers.

4.4. Macro stability

In the end the level of the phreatic surface influences the stability of the inner slope. In the first place by the straightforward principle of Terzaghi: The effective soil stresses equal the total soil stresses minus the water pressure or

$$\sigma' = \sigma - p_w \tag{4.18}$$

The effective soil stress determines the strength and friction of the soil. Therefore a high water pressure induces a smaller friction coefficient between soil particles. Macro instability occurs over a slide plane as shown in Figure 2.1. Several models exist on ow this plane and stability of this plane needs to be assessed: Bishop (1955), LiftVan (1999), Spencer - Van der Meij (1967, 2012). The are all so called Limit Equilibrium Models(LEM) since they assess the force equilibria for slices of soil. While Bishop has been common practice for years it has been discarded in the new WBI and been replaced LiftVan and Spencer. The aim of this Section is merely to indicate how and why the phreatic surface influence inward macro stability. Therefore, only the simplest method of Bishop is used as an example. The method checks the moment equilibrium of a circular slip plane as depicted in Figure 4.8. The plane is divided into slices.

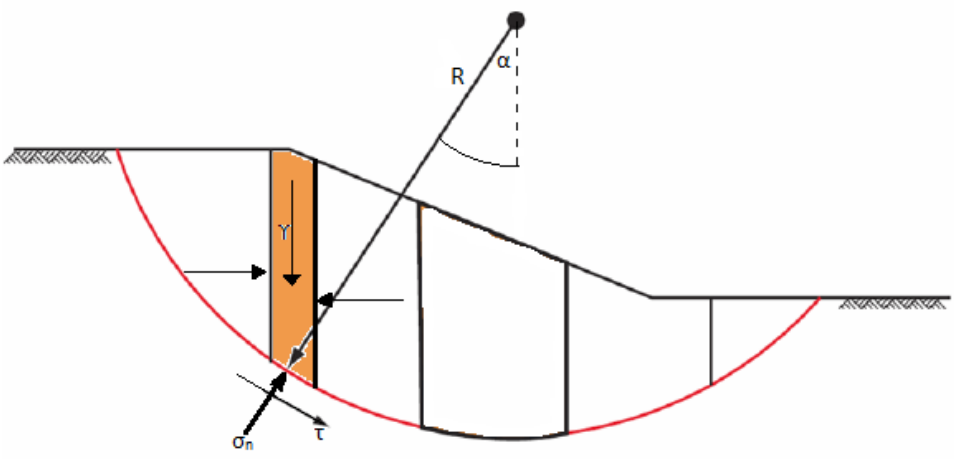

Figure 4.8: Simple indication of the method of Bishop. Source: Flood Defences Lecture Notes, [7].

In the end the failure mechanism is a too large driving moment compared to the resisting moment. The driving moment is cause by the weight of the soil. And since there is more soil in the dike body than behind the dike the dike wants to collapse by pushing up the soil in the polder while the embankment while the dike body slides downward. However, there is another resisting force which prevents all this from happening instantly. The friction of the soil particles along the sliding plane, presented in Figure 4.8 as τ. This reactionary resistance can be calculated with

$$\tau = (c + \sigma'_n \tan\phi) \tag{4.19}$$

Thus that the sliding friction equals the cohesion plus the effective stress times the tangent of the angle of internal friction. And as mentioned above this effective stress, declines with higher pore water pressures. A higher phreatic surface inside the dike causes the pore water pressures deeper in the soil to become higher, due to hydrostatic pressure. Thus a higher surface has a negative effect on the dikes safety with respect to inward macro stability.

4.5. The FEM program, PLAXIS

The actual research where different dikes are subjected to several extreme loads is done with the Finite Element Method (FEM). This is a numerical method where the 2D dike and subsoil gets divided into a number of smaller elements for which the balance equations are simplified. Every time step the equations for all the smaller, simpler elements are solved and are then put together to approximate the solution for the entire, large, complicated model.

For soils and groundwater flow PLAXIS is a widely used FEM-program as it is user friendly but can still incorporate a lot of feature found in the real world. As the posed problem is represented in 2 dimensions, PLAXIS 2D is used for the calculations. Within PLAXIS a special module is developed called PLAXflow which is needed to calculate pore water pressures in the soil subjected to changing hydraulic circumstances. In order to reduce computation times the transient groundwater flow calculation type is picked. This method treats the soil as a rigid structure and only calculates the flow through it.

The model can be constructed by drawing lines which come together as soil polygons to which certain attributes can be assigned. Loads can be applied on the boundaries of these polygons to simulate rain or water levels. To calculate the differential equations in practice these boundary conditions need to be indicated. For this research three types of boundary conditions are relevant: Seepage, Head and Infiltration.

The head boundary condition is rather direct.

$$\phi = \bar{\phi} \tag{4.20}$$

Where ϕ = the actual exerted head at the boundary and $\bar{\phi}$ = the value of the imposed head by the user.

For infiltration boundaries the applied head is defined as:

$$\begin{cases} \phi = z + \bar{\phi}_{p,max} & \text{if ponding} \\ q_x n_x + q_z n_z = -\bar{q} & \text{if } \phi < z + \bar{\phi}_{p,max} \cap \phi > z + \phi + \bar{\phi}_{p,max} \\ \phi = z + \bar{\phi}_{p,min} & \text{if drying} \end{cases} \tag{4.21}$$

Herein are $\bar{\phi}_{p,max}$ and $\bar{\phi}_{p,min}$ user defined boundaries before water respectively runs off or can evaporate out of the ground ($\bar{\phi}_{p,min}$ is usually negative). If these boundaries are not reached the precipitation creates an inflow $\bar{q}$. The inflow in the soil equals to the infiltration capacity of the soil in x and z direction where n_x and n_z are outward pointing normal vector components on the boundary.

A seepage boundary is the standard type of boundary. Seepage is mathematically defined as

$$\begin{cases} \phi = \bar{\phi} & \text{if } \bar{\phi} \leq z \\ q_x n_x + q_z n_z = 0 & \text{if } \bar{\phi} < z \cap \phi < z \\ \phi = z & \text{if } \bar{\phi} < z \cap q_x n_x + q_z n_z > 0 \end{cases} \tag{4.22}$$

Thus if the water level if above point z the accompanying head is applied. Infiltration equals zero if the head is below the point z, meaning also no evaporation takes place when the head is lower than z. At atmospheric pressure the outflow of water can take place. It is also possible to close the boundary when the water level is below z. Then the last condition does not apply.

After the boundary conditions and the functions applied to it are defined, the calculation can start. After several minutes or hours, depending on the type of load, of run time the results can be presented. Pore water pressure, saturation, hydraulic head and many more characteristics are stored for every time step and can thus be used to show development in time.

5

Research setup

5.1. Dike models

5.1.1. Case study selection

The PLAXIS model will be based on a real case to make the research more applicable and realistic. Therefore, a location needs to be found where Hydra-NL and IV-Infra both have a lot of information about. Furthermore there need to be only soil solutions and thus no hard constructions to support the choice of a 2D approximation. Finally the location need to be as far upstream as possible to reduce influences of the sea and barriers. The resulting location is a dike near the town of Groot-Ammers at the Lek river, see Figure 5.1. The raw data sets provided by IV-Infra B.V. can be found in Appendix C.

Figure 5.1: Case location. Groot-Ammers, Lek river

The chosen dike segment is part of dike ring 16, called 'Alblasserwaard en Vijfheerenlanden'. Both Hydra-NL as well as the company have a lot of information about this location; both about hydraulic loads as the

soil and subsoil. Figure 5.2 shows the Hydra-NL measure points (Dark Blue), CPT locations (Orange), boring locations (Red), and hydraulic head piezometers (Cyan). Furthermore several cross sections in the area are known indicated by the green dotted lines.

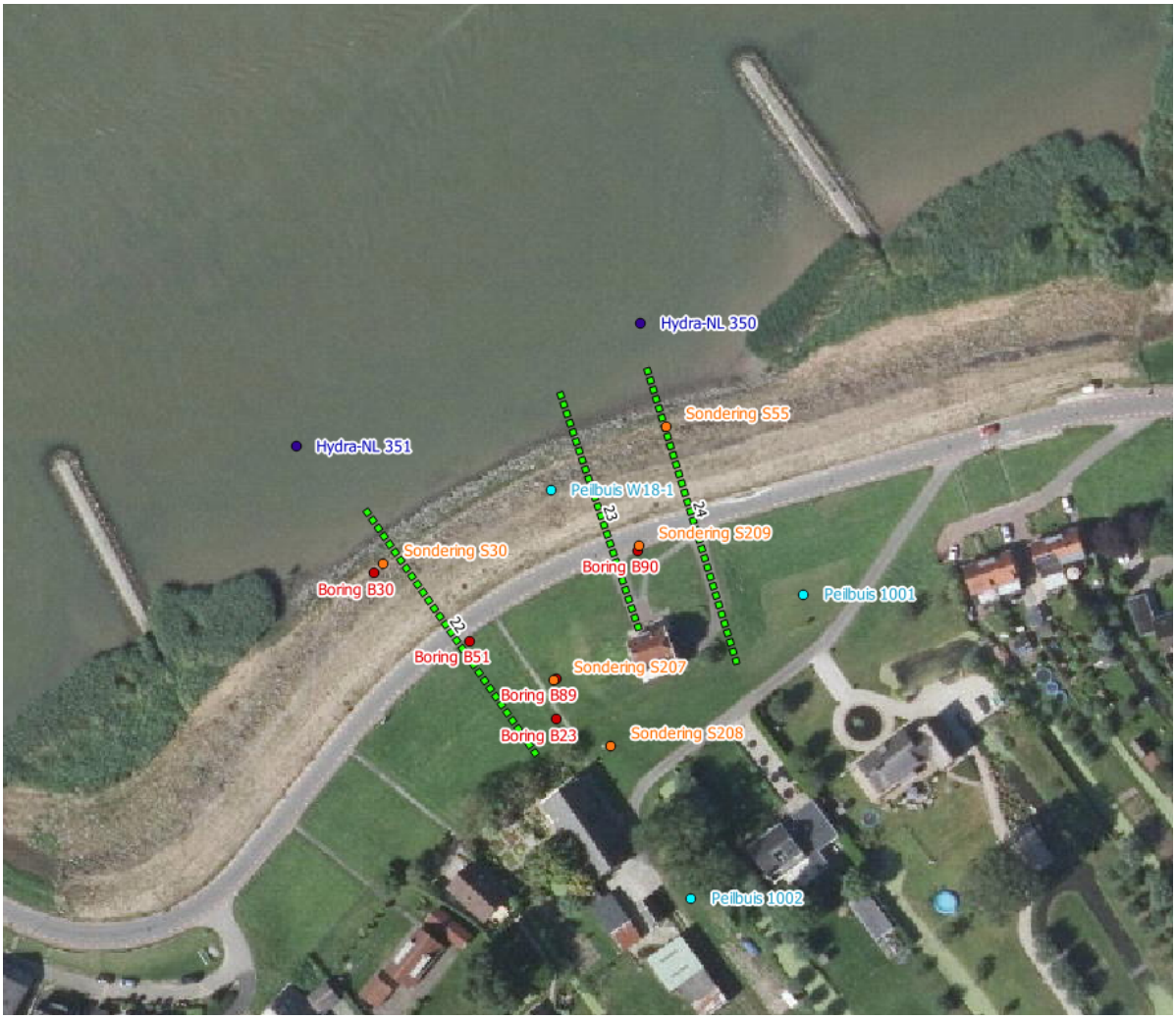

Figure 5.2: Available data in the region.

The location used for this thesis is cross section 22. The surface geometry is depicted in Figure 5.3. On this location the Hydra-NL point, absence of buildings and hinterland roads and presence of borings and CPT's all come together.

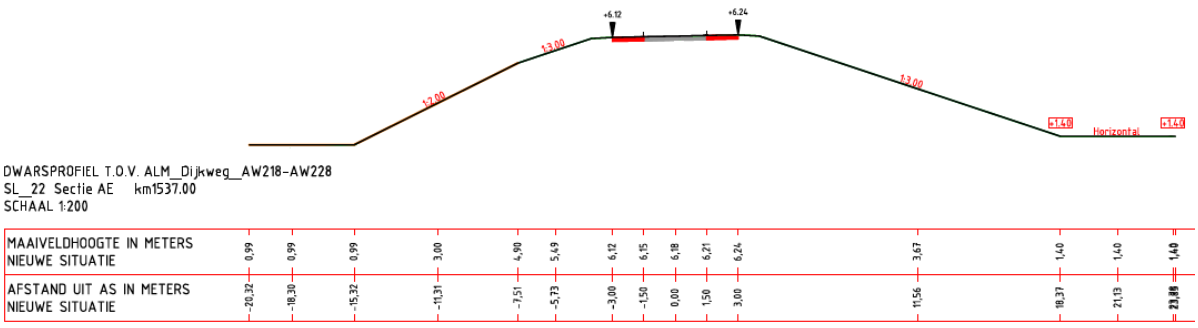

Figure 5.3: Used dike cross section, number 22. Values are in meter N.A.P.

A disadvantage of this location is that the influence of the sea level is still noticeable in the calculation of the design water levels. According to the Hydra-NL classification it is treated as a downstream river. A tidal signal is thus included in the probability calculations as well as the influence of the storm surge barriers. The results of the Hydra-NL Basic calculation are used as they are produced, so including influence of open/closed storm surge barriers and tidal influences. The oscillating character of the water level due to tide is ignored for the input signal of the PLAXIS model.

The dike layout is copied from the case and is thus cross section 22 of dike stretch 16-3. The design drawing presented in Section 5.1.1 does not include the foreshore up to the Lek river. Therefore the older cross section drawings from the 80's (see Figure C.2 in Appendix C) are combined with the new design. Also the thickness of the aquitard of 7 meters is based on this drawing. The initial ground water level at the edges of the model is based on piezometer data for the winter season. Piezometer W18-1 (outside of the dike) gives an average winter season value of +0.85 N.A.P. While the piezometer 1001 (inner dike toe) gives an average value of -0.4m N.A.P. for the Pleistocene sand layer and a -0.6m N.A.P. for the Holocene clay layer. Between this inner and outer toe value it is assumed that the pressure decreases linearly both in the sand as well as in the clay layer.

Furthermore in order to define the top layer subjected to soil structure deterioration and macro pores and the clay/sand core of the dike, and outer layer with a thickness of 1 meter is defined (z_{lay}). Below the dike, the boundary between the clay subsoil (z_{sub}) and the core is assumed to increase linearly from +0.99m N.A.P to +1.4m N.A.P. These are not coincidentally the same values as the outside surface level and are picked this way to avoid small boundary angles which will increase the number of grid elements greatly.

This leads to the following starting values, presented in 5.1.

Borehole nr.	1	2	3	4	5	6	7	8	9	10	11
$x(m)$	0	4	20	24	30.68	38.49	42.15	49.85	64.37	70	100
$z_{sur}(m)$ (w.r.t. NAP)	-1.5	-1.5	-0.3	0.99	0.99	4.93	6.12	6.24	1.4	1.4	1.4
$z_{lay}(m)$ (w.r.t. NAP)	-1.5	-1.5	-0.3	0.99	0.99	3.81	5.07	5.24	1.4	1.4	1.4
$z_{sub}(m)$ (w.r.t. NAP)	-1.5	-1.5	-0.3	0.99	0.99	1.07	1.12	1.24	1.4	1.4	1.4
$h_0(m)$ (w.r.t. NAP)	0.85	0.85	0.85	0.85	0.85	0.75	0.36	0.02	-0.6	-0.6	-0.6
$d(m)$(w.r.t. NAP)	-7	-7	-7	-7	-7	-7	-7	-7	-7	-7	-7

Table 5.1: Borehole characteristics. x,z-Location, head at beginning simulation, h_0, and depth of the aquitard ,d

The hinterland is extended to 100 meters (35 meter from inner toe) to allow for any inward slope stability calculations. In the PLAXIS model, an extra borehole is placed at 70 meters. This extra borehole is placed so an extra boundary is defined in the model, between the inner toe and the rest of the hinterland. This is needed to apply overtopping water directly behind the dike without applying it to the entire hinterland.

This thesis will consider several dike types. A homogeneous clay dike, a clay dike with soil structure deterioration in the top layer and a sand dike with a top clay layer also subjected to weathering and macro pores. The geometry of the embankment and the boundaries of different soil layers will be the same for all types so only properties of layers are altered. Table 5.2 shows the soil type per layer polygon, which can be seen in Figure 5.6. For the detailed soil properties Table 5.3 can be consulted.

Dike type	Subsoil	Dike core	Top layer (1m) Outer slope	Supra top layer (0.5m) Crest & inner slope	Sub top layer (0.5m) Crest & inner slope
Homogeneous clay	$Clay_{core}$	$Clay_{core}$	$Clay_{core}$	$Clay_{core}$	$Clay_{core}$
Clay, soil structure	$Clay_{core}$	$Clay_{core}$	$Clay_{top}$	$Clay^{*}_{top}$	$Clay_{top}$
Sand, soil structure	$Clay_{core}$	$Sand_{core}$	$Clay_{top}$	$Clay^{*}_{top}$	$Clay_{top}$

Table 5.2: Soils per layer for simulated dikes types. * Altered $k-$values.

After these have been entered, soil properties for the layers need to be entered. The soil classification is done via the Staring definition. The properties are chosen as presented in Table 5.3.

Soil type	$Clay_{top}$	$Clay_{core}$	$Sand_{core}$	$Sand_{sub}$
Material model	Mohr-Coulomb	Mohr-Coulomb	Mohr-Coulomb	Mohr-Coulomb
Drainage type	Undrained (A)	Undrained (A)	Drained	Drained
γ_{sat} $[kN/m^3]$	18	17	19	19
γ_{dry} $[kN/m^3]$	14	14	16	-
ϕ' [°]	20	15	30	30
c' $[kPa]$	4	10	0	0
E' $[MPa]$	4.5	4	9.2	14.8
ν	0.2	0.2	0.3	0.3
e	1.48	0.86	0.81	0.81
k_x $[m/day]$	0.005	0.0003	15	20
k_y $[m/day]$	0.01	0.0001	5	10
Staring	B11	O12	O5	O2
	Heavy Clay	Heavy Clay	Coarse Sand	Loamy Sand

Table 5.3: Soil parameters. Based on old field tests from the 80's.

Four different soil types are used for this thesis which are presented and named in the top line of the table. The parameters of the top layer are used for the outer slope and lower 0.5 meter of the crest and inner slope. For the top 0.5 meter, the k_x and k_y values are sometimes altered while keeping the rest of the characteristics the same. This is then explicitly mentioned in the text.

The material model decides how the strength of the soil is calculated and how it reacts under certain loads. In all cases the Mohr-Coulomb model is chosen. Although it is of no importance for the ground water flow calculations, a model has to be picked in order to run PLAXIS.

The drainage type can be either drained or undrained. Within the undrained types (A, B, or C) only differs in which input parameters are needed. Type A is applied as its necessary input is available. The sandy soils are set as drained while the clayey ones are treated as undrained. This is a rather common assumption as the water entrapped in clay, compared to loads, has relative very little time to escape. As a result water tensions within the pores change rather than that the water flows away immediately. This is the case within sandy soils where water can flow away relatively quickly and pore water pressure build-up is non-existent or stays limited.

The volumetric weight, angle of internal friction and cohesion are based on both measurement as well as general used values for these soil types. As much as possible was concluded from the data provided but some characteristics needed to be supplemented with rules of thumb. The rules are mainly retracted from study books such as [20] and papers, [19]. This is also the case for the elasticity module, Poisson ratio and void ratio.

The hydraulic conductivity of the soil is split in a vertical y-direction and a horizontal x-direction. In this way the often mentioned an-isotropic soil behaviour can be modeled. This parameter is extremely (probably the most) important for this thesis. The values above are based on literature and expert opinions. They are not measured values from the field and will also be altered manually later on for the sake of research. In general for soils it is found that the horizontal permeability is larger than the vertical one. For sand this relation can be 2 while for clay this can become even larger. Therefore, all the original un-weathered soils have a larger horizontal hydraulic conductivity. The clay top layer however, the relationship is turned around since soil structure cracks and pores mainly enlarge the vertical hydraulic conductivity.

For the unsaturated soil the Van Genuchten-model is picked to calculate flow though the unsaturated zone. The parameters used for this model are the standard given by PLAXIS and thus unaltered but are dependent on the picked Starting soil type. The resulting WRC and HCF are shown in Figures 5.4 and 5.5. Why these soil types and these parameters are picked can be found in Appendix D. The Pleistocene sand layer is not presented in these graphs as it is naturally submerged at all time and its WRC and HCF are thus not of interest.

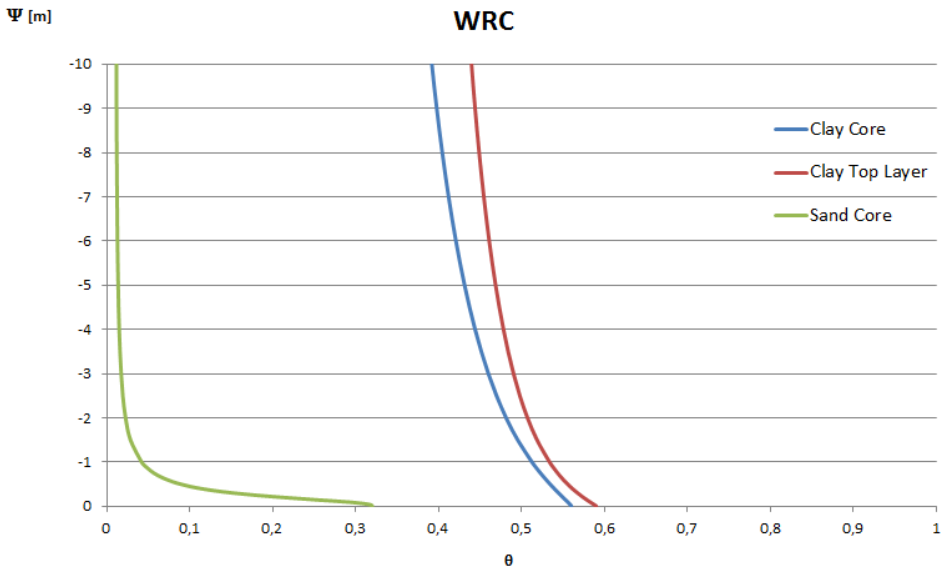

Figure 5.4: Water Retention Curve

In both of these graphs set out across the vertical axis is suction Ψ. The horizontal axis in the WRC is water content defined as

$$\theta = \frac{\text{Volume of water}}{\text{Total volume of wet material}} = \frac{\text{Volume of water}}{\text{Volume of solids + Volume of pores}} \tag{5.1}$$

As can be expected, the saturation degree drops really quick for sand and finish at a residual saturation which is rather low. Clay on the other hand stays saturated at very high suction.

The horizontal axis of the HCF graph gives the relative hydraulic conductivity. The 'local' hydraulic conductivity depends on the suction: $k_{local} = k_{sat} * k_r$.

The values for k given in Table 5.3 are the hydraulic conductivities in fully saturated condition, k_{sat}.

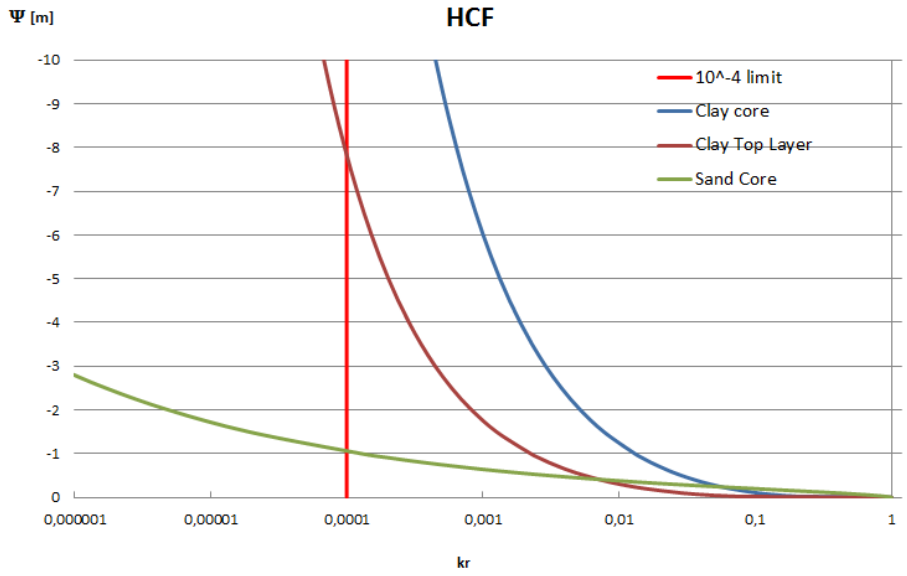

Figure 5.5: Hydraulic Conductivity Function

The relative conductivity of the two soil types behaves rather differently. While the conductivity of the clay soil diminishes rather quickly at low suction levels, the hydraulic conductivity of the sand stays high. With a

suction head of 2cm the conductivity of the sand is 90.2% of the saturated conductivity whereas for clay it is only 9.1%. In PLAXIS the relative permeability can't become smaller than 10^{-4} times the saturated hydraulic conductivity. This is most likely because of numerical stability issues.

Next the mesh is constructed. This done by PLAXIS automatically, but some refinements are made. As can be seen in Figure 5.6 the relevant boundaries of the model are numbered from 5 to 9. For every boundary the mesh can be locally set to finer or coarser than average. Also the boundaries between soil layers and per soil layer different mesh coarseness can be picked. The clay dike gets a coarseness factor 0.2 (making the mesh finer) and boundaries 1 to 9 are set to 0.3. The rest of the mesh is set to 'Fine'. In order to assess the pore water pressures inside the dike, an output location directly below the inner crest is selected. All the graphs in Chapters 6 and 7 are for this point, which is located at a depth of -0.83 meter N.A.P.

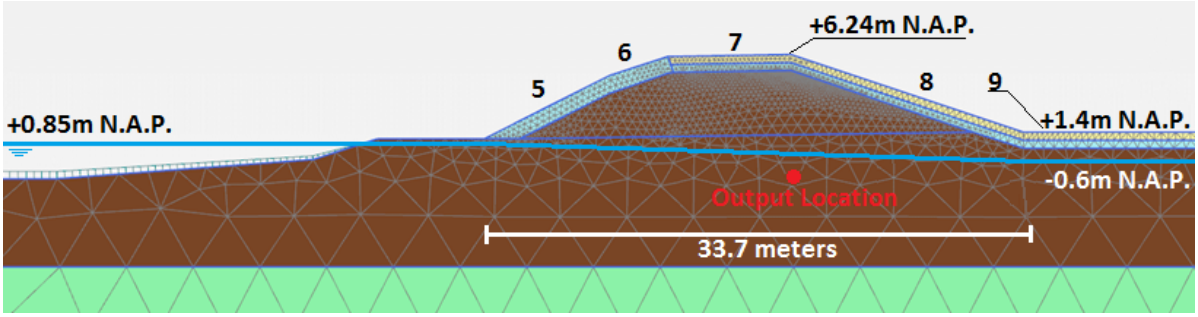

Figure 5.6: Mesh as generated by PLAXIS after defined input. Also handled boundary numbers, output graph location, and equilibrium winter water level are shown.

The inner crest is chosen as it is an important location for inward macro-stability; most of the slip circles cross this line (from output location point towards the crest), but at the same time the resulting pore water pressures are not limited by the height of the soil above the output location. If a point, located more to the hinterland, would have been selected, this could be the case. The depth of $-0.83 mN.A.P.$ is needed because the output location always need to be below the equilibrium ground water level in the subsoil, otherwise a rise below the output location would not be signaled. This is furthermore a realistic depth where a large part of the slide plane occurs.

The resulting mesh consists out of 3236 elements which leads to average calculation times for overtopping and rain of about 3 hours. Also shown in the Figure is the top layer, affected by some soil structure deterioration (blue color), and the top 0.5 meter of heavily deteriorated clay (sandy color) at the inner slope and crest.

5.1.2. Top layer

To simulate soil structure deterioration the top 1 meter of the dike can be given different properties. The thickness of the top layer of 1 meter is based on the paper of Van Hoven et. al. (2010), [19]. The choice to divide the crest and inner slope into two layers of 0.5 meters of which the top one is very permeable is based on the IV-report mentioned in Section 4.3. Also the thickness, 0.5 meter, of this supra top layer with macro cracks is based on the deepest crack found and presented in Figure 4.3.

The clay dike with soil structure deterioration for the top 1m the outer slope and lower 0.5 meter of the crest and inner slope will get a standard topsoil characteristic with a k_y of $0.01 m/day$ (see Table 5.3). For the crest and inner slope the top 0.5 meter gets an extra high permeability of $k_y = 2.07 m/day$ to simulate macro pores (holes and cracks). The sand dike with a clay top layer with soil structure deterioration, thus a k_y of $0.01 m/day$. The top 0.5 meter at the inner slope and crest is simulated with with macro pores and will get three different vertical permeabilities;

- Maximum value of $k_y = 0.6 \cdot 10^{-4} m^3/s/m^2$ or $5.18 m/day$
- Mean value of $k_y = 2.4 \cdot 10^{-5} m^3/s/m^2$ or $2.07 m/day$
- Low value of $k_y = 9.6 \cdot 10^{-6} m^3/s/m^2$ or $0.83 m/day$

Due to the vertical nature of the macro pores the permeability in the horizontal direction is set ten times lower. The hydraulic conductivities for the top 0.5 meter of clay are based on the paper of Van Hoven et.al.(2010), [19]. The average and top value are mentioned directly. Based on assumption of a log-normal distribution of

k, mean value, max value, and number of tests (21) the lower value is calculated. This gives 5 different dikes for to which the loads are applied.

5.2. Loads

This section will walk through all load settings and input of the PLAXIS simulations. Also the PlaxFlow needs to be available for the user in order to fully replicate the results. The section will be in close relation with the findings of Chapter 3 and 4. All three types of loads will be treated separately here, while load combinations are explained in the next section.

5.2.1. Water level

Maximum water levels are given by Hydra-NL and are a result of a combination of high seas, winds and high discharge. The shape of the flood wave comes from the WAQUA simulation at the Krimpen aan de Lek location. The shape is adjusted for the starting and peak values. Figure 5.7 gives the input for the 10,000 year high water level. It starts at a height of +0.85 N.A.P. as this is the average water level in the river for the winter semester. It is good to realize that the 1 in 10,000 year water level when no overtopping is considered is higher than when overtopping is considered. Due to the need for wind of a certain force and direction and thus extra demands for the 1 in 10,000 year load, the water level associated with the 1/10,000 discharge will occur more often than 1/10,000 and is thus lower. Also, in order to be able to simulate overtopping in PLAXIS, the water level during the actual overtopping needs to be constant. As a 48-hour storm is chosen the top water level is kept constant for two days, which is a rather conservative assumption.

Figure 5.7 gives the 1/10,000 water level, 4.112m. This is consistent with a Rhine discharge at Lobith of 18,275 m^3/s.

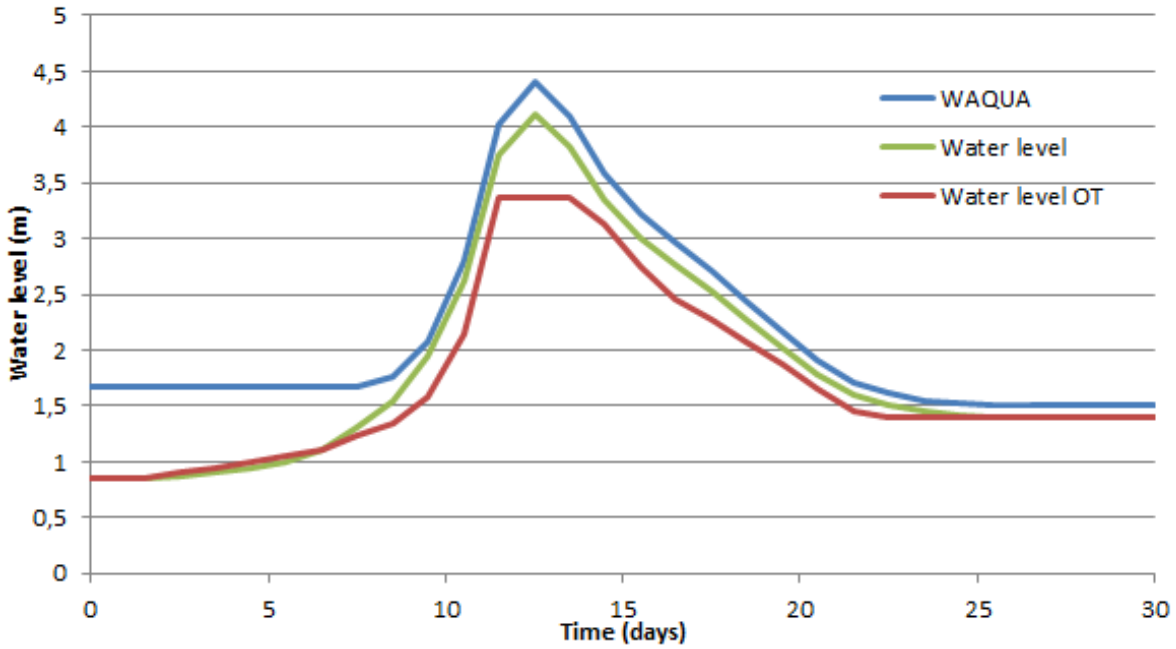

Figure 5.7: Water level with 1/10,000 year return period (green) and shape as predicted by Deltares (blue). Water level for 1/10,000 year return period for overtopping (red).

5.2.2. Overtopping and run-up

For overtopping Hydra-NL calculates several values. For this section, a arbitrary overtopping scenario is picked. It is consistent with a 1/10,000 year overtopping event. For this case:

$h[m]$	$q[m^3/m/s]$	$H_{m0}[m]$	$T_{m-1,0}[s]$	$z_{2\%}[m]$
3.99	$2.73 \cdot 10^{-4}$	0.77	2.89	6.26

Table 5.4: Overtopping and run-up characteristics for 1/10,000 year event.

It can also calculate the 1/10.000 the wave run-up height as $z_{2\%}$. The dike is divided into the outer slope, crest, and inner slope and hinterland. These zones are numbered 3, 4, and 5 respectively in Figure 4.3.

Run-up follows a Rayleigh distribution, for this case 4.4 % of the incoming waves will overtop and thus proceed from area 3 to area 4 and is responsible for the 0.273 l/m/s. Figure 5.8a shows the cumulative density function of the wave run up.

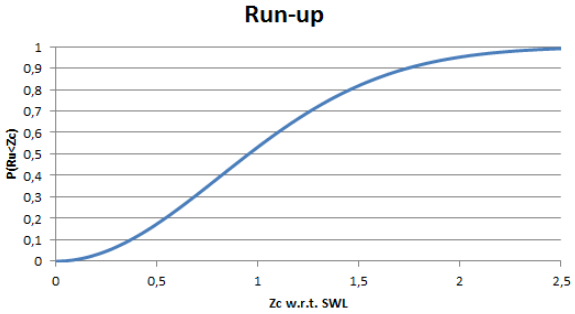

(a) Cumulative Rayleigh distribution of wave run-up heights

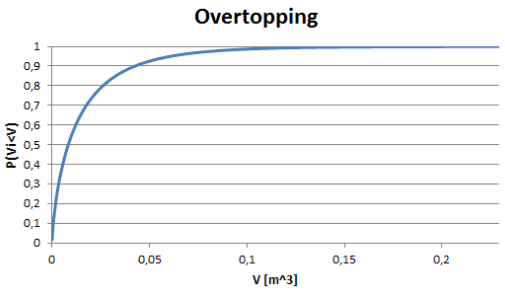

(b) Cumulative two parameter Weibull distribution of individual overtopping wave volumes

Figure 5.8: Wave load distributions

The total number of overtopping waves during this storm event can now be easily calculated. It is assumed that the storm occurs during the peak and lasts for the entire 48 hours. This means that 2856 waves reach the crest of the dike. When looking at the overtopping volume distribution the following graph can be created, see Figure 5.8b.

So for the storm to be implemented in PLAXIS it is known how many waves need to be sampled from which distribution to get a representative overtopping load on the dike. To implement the overtopping load in PLAXIS the head function needs to be used. Thus for boundary 5 and 6 the run-up needs to be translated to a head load and for boundaries 7, 8, and 9 the overtopping needs to be translated. For this random generation of waves a MATLAB is written to generate the overtopping and run-up values and eventually a head function for each boundary in PLAXIS. The steps of the script are described below.

1. Draw waves

A storm duration of 48 hours is assumed with the characteristics from Table 5.4. This means that for the waves every 2.65 seconds a wave needs to be 'drawn' for the duration of the storm. However, since PLAXIS can only have a maximum number of steps per simulation phase, the minimum step duration is 20 seconds for a 48-hour storm. As a consequence several waves need to be aggregated to one average head load for that 20 seconds. Appendix D explains in more detail why this is necessary

From the distribution in Figure 5.8a the run-up is drawn. If the drawn run-up exceeds the crest level of 6.12 meter the overtopping processes come into play.

2. Run-up boundaries

As stated above the SWL is at 3.99. Thus boundary 5 is split at this level in boundary 5a (below SWL) and 5b (subjected to run-up). Run down below the still water level is ignored altogether, so 5a is just a regular seepage boundary.

For both 5b and 6 a representative z_c value needs to be calculated to represent the whole boundary. This has to be done in such a way that about the total wetting time of the dike and accompanying head are representative for reality. To find this representative height the probability belonging to the height of the top of the boundary and the probability belonging to the height of the bottom of the boundary are averaged. From this average the representative height is constructed. Thus for 5b:

$$\begin{aligned} z_c^+ &= 0.94 \quad \rightarrow \quad P(R_u < 0.94) = 0.49 \\ z_c^- &= 0 \quad \rightarrow \quad P(R_u < 0) = 0 \\ P(R_u < z_{c,rep}) &= \frac{0.49+0}{2} = 0.244 \quad \rightarrow \quad z_{c,rep} = 0.61[m] \end{aligned} \tag{5.2}$$

For boundary 6 a value of 1.31 is found. So if the run-up value of a drawn wave exceeds this level the head function is activated on the boundary and otherwise it is not.

Due to limitations in PLAXIS the head calculated for the representative height is applied uniform over the entire boundary. As is depicted in Figure 5.9.

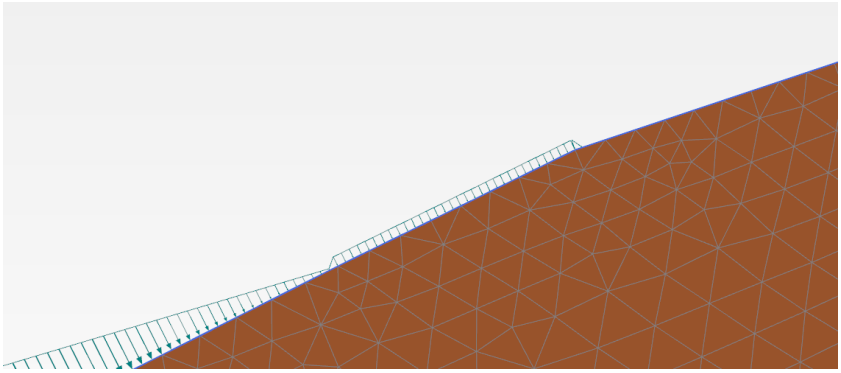

Figure 5.9: Run-up load uniformly applies perpendicular to the boundary. Boundary 5b is wetted while, 6 remains dry for this particular wave.

This flow thickness is the maximum flow thickness for a run-up event. However, the head generated by the incoming wave upon the subsoil peaks first and then diminishes over time. A simplified function is chosen to approximate the pattern shown in Figure 4.4.

Of this total wetting time, 25% is the calculated max head, then 25% 1/3 of the thickness is applied and for the final 50% of the time only 5% of the initial head is applied. Due to the short nature of the river waves and the face that the smallest amount of time in PLAXIS is seconds the total time for a single wave is taken as 4 seconds. In reality the wetting time varies. Analytically when assuming a quadratic decelerating flow velocity compared to v_{max} the wetting time ranges from 2.89 to 5.80 (1% wave) seconds for boundary 5b and 3.22 to 4.4 seconds for boundary 6. For the 2% run-up wave the wetting time would be 5.57 and 4.24 seconds respectively. Therefore 4 seconds is a reasonable wetting time to assume.

Finally, to create the input table for PLAXIS for boundary 5b and 6: If a new wave runs up before the other has run off, the wave is overwritten by the new wave. With the current set-up this is not necessary since the wetting time is assumed the same as the wave period. For the crest and dike toe area it is of importance.

This gives a signal changing in value per second. Unfortunately as mentioned above and in Appendix D every input entry for a load needs to be at least 20 seconds long otherwise PLAXIS will skip the load altogether. Therefore the exerted load is averaged over 20 seconds and the applied for that 20 seconds. This thus creates a simplified load signal for the run-up and overtopping boundaries. The underlying this average head however are still the randomly drawn 5 waves and their distribution in time.

3. Overtopping boundaries

The overtopping boundaries are 7, 8 and 9. Boundary 7 is the crest of the dike and has a tiny inclination of 1:67 and it is thus assumed that overtopped water remains on the dike way longer than on the steep slopes. The flow thickness is reduced by $1/3^{th}$ and then stays the same for the entire crest. The pattern of the head is slightly different because the water will remain on the crest much longer. The time the max head is exerted on the crest is largely based on Figure 4.4 which is an actual measurement at the crest of the dike. The peak value is exerted for 2 seconds and then a head of 30 mm is applied, with a duration of 2 minutes. This is thus independent of run-up height.

Boundary 8 is the inner slope of the dike and the flow thickness is calculated as described in Chapter 4. The same time distribution as for boundaries 5b and 6 is used. The boundary is activated for waves with a run-up larger than 6.24 meter. The maximum is applied for 1 second, then $1/3^{th}$ of the maximum for 1 second and then 5% for two seconds.

Boundary 9 is the horizontal hinterland, if a wave flows over the outer crest also boundary gets wetted. Only the same way as boundary 7, the crest, but with the maximum flow thickness of boundary 8. Of course the same aggregation of the load,s by taking the average, is applied for these boundaries to create a signal which changes only every 20 seconds.

5.2.3. Precipitation

In PLAXIS precipitation is implemented as a discharge in $[m^3/day/m^2]$ furthermore a maximum pore pressure head relative to the elevation of the boundary, $\psi_{max}[m]$ needs to be specified to simulate run off. In case of precipitation a $\psi_{max} = 0.03m$ is handled. If the boundary has an angle the puddle maximum is lowered with the cosine of the slope.

For now precipitation input is based on the STOWA 2015, [4], and STOWA 2004, [13], reports. To limit the number of precipitation scenarios the duration is set to the maximum as handled by the STOWA report, 196 hours or 8 days. This choice is also based on the thesis of Ten Bokkel Huinink, as he concludes that for relative impermeable soil, such as clay, a long duration with a low intensity has the largest effect on the phreatic surface. The total volumes for 8 days with different return periods are presented below in Table 5.5.

Ret. Per.	1	5	10	20	50	100	200	1,000	*10,000*	*100,000*
Year	77.9	104.8	115.9	126.5	140.1	150.0	159.6	180.8	*205.0*	*226.0*
Nov-Mar	65.6	89.4	99.1	108.5	120.5	129.3	137.7	156.4	*181.0*	*202.0*

Table 5.5: 8-Day precipitation totals volumes in mm for different return periods in the Netherlands (De Bilt) in 2014 for the entire year and for the period November-March. The longer return periods are not in the report but extrapolated from the published data.

Figure 5.10 shows the total amount of rain against the return period. Values with intermediate return periods can be estimated from these graphs. Furthermore the values with return periods of 10,000 and 100,000 year are not from the report but from visual extrapolation of the graph. So the correctness of these number is not guaranteed as they are not directly simulated by KNMI or STOWA.

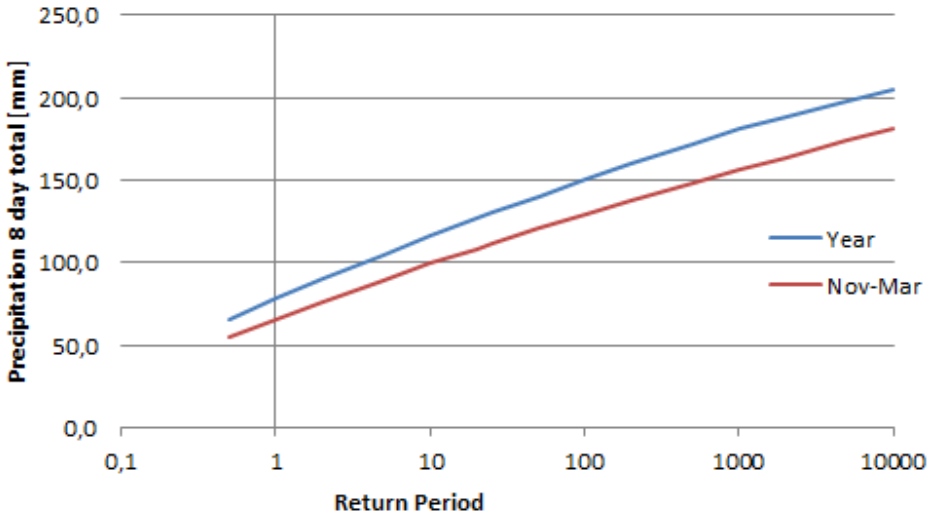

Figure 5.10: Total 8-day precipitation in the Netherlands (De Bilt) for the entire year and for the period Nov-Mar. Values are not corrected for future climate scenarios.

For this research the November-March values are used. This total volume falling in this 8 days time has a certain pattern. As stated before STOWA defined 7 different patterns. One with no peak, two with 2 peaks and 4 with one peak. The different patterns are supposed to be the same for different return periods, but differ slightly per season. This seasonal difference is smaller for the long duration of 8 days and is thus neglected here.

Table 5.6 shows the characteristics in fraction of the total volume per shape type. The last column shows the probability of occurrence for that type. Type 2A has a short duration between peaks while type 2B has a long one. Type 1A has the lowest peak value while type 1D has the highest.

Type/Time	32h	64h	96h	128h	160h	192h	Pr
No peaks	0.16	0.15	0.19	0.19	0.15	0.16	0.14
1 Peak A	0.14	0.13	0.31	0.15	0.13	0.14	0.14
1 Peak B	0.10	0.09	0.46	0.14	0.12	0.09	0.14
1 Peak C	0.06	0.07	0.60	0.12	0.09	0.06	0.14
1 Peak D	0.03	0.05	0.74	0.10	0.05	0.03	0.14
2 Peak A	0.05	0.40	0.07	0.39	0.05	0.04	0.18
2 Peak B	0.43	0.05	0.04	0.05	0.38	0.05	0.12

Table 5.6: Relative distribution of precipitation per pattern. Last column is probability of occurrence for each type.

5.3. Situation at the beginning of the scenarios

In order to adequately assess the effect of the different loads it is evident that the same starting point needs to be taken for every simulation. What should that starting point be and should it differ per dike type? Four possible options are considered.

1. Only global water level as in Figure 5.6; The dike has the water content as if is has just been constructed without any rain events.

2. Prewet the dike once; Before applying the hydraulic loads one simulation is done where it rains for 300 days straight to completely saturate the dike, then a cooling down period of another 700 days is simulated to give the water time to return to its equilibrium. The difference with the first option is that the saturation degrees high up in the dike are more realistic and closer to what they would be in reality.

3. Apply several years of actual precipitation and evaporation data for the region Rotterdam.

4. Set the level to an actual measurement in the dike given in Figure C.15. This means that the phreatic surface is at +3m N.A.P.

Especially for the clay dikes the difference between the four starting scenarios is significant. To keep as close to reality as possible, the combination of the last two options is chosen. Where the actual measured precipitation and evaporation at Rotterdam is applied until the measured level of +3m N.A.P. is reached. This last requirement is only used for the clay dikes, as the sand dike will virtually never reach this point. The only issue with this measured value in the dike is the fact that it is only one measurement point in time and that it is not known at what time of year the measurement was taken. Ergo, it is unknown whether this is a winter or summer measurement and if that matters at all. It is however the best option available. The resulting starting positions for the three different dike types are shown in Figures 5.11 to 5.13.

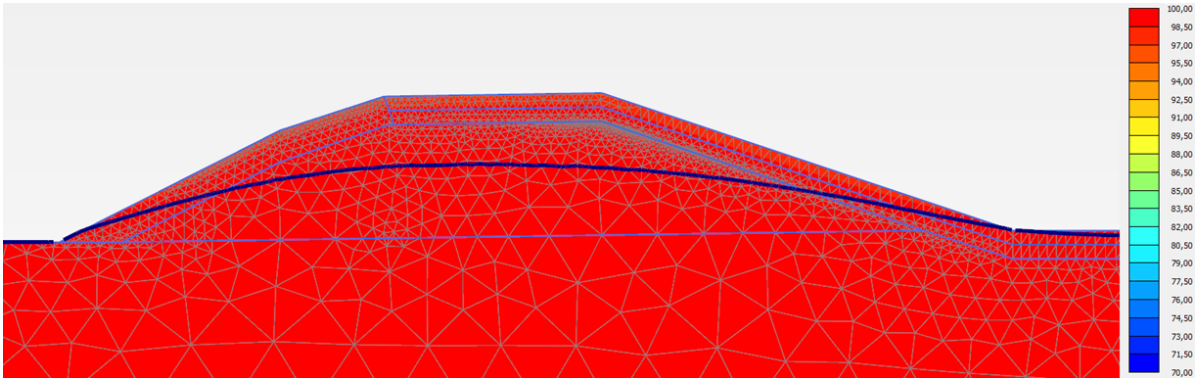

Figure 5.11: Starting position of the phreatic surface for the homogeneous clay dike. Colours indicate effective saturation.

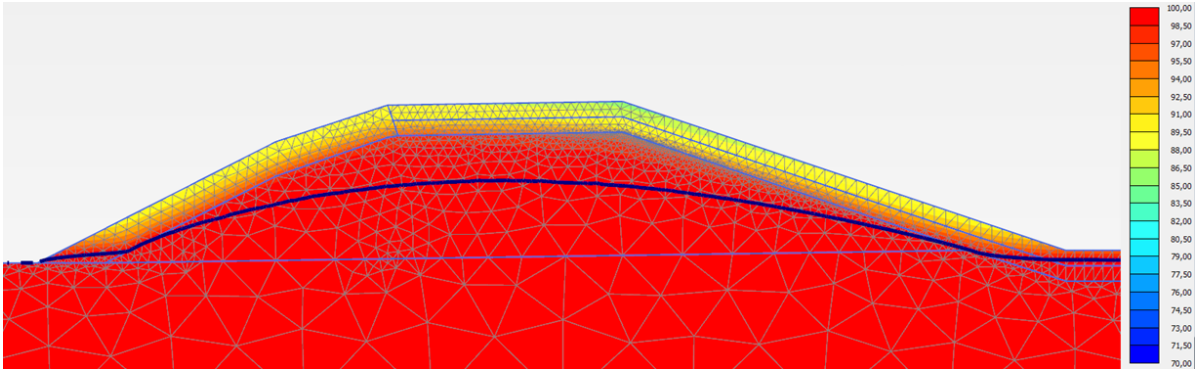

Figure 5.12: Starting position of the phreatic surface for the clay dike with soil structure deteriorated in top layer. Colours indicate effective saturation.

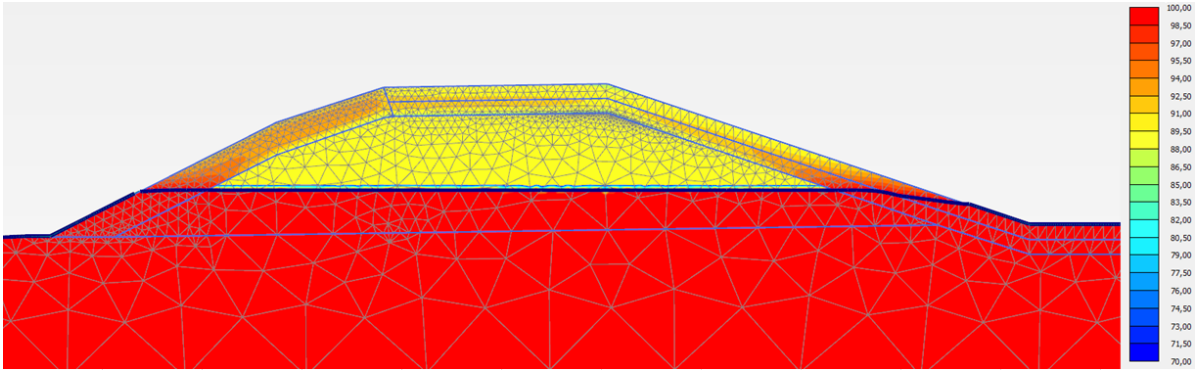

Figure 5.13: Starting position of the phreatic surface for the sand dike with a clay top layer with soil structure deterioration. Colours indicate effective saturation.

Another requirement for the starting position of the phreatic surface is that the pressures below the phreatic level are close to hydrostatic and no areas filled with air are present in the subsoil. In the clay dikes this state is not reached by applying the realistic rain. In order to reach this state, an artificial pre-wetting scenario for the clay dikes was needed. Even then it took a really long time, but also needed a long period of rest to reach the desired starting level again. The required rain time and resting period to reach the +3m N.A.P. are summarized below.

1. Homogeneous clay dike with k = 0.1 mm/day; 54 years of rain and 2.5 years of drought.
2. Clay dike with soil structure deteriorated top layer. Clay core of dike and subsoil have k = 0.1 mm/day; 27 years of rain and 2.5 year of drought.
3. Sand dike with soil structure deteriorated top layer. Clay subsoil has k = 0.1 mm/day; 5 years of rain, 140 days of drought.

It is evident that for the clay dikes the procedure needed to reach the measured value is far from realistic. In reality the years of rain needed and the following drought are both extremely long. This is mainly caused by the layer build-up of the dike in the model. Due to the lack of sandy layers in the model, the water can escape and penetrate way slower. Although this start isn't perfect as well, at some point decisions need to be made.

However, some interesting things can already be concluded from these three simple pre-runs. The effect of the soil structure deterioration in the top layer of the dike is crucial for the penetration of incidental hydraulic loads. Only the top 1 meter has a different hydraulic conductivity when comparing the first two dikes while the core and subsoil have the same characteristics. However, the difference in time in order to reach the same phreatic level is a factor 2. It is clear that the top layer with soil structure deterioration acts as a buffer basin for precipitation (and overtopping). It captures most of the water in its pores in a rather short time and

then releases it slowly in the less permeable dike core. If this layer is not present, as is the case with the homogeneous clay dike, the main part of the precipitation will run off and/or evaporate before any significant penetration takes place. It thus takes a long time to let enough water penetrate into the dike if no top layer with soil structure deterioration is present.

6

Results individual extreme events

This chapter presents the results of the PLAXIS runs. The images (if presented) are either the effective saturation or the active pore water pressure. The key in all of these images is also the same; Saturation plots: Blue is 70% saturation, Red is 100% saturation; Pore water pressure plots: Blue is $10kN/m^2$, Red is $-30kN/m^2$. What the exact definition of these variables is, is explained in Appendix D.1. The dark blue line is the phreatic surface, or more general, the point where pore water pressures become positive.

The data presented in the graphs is the value generated in the output point below the inner crest. The phreatic surface rise in time is presented in meter water column and is always relative to a scenario where no loads are applied. So, from the raw pressure data for each simulation, the pressure data from a scenario where no loads are applied, is subtracted. As a consequence, it is possible that the pressure rises while in absolute sense it decreases and the other way around. Furthermore, on the secondary axis, the rain and water level loads are presented in cm/day and $mN.A.P.$ respectively. There are also two vertical red lines to indicate the period where the overtopping load is applied.

In all the graphs WL 1/100,000 stand for the 1 in 100,000 year Water Level. Rain 1/100,000 or U0 1/100,000 stands for the 1 in 100,000 year uniform shaped precipitation load. With OT 1/100,000 the 1 in 100,000 year OverTopping combined with its water level is signaled.

To give the simulation time to start-up the first ten days no loads are applied. This time is therefore not shown in any of the graphs. Table 6.1 shows when the loads are applied in simulation time. Each of the simulations has a total duration of 200 days.

Load	Start time	Peak time	End time
High water wave	10	22.5	40
Precipitation (U0)	10	-	18
High water wave OT	10	21.5 - 23.5	40
Overtopping waves	21.5	-	23.5

Table 6.1: Times of the loads (in the simulation time).

6.1. Homogeneous clay dike

First, the effects of different loads on a homogeneous clay dike without any soil structure deterioration in the outer layer is tested. The complete dike thus has a maximum hydraulic conductivity of $0.0001m/day$ or $0.1mm/day$ which is a realistic value for intact homogeneous clay.

Figure 6.1 shows the phreatic surface development in time for several different loads. It is immediately clear that the development in time of all three cases is none whatsoever.

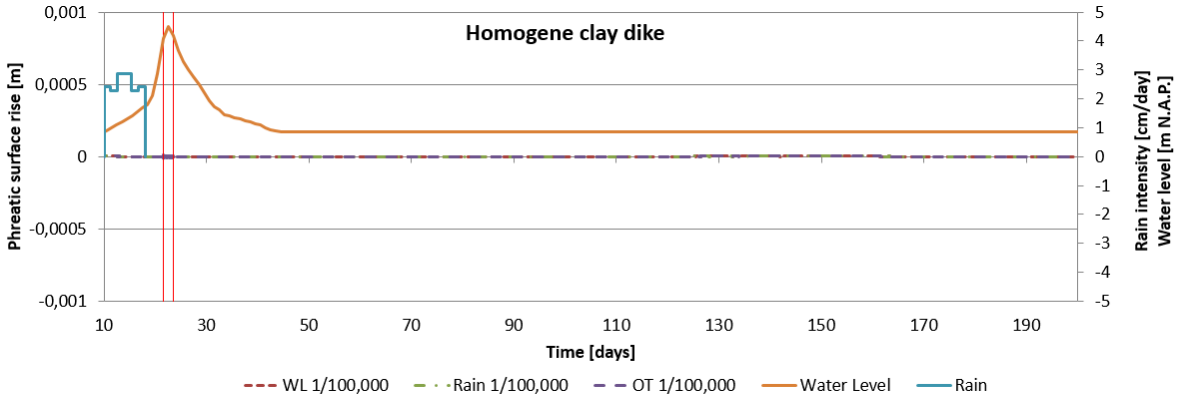

Figure 6.1: Relative phreatic surface rise for a homogeneous clay dike. Hydraulic loads are on the secondary axis. The two red lines signal the period where overtopping is applied.

In the 160 days after the loads are applied still no reaction caused by the loads is noticeable in the pore water pressures in the soil. When looking at the dikes just after the loads are applied it becomes clear why.

6.1.1. Water level

Figure 6.2 shows the dike just after the peak of the high water wave has passed. During the first several days of the flood wave only several centimeters of infiltration distance at the river side of the dike are observed. This distance is really small, despite the already highly saturated starting situation of the soil.

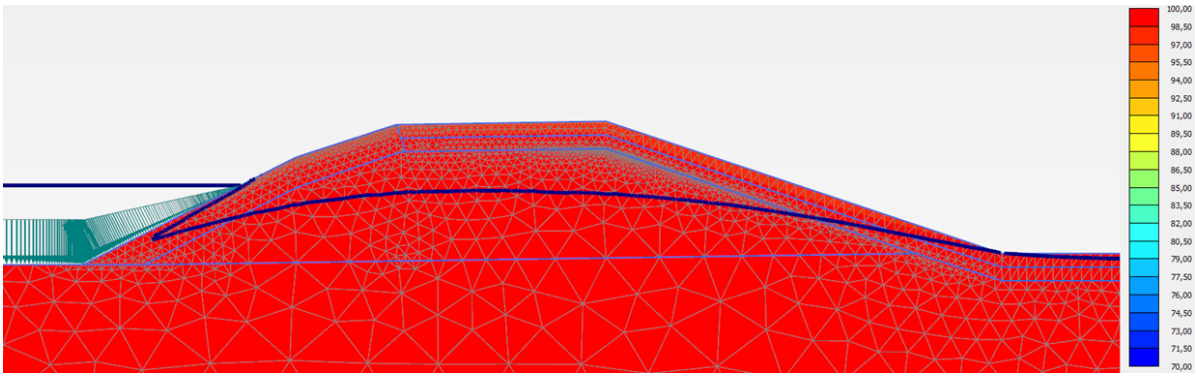

Figure 6.2: S_{eff} just after the peak of the 1/100,000 year high water wave, at t=24 days. (Red =100% saturated, Blue =70%)

It is clear that this small infiltration in the highly impermeable clay barely influences the surface at all. Especially below the outer crest, where the chosen output location for the pore water pressures is located, the influence is nonexistent.

6.1.2. Precipitation and overtopping

When rain and overtopping are regarded, Figure 6.3 and 6.4 respectively, the same issue of little infiltration is observed.

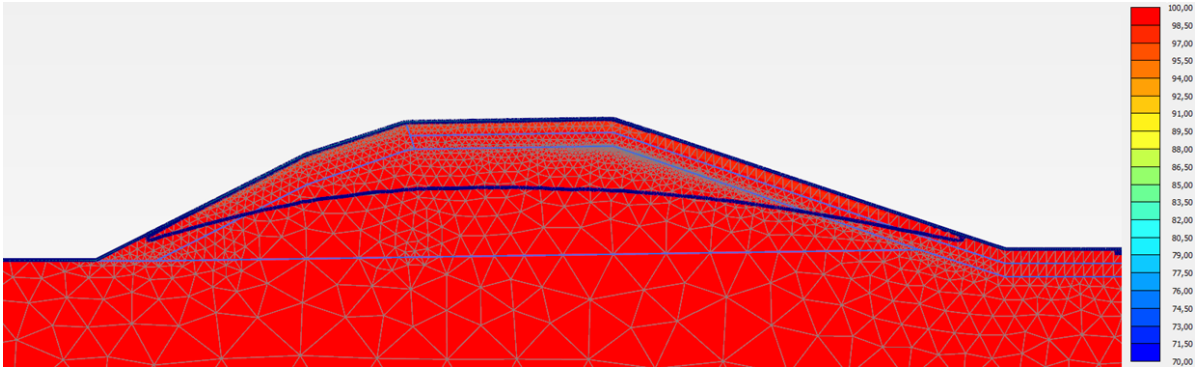

Figure 6.3: S_{eff} after 1/100,000 year uniform rain event at t=18 days. (Red =100% saturated, Blue =70%)

For rain, the results of the uniform shape are presented, both in the graph before as well as the figure above. However, this could have been any of the picked shapes as no visible differences occurred for this dike type and settings.

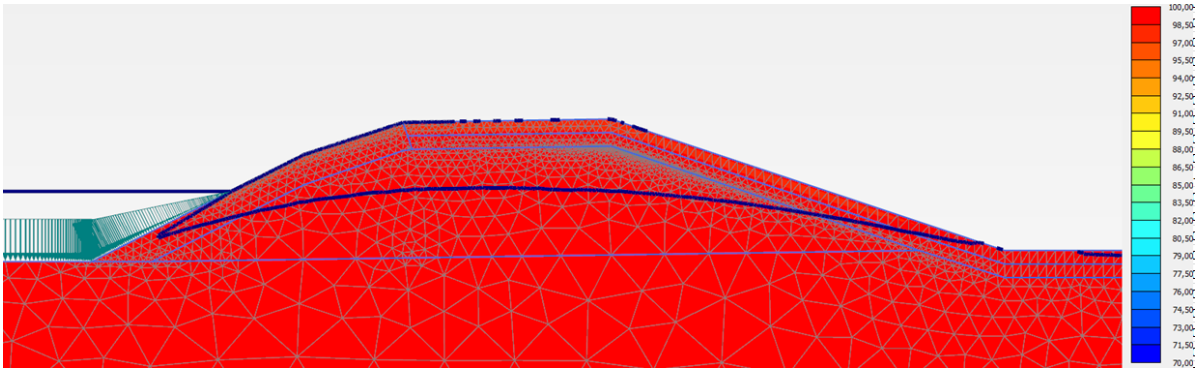

Figure 6.4: S_{eff} after 1/100,000 year overtopping event at t=23.5 days. (Red =100% saturated, Blue =70%)

For both precipitation and overtopping the load duration compared to the permeability is too short. The eight days of rain create a small fully saturated upper layer in the soil. In this layer the rain causes the pressure to rise in the pores and thus the blue line, indicating where active pore water pressures are larger that atmospheric pressure, is also computed there by PLAXIS. For the two day lasting overtopping, even though head values are larger than in the precipitation case, the infiltration at the surface is even less. Although it is nice to notice the asymmetric distribution of this fully saturated front: the run-up boundaries being fully saturated and a less saturated crest and inner slope. The hinterland however, where the overtopping water can accumulate, does show some heightened surface. This indicates that the simulation of the overtopping waves works rather well.

As these are the maximum 1/100,000 year loads for all hydraulic load types, the smaller ones are not tested at all, as even less water will infiltrate in these cases. It could be possible that further away in time some slight differences between the different scenarios do occur. However at some point the simulation has to be cut off and more than 160 days reaction time for one event could be classified as enough. Waiting even longer to monitor the effects makes less sense as seasonal influences have changed entirely. The effect of a series of effects however, could still be very interesting, but as this is a different kind of research it is not regarded in this chapter.

6.2. Clay dike with soil structure deterioration in top layer

The clay dike with soil structure deterioration is expected to behave slightly different than the homogeneous clay one. No clear differences were observed between the three different hydraulic conductivity values of the top 0.5 meter. So in order to keep the results orderly only the results for the average conductivity of the supra top layer, $k_y = 2.07$, are presented in this section.

Comparing the graphs in Figure 6.5 to those in Figure 6.1 no significant differences can be observed. Only

difference would come from a small numerical instability at the beginning of the overtopping phase, but this has no physical meaning at all.

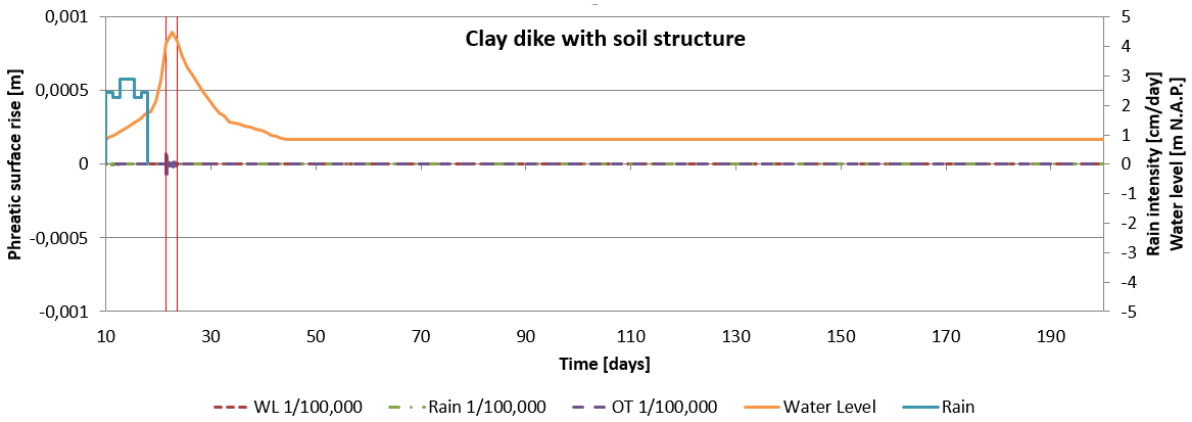

Figure 6.5: Relative phreatic surface rise for a clay dike with soil structure deterioration in the top layers. Hydraulic loads are on the secondary axis. The two red lines signal the period where overtopping is applied.

All scenarios are again identical for the entire 200 days. Indicating that the effect of a 30-day 1/100,000 year flood wave is not felt deep in the dike and its effects do not surpass the outer crest. Also overtopping and rainfall do not have any influence within the 200 day simulation span. However, the rest of the results later on suggest that this is caused by the time where the simulation is cut off rather than that there is no effect at all, as is the case with the homogeneous dike.

Again the one peak rainfall shape (1C) and two peak rainfall (2B) shapes are also applied to the dike but within the 200 days range no significant differences are visible. Therefore, in the graph above, the precipitation is referred to as rain, as distinction between different shapes makes no sense for these dikes. So again, it can be concluded that the individual events do not influence the phreatic surface significantly.

6.2.1. Water level

For the water level scenario the effective saturation just after the peak of the high water wave is shown in Figure 6.6.

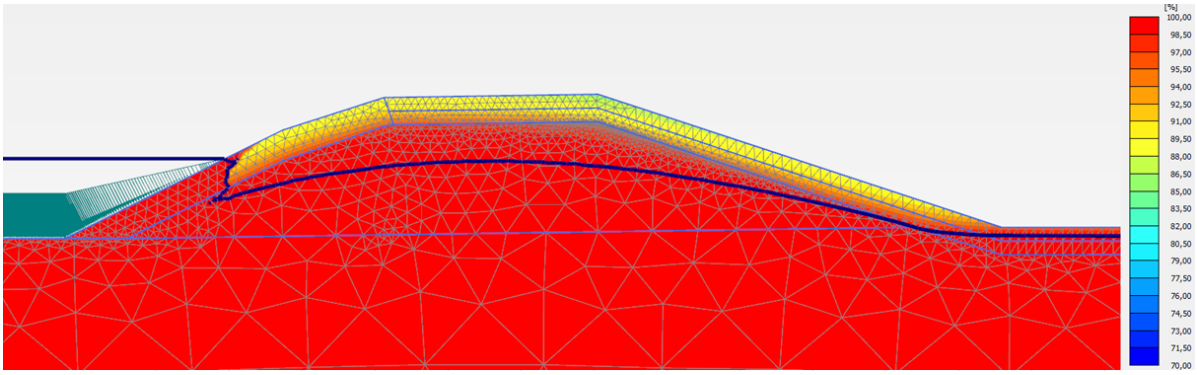

Figure 6.6: Effective saturation in the clay dike after the 1/100,000 year high water wave has occurred.

It is clear that compared to the homogeneous dike the infiltration in the outer layer, with a $k = 0.01 m/day$ rather than $k = 0.0001 m/day$, is much more. However as soon as the less permeable core is reached the flow is becoming really slow again, thereby prohibiting the water level to influence pore water pressures deeper inside the embankment.

6.2.2. Precipitation

The effective saturation plots for the precipitation event are shown in Figures 6.7 and 6.8. The Figures show the dike directly after the precipitation and 12 days after the rain respectively.

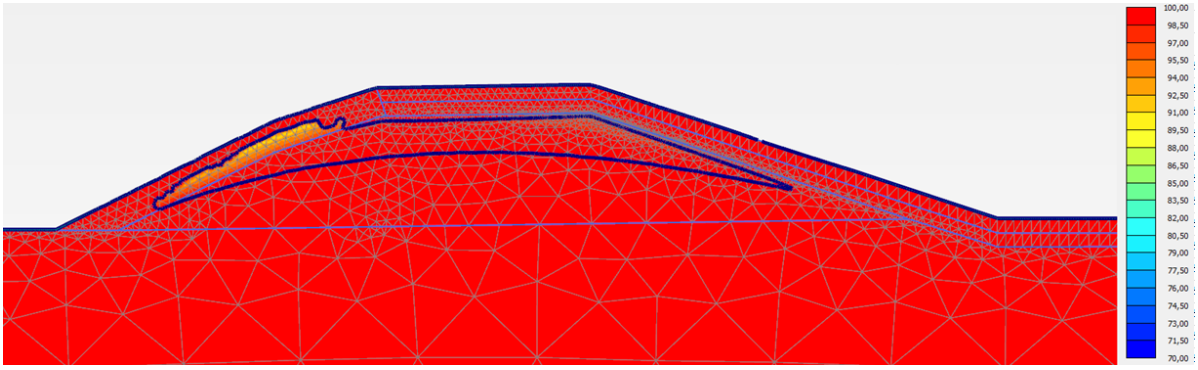

Figure 6.7: Effective saturation in the clay dike directly after the uniform 1/100,000 year rainfall has occurred.

The figure above shows some interesting results. The very permeable top layer quickly fills up with water during a precipitation event. It acts like a catch basin, quickly absorbing the water and then slowly releasing it to the subsoil below. This hypothesis is backed-up by the fact that the infiltration at the inner slope is higher than at the outer slope. At the outer slope the rain has penetrated roughly half a meter into the soil, while at the inner slope it has penetrated the full top layer and even several centimeters into the barely permeable core. The logical explanation for this difference is twofold. The first thing being that the top very permeable 0.5 meters catches most of the water, preventing it to run-off. The second reason is that once the water is caught by the top 0.5 meter a layer of hydrostatic pressure forms. The water gets pushed into the less permeable lower 0.5 meter while at the outer slope the maximum pond depth is set to only 3 centimeter, the difference being roughly 47 centimeter of watercolumn.

Figure 6.8 shows the situation 12 days later; again without any additional loads.

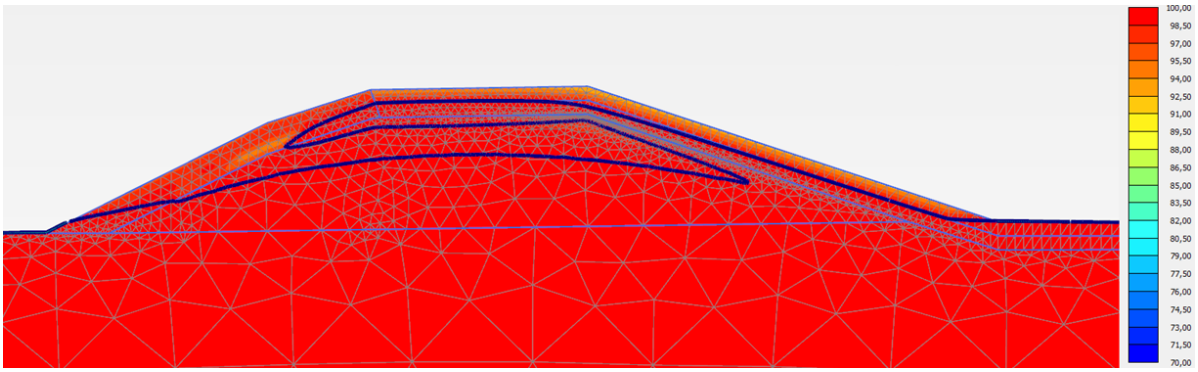

Figure 6.8: Effective saturation in the clay dike 12 days after the uniform 1/100,000 year rainfall has occurred.

Comparing Figure 6.8 to 6.7, it is apparent that the infiltration front has barely advanced into the dike core, while the top 0.5 meter is empty entirely. In this layer, the water has mainly flowed to the side towards the inner dike toe. The same is already starting to happen with the lower top layer and can be seen at the inner crest. Here, the water flows parallel to the embankment slope, inside its own layer rather than penetrate the core body. Below the outer crest this phenomenon is also visible as the larger part of the water flows in the top layer rather than through the core.

At simulations' end Figures 6.9 and 6.10 depict the situation in the soil.

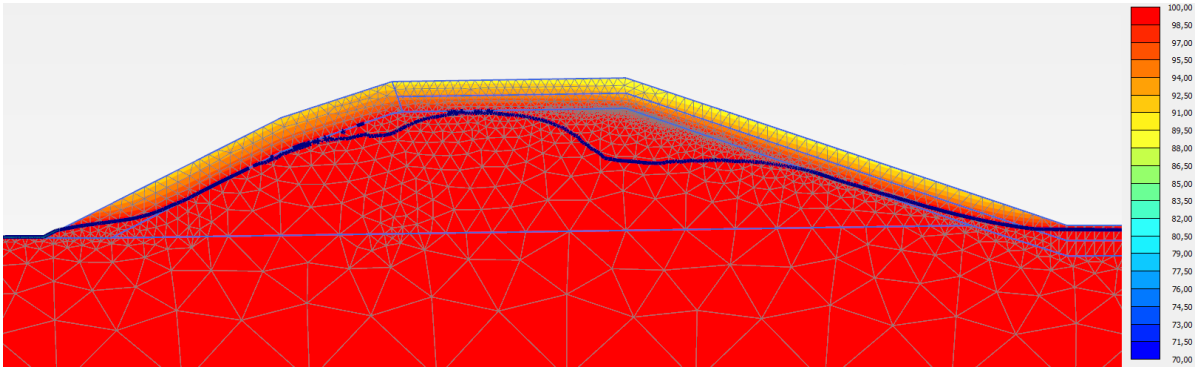

Figure 6.9: Effective saturation in the clay dike 182 days after the 1/100,000 year rainfall has occurred.

In 176 days time, the water infiltrated in the top found its way to the phreatic surface below. This gives a strange shape of the phreatic surface. The bulge in the center is caused by the large amount of water which could infiltrate through the top as little water flows off through the sides. That the phreatic surface at the left is higher than at the right is also caused by the fact that less water flows of sideways compared to the inner slope. Even though less water will infiltrate at the outer slope compared to the inner slope, eventually the phreatic surface rises more at the inner slope. This is likely to be caused by the fact that once the water has penetrated at the outer slope, it is more likely to reach the phreatic surface, as less water flows away sidewards through the permeable top layer. This means that shortly after the rain event the inner slope of the dike is affected more by rainfall than the outer slope, but after a while it is the other way around.

For the final interpretation of these results, Figure 6.10 shows something important. Even though Figure 6.9 suggests that the phreatic surface is heightened, the actual pore water pressure below the surface is not hydrostatic. There is a large area where the pore water pressure is between $0-2kN/m^2$. And even though the saturation degree is 100% it does not contribute to a higher pore water pressure deeper in the soil. Therefore it does not influence the effective shear stress and the probability of failure with respect to macro-stability. It also explains why the pressure in the output point in Figure 6.5 does not increase in the entire 200 days.

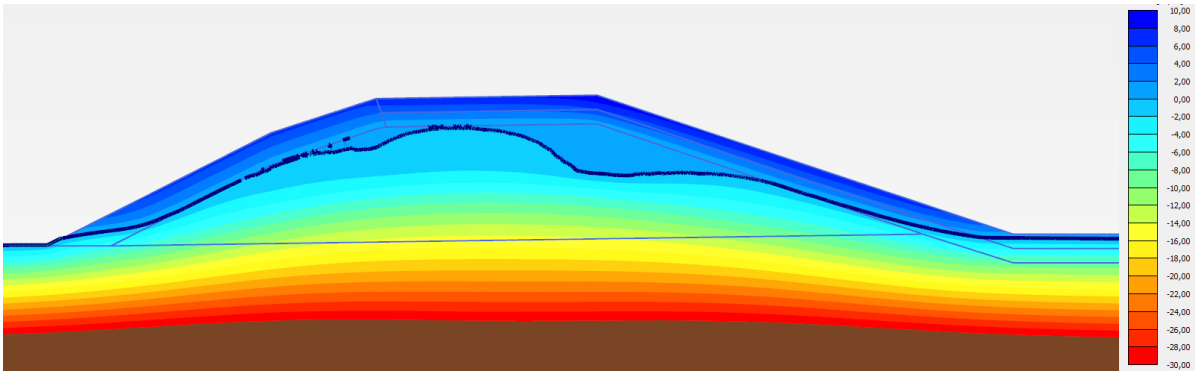

Figure 6.10: Active pore water pressure in the clay dike 182 days after the 1/100,000 year rainfall has occurred.

6.2.3. Overtopping

Figures 6.11 and 6.12 present the results after the overtopping event.

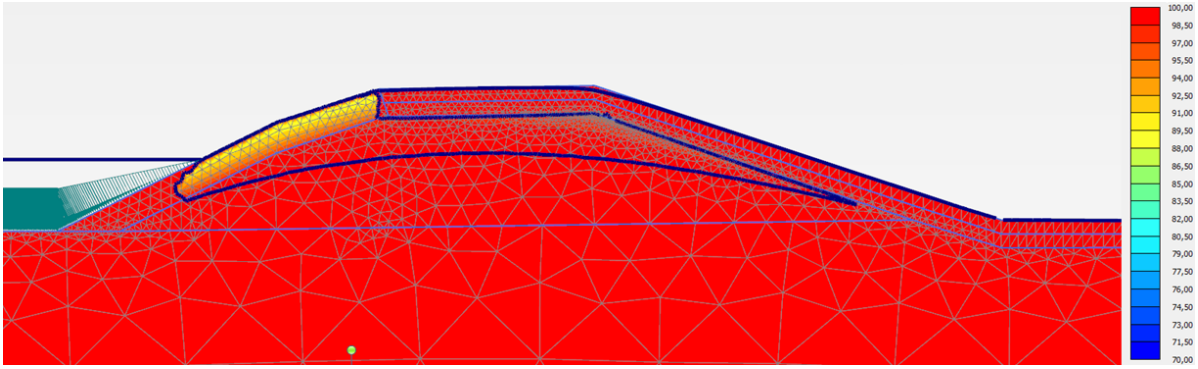

Figure 6.11: Effective saturation in the clay dike directly after the 1/100,000 year overtopping has occurred.

Again, it is clear that the very permeable top layer at the inner slope and crest absorb the water very well and in a short amount of time. The two day alternating head load is, again, not enough to penetrate the less permeable outer slope. Here the importance of the permeable top layer is even stronger. Even though the inner slope and crest are loaded less often and with a lower head the water penetrated the entire 0.5m sub top layer, while this layer has the same properties as the top layer on the outer slope. The explanation remains the same as with the precipitation case. There is however a small chance that the bad infiltration at the outer slope is partly cause by some numerical influences. See Appendix D.8 for the elaborate review of this problem.

Figure 6.12 shows the saturation at the end of the 200 day simulation. So almost 180 days after the last wave. The surface is indeed higher at the inner slope than at the outer slope. Also, there is a bulge of where the crest water penetrated the core body. This water is still flowing and the pressure distribution below the bulge is, again, not hydrostatic. This can be seen in Figure 6.13 where the actual pore water pressures are depicted. The same consequences for this phreatic surface bulge apply as for the precipitation case.

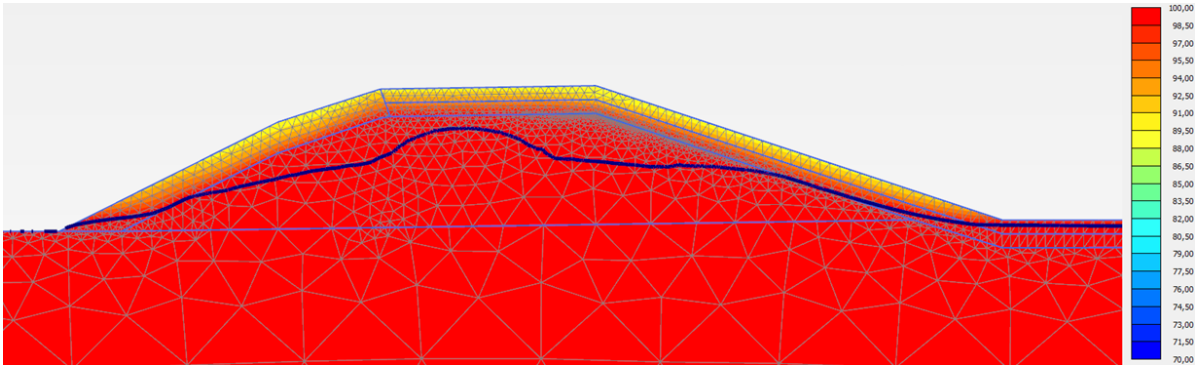

Figure 6.12: Effective saturation in the clay dike 175 days after the 1/100,000 year overtopping has occurred.

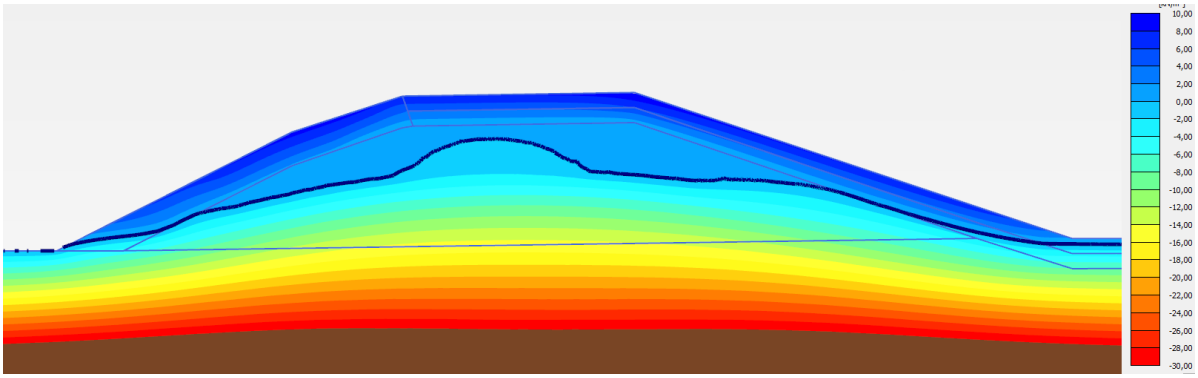

Figure 6.13: Active pore water pressure in the clay dike 175 days after the 1/100,000 year overtopping has occurred.

Notice that the shape between the precipitation and the overtopping case differs mainly at the outer slope, while the inner slope remains roughly the same. Explanation for this difference can likely be found in the load durations and the influence of the permeable supra top layer. Due to the smaller permeability of the outer layer, the limiting factor of the infiltrating water is the duration of the load and not the total amount of water flowing over it. As the total amount of water is roughly the same for both scenarios (based on the same results for the inner slope after the same amount of time), the difference is caused by the part of the water that actually infiltrates. Of course, if the same amount of water is spread out over 8 days rather than 2, a much higher percentage will infiltrate which causes the phreatic surface to rise more in the precipitation scenario.

6.3. Clay cover on sand core

Again, to check the influence of the different hydraulic loads, the scenarios with the heaviest loads have been applied first. In all figures the effective saturation (S_{eff}) is shown at the peak of the phreatic surface value. Always with the same key (Red =100% saturated, Blue =70%) for easy comparison purposes. The yellow color of the sand core, however, is not the degree of saturation, but the color given to sand in PLAXIS. For sand, 1 meter above the phreatic surface gives a residual saturation of less than 5% while directly above the phreatic surface a saturation of 32% is present, confirm the graph in 5.4. This is all well below the 70% limit of the saturation key, hence PLAXIS just depicts the soil color picked by the user.

Figure 6.14 shows the phreatic surface rise, relative to the 'no-loading' scenario, for the different hydraulic loads.

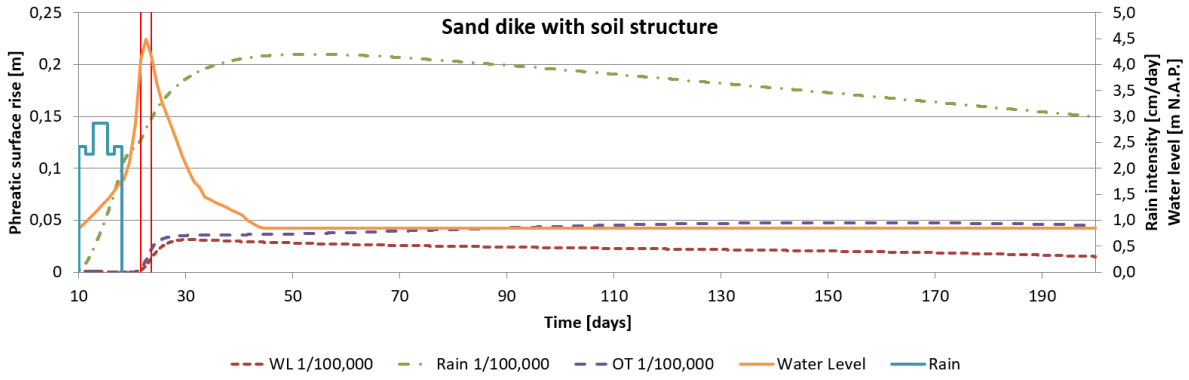

Figure 6.14: Relative phreatic surface rise for a sand dike with soil structure deterioration in the top layers. With top 0.5 m k_y = 2.07. Hydraulic loads are on the secondary axis. The two red lines signal the period where overtopping is applied.

For this dike type, at least some distinct differences are registered when the loads are applied. Due to the sand core and top layer with soil structure deterioration, the loads influence the surface relatively quick. Of all the loads, the uniform rain clearly jumps out with a surface level which is 21cm higher than the reference level. Although this is still not dangerously high. The maximum level rise is simulated at 50 days, so 32 days after the last drop of rain fell. The clay cover thus acts as a zone delaying the infiltrating water. The difference between the overtopping load and rain load is an important observation as the overtopping can be seen as a short intense event while the rain has a longer uniform character. The difference in phreatic surface between the overtopping and just high water level, is 3cm after 200 days, with both lines already decreasing.

6.3.1. Water level

This is the only dike type where the river water level itself has influence on the phreatic surface within the dike. Figure 6.15 shows the point where the phreatic surface is at it's maximum.

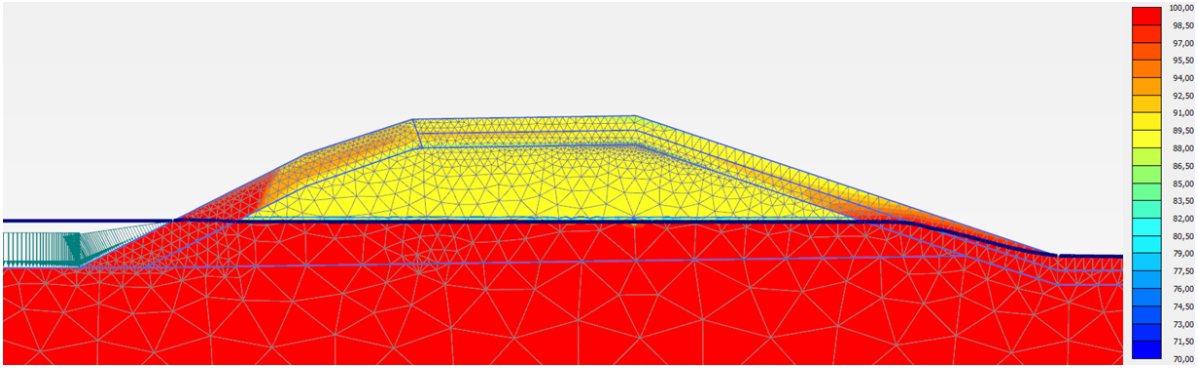

Figure 6.15: Effective saturation in the sand dike while the 1/100,000 year high water wave occurs. Four days after the peak value has occurred. Water is dropping. Top 0.5 m $k_y = 2.07$

Not surprisingly, this is the moment where the river water level is the same as the phreatic surface within the dike. As the water rose at the beginning of the flood wave it started penetrating the cover layer, but the water needs time to reach the core. After reaching its highest point (the saturation pattern in the top layer of the outer slope shows where that point was), the water started dropping again. At some point it has the same level as the delayed phreatic surface within the dike core. As soon as the outer water level drops even lower, not only the force pushing the water into the dike stops, but the direction actually reverses, pushing the water back out. That is why the water level and the reference lines in 6.14 are not parallel but the water level graph declines faster. This is naturally also the highest point the phreatic surface will reach for this simulation.

6.3.2. Precipitation

For the uniform rain shape, the situation directly after the rain and the moment of the maximum phreatic surface are presented in Figures 6.16 and 6.17 respectively. Just as with the clay dike, which has the same top layer characteristics as this sand dike, the top layer is entirely saturated. Main difference is at the core; rather than encountering an impermeable body where the pore water pressure can build, the water can flow relatively easy towards the phreatic surface below. As if water is seeping through a leaking ceiling.

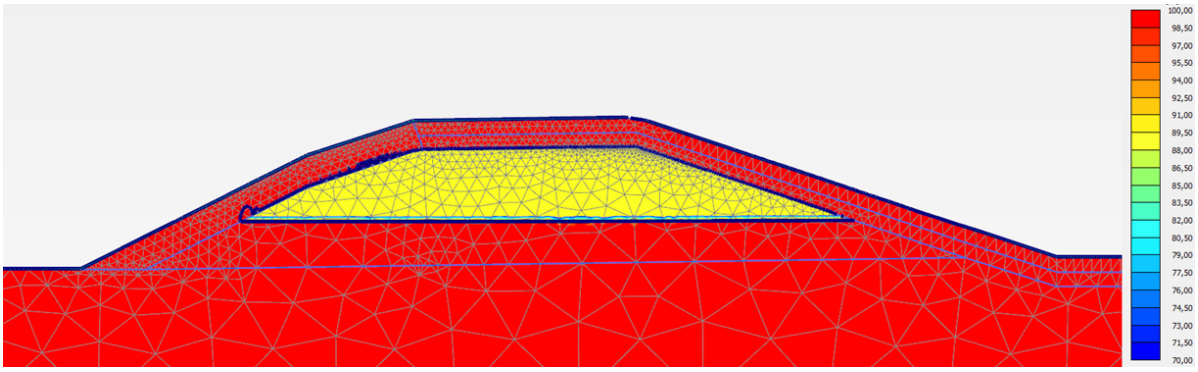

Figure 6.16: Effective saturation in the sand dike directly after 1/100,000 year uniform rain occurred. Top 0.5 m $k_y = 2.07$

At the maximum phreatic surface, the top layer transferred all its water to the body below. With no more water leaking though the figurative ceiling, the water starts dropping again.

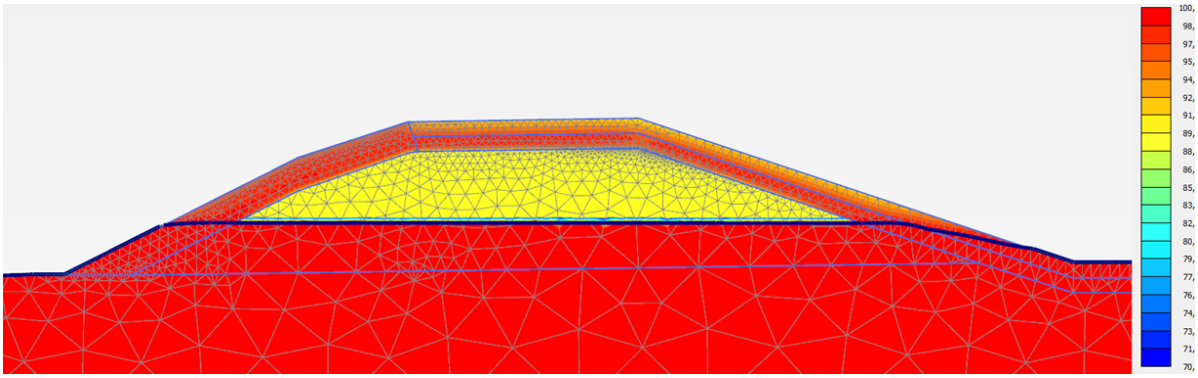

Figure 6.17: Effective saturation in the sand dike 18 days after 1/100,000 year uniform rain occurred. Top 0.5 m $k_y = 2.07$

The results above are only for the uniform rain shape. Other rainfall shapes have also been applied to the dike. Figure 6.18 shows the influence of the shape on the phreatic surface in time. Only the two peak rainfall with a long duration between peaks (B2) and the second to highest one peak rainfall (C1) are shown to keep things orderly. The differences between the shapes are not that large as can be seen in the graph. Notice that the reference level, uniform, and overtopping scenario are the same as in Figure 6.14 but that the time scale is set to logarithmic.

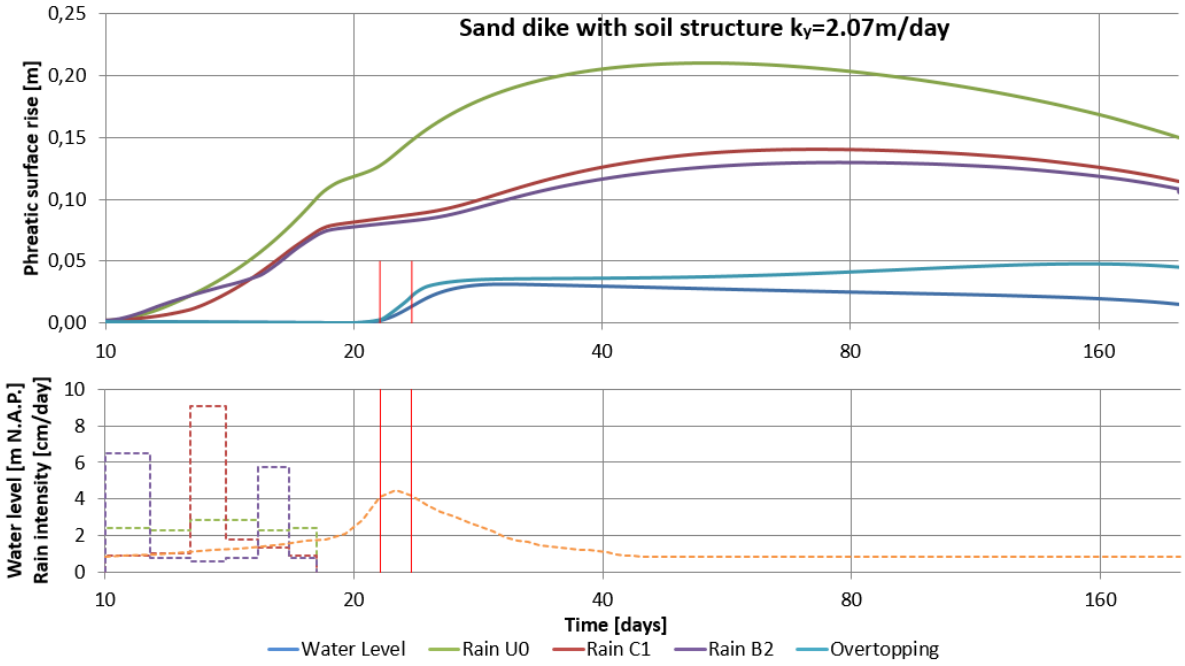

Figure 6.18: Difference in precipitation patterns in time. Top 0.5 m $k_y = 2.07[m/day]$. Loads are plotted below on the same time scale. Red bars indicate overtopping period.

The uniform shape clearly has the largest influence on the surface. Both the C1 as well as the B2 pattern heighten the surface less. This is caused by the fact that peaks are probably less profitable with respect to infiltration. Above a certain threshold value the water starts running off rater than infiltrating. Two things could be happening:

- The threshold value is not reached by the uniform shape but with any peak shaped rain it is, thus losing water to run-off.
- The threshold value for run-off is also reached by the uniform shape but it is reached constantly for the entire 8 days. For the other patterns there are days where the threshold is far from being reached, while at other days relatively more water is lost to run-off.

Although with the current results it is not possible to check whether the uniform shape reaches the threshold or not, the rest of the explanation is about the same.

6.3.3. Overtopping

Figure 6.19 depicts the dike 30 minutes after the last overtopped wave, 23.5 days after the simulation started. Here again, as also explained in Section 5.3, the importance of the permeability of the top layer for further infiltration of water is clear. While at the outer slope, where no macro pores, holes, and cracks are simulated, the water barely infiltrates during these two days of overtopping. Even though compared to the inner slope, both the frequency of waves as well as the corresponding head is higher for these outer slope boundaries.

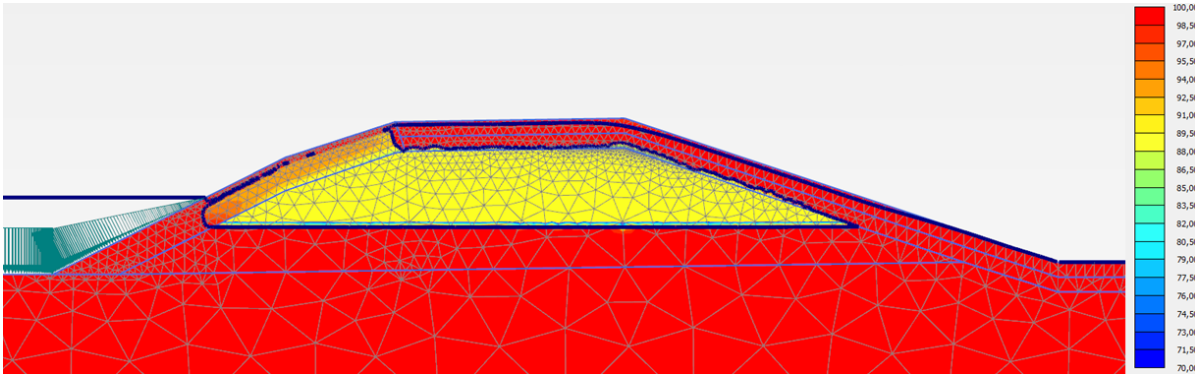

Figure 6.19: Effective saturation in the sand dike 30 minutes after the high water wave with 1/100,000 overtopping has occurred. Top 0.5 m $k_y = 2.07$

In general it can be said that for the three investigate dike types, the sand core is the most reactive one. But even with this dike type, the reaction to single events is small and spread out in time due to the clay layer. So for none of the dike types, even though subjected to the most extreme scenarios, the phreatic surface reacted enough to cause any significant danger with respect to inward macro stability due to phreatic surface rise.

6.3.4. Different k-values top layer

For the supra top layer, different hydraulic conductivity values have been applied. This means that only the top 0.5 meter of the crest and inner slope has been changed. The lower 0.5 meter of the clay top layer and the outer slope kept their original value of 1 centimeter per day. These three different dikes with top layer permeability of 0.83, 2.07, and 5.18 [m/day] all have been subjected to three different precipitation shapes (U0, C1, and B2) and an overtopping event. All these loads have a probability of occurrence of 1/100,000 per year. The water level scenario is left out, as the outer slope characteristics have not changed.

Figures 6.20 to 6.22 give the results of the runs. In contrast to some of the graphs before, the x-axis is log scale as the main differences occur in the first 30 days. As can be seen, the influence of the hydraulic conductivity of these top layers is little. The reaction time to the load decreases as the hydraulic conductivity increases, but the maximum values reached for each scenario are not significantly different.

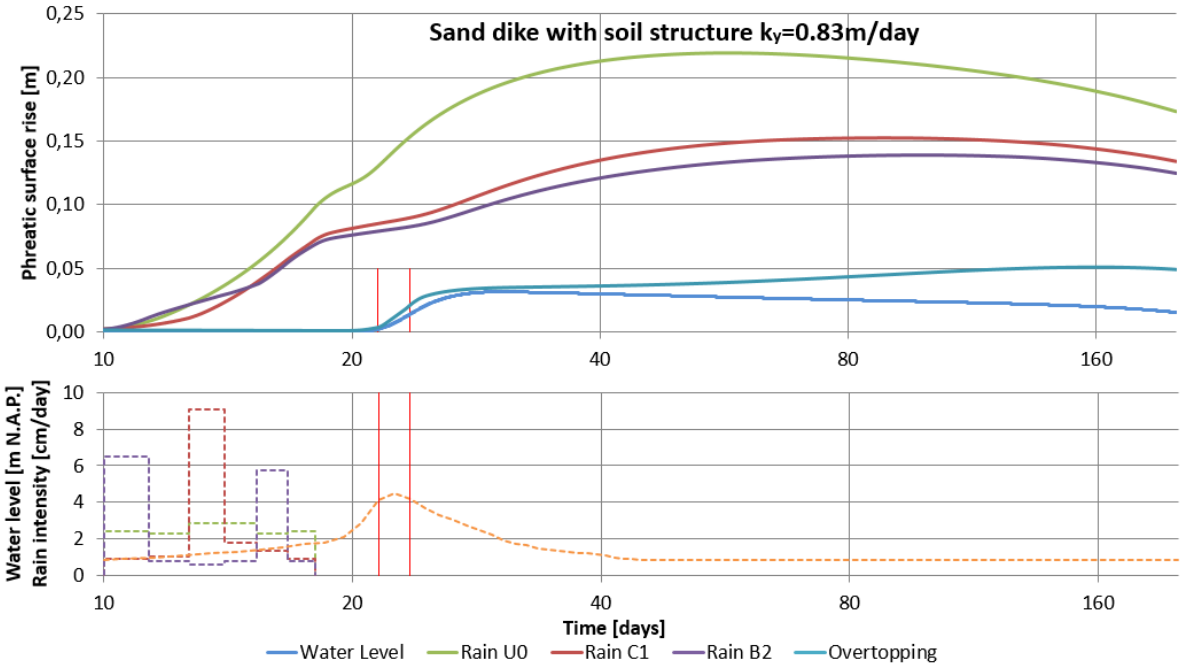

Figure 6.20: Influence of precipitation and overtopping on phreatic surface. Top 0.5 m $k_y = 0.83[m/day]$. Loads are plotted below on the same time scale. Red bars indicate overtopping period.

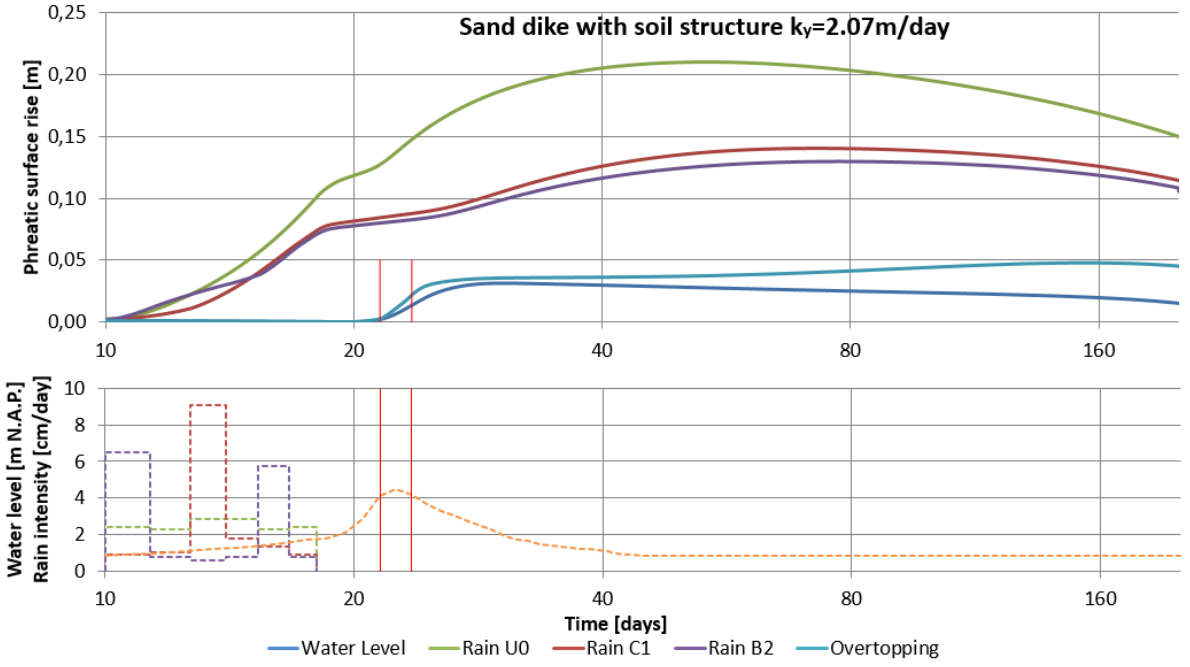

Figure 6.21: Influence of precipitation and overtopping on phreatic surface. Top 0.5 m $k_y = 2.07[m/day]$. Loads are plotted below on the same time scale. Red bars indicate overtopping period.

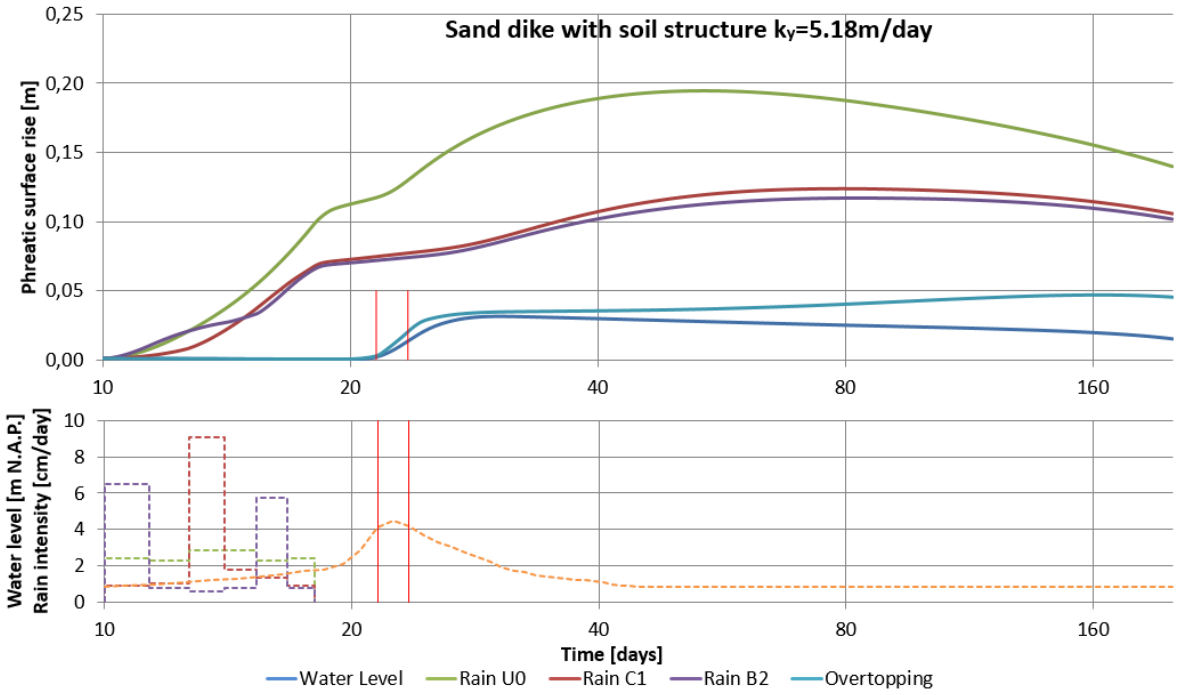

Figure 6.22: Influence of precipitation and overtopping on phreatic surface. Top 0.5 m $k_y = 5.18[m/day]$. Loads are plotted below on the same time scale. Red bars indicate overtopping period.

For the overtopping scenario, the difference in hydraulic conductivity of the supra top layer is very small and only differs less than $1mm$.

In general the influence of the hydraulic conductivity of the top 0.5 meter is very little, at least with the picked values. The largest difference occurs during the uniform rainfall between the $k = 0.83m/day$ and $k = 5.18m/day$ and is roughly $3mm$. Based on the previous sections, however, the presence of the layer is of importance to catch the overtopping and rain water, but once it is there its conductivity matters little. It does mean that somewhere between a hydraulic conductivity of $0.01m/day$ and $0.83m/day$ there is a conductivity range where its value does have a large influence. What this value is, depends on the intensity of the load, as the hydraulic conductivity of the soil needs to be as high as this intensity. Only if the load has a higher discharge than the soil run-off occurs, otherwise the entire load will be caught in the top 0.5 meters of the soil and then released slowly to the deeper part in time. The loads tested here are all fully absorbed by the top layer.

There is, however, a somewhat counter intuitive relation between the permeability of the supra top layer and the rise of the phreatic surface. As the higher permeability lead to a lower surface. This is true for all rainfall shapes and overtopping. Its explanation is the same as for the asymmetric phreatic surface in Figures 6.9 and 6.10. All layer are permeable enough to quickly catch any precipitation, but the less permeable soil losses less water due to sideward flow inside the top layer; therefore more water can infiltrate in the layers below. This will thus have a large effect on the phreatic surface inside the dike. On the other hand, if the hydraulic conductivity becomes too small, not enough water can penetrate in the outer layer and will thus run-off at surface level. This means that there is a optimal hydraulic conductivity which leads to the highest infiltration. This optimal value ensures both a high infiltration in the outer layer as well as minimal sideward flow inside the outer layer. This research did not try to find this k-value. Partly because the optimal value is dependent on load duration, load intensity, and permeability of the soil layer below itself.

It is likely that altering the hydraulic conductivity of the sub-top layer and outer slope has a larger influence on the effect loads have on the surface, as this is the limiting factor and not the supra-top layer. However, as explained before, the large soil structure deterioration and macro-pores are only signaled in this top 0.5 meter. The influence of hydraulic conductivity of the sub-top layer rather than that of the supra-top layer is not within the scope of this thesis, but is definitely an interesting variable for sand core dikes.

7

Results of additional tests

7.1. Long term realistic precipitation

In Chapter 6 it became clear that individual extreme events do not have much influence on the phreatic surface when they are isolated in one simulation. In order to conclude whether the extreme precipitation has any significant influence at all, it is interesting to look at the simulation results behind the background of 'realistic' precipitation. In order to do this, a baseline scenario needs to be set. This baseline will be given by a simulation with 9500 days of rain (26 years) as measured in Rotterdam. To make it more realistic, the evaporation of each day is subtracted from the fallen rain. The location difference between Rotterdam and Groot-Ammers is neglected.

The input file for the precipitation and evaporation comes from the KNMI and is shown in Figure 7.1. From this loading file only the first 9500 days are used.

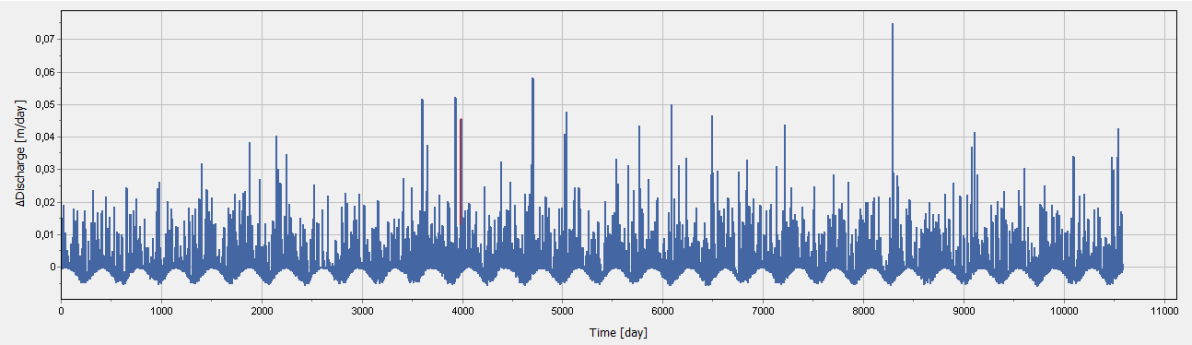

Figure 7.1: 29-year net precipitation at Rotterdam as documented by the KNMI.

Applying this to the clay dike with soil structure deterioration and the sand dike gives quite a different result compared to the individual events. If the first 26 years of the signal above are applied to the clay dike, its phreatic surface rises to the top layer and saturates the entire core. See Figure 7.2 for the begin situation and Figure 7.3 for the situation after 26 years of normal rain. As one can see, the dike gets entirely saturated in that period.

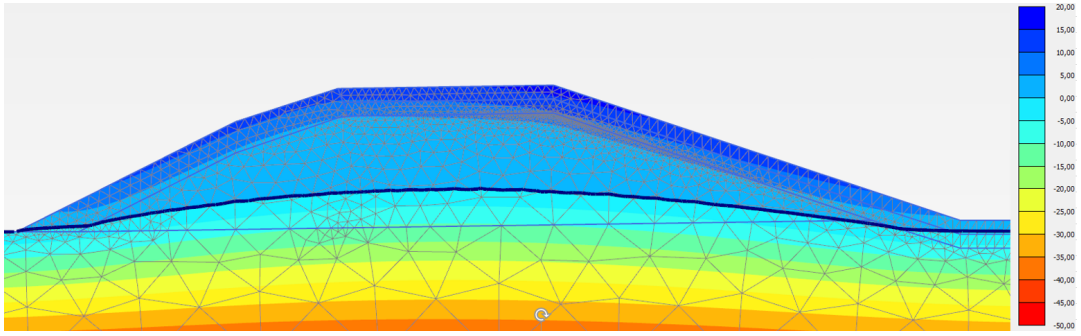

Figure 7.2: Active pore water pressure in clay dike with soil structure deterioration at the beginning of the 26 year period of measured precipitation.

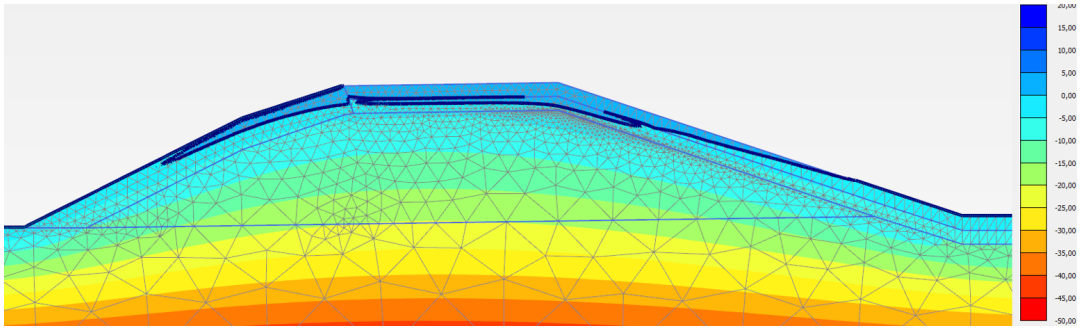

Figure 7.3: Active pore water pressure in clay dike with soil structure deterioration at the end of the 26 year period of measured precipitation.

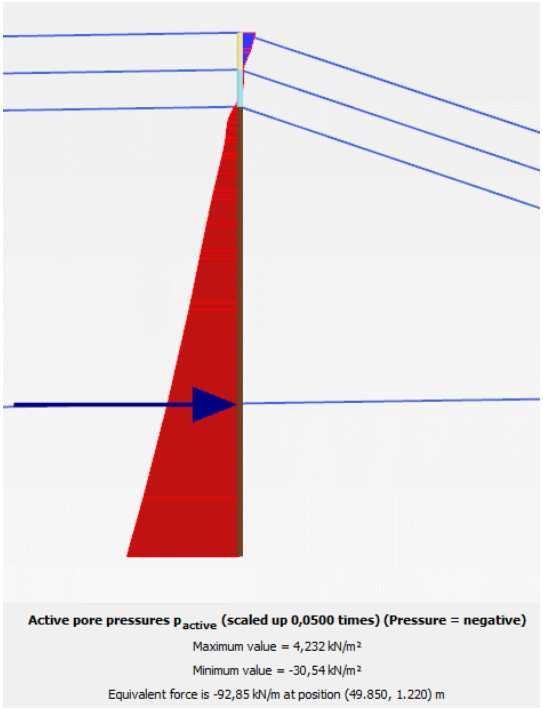

(a) Active pore water pressure over depth in clay dike with soil structure deterioration at the end of the 26 year period of measured precipitation.

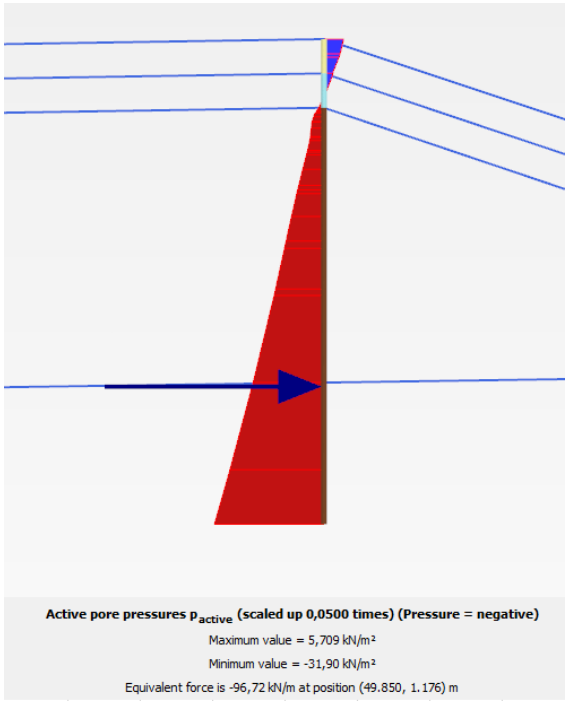

(b) Active pore water pressure over depth in clay dike with soil structure deterioration at the end of the 52 year period of realistic precipitation.

Figure 7.4: Active pore water pressure over depth in clay dike with soil structure deterioration at the end of the 26 and 52 year period of realistic precipitation.

However, something remarkable is happening. While the phreatic surface, being the pores where the water pressure is larger than the atmospheric pressure, has risen by several meters, the active pore water pressure in the subsoil barely changes. Every shade change in color in the Figure 7.3 is consistent with half a meter water column change in pressure. In Figure 7.4a, the actual pore water pressure over depth below the inner crest is shown. The Figure gives a pore water pressure at $-0.83mN.A.P$ of $30.54kN/m^2$, while the phreatic surface is located at $+5.39mN.A.P$.

This pore water pressure is linearised from the phreatic surface to the depth of the output point and compared to the hydrostatic pressure in Figure 7.5. The difference between both line is almost a factor 2, which is quite a lot. It would mean that in reality the pore water pressures inside the dike are much lower in reality, and therefore the effective soil stresses much higher. Thus the level of safety with respect to inward macro stability is actually higher than is assumed now, as the friction forces along the slide plane are higher.

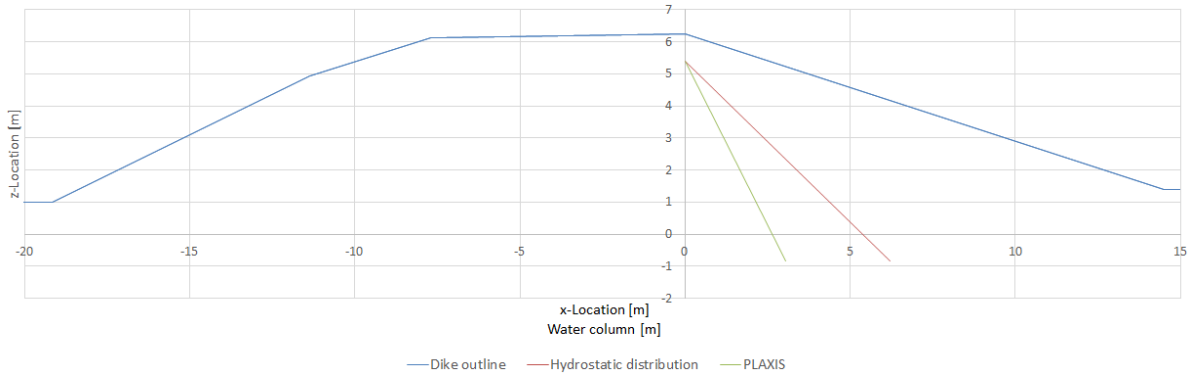

Figure 7.5: Linearised pore water pressure distribution below the inner crest compared to hydrostatic pressure in a clay dike after 26 years of rain.

The simulated phreatic surface rise in the graphs is based on the pore water pressure simulated roughly 1 meter below N.A.P.. As a consequence, the phreatic surface rise in all the graphs presented before can actually be higher than the pore water pressures suggested. To check whether this effect gets less in time, the simulation with real rain is doubled in time to 52 years and the cross section pore water pressures are checked again, see Figure 7.4b. This Figure gives a pore water pressure at $-0.83mN.A.P.$ of $31.90kN/m^2$, while the phreatic surface is located at $+5.40mN.A.P.$. Comparing these values to the hydrostatic pressure, gives Figure 7.6. This Figure is of course roughly the same as the 26 year case.

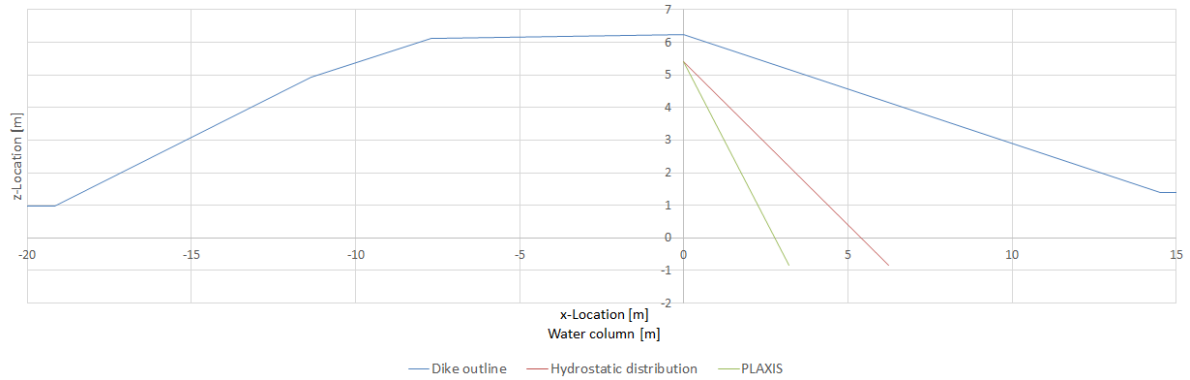

Figure 7.6: Linearised pore water pressure distribution below the inner crest compared to hydrostatic pressure in a clay dike after 52 years of rain.

To check the development of the pore water pressure in the output location in time, three line are plotted in the graph in Figure 7.7: the pore water pressure as simulated in the output location, the pore water pressure development in a scenario without rain, and the relative pore water pressure. The last one is the same as all the other graphs, ergo the simulated one minus the reference scenario.

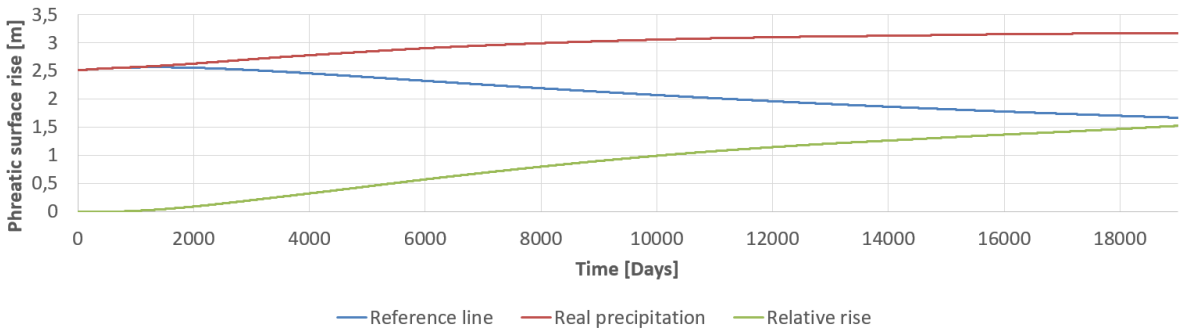

Figure 7.7: Simulated pore water pressure, reference scenario pore water pressure, and relative pore water pressure over 52 years time.

As can be seen the values of the red line around 9500 days (26 years) and 19,000 days (52 years) are indeed the values found in Figure 7.4: 30.5 and 31.9kN/m^2 or 3.05 and 3.19 meter water column. The reference scenario is shown separately to show the influence of the reference scenario on the relative phreatic surface rise. It becomes clear that by far the largest part of this relative rise is due to the lowering of the pore water pressures after the prewet scenario. The development of the actual pore water pressure in the output point is already nearing an asymptote, suggesting an equilibrium but transient state. The pressure distribution in this state is still far from hydrostatic. For a very small part, it is caused by the flow velocity of the water. The flow velocity in the almost impermeable clay core is however so small that it definitely cannot explain the total difference. Maybe it is caused by the suction properties of the soil, trapping the water as a sponge and prohibiting the pore water to fully add its weight to the water column. Of course it could also be in the chosen soil properties or PLAXIS settings. This all is, however, speculation and the exact cause is not within the scope of this thesis.

Figure 7.8 shows the development of the sand dike and the clay dike over the course of the first 26 years. In reality, the influence of rain on the phreatic surface is less than the graphs suggests, as for each day the 24-hour sum of the precipitation is applied uniformly over the day. And as concluded in the previous chapter, this is the most preferable loading case, infiltration wise. Nevertheless, the effect is ignored.

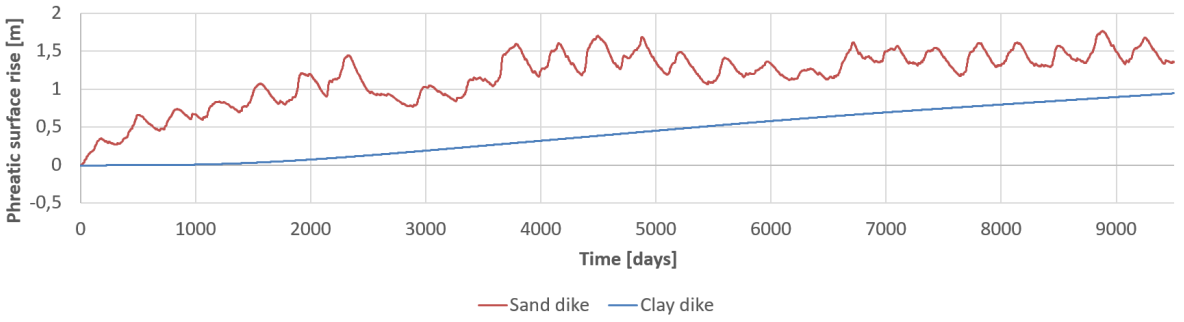

Figure 7.8: Relative phreatic surface rise of the sand and the clay dike when 26 years of realistic precipitation is applied.

The first thing that catches the eye, is of course the turbulent character of the sand dike versus the steady climb of the clay dike. This difference in behaviour is as one would expect, based on prior knowledge. However, comparing Figures 7.3 and 7.10, both depicting the dike at t = 9500 days, the difference between the phreatic surface rise of the clay dike and sand dike would be somewhere around 3 meters rather than $-0.5m$. Again this is due to the non-hydrostatic character of the clay dike. Whereas the pore water pressures in the sand dike are approximately hydrostatic, see the area below the phreatic surface in Figure 7.10.

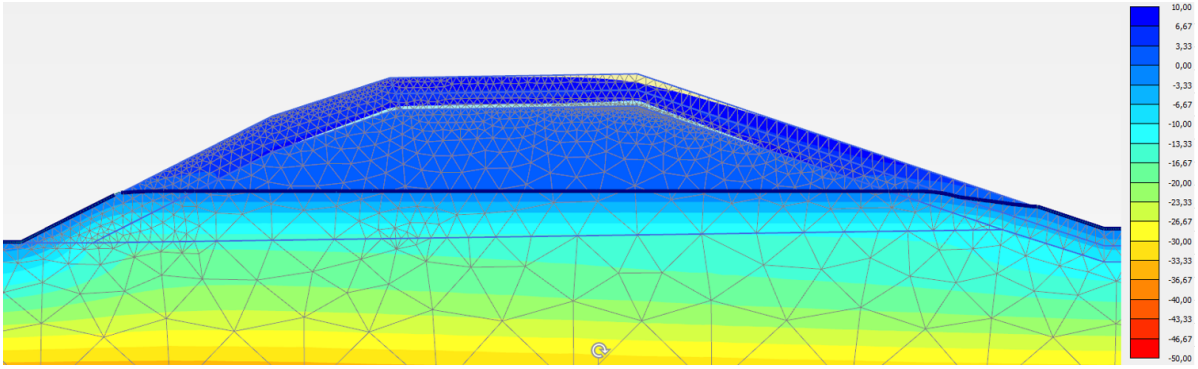

Figure 7.9: Active pore water pressure in the sand dike with soil structure deterioration at the beginning of the 26 year period of measured precipitation.

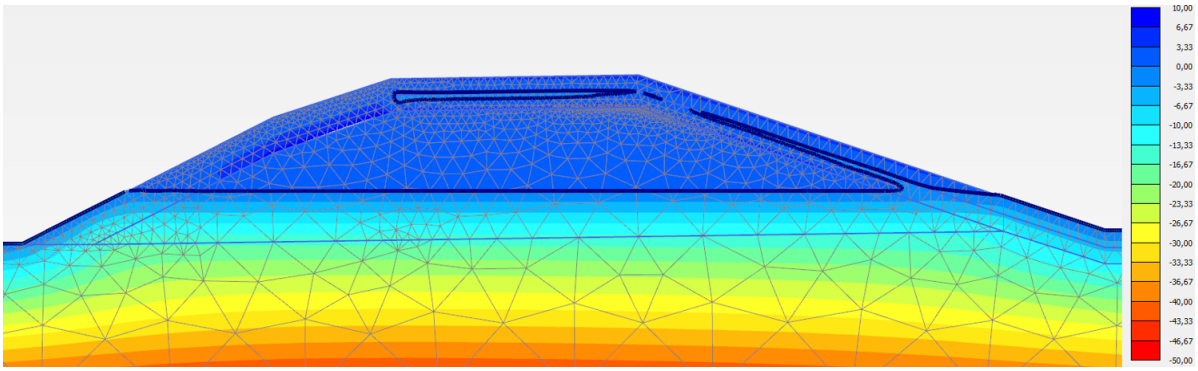

Figure 7.10: Active pore water pressure in the sand dike with soil structure deterioration at the end of the 26 year period of measured precipitation.

The pressure distribution in the sand dikes are more or less hydrostatic, also the equilibrium state of the phreatic surface is reached rather quickly and it then fluctuates with the seasons around a certain level.

In this section it becomes clear that within clay dikes there is a difference between the phreatic surface level as the point where the pore water pressure is equal to the atmospheric pressure ($p = p_{atm}$) versus the definition based on pressure points 1 meter below N.A.P. used in this thesis. The question is whether this difference is a problem. To answer that, first remember the research question:

How do water levels, precipitation, overtopping and soil properties influence the inward macro-stability through the shape and level of phreatic surface in river dikes?

The phreatic surface is related to inward macro-stability. That is why the output point below the outer crest is picked and this is also why the phreatic surface based on the pressure deep in the soil is more important than where the actual surface is. Slide planes observed with macro-instability, especially the severe ones, are rather large and reach below the surface level of the hinterland. The resisting friction force of the slip plane is affected by the pore water pressure at that location and not by how much of the dike above it is fully saturated. Therefore, this theoretical surface rather than the location of the $p = p_{atm}$-line is more useful here.

On the other hand; what is ignored in these PLAXIS calculations, but is of important for macro-stability is the weight of the soil on the driving side of the slip plane. The $p = p_{atm}$ phreatic surface line is off course of importance for the weight of the soil as wet soil is heavier. However, this effect is expected to be rather small, as the clay dike already has a saturation of at least 95% (see all the Figures in Section 6.2). So increase in weight by the surface is little. In the case of the sand dike, it would matter a lot, but there the pressures are more hydrostatic and thus the difference between the simulated pressures at the output location and the $p = p_{atm}$ saturation surface will be much less.

7.2. Results based on altered real precipitation input

In order to check the influence of extreme event against a more natural background, four extra experiments are conducted. The input signal of a 8-day uniform rain event is substituted in the original signal in Figure 7.1. This is done at three different times: fairly at the beginning on day 11, in the middle at day 3018 and near the end at day 8436.

Furthermore, to check whether extreme precipitation events matter at all the input signal is altered a lot by replacing every day it rains by the 1/10 year 24-hour precipitation, $40.7mm$. This way, it is tested if only the number of rainy days matter rather than the intensity of the rain. The results for these four experiments applied to the clay dike are presented in Figure 7.11. Mind that this is the only graph where the results are presented compared to the starting situation and not a reference scenario. The aim of the graph, however, allows interpretation compared to each other.

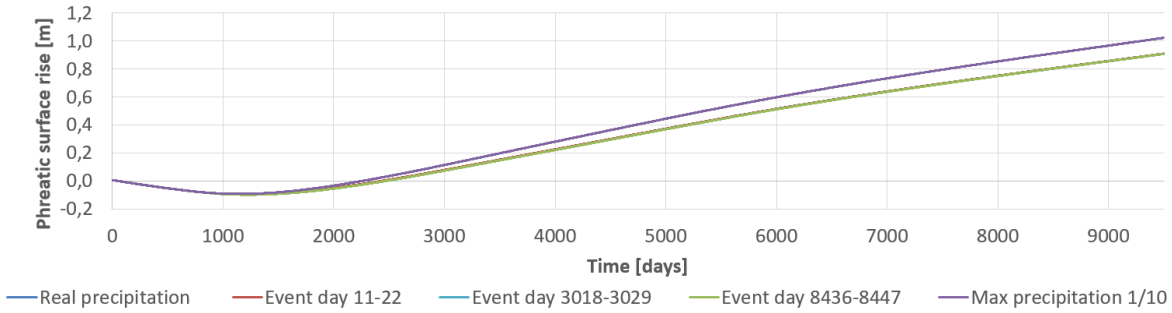

Figure 7.11: Phreatic surface rise of the clay dike for several 26 years scenarios. Blue, red and cyan lines are below the green one.

It becomes immediately clear that replacing the precipitation sum of every rain day with the 1/10 year volume does have a influence on the pore water pressures in the dike. Although it might not be as much as one would expect. Over the course of 26 years of rain only an extra $15cm$ is added. This is very little considering the fact of the extreme loading nature of the simulation.

Also, when only one 1/100,000 raining event is added to the loading series, almost nothing changes, the effect of this intense rain event of 8 days, does next to nothing when placed in the entire precipitation measurements of 26 years. The placing of this event in time also doesn't matter (blue, red and cyan lines are below the green one).

For the sand core, the results are presented in 7.12. Here the influence of the 1/100,000 year uniform rainfall is noticeable. It lifts the surface with about $25cm$ and then returns to its reference state within 500 days or so.

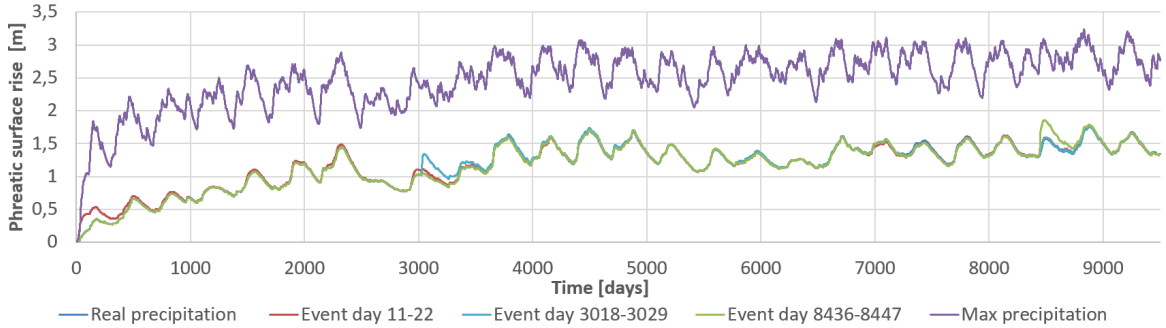

Figure 7.12: Relative phreatic surface rise of the sand dike for several 26 years scenarios.

The extreme case lifts the surface to an entire new level. However, around this new equilibrium level, the rise keeps having the same kind of pattern as the real precipitation. Although the standard deviation around this new mean is larger. This can be explained by the fact that when the surface is higher, so are the pressures inside the dike. Thus, when several dry days occur, the dike empties faster due to higher pressure. It also gets filled up again quicker due to the heavy rains, leading to the higher standard deviation in the signal.

7.3. Deterministic calculations based on WBI 2017

In Chapter 3, the TAW[2004] is mentioned as the current method to implement the phreatic surface in a deterministic way. For the dike designing engineer this is the standard method that should be used when more detailed data is not available. To recap:

Using Figure 7.13, the phreatic surface for an impermeable dike on an impermeable subsoil for a high water level scenario without any numerical modelling needs to be calculated as follows (so no precipitation or overtopping influence):

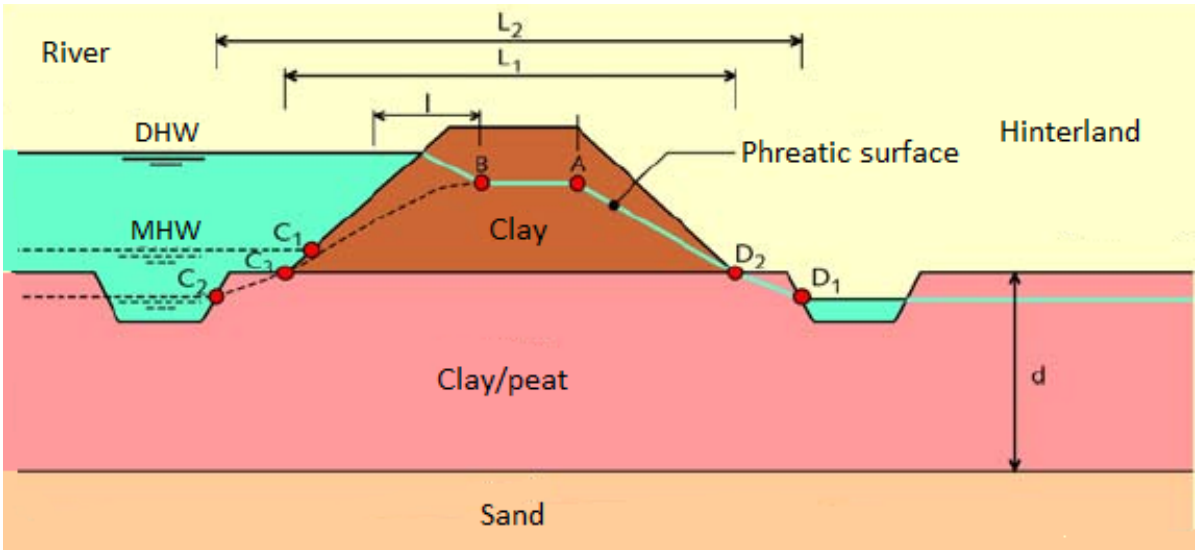

Figure 7.13: Clay dike and peat/caly as subsoil. Phreatic surface during DHW. Dotted line gives phreatic surface during normal conditions. Source: TAW [2004], [11].

$$A = \min(C + \frac{L}{X}, \quad D + \frac{L}{X}, \quad h_{crest} - 0.3) \tag{7.1}$$

where

$$X => \quad \text{if} \quad d < 4.0m \qquad X = 10$$
$$\text{if} \quad d > 4.0m \qquad X = 8$$

Using the case study all the numbers can be inserted in the formulas. The thickness of the aquitard, d, was set to 7 meters based on the measurements in Appendix C, so $X = 8m$. This leads to a phreatic surface level below the inner crest of:

$$A = \min(0.99 + \frac{33.69}{8}, \quad 1.4 + \frac{33.69}{8}, \quad 6.12 - 0.3) = 5.201m, \tag{7.2}$$

where the first constraint leads to the lowest result. The formula used by the TAW for the level of the phreatic surface in a clay dike seems pretty good for a first estimate. Since the level of the phreatic surface in the clay dike when realistic precipitation was applied, is around 5.4m N.A.P. However, another problem is encountered for this primary river dike: this combination of levels, gives an interpretation issue for the dike used in this thesis. As the standard level of A, is already higher than the 1/100,000 high water wave. The method suggested by the TAW does not include this scenario, and is thus incomplete. With respect to inward macro stability this incompleteness is not of any interest, but for outward macro stability it is. First, ignoring this incompleteness, the method of the TAW is applied blindly: The horizontal location of point B is given by the horizontal intrusion length as seen from the point where Mean High Water (MHW) touches the dike, see Figure 3.9. This is a time dependent process, as can be seen in both the formula and the figure. The intrusion length can be calculated with:

$$I = \sqrt{\frac{2 * k_z * h_0 * t}{n_z}} = \sqrt{\frac{2 * 0.01 * 3.285 * 7}{0.597}} = 0.88m \tag{7.3}$$

where

$$k_z = 0.01 \text{ Hydraulic conductivity dike material } [m/day]$$
$$h_0 = (2 * (4.17 - 0.99) + 4.485 - 0.99)/3) = 3.285 \text{ Water depth } [m]$$
$$t = 7 \text{ Duration high discharge causing DHW } [day]$$
$$n = 0.597 \text{ porosity dike material } [-]$$

To say something about the infiltration distance in time by a high water wave, Figure 6.6 is used. I is the horizontal distance from the point where mean high water touches the dike to where it connects to the surface already in the dike. In this case the dikes toe is taken as the mean high water in winter season. The peak of the high water wave occurs 7 days after the quick rise of the water level starts. This leads to an infiltration distance slightly less than the top layer thickness. In this case however, the resulting surface would be outside of the dike, see Figure 7.14.

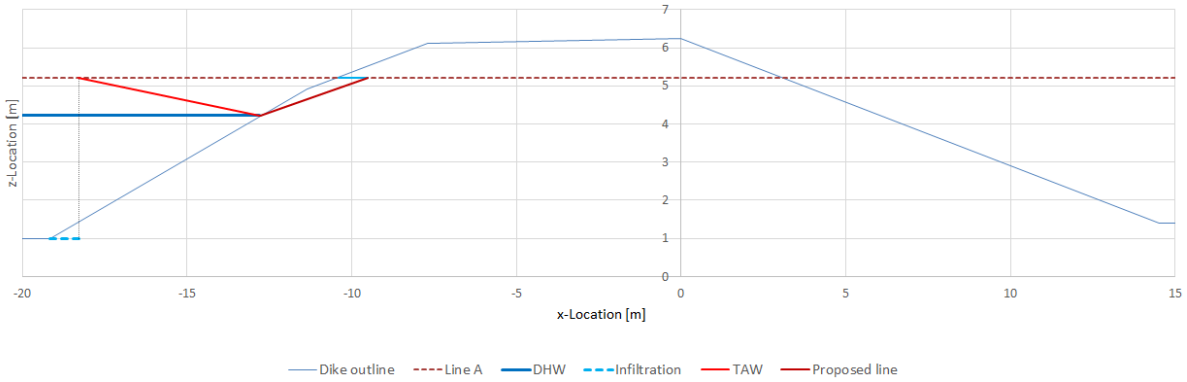

Figure 7.14: Phreatic surface when design high water is below internal phreatic surface. In addition; proposed phreatic line is presented.

There is also a line within the dike; this is a proposed surface location, based on Figure 7.3. Point B, still somewhere on line A, is some distance inside the dike. For now, the same 0.88 meter as the calculated infiltration distance is used as an example. This gives roughly the right location, but that is merely a coincidence. A new formula for this horizontal distance needs to be developed; again dependent on hydraulic conductivity and probably porosity, but independent of design high water and time. Other research will have to investigate this further. The resulting phreatic surface is proposed to be drawn from the point where design high water touches the outer slope to the calculated point on line A. So now, the proposed method would be:

1. Calculate location point A (as in TAW)
2. Check if proposed point B is outside of dike
3. If not; proceed with TAW method. If so apply new proposed method with still to be calibrated formula.

For the sand core dike, the TAW proposes another method. The sand on clay scenario is rather straight forward. According to the TAW on needs to apply half of the design high water as to where the water penetrated through the clay surface. In this case it would be $0.5 * (4.485 - 0.99) = 1.75m$.

Comparing this to Figures 6.15 and Figure 6.14 this rule of thumb is reasonable. Especially in Figure 6.15 it is clear that the max phreatic surface inside the dike is roughly half the height of the maximum level of the high water wave.

The rules of thumb above are for the cases when no measurements are available. If there were measurements Figures 3.6 and 3.7 are to be used. The correctness of the second is already treated above, the method of the rainfall scenario however, is not. For rainfall, it states one should take the measured level under normal conditions and then apply an extra head of $0.8m$.

However in this research, the adding of extra head to the phreatic surface based on one extreme precipitation event is not backed up by any of the results. This method of coping with precipitation influence of the phreatic surface seems quite off and no addition at all seems closer to reality than 0.8 meters. Naturally, the research presented in this thesis is not backed up by any measurements or practical experiences, while this might be the case for the method in the TAW[2004].

8

Conclusions

8.1. Conclusions

This thesis aims to extend the existing knowledge on the influence of hydraulic loads on the phreatic surface in primary flood defences. Especially the effect the phreatic surface level would have on the inward macro-stability failure mechanism is considered. The starting point for this research is the new WBI2017 which introduces a new way to look at failure probabilities: rather than calculating the return period for a load and then applying that load, one looks at a (failure) probability per year. This new way of looking at probabilities allows for a more natural incorporation of length effect, combining of failure mechanisms, and full probabilistic approaches.

In continuation of these renewed ways, this thesis aims to aid in the probability per year that a dike fails due to macro-instability of the inner slope induced by a high phreatic surface inside the dike. Therefore, loads, soil parameters, and their influence on the phreatic surface need to be simulated. Simulated, because none of these extreme loads have been measured by man, but they are the result of statistical research and extrapolation. The research question as presented in Chapter 2 summarizes this problem:

How do water levels, precipitation, overtopping, and soil properties influence the inward macro-stability through the shape and level of phreatic surface in river dikes?

The initial set up to answer this question was a semi-probabilistic approach; where different loads and combinations of loads, with different probabilities of occurrence per year, were applied to a FEM-computer model of a real dike. These loads were to influence the phreatic surface each in their own way and subsequently have influence on the failure probability of the dike. The runs, done in PLAXIS, consist of 200-day simulations where loads are applied to either a clay dike or a dike with a sand core. The geometry is based on a case study of a dike near Groot-Ammers and the loads are extracted from the Hydra-NL program and STOWA reports.

However in none of the simulations, the phreatic surface rise was of such severity that it could cause a dike failure. This statement is made, not because all loads were actually applied in simulations, but based on the fact that this research starts with applying the heaviest loads, with a probability per year of 1/100,000, and even then no significant influences were registered.

So to answer the research question: In the chosen case study, with the given dike geometry, soil characteristics, dike types, and soil layer build-up, the influence of water levels, precipitation, and overtopping on the phreatic surface and the subsequent macro-stability is too small to be of any significant influence. Ergo, in none of the simulations the phreatic surface rise was of such severity that it could actually cause failure of the flood defence. This is especially true for individual events. For these single hydraulic loads, no reaction in any of the clay core dikes was registered. In the sand core dike a maximum relative rise of 21 centimeter was computed.

The study also shows that a sequence of smaller regular events lifts the phreatic surface in clay dikes more than an extreme event. When 26 years of rain are applied to the surface of the clay dike with soil structure deterioration, the dike slowly fills with water over a very long period of time. Thus a wet season or even a wet decade is more dangerous for the stability of the dikes than a rainy week or a single flood wave.

Another finding of this study is the necessity of a weathered top layer of the soil. This so-called soil structure deterioration allows water to infiltrate in the top layer. Soil structure deterioration is caused by holes

dug by animals, root canals, or by shrinkage and expansion under different weather conditions. It allows the water to be absorbed quickly and thus acts as a buffer basin. Then, the water infiltrated in this top layer can infiltrate the less permeable deeper parts over a longer period of time. Experiments with no soil structure deterioration at all, showed no reaction of the phreatic surface, as all water applied to the surface would simply run off or evaporate.

This study is the first to incorporate overtopping influences on the phreatic surface. So far, the methods would not include its effects, but these assumptions were never checked by any simulations. This thesis finds that the influence of overtopping is indeed negligible compared to certain precipitation scenarios. This conclusion is true for all dike types tested in this thesis and current methods thus need no alterations with respect to this hydraulic load.

The research also concludes that for the given soil characteristics, the uniform rainfall shape leads to the highest infiltration volumes, as all other rainfall shapes lead to more run-off. For the dike with a sand core, the maximum observed phreatic surface rise difference between a uniform and a peaked shape is 50%.

A final observation with respect to the cracked top layer, is the counter intuitive relation between the hydraulic conductivity of the top 0.5 meters and the rise of the phreatic surface. The sand dike simulations showed a higher rise with a lower hydraulic conductivity of the top layer.

There seems to exist an optimal permeability to achieve the highest infiltration into the core. This permeability is dependent on the load intensity. The optimal value ensures that almost all the water can infiltrate in the top layer with little surface run-off, while at the same time the smallest amount of water can flow sidewards inside the top layer, thus inducing more infiltration into the dike core. This effect is observed with all the precipitation shapes as well as the overtopping load. Furthermore, it explains the asymmetric phreatic surface shape observed within the clay dike when subjected to precipitation.

When comparing the results to the current methods, as given by the TAW[2004],[11], and WBI2017 ,[1]; it turns out these are sometimes supported by the findings of this thesis, while in other cases they are not. The choice not to incorporate overtopping as a phreatic surface lifting load can be defended, as this is a load with a very small probability of occurrence and can only be seen as an individual event. Therefore, it will not influence the phreatic surface notably. Furthermore, the method used on sand core dikes with a high water level load is a good first estimate, as is shown by the simulation results of this research.

However, some of the current methods are not backed-up by this study. First of all, the method to estimate the phreatic surface in a clay dike on an impermeable subsoil appeared to be incomplete: the case where the phreatic surface in the core is above the design water level is not included; while the issue is hardly unique for primary flood defences. Based on the results in this rest of the study, this thesis proposes a rough sketch of a method that could be applied, although more research and calibration will be needed. The assumption that the phreatic surface in the core is independent of river water levels is supported by the results in this report.

Secondly, the method to estimate the phreatic surface in an extreme precipitation event appears to be too safe. From this research it can be concluded that both in sand and especially in clay dikes the addition of 0.8 meters to the measured phreatic surface as the consequence of a single extreme event is unnecessary. For sand dikes an impact of 25 centimeter is found, while for a clay core no effect is registered.

Thirdly, the results of this research also suggest that the assumption of the TAW[2004], that the pore water pressure has a hydrostatic distribution below the phreatic surface, is on the safe side. The simulations done in Chapter 7 suggest that the pore water pressure distribution in clay dikes below the surface is not really hydrostatic. However, more experiments are needed to back-up this claim, since the differences are too large to explain fully. In general, based on this study, it can be said that some of the deterministic methods in the TAW[2004] and WBI2017 are too safe.

8.2. Discussion

The conclusions above and the research behind it need to be interpreted with some footnotes due to assumptions, model limitations, and factors not taken into account. First and foremost, the chosen test case which is not the most common one. This whole thesis is based on one specific case of a primary flood defence at the river Lek. The geometry is assumed to be constant and is not considered as one of the variables, but the chosen case had a larger influence on the results than initially assumed. First of all, the dike has just been upgraded and strengthened by IV-Infra. Furthermore, as the dike is a primary flood defence, the distance between the crest of the dike and the actual 'equilibrium' phreatic surface is relatively large. As stated in Chapter 5, under normal winter conditions the equilibrium water level in the river is around +0.85m N.A.P. and -0.6m N.A.P. in the hinterland, both well below surface level. Therefore, the dike is permanently losing water to the

subsoil and every day without rain or a flood wave the dike is drained further. Also, as it is a large embankment, the flowing path from a load applied to surface level to the actual phreatic surface is very long. Because of diffusion, the load is 'stretched out' in space and arrives at the phreatic surface over a longer period of time, resulting in a smaller effect of the load. In that sense, the chosen dike is a difficult case with respect to the phreatic surface.

Another consequence of the depth or the equilibrium phreatic surface was the complexity to define a good begin state for the simulations. But this begin situation does influence the results, especially for the clay dike. The starting position was based on the measured phreatic surface below the crest. However, to reach this level, the procedure of pre-wetting with extreme rain followed by a long period of time with no precipitation is questionable. The water is already dropping and the soil above the surface contains less water than it would have in reality. To tackle this problem, the reference scenario is introduced and the results are presented corrected for this scenario. Still, it is not ideal, as the influence of the pre-wetting is present in the results of Chapter 6. For the results in Chapter 7, the effects of the pre-wetting are less and probably negligible. To have the correct starting situation of the dike for the simulations would require more measurements of the phreatic surface inside the embankment as a time series. It could then be related to the actual precipitation, but even then, the soil build-up and soil parameters should be modelled more precisely to approximate this 'real' begin state.

As is with most simulation research, the soil is not realistic. The complex and unknown layer build-up and the different parameters per layer are nearly impossible to simulate. Hidden sand layers, both horizontally as well as diagonal, can act as water infiltration paths. The sounding of the dike crest, in Appendix C, suggests that this far more complicated layer build-up is present within the used dike. With respect to hydraulic conductivities, some often observed an-isotropic behaviour is used in the model. But important parameters, such as the porosity of the soil and the residual saturation, are not backed up by any measurements or data. The same goes for the "Van-Genuchten"-parameters. Furthermore, the effect of the third dimension is not taken into account. Again, water could also flow inside the dike parallel to the river and thus be lost to a dimension not considered in these simulations. By assuming homogeneous clay cores and top layers, the saturation process could take longer in the simulation than it would in real live. The clay dike in Figure 7.11 is still getting filled and has not yet reached a equilibrium after 26 years of 'realistic' precipitation. The question is if it would take that long in reality or, due to more sandy layers, would go faster in reality.

Furthermore, there are some smaller points where one could ask if it is a right or justified decision. This thesis uses only the pressure development in a single output point, 7 meters below the inner crest, to represent the entire phreatic surface. The influence of overtopping and precipitation loads could me more severe and more direct closer to the inner dike toe.

The influence of load combinations was, in the end, not tested. This was mainly caused by some technical problems in PLAXIS, but also due to the minimal effects of individual events. The testing of rainfall in combination with overtopping or water levels need to be tested in further research. However, based on the results in this study, little extra insight will probably be obtained.

Finally some remarks on the overtopping loads and scenarios are to be made. In order to properly apply the overtopping loads, the head files have been averaged over a period of twenty seconds. In Appendix D it is checked whether the averaging of five waves of four seconds into one, twenty second load, has significant influence on the results. The distribution of one wave load, with a high peak followed by lower pressure is also averaged, but the implications are unknown. Also with the overtopping scenario, some small numerical instabilities occur at the outer slope, as the coarse grid cannot cope with the highly alternating character of the load. Therefore the infiltration in the outer slope might be slightly more than simulated now.

8.3. Recommendations

All the results in the report should be checked with field measurements. Also the input of soil characteristics and layer build-up needs to be checked. Measurements of the phreatic surface in time are needed to calibrate the model correctly and results from such a model would be more valuable.

Another recommendation would be to check the method of the TAW[2004] to add 0.8 meters for a heavy precipitation scenario because none of the results of this thesis support that method. However, if the dike would be less homogeneous it might be a correct rule of thumb. More research should be conducted to verify this. Also the method should be expanded for dike with the design high water below the proposed level of the phreatic surface.

The influence of the geometry is not included in this thesis and further research on its influence on the

phreatic surface might be interesting. Also the influence of the equilibrium phreatic surface is an important factor to consider. With regional dikes, for example, the equilibrium phreatic surface is always higher in the dike.

Another recommendation for further research would be to investigate the influence of the permeability of the sub top later and outer slope and maybe other soil parameters, besides the hydraulic conductivity.

Final recommendation is to investigate the non-hydrostatic pressure distribution in the clay dikes. At the moment, no logical explanation can be given, besides it being a fallacy in the program settings or program.

Bibliography

[1] WBI 2017. *Schematiseringshandeling macrostabiliteit.* Ministerie van Infrastructuur en Milieu, 2.1 edition, 2016.

[2] WBI 2017. *Bijlage II Voorschriften bepaling hydrailische belasting primaire waterkeringen.* Ministerie van Infrastructuur en Milieu, 2017.

[3] R. Agtersloot and A.J. Paarlberg. *WAQUA Productieberekeningen Bovenrivieren Rijntakken.* Deltares, 2016.

[4] J. Beersma, J. Bessembinder, T.o Brandsma, R. Versteeg, and H. Hakvoort. *Actualisatie Meteogegevens voor Waterbeheer 2015.* Stichting Toegepast Onderzoek Waterbeheer, 2015. ISBN 978.90.5773.706.0.

[5] R.W. Bijlard, G.J. Steendam, H.J. Verhagen, and J.W. van der Meer. Determining the critical velocity of grass sods for wave overtopping y a grass pulling device. *Coastal Engineering*, 2016.

[6] W.S. de Raadt, D.J. Focks, A. van Hoven, and E. Regeling. How to determine the phreatic surface in a dike during storm conditions with wave overtopping: A method applied to the afsluitdijk. *Geotechnical Safety and Risk*, 5:509–515, 2015. doi: 10.3233/978-1-61499-580-7-509.

[7] S.N. Jonkman, R.E. Jorissen, T. Schweckendieck, and J.P. van den Bos. *Flood defences Lecture notes CIE5314.* Delft University of Technology, 2nd edition, 2017.

[8] L.A. Ponsioen. Overflow and wave overtopping induced failure processes on the land-side slope of a dike. *Thesis TU Delft*, 2016. URL `uuid:a6ef81da-53a2-4e84-8829-b9a08afea2ef`.

[9] A. Rippi. Structural reliability analysis of a dike with a sheet pile wall: Coupling reliability methods with finite elements. *Thesis TU Delft*, 2015. URL `uuid:09edf3ae-6818-4c17-bd25-8b3f3414b6b8`.

[10] TAW. *Technical report on the use of clay for dikes.* Technische Adviescommissie voor de Waterkeringen, 1996.

[11] TAW. *Technisch Rapport Waterspanningen bij dijken.* Technische Adviescommissie voor de Waterkeringen, 2004. ISBN 90-369-5565-3.

[12] J.G.F. ten Bokkel Huinink. Assessment of the probability distribution of the phreatic surface in a regional flood defence. *Thesis TU Delft*, 2016. URL `uuid:7b3841dd-1eda-4fd9-aa32-5e1b074cf7c1`.

[13] J. van Dansik, C. Griffioen, T. de Meij, J.Strijker, and M. Talsma. *Statistiek van extreme neerslag in Nederland.* Stichting Toegepast Onderzoek Waterbeheer, 2004. ISBN 90.5773.261.0.

[14] J.W. van der Meer. The wave run-up simulator. idea, necessity, theoretical background and design. *Coastal Engineering*, 2011.

[15] J.W. van der Meer, P. Bernardini, W. Snijders, and H.J. Regeling. The wave overtopping simulator. *Coastal Engineering*, 2006.

[16] J.W. van der Meer, G.J. Steendam, G de Raat, and P. Bernardini. Further developments on the wave overtopping simulator. *Coastal Engineering*, 2008.

[17] J.W. van der Meer, N.W.H. Allsop, J. De Rouck, H. Schüttrumpf, and B. Zanuttigh. *Manual on wave overtopping of sea defences and related structures.* EurOtop, 2nd, pre-release october 2016 edition, 2016.

[18] A. van Hoven. Strength of clay cover layers, the influence of grass and soil structure on the shear strength of clay. *Delft Cluster*, 2008.

[19] A. van Hoven, B. Hardeman, J.W. van der Meer, and G.J. Steendam. Sliding stability of landward slope clay cover layers of sea dikes subject to wave overtopping. *Proceedings of 32nd Conference on Coastal Engineering*, 32, 2010. doi: https://doi.org/10.9753/icce.v32.structures.5.

[20] A. Verruijt and S. van Baars. *Grondmechanica*. VSSD, Delft, 7 edition, 2009. ISBN 978-90-71301-45-2.

[21] X.Yang and X.You. Estimating parameters of van genuchten model for soil water retention curve by intelligent algorithms. *Applied Mathematics Information Sciences*, 7:1977–1983, 2013. doi: http://dx.doi.org/10.12785/amis/070537.

List of Figures

List of Tables

A

Glossary

Translations & Definitions

Cunet	Road foundation
Custumized test	Toets op maat
Dike compartment	Dijkvak
Dike section	Dijktraject
Piezometer	Peilbuis
Sounding	Sondering
Surface level	Maaiveld
Cross section	Dwarsprofiel

Abbreviations

DHW	Design High Water	Maatgevend Hoog water
FEM	Finite Element Method	Eindige Elementen Methode
HCF	Hydraulic Conductivity Function	Hydraulische Doorlatendheidsfunctie
KNMI	Koninklijk Nederlands Meteorologisch Instituut	Royal Dutch Meteorological Institute
LIR	Lokaal Individueel Risico	Local Individual Risk
MHW	Mean High Water	Gemiddeld Hoog Water
MKBA	Maatschappelijke Kosten Baten Analyse	Social Cost Benefit Analysis
OT	Overtopping	Golfoverslag
RWS	Rijkswaterstaat	Department of Waterways and Public Works
STOWA	Stichting Toegepast Onderzoek Waterbeheer	Organization for Applied Water Control Research
TAW	Technische Adviescommissie voor de Waterkeringen	Technical advisory committee for Flood Defences
WBI	Wettelijk Beoordelings Instrumentarium	Legal Assessment Toolkit
WL	Water Level	Waterpeil
WRC	Water Retention Curve	Zuigspanningscurve

B

List of Symbols

Roman letters

c	Cohesion	$[N/m^2]$
d	Thickness Aquitard	m
e	Pore number	
E	Young's modulus	$[N/m^2]$
f	Slope friction (0.01 for grass)	
g	Gravitational constant	$[m/s^2]$
h	Water depth river	$[m]$
H	Wave height	$[m]$
I	Intrusion distance	$[m]$
k	Hydraulic conductivity	$[m/s]$
p	Pressure	$[N/m^2]$
q	Discharge per meter stretch (often overtopping)	$[m^3/s/m]$
R_u	Run-up height wave	$[m]$
n	Porosity	
N_i	Number of i	Integer
S	Saturation degree	
T	(Wave) Period	$[s]$
u	Current velocity	$[m/s]$
v	Velocity	$[m/s]$
z	Height	$[m]$

Greek letters

α	Slope angle	$[\circ]$
γ	Volumetric weight	$[kN/m^3]$
θ	Water content soil	
ν	Poisson ratio	
ρ	Density	$[kg/m^3]$
σ	(Soil) Stress	$[N/m^2]$
τ	Shear stress	$[N/m^2]$
ϕ	Angle of internal friction	$[\circ]$
ψ	Suction	$[m]$

Subscripts

c	crest
e	effective
r	relative
x	in x-direction
y	in y-direction

Mathematical Operators

$P(A)$	Probability of event A
$P(A\|B)$	Probability of event A given event B
$\Gamma(\cdot)$	Gamma function

Abbreviations

B2	2 Peak Precipitation Shape
C1	1 Peak Precipitation Shape
U0	Uniform Precipitation Shape

C

Data provided by IV-Infra

The data shown in this chapter comes from the measure locations show in Figure C.1. Plus the more elaborate drawings of the dike made in the 80's.

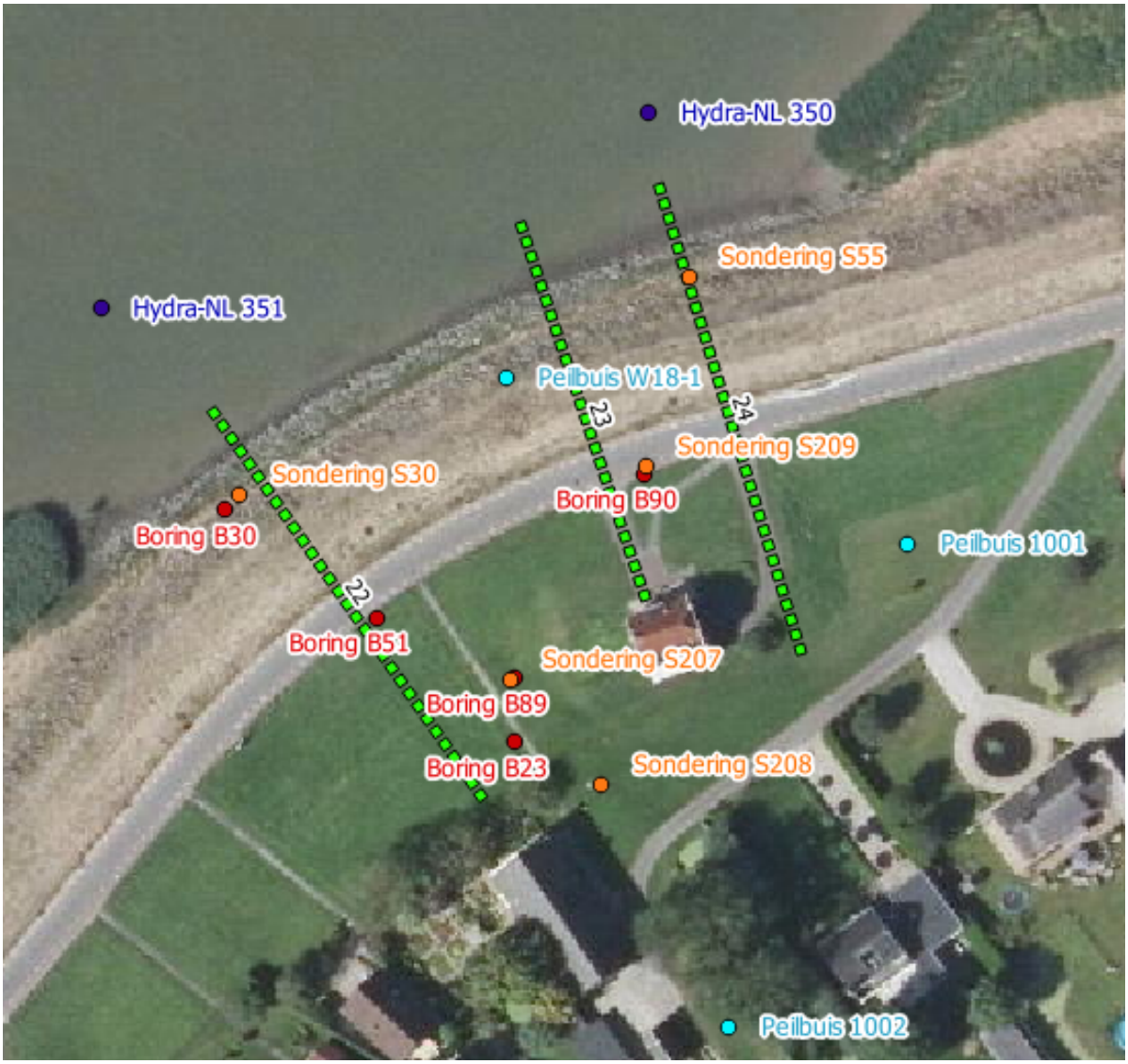

Figure C.1: Available data in the region.

C.1. Cross sections

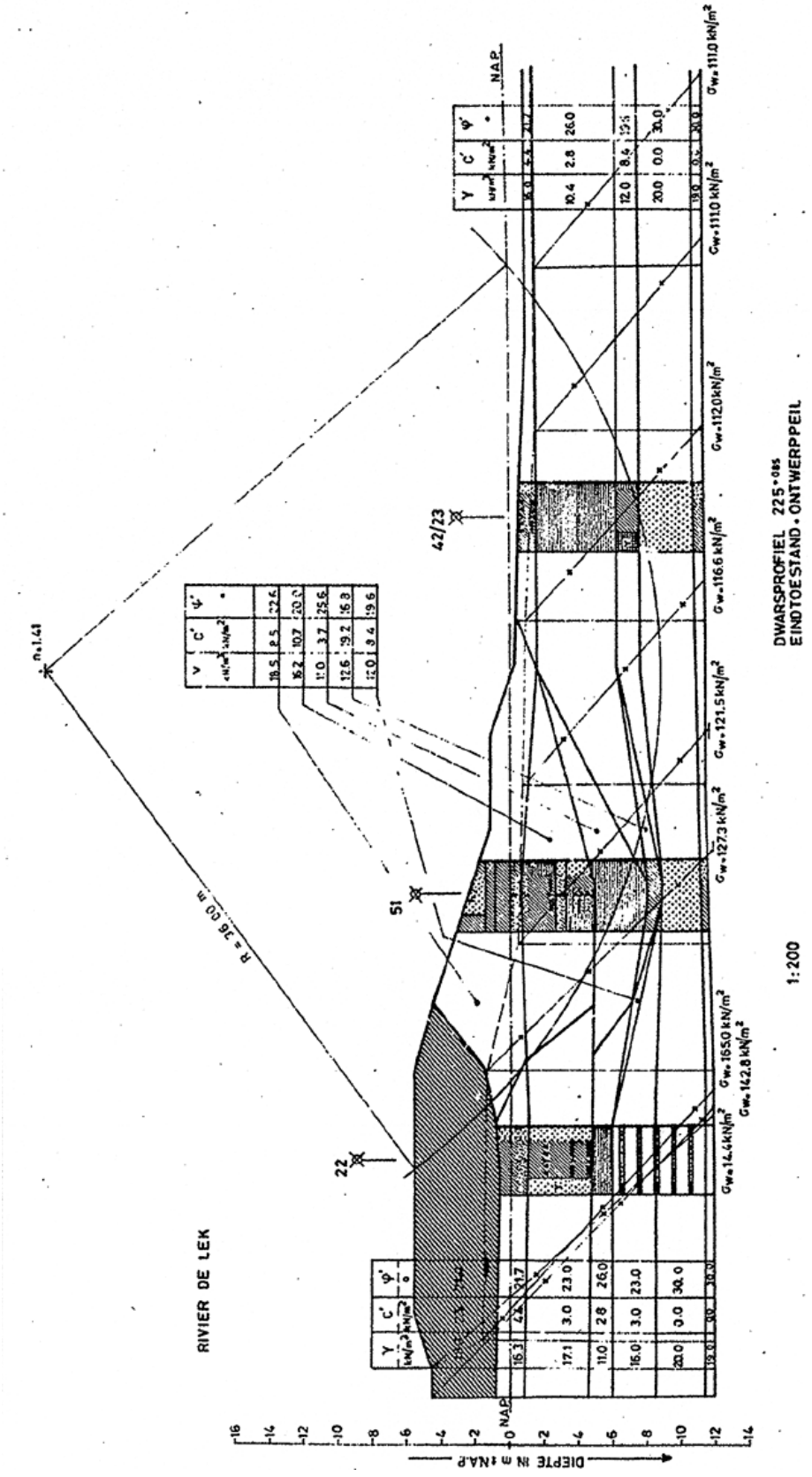

Figure C.2: Cross section made in 1982, used for geo data

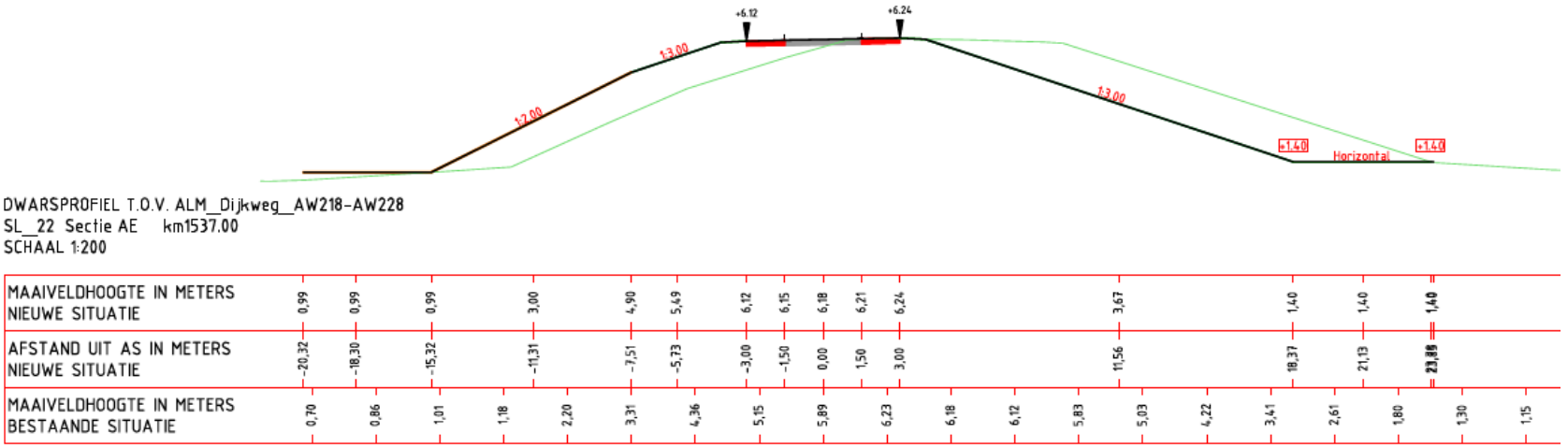

Figure C.3: Cross section 22, used as profile for runs

C.2. Borings

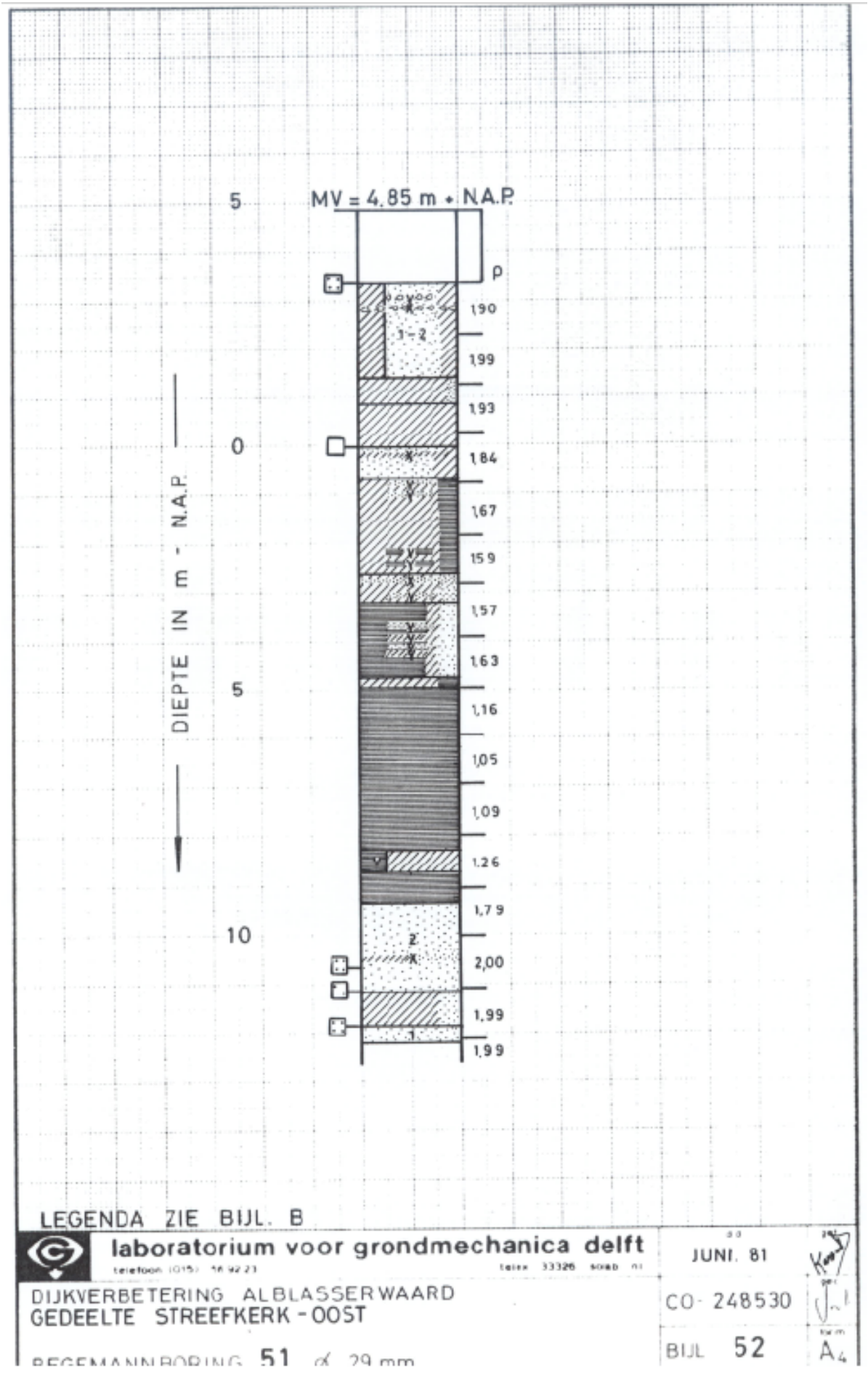

Figure C.4: Boring 51, part 1

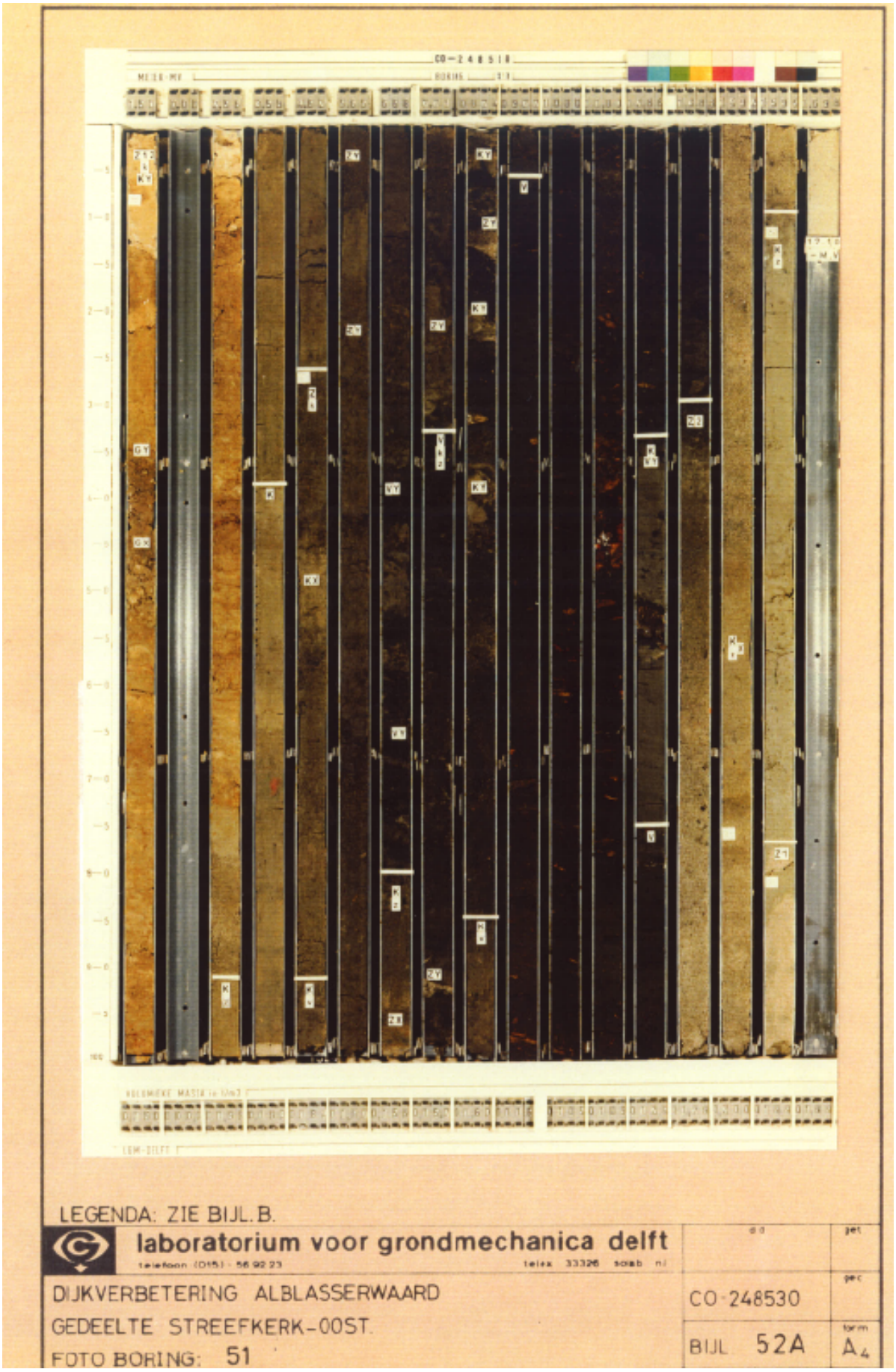

Figure C.5: Boring 51, part 2

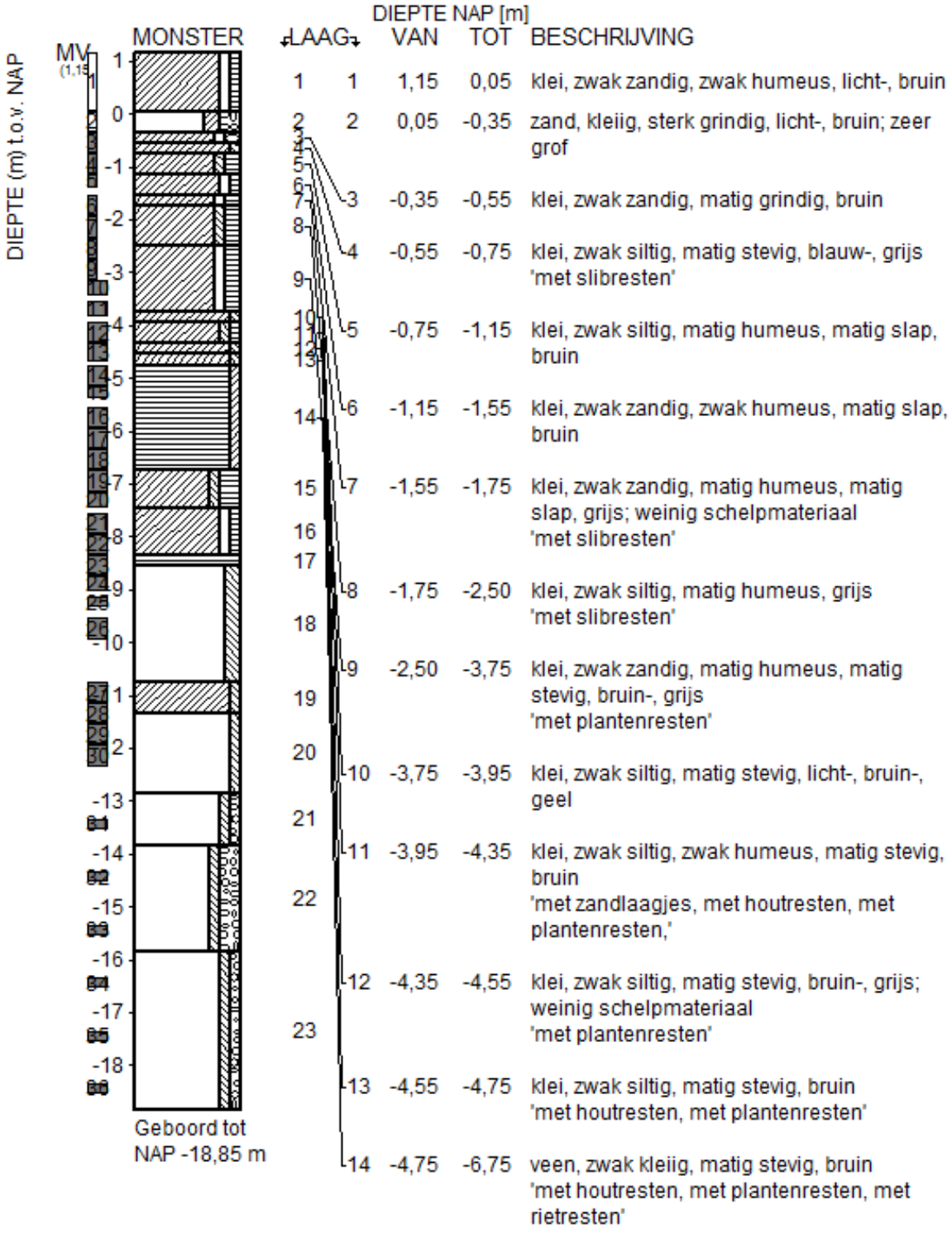

Figure C.6: Boring 89, part 1

maaiveld: NAP 1,15 m
X = 115322,57 m Y = 437194,38 m (RD)

DIEPTE (m) t.o.v. NAP

DIEPTE NAP [m]

MONSTER	LAAG	VAN	TOT	BESCHRIJVING
Geboord tot NAP -18,85 m	15	-6,75	-7,45	klei, zwak siltig, sterk humeus, matig stevig, grijs 'met houtresten, met plantenresten, met rietresten'
	16	-7,45	-8,35	klei, zwak zandig, zwak humeus, matig stevig, bruin-, grijs 'met houtresten, met plantenresten'
	17	-8,35	-8,55	veen, mineraalarm, matig stevig, bruin 'met houtresten, met plantenresten'
	18	-8,55	-10,75	zand, matig siltig, grijs-, bruin; matig grof, gelaagd, met kleilagen 'met houtresten, met plantenresten'
	19	-10,75	-11,35	klei, zwak siltig, matig stevig, grijs; kalkarm
	20	-11,35	-12,85	zand, zwak siltig, grijs; zeer grof
	21	-12,85	-13,85	zand, zwak siltig, zwak grindig, grijs; zeer grof
	22	-13,85	-15,85	zand, zwak siltig, sterk grindig, grijs; zeer grof
	23	-15,85	-18,85	zand, zwak siltig, zwak grindig, grijs; zeer grof
				Einde Boring B89

Figure C.7: Boring 89, part 2

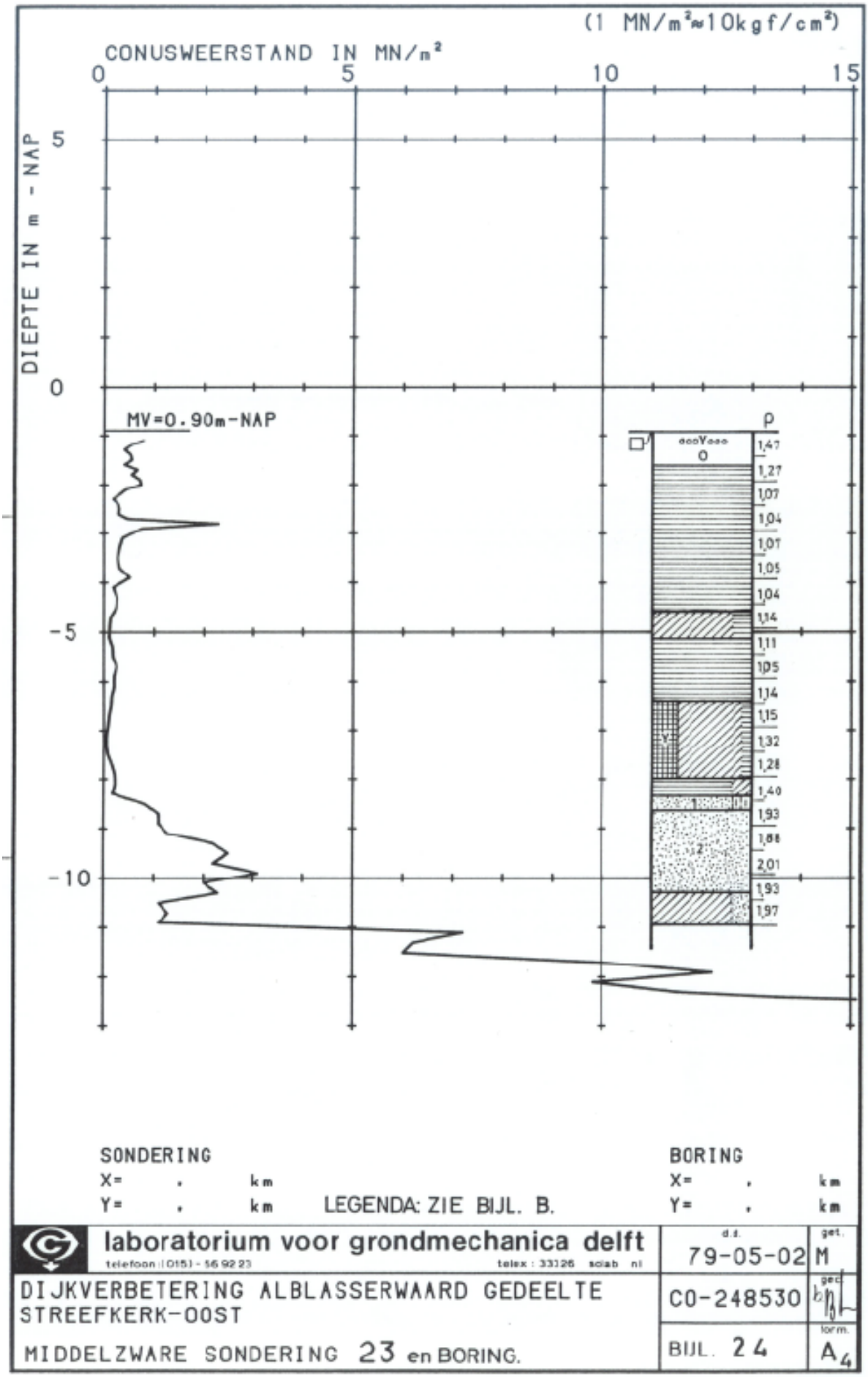

Figure C.8: Boring 23, part 1

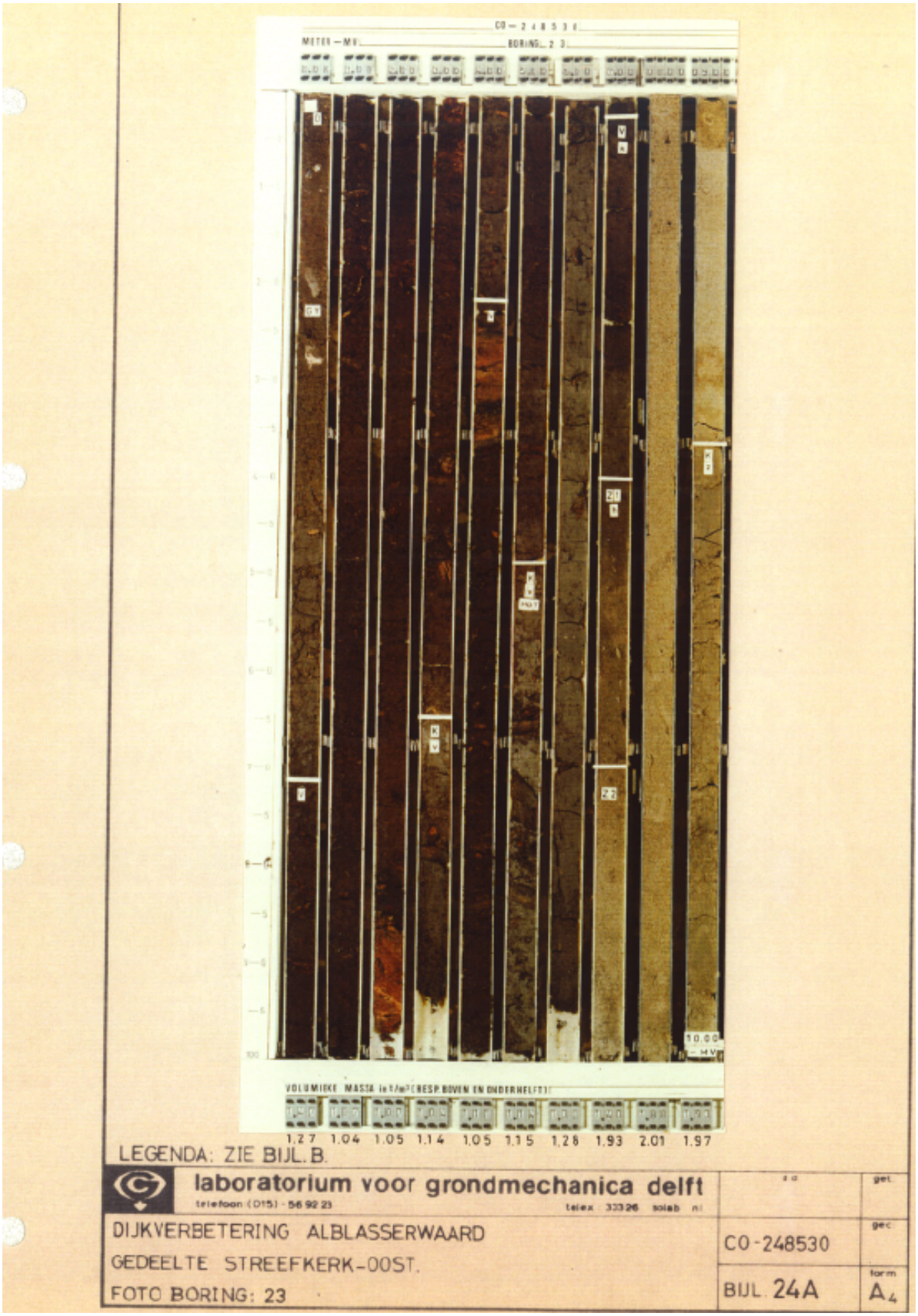

Figure C.9: Boring 23, part 2

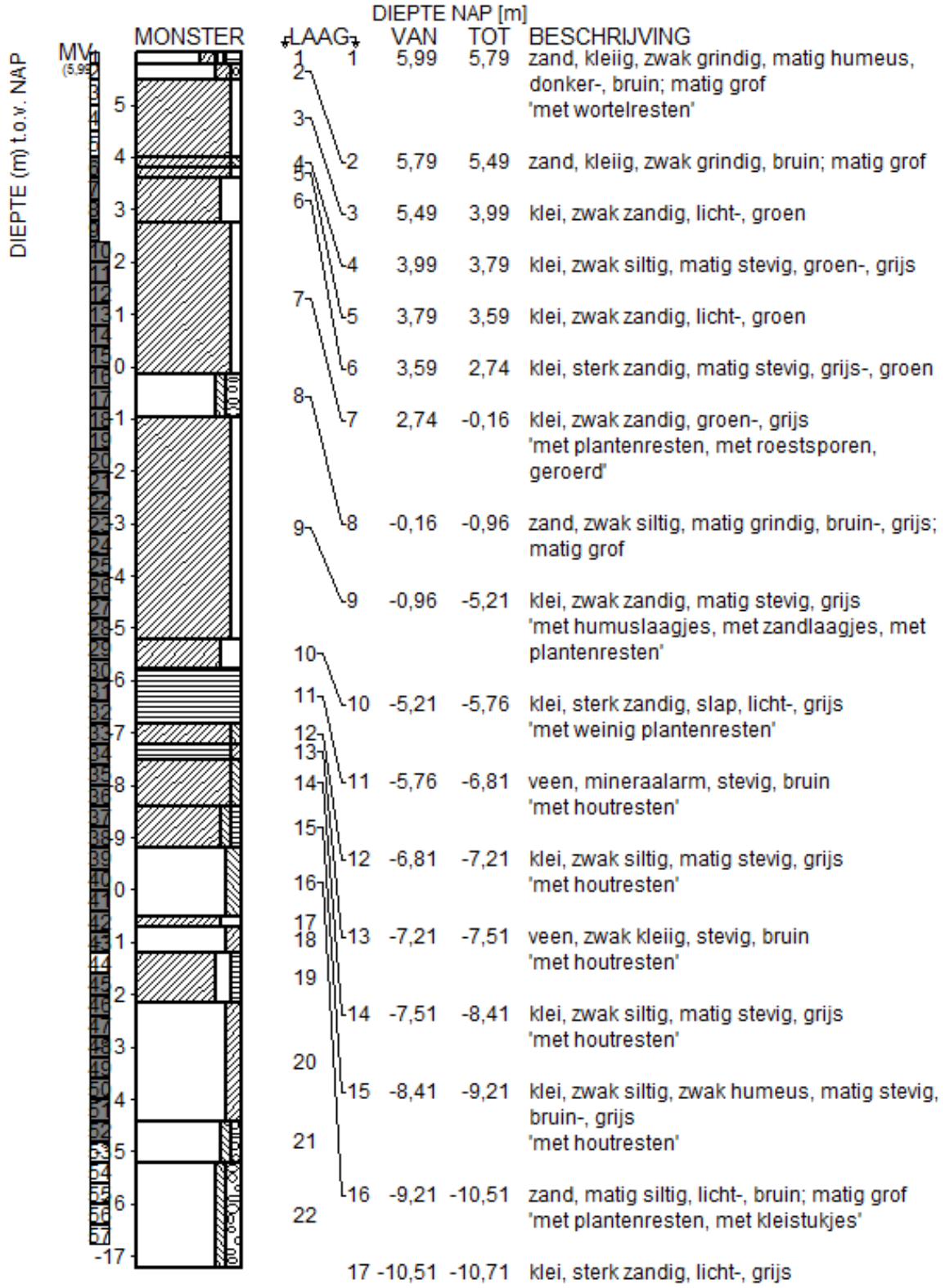

Figure C.10: Boring 90, part 1

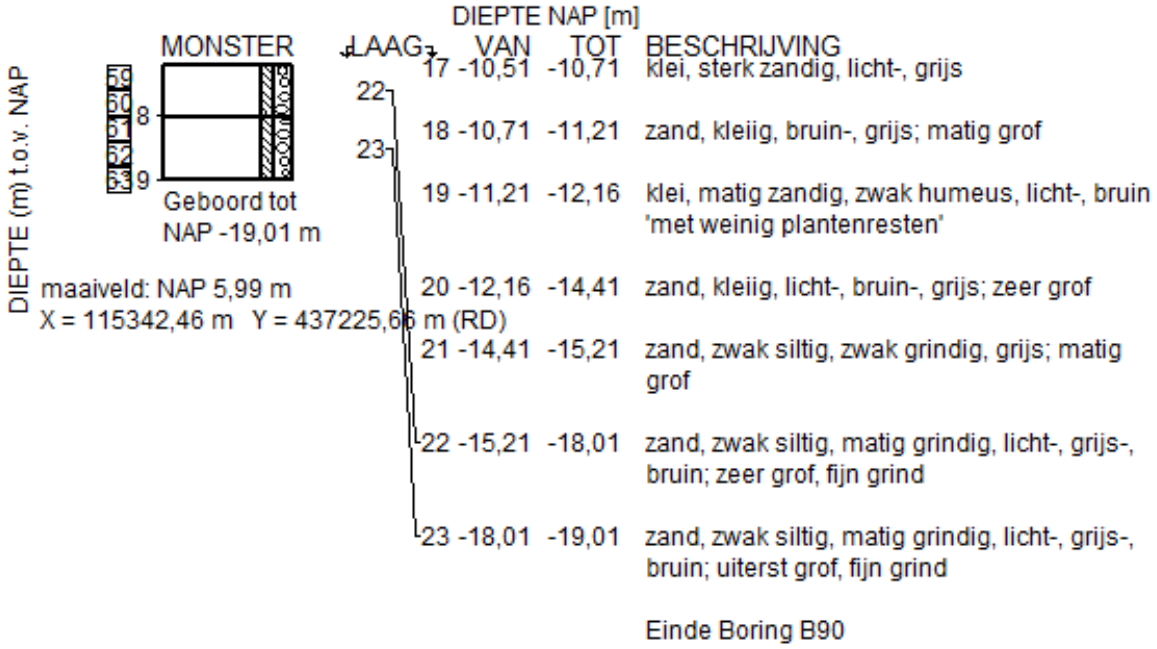

Figure C.11: Boring 90, part 2

C.3. Soundings

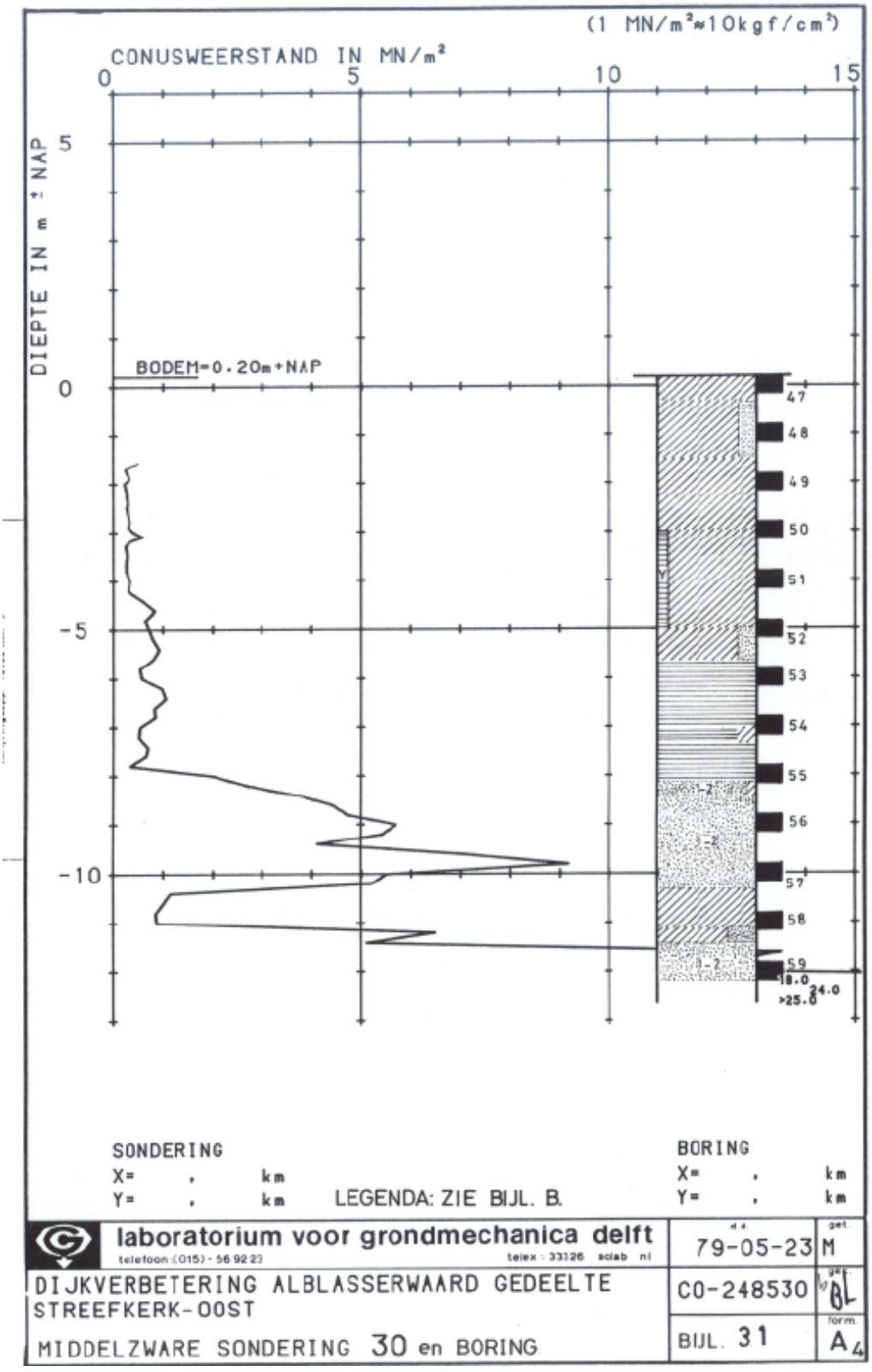

Figure C.12: Sounding and boring 30

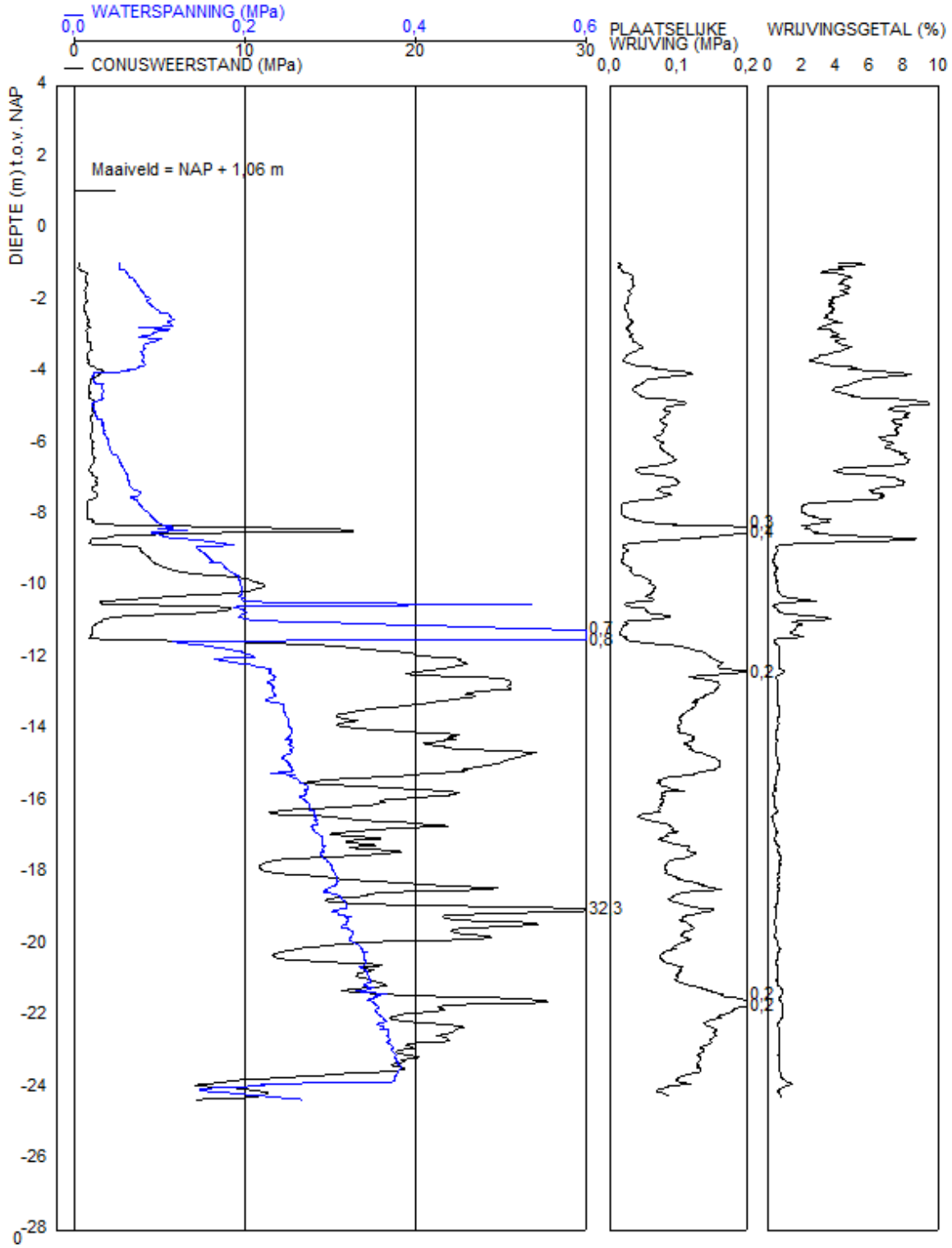

Figure C.13: Sounding 207

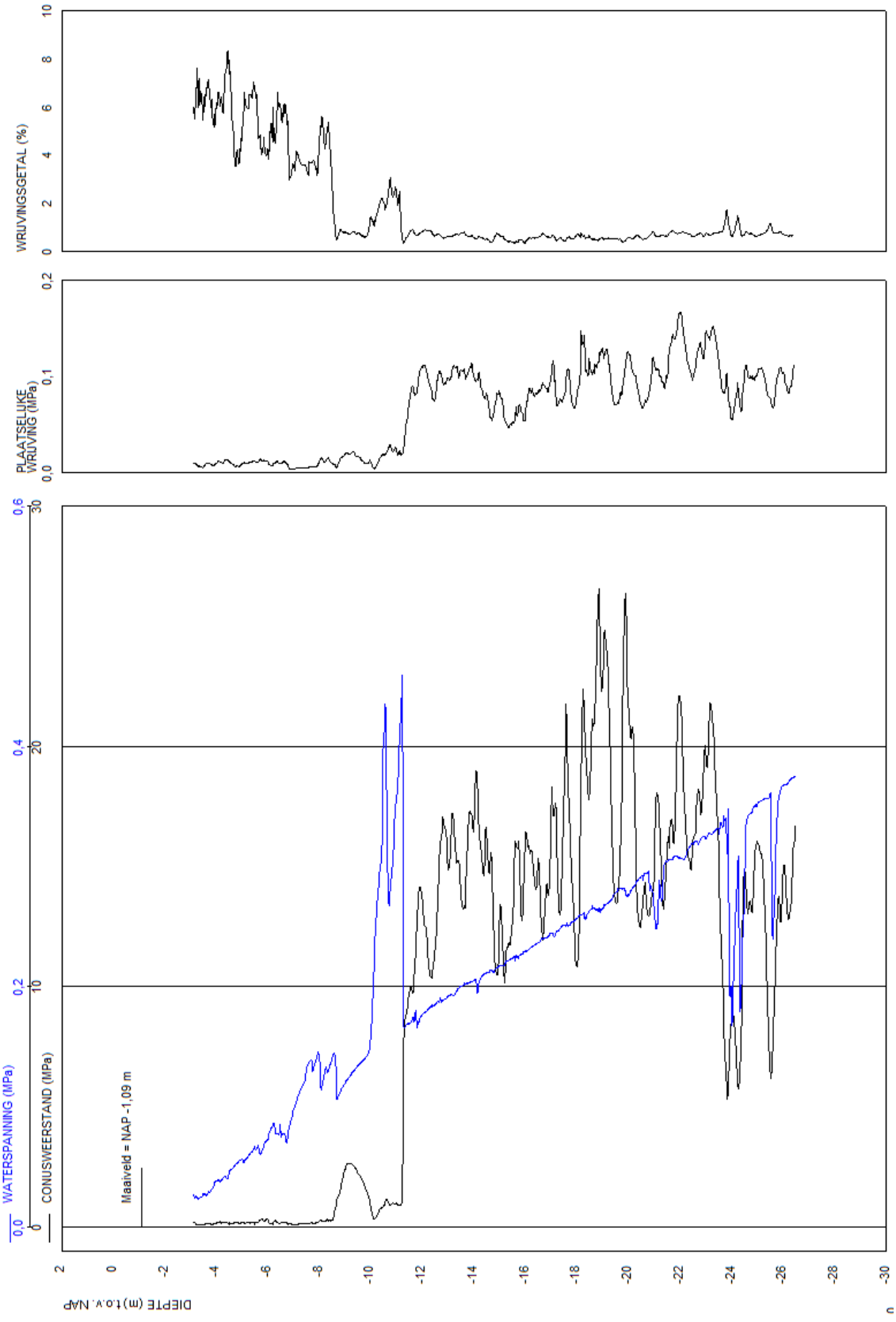

Figure C.14: Sounding 208

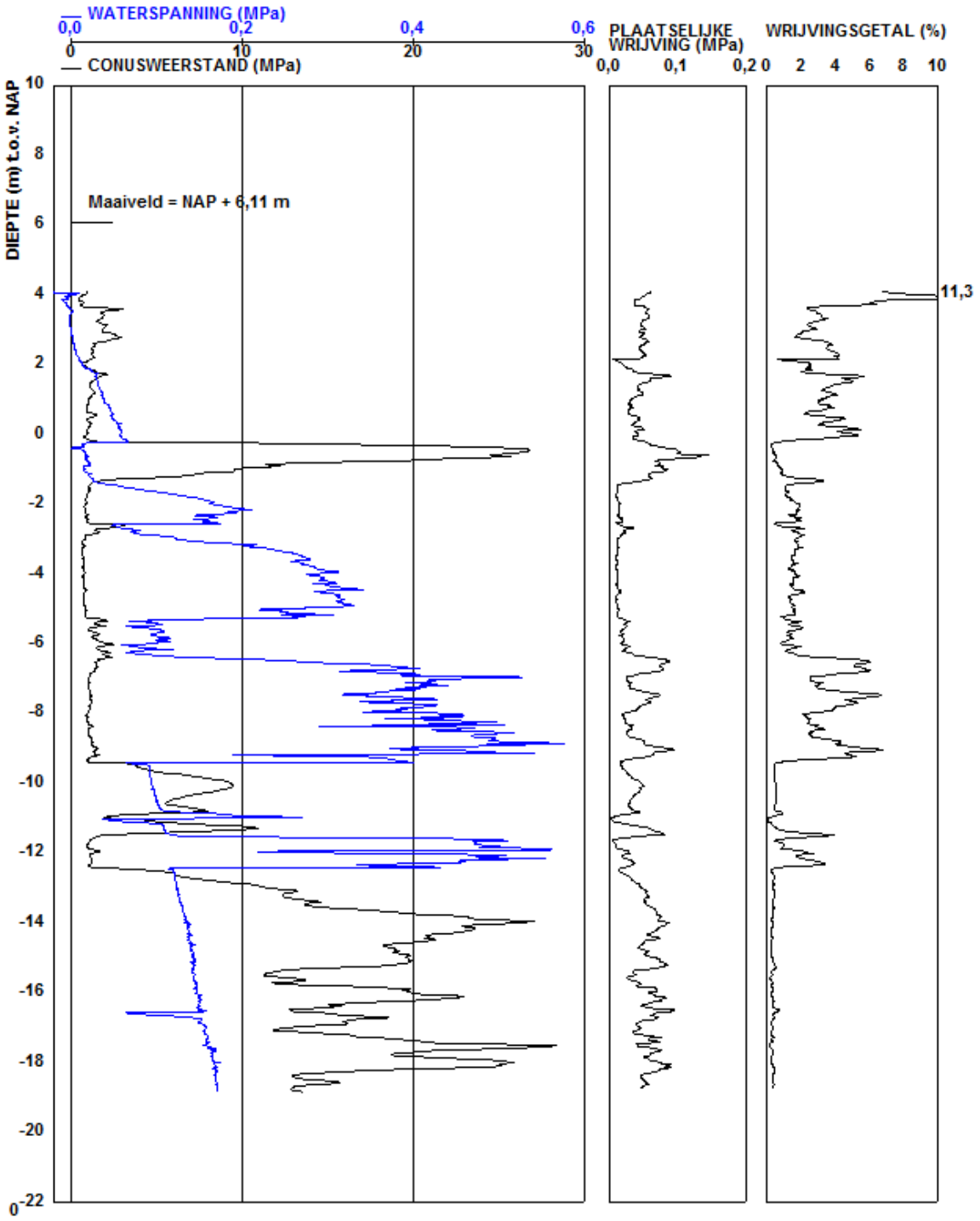

Figure C.15: Sounding 209

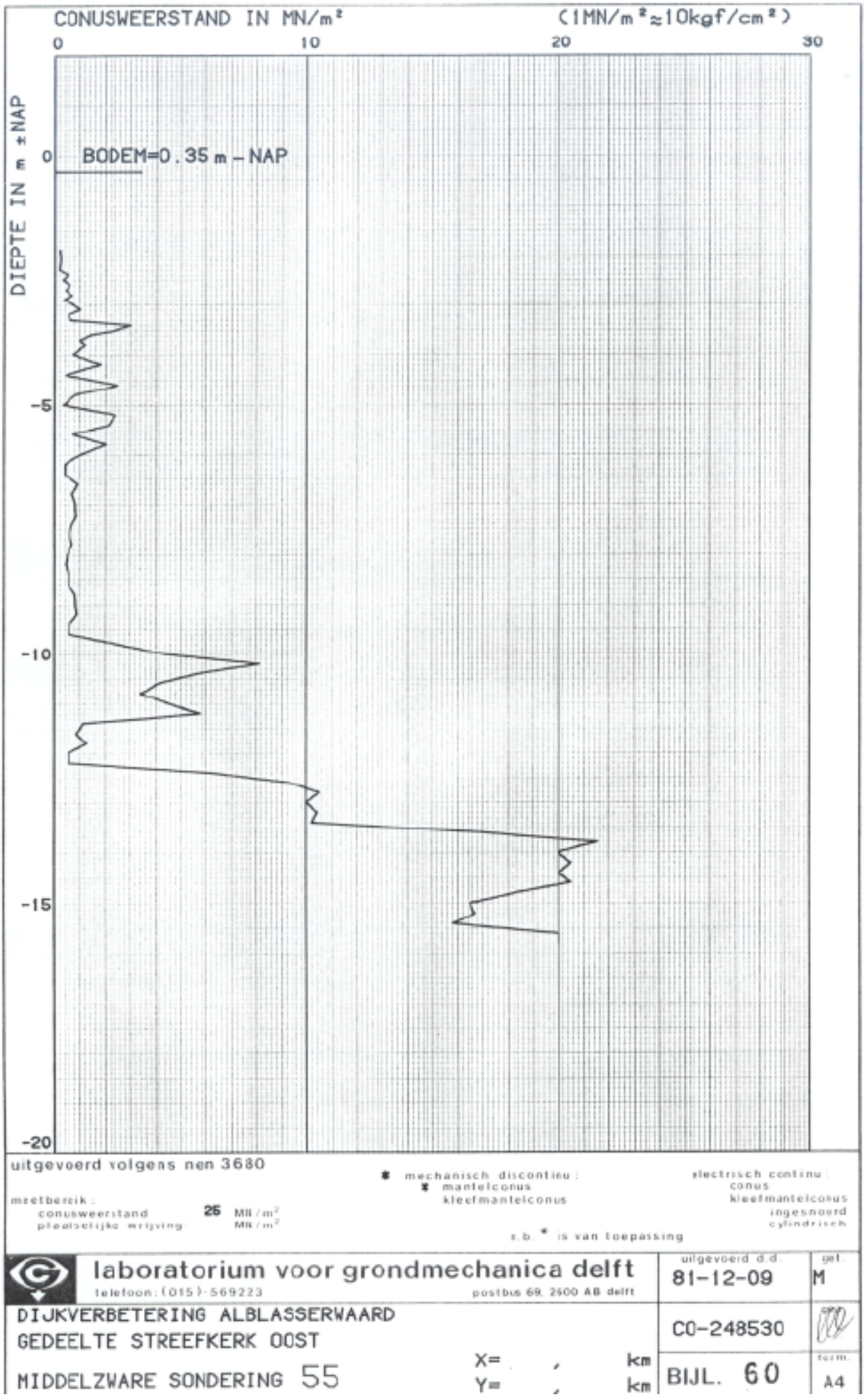

Figure C.16: Sounding 55

C.4. Piezometer measurements

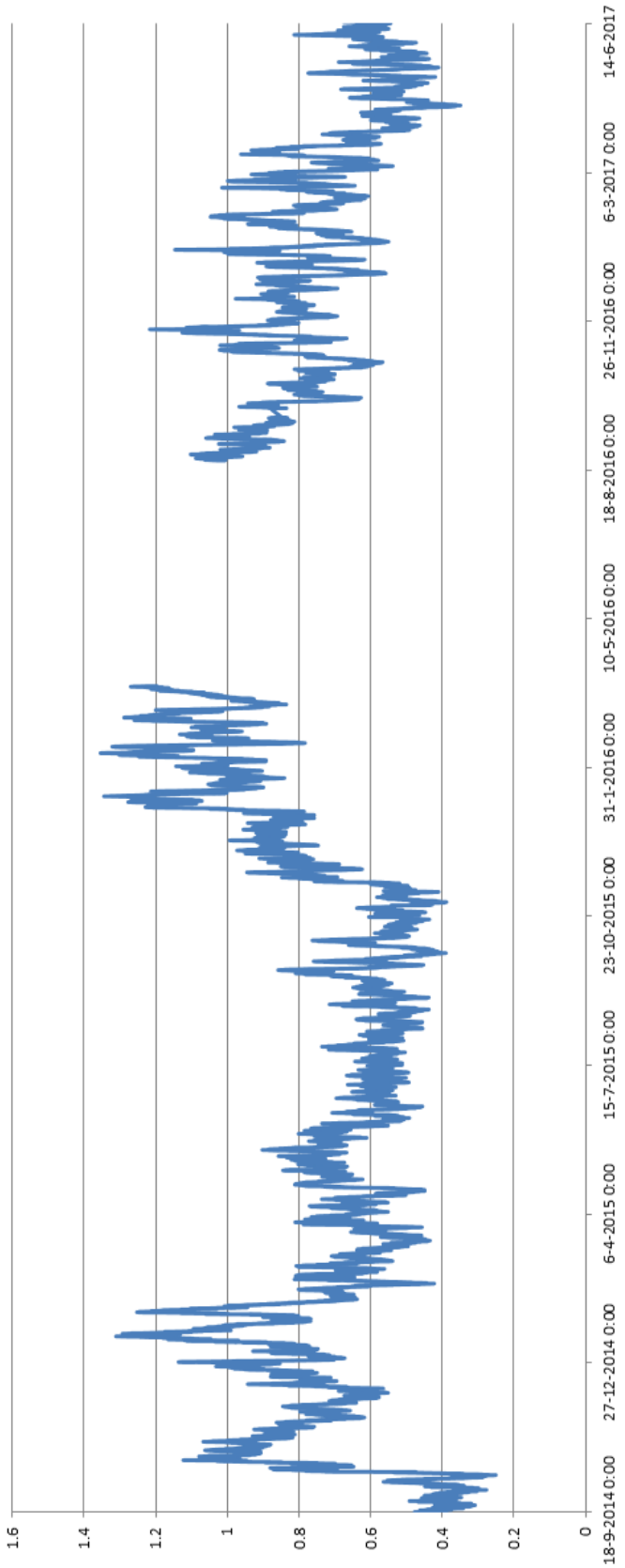

Figure C.17: Data series from piezometer W18-1. Not corrected for settlement.

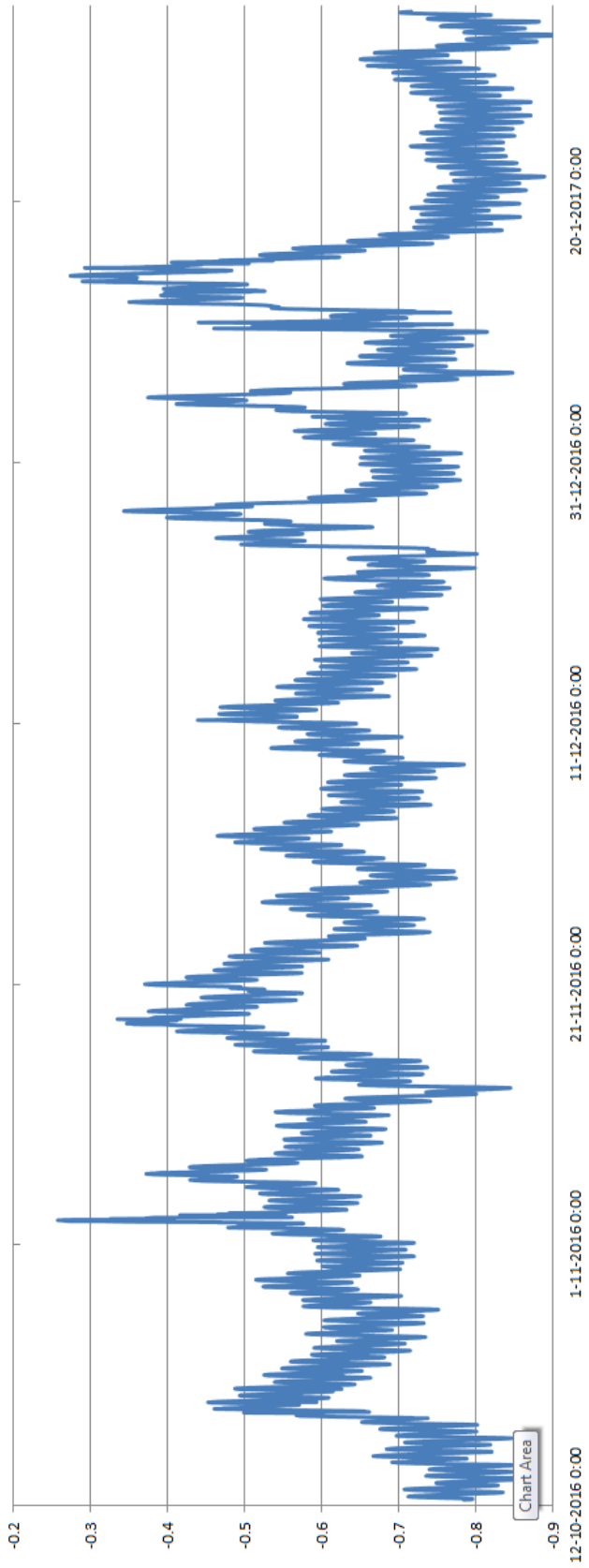

Figure C.18: Data series from piezometer 1001 at -8.46 meter N.A.P. Not corrected for settlement.

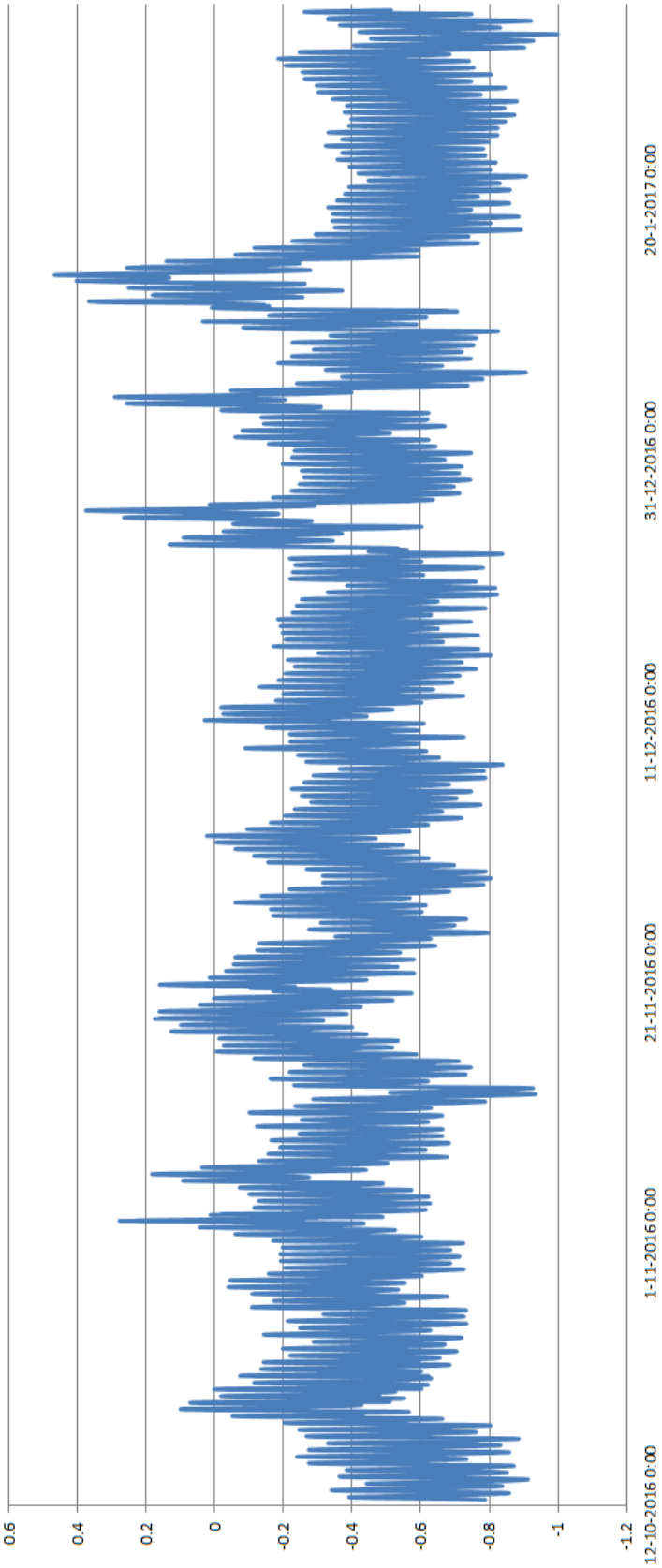

Figure C.19: Data series from piezometer 1001 at -12.45 meter N.A.P. Not corrected for settlement.

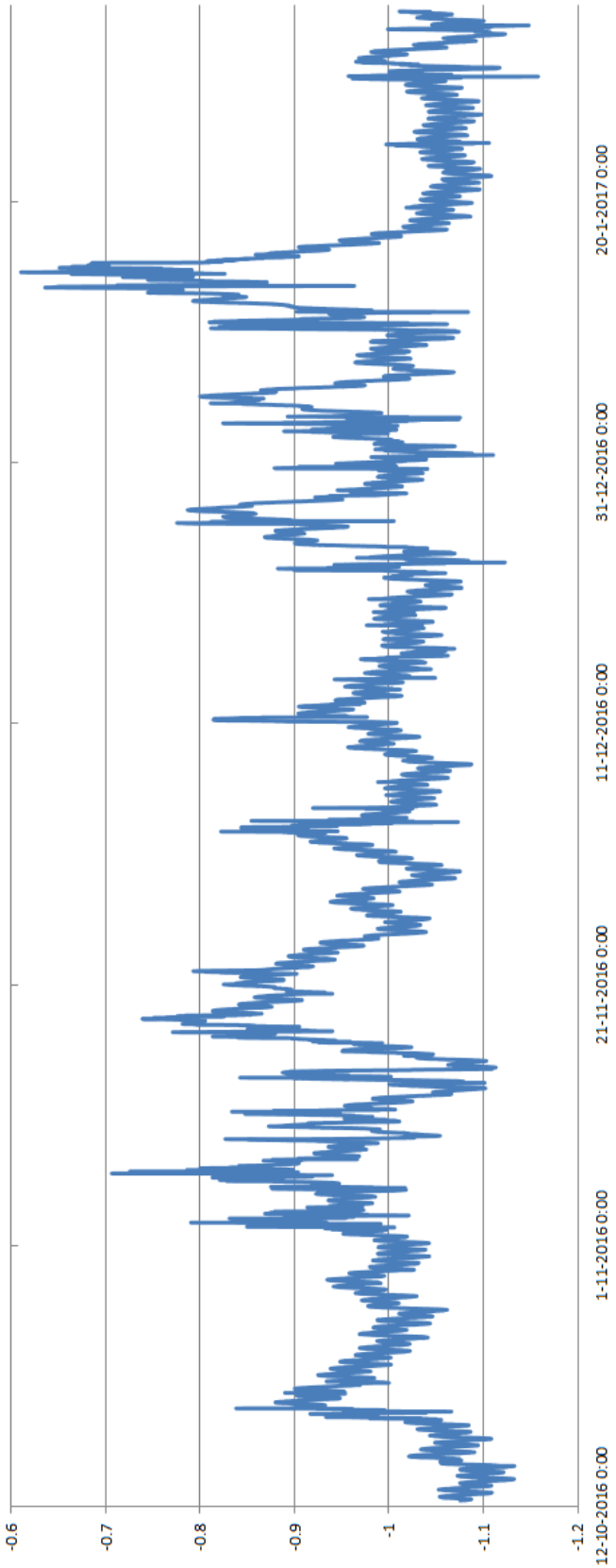

Figure C.20: Data series from piezometer 1002 at -8.64 meter N.A.P. Not corrected for settlement.

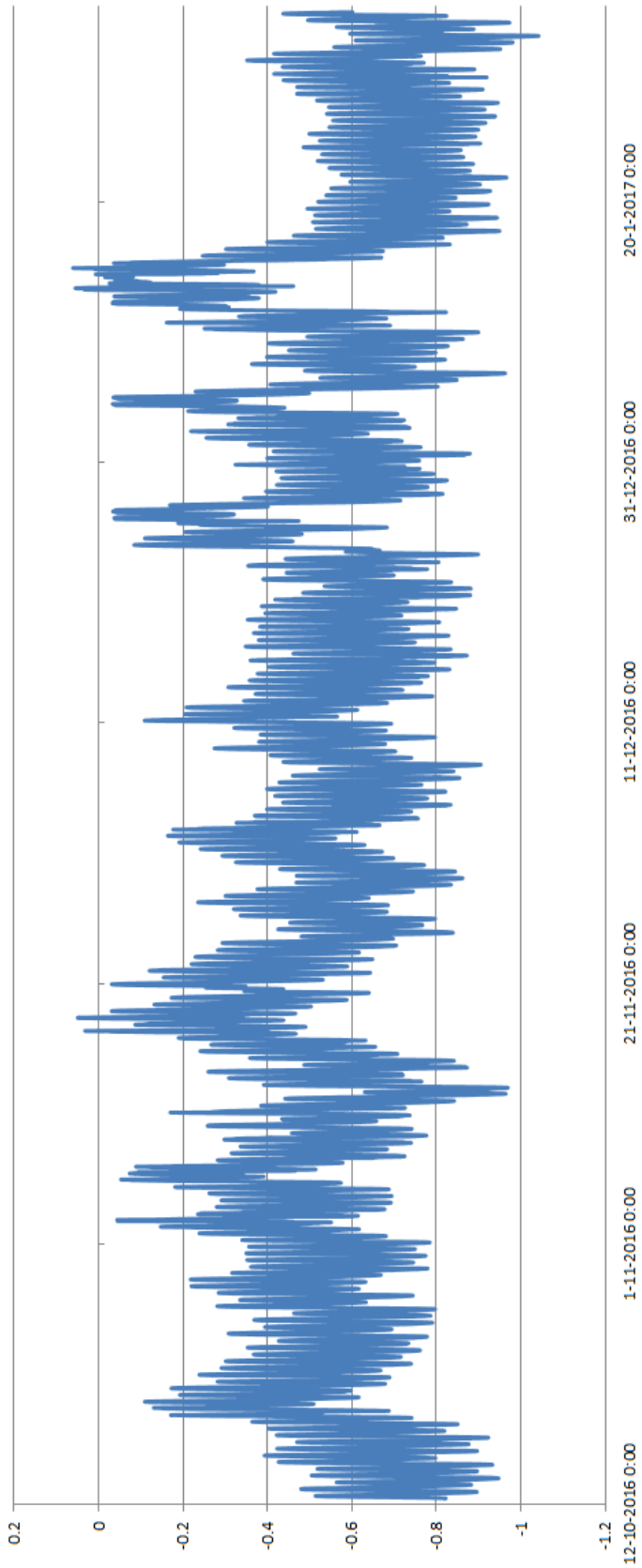

Figure C.21: Data series from piezometer 1002 at -12.12meter N.A.P. Not corrected for settlement.

D

Analysis and validation of PLAXIS settings

This Appendix handles PLAXIS interpretation issues and problems as encountered during the first runs. It also investigates the influence of the hydraulic conductivity of the soil, the 'k'-parameter, and the influence of several unsaturated flow parameters. Four main issues encountered during the first runs:

- Phreatic surface shows a strange backwards angle just after water level rise.
- A strange water pressure drop between phases.
- Overtopping signal is not recognized by PLAXIS.
- Area just below surface level where the saturation dropped

Solutions and analyses of these problems are presented in this Appendix. Furthermore a sensitivity analysis is performed on certain soil parameters to gain an understanding of their effect. Also several settings for clay are investigated and compared.

D.1. General interpretation results and parameters

Pressures and saturation

In PLAXIS a lot of different values and graphs can be obtained. All with its own definition an applicability. It is of importance to consider which type of result need to be interpret in which way. In order to do so a general introduction is given here. First of all in PLAXIS; pressures are negative while suction is positive! (except hydraulic head which is explained later on). So below a meter of water, a pressure of $-10 kN/m^2$ is registered.

The most important variable which is of direct interest for macro stability analysis is what PLAXIS calls the 'active pore water pressures', p_{active}. This is the pore water pressure used in Terzaghi's formula. It is defined as the pore water pressure times the effective saturation, $S_{eff} * p_{water}$. As a consequence below the phreatic surface p_{active} equals the hydrostatic pressure as the effective saturation is equal to 1. Far above the surface the active pore pressure is zero as effective saturation is 0. Only in the zone above the phreatic surface the small positive value for effective saturation combined with the positive values of the pore water pressure produce a layer of small suction, the capillary fringe. The effective saturation is defined as the saturation degree between the boundaries of the residual saturation S_{res} ($S_{eff} = 0$) and the maximum saturation degree S_{sat} ($S_{eff} = 1$).

In this Appendix the same geometry of the dike is handled in all examples. The outer geometry is the same as in the rest of the thesis, meaning that:

- Toe to toe distance is 33.7 meters.
- Inner crest is $+6.24 mN.A.P.$.
- Outer crest is $+6.12 mN.A.P.$.
- Foreshore is $+0.99 mN.A.P.$.
- Hinterland is $+1.40 mN.A.P.$.
- Starting level ground water $+0.85 mN.A.P.$ for entire model! (Differs from main file).

So, main difference is the starting level of the phreatic surface. Other difference is that only homogeneous dikes are considered.

Figure D.1 to D.3 show the starting situation for p_{water}, S_{eff}, and p_{active} respectively. It is important to notice that the p_{water} is a more hypothetical pressure distribution! There is no suction of $54kN/m2$ in the top of the dike as there is mainly air in the pores. If the dike would be filled with water hanging in the dike without actually altering the phreatic surface this would be the suction in the top of the dike. Or, if one were to put a vacuum cleaner on over the dike it would have to suck with $54kN/m2$ to pull the water up to that height. So, p_{water} above the phreatic surface can be seen as the suction power a vacuum would need to have to suck the water, from the water table below, up to that point. It has no practical meaning in that sense.

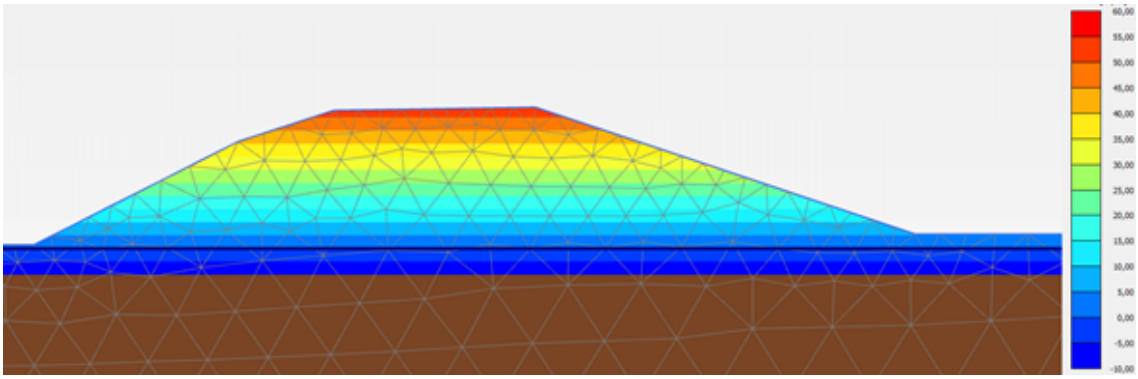

Figure D.1: $p_{water}(t=0)$ (Red = 55 to 60 kN/m2, Blue is -10 to -5 kN/m2)

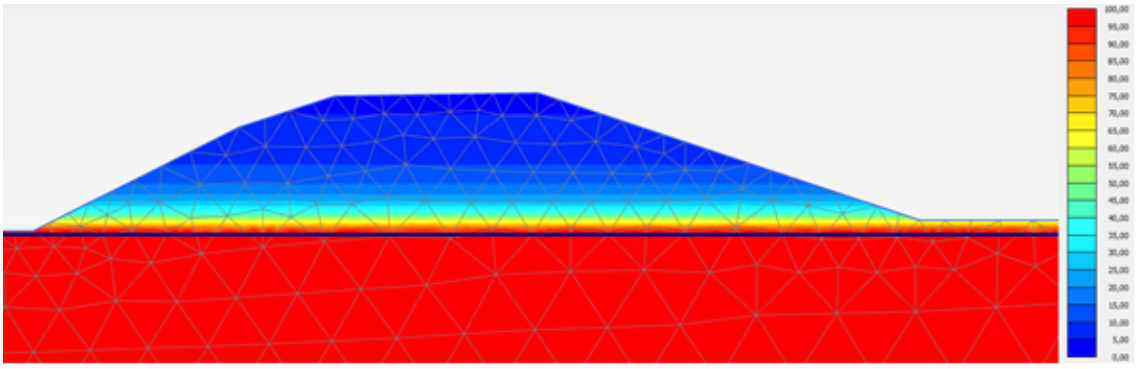

Figure D.2: $S_{eff}(t=0)$ (Red = 95-100%, Blue is 0-5%)

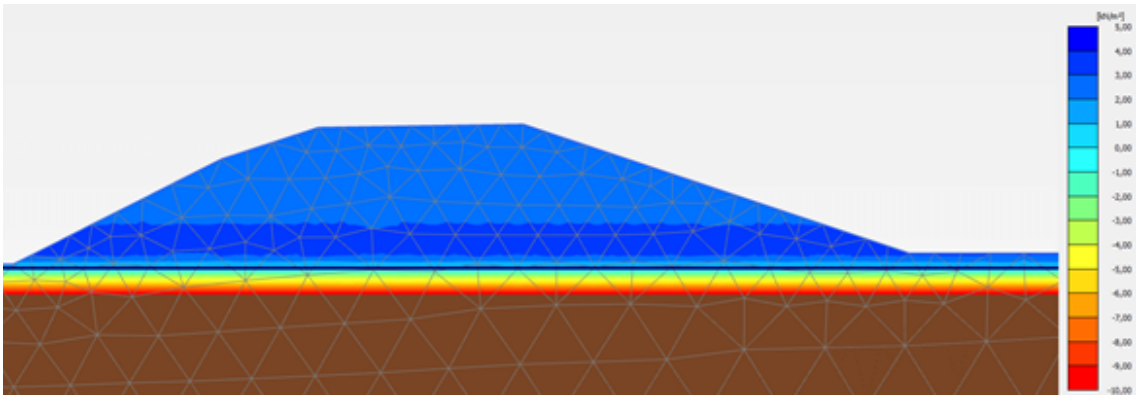

Figure D.3: $p_{active}(t=0)$(Red = -10 to -9 kN/m2, Blue is 4 to 5 kN/m2)

The figures above show the dike as calculated by the initial phase of PLAXIS, so no external water has been

applied to the dike ever. The dark blue line is the phreatic surface as calculated by PLAXIS. Or more precise; it is the line from where pore water pressure rather than suction occurs. The effective saturation degree is not equal to 0 throughout the dike, even all the way in the top an effective saturation degree between 0 and 5% is measured. This has to do with the water retention curve which PLAXIS applies during starting conditions. For the used parameter set, the effective saturation degree at a suction of $48.9 kN/m^2$ is 5.0% which is consistent with the height of $4.89 m$ above the phreatic surface where the shade changes.

As a consequence, the active pore pressure in the clay is not entirely 0 at starting point. There is a small active suction between the soil particles as some pores are not entirely drained and some water is retained. This suction forces are created due to the water still entrapped between the clay particles and wants to escape downward due to gravity, but can't due to cohesive effects. This generates a small suction, pulling the soil particles together. However, some small distance above the phreatic surface more and more pores get filled due to capillary suction. The suction generated in this area thus actually aids to the strength of the soil.

In the scenario above the dike is in its driest possible situation. For the Netherlands however this is not a realistic starting point as is common knowledge. In order to make the starting point of simulation somewhat more realistic; the dike is pre-wetted before every scenario. For this Appendix it is done by a period of extreme rain and a period of drought before the other loads are applied. There will be rain of 50 centimeter a day for 300 days, literally soaking the dike and bringing up the phreatic surface to surface level. Then nothing will happen for another 200 days, giving the soil water time to approximate a somewhat more realistic equilibrium than the case above. With a hydraulic conductivity of $0.1 m/day$ this should be enough to get close enough to the equilibrium. Then the graphs of p_{water}, S_{eff}, and p_{active} respectively look as such:

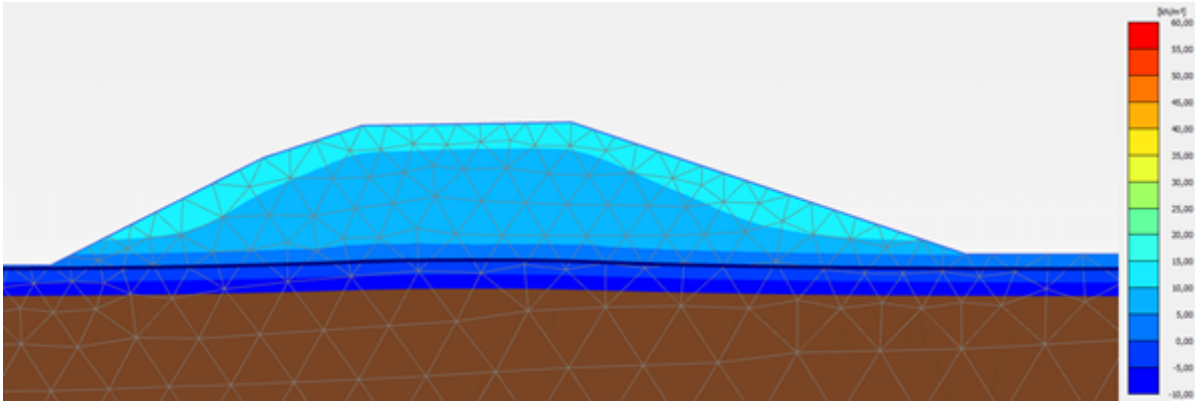

Figure D.4: $p_{water}(t = 500)$ (Red = 55 to 60 kN/m2, Blue is -10 to -5 kN/m2)

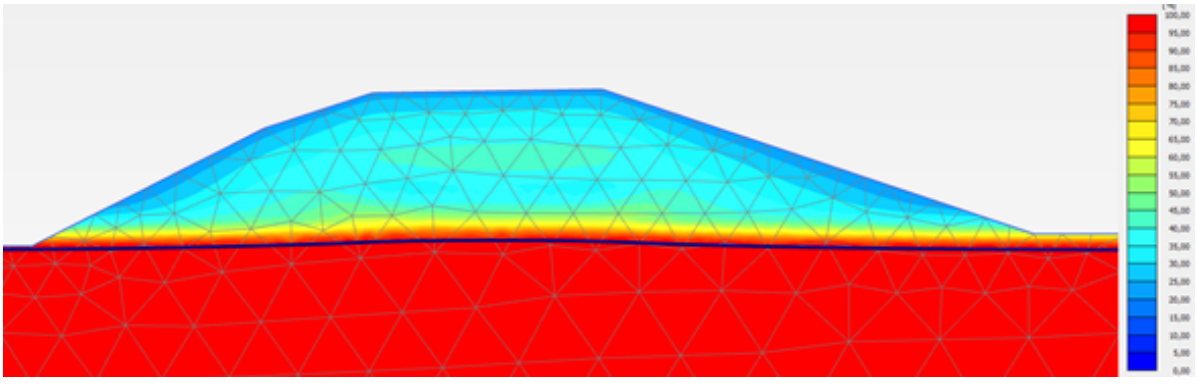

Figure D.5: $S_{eff}(t = 500)$ (Red = 95-100%, Blue is 0-5%)

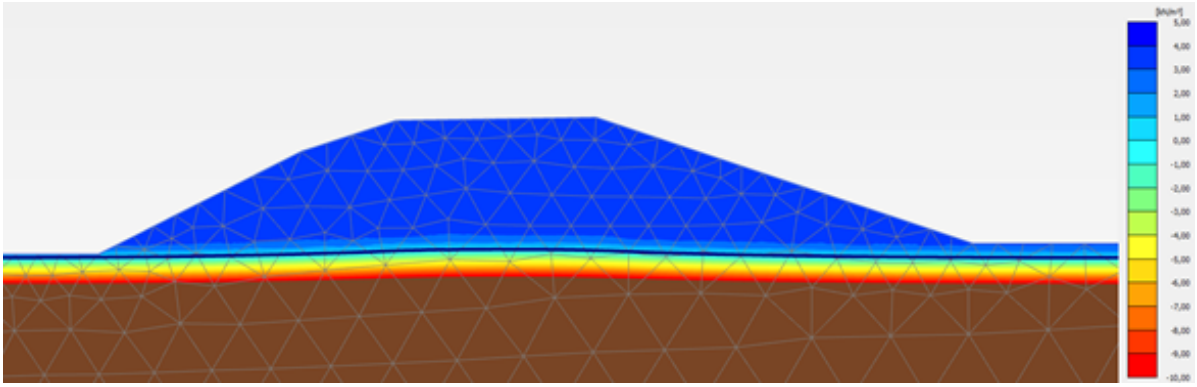

Figure D.6: $p_{active}(t = 500)$(Red = -10 to -9 kN/m2, Blue is 4 to 5 kN/m2)

The p_{water} graph and saturation graphs have changed quite a lot, while the active pore water pressure stayed roughly the same. Due to local saturation the suction in the dike drops, lowering p_{water}. The saturation graph in turn shows the effective saturation. These two variables again result in the effective pore water pressure. As one can see there is a small effective suction, between $3-4kN/m2$ throughout the entire dike.

Head

In PLAXIS hydraulic head, h, is defined as:

$$h = z - \frac{p_{water}}{\gamma_w}$$

Where z is the location in vertical direction, γ_w the volumetric weight of water, and p_{water} the pore water pressure as defined above. So, because of the minus and pressure being negative hydraulic head is the other way around again. Thus more pressure generates a higher hydraulic head and suction lowers the head. In the end head differences induce ground water flow. Below the hydraulic head plots at the very beginning and after the pre-wetting phase are shown.

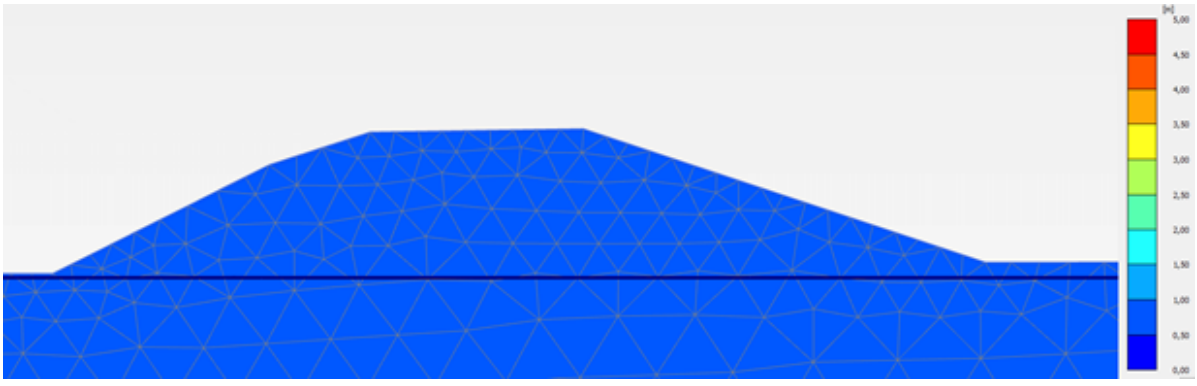

Figure D.7: $h(t = 0)$ (Red = 5m, Blue 0m)

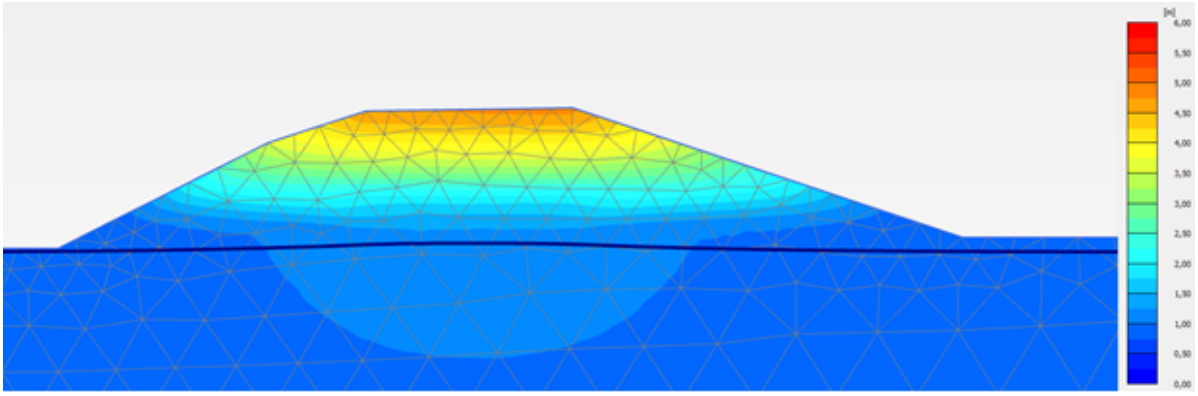

Figure D.8: $h(t = 500)$ (Red = 6m, Blue 0m)

Before any hydraulic loads are applied the head is equal to $0.85m$ everywhere, as this is the water level compared to N.A.P. which is the reference point for the model. After the rain and rest period passed, the head throughout the embankment is clearly influenced. On either side and far below the dike the equilibrium is already reached since head values returned to 0.85 meter again. However, in the dike the situation is not normalized yet after 200 days. A slight bulging of the phreatic surface is noticeable, leading to the slightly higher head directly below the bulge.

Above the phreatic surface the hydraulic head is becoming larger with the height position, indicating that the suction increases slower than hydrostatically would be expected thus inducing a flow downward. This lower suction in turn is the consequence of heightened saturation degrees. Due to the suction and the resulting lowered hydraulic conductivity the flow becomes really slow. Thus taking a long time to approximate the equilibrium even though the head gradient is quite high (flow in the end depends on head gradient and hydraulic conductivity).

D.2. Phreatic surface bend

The unexpected observation which raised doubt about the legitimacy of the model is depicted below.

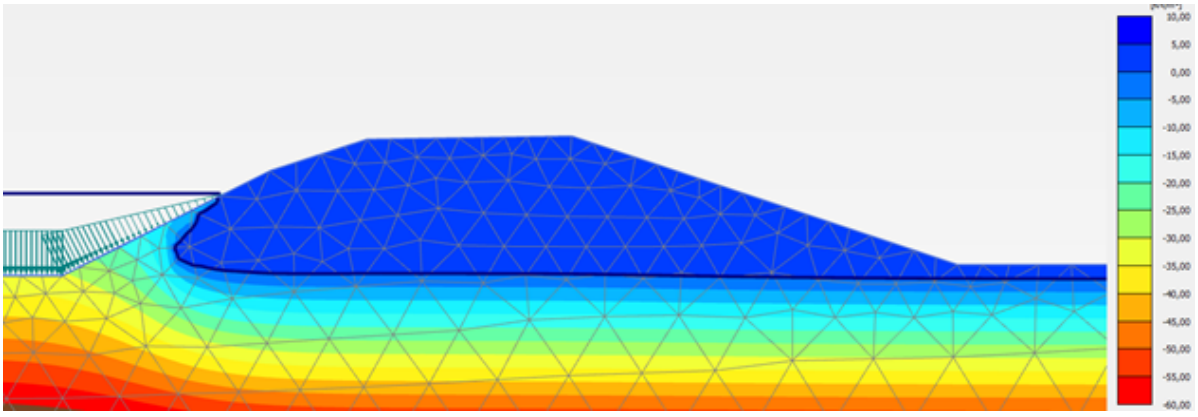

Figure D.9: Example of the simulated bend in the phreatic line.

As one can see there is a strange bend (knik) in the phreatic surface after the water rose, which was not expected. One would expect a more sloping surface towards the hinterland and no 'Z'-like shape. I argue that this 'Z'-shape is actually correct and is the consequence of the relatively quick water level rise compared to the hydraulic conductivity and most importantly the slope angle of the dike.

Two main arguments can be given about the correctness of the observation. One in the form of an extra experiment and one by prolonging the run. First, the additional experiment of which the initial phase is shown below. A $10x10m$ block subdivided into 4 $5x5m$ blocks three of them filled with soil with a k of $0.01m/day$ and half of the block saturated. The p_{water} and not the p_{active} is shown.

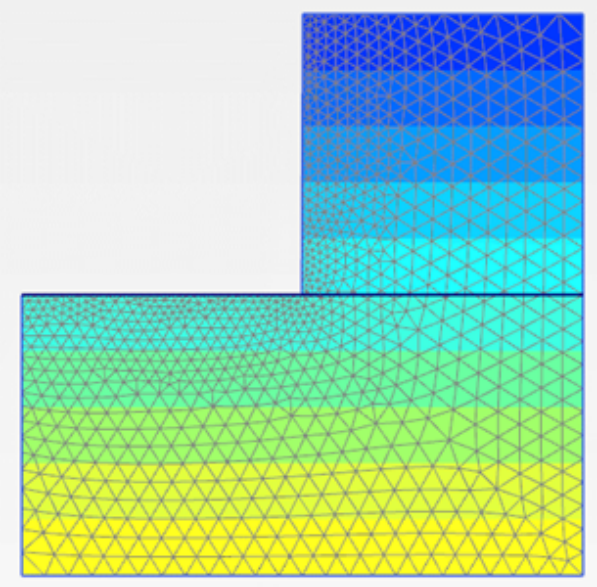

Figure D.10: Starting situation of experiment at t=0.

Then a rising water level over 15 days' time is applied, then the water level is kept high for another 15 days. That gives these infiltration patterns after respectively 15 and 30 days.

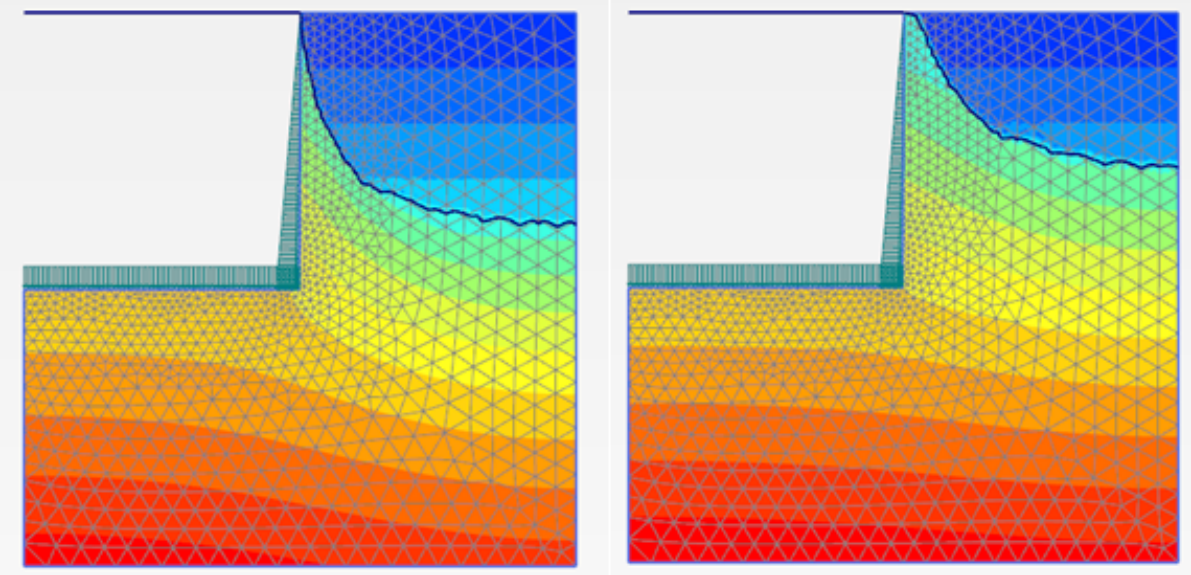

Figure D.11: Infiltration pattern at t=15 and t=30.

As one can see a quadratic/hyperbolic infiltration pattern is visible after 15 days. If one would apply this shape to the slope of a dike, thus tilting it, a Z-like shape as observed in the first figure would appear. As it would curve in a parabolic shape until it hits the already existing phreatic surface, thus creating a Z.

Second argument would be that if the run is extended in time, the expected shapes would turn up. Take a look at the following Figure of $0, 15, 30, 100$, and 1000 days. In a relative short time the Z is filled up; at $t = 30$ so within 15 days. The p_{water} and not the p_{active} is shown.

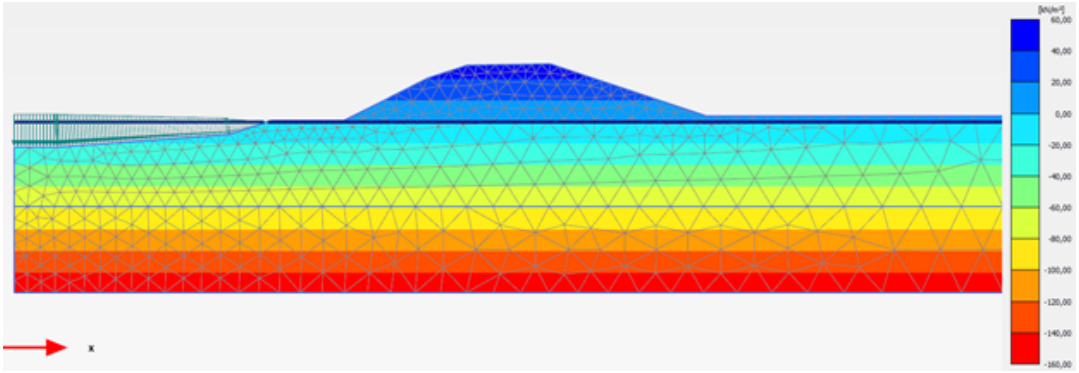

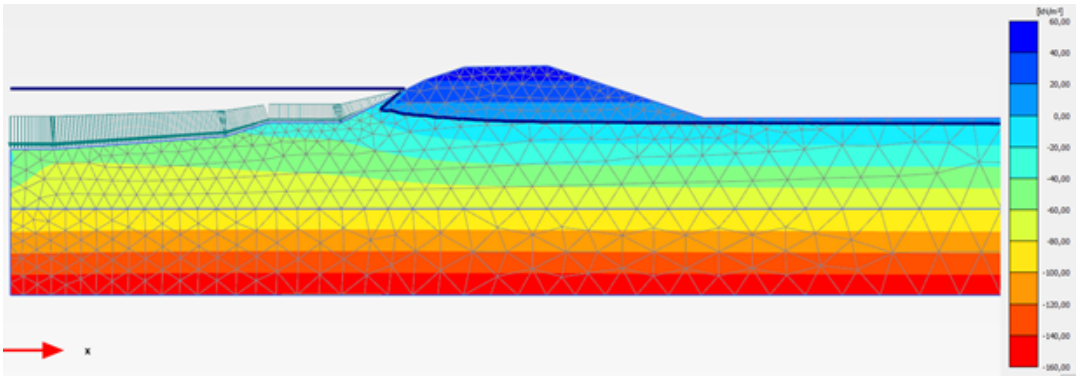

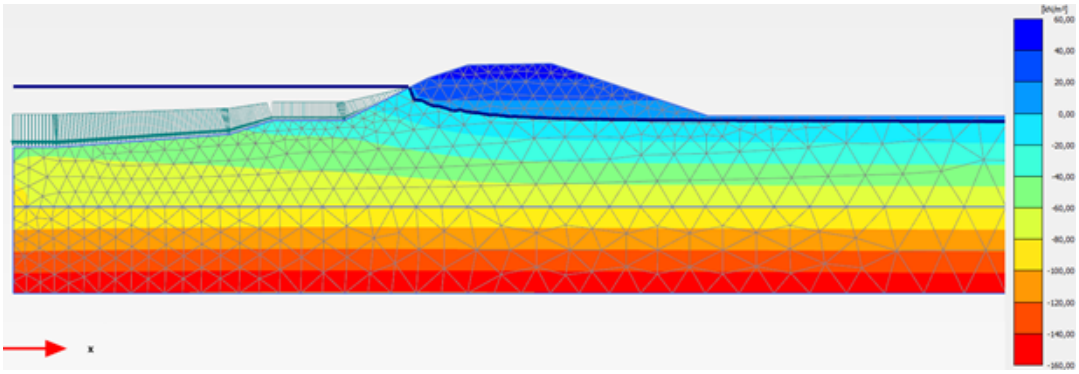

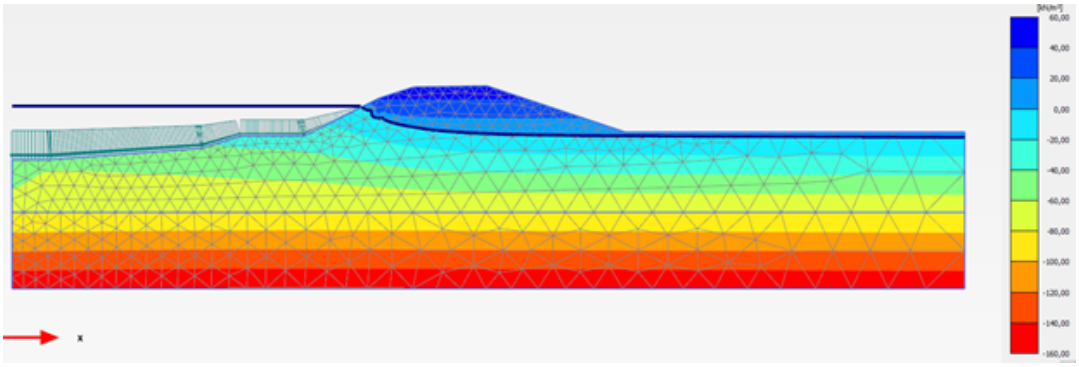

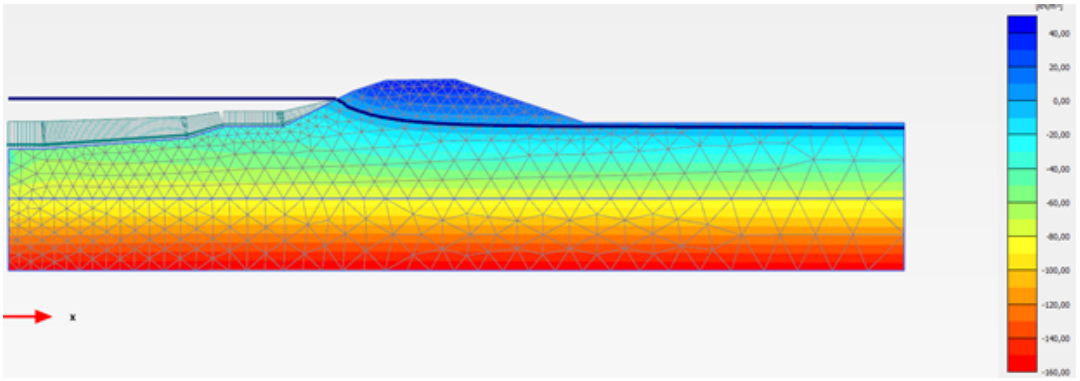

Figure D.12: Development of bend in time. Respectively; t=0, t=15, t=30, t=100, and t=1000 days.

The strange shape thus appears for a short time only, dissipating quickly. With higher k-values, different $k_y - k_x$ ratios or a higher k-value for the top layer, the Z-shape will become less or disappears altogether.

D.3. Water pressure drop between phases

Second problem would be that between consecutive phases a groundwater head drop is clearly noticeable. This is illustrated in the graphs below. Point A is below the outer crest while point B is below the inner crest.

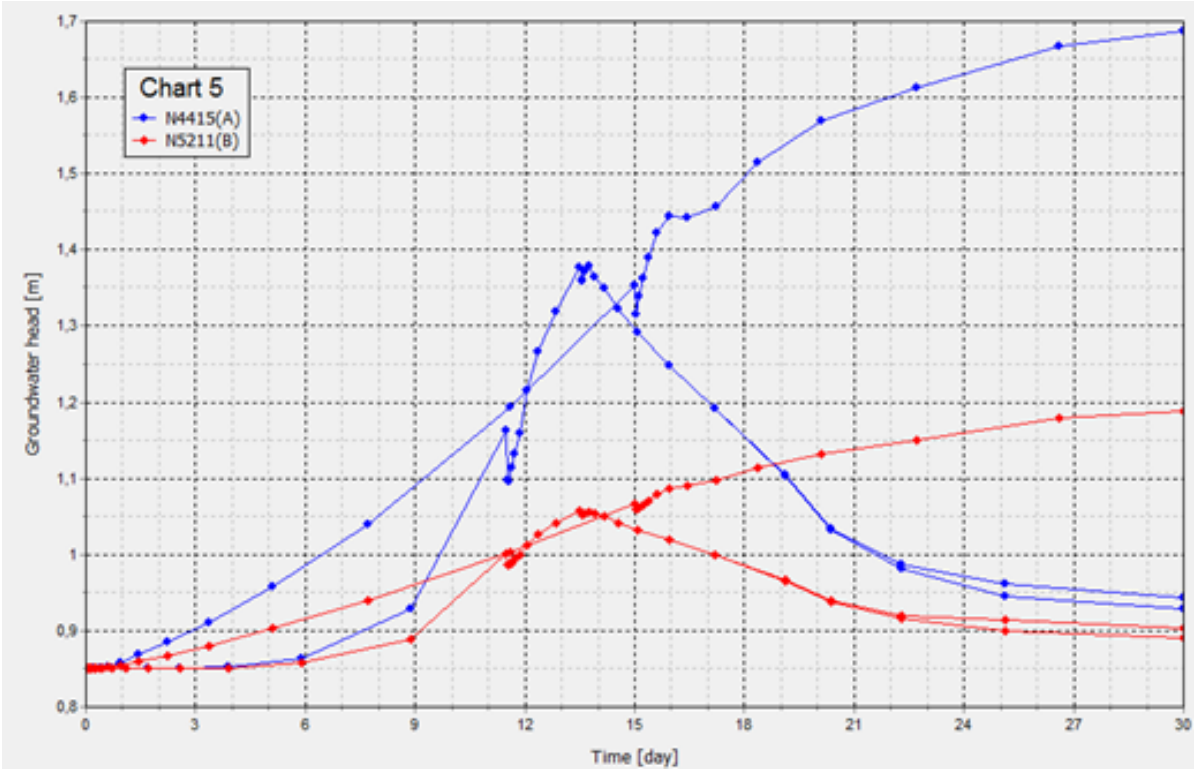

Figure D.13: Pressure drop in pores between two phases.

Four lines are constructed at two locations for two different scenarios. The rising blue and red lines belong to a scenario where a water level rising for 15 days is applied and then another 15 days where the water level is constant. The rising and the constant level are a different phase each. For both point A and B a pressure drop is present when the new phase starts. After this drop the model returns to the old value after 8 steps (2 days and a little bit). So it seems that, although the settings indicate to continue with the values of the old phase, a new numerical balance needs to be found inducing the drop. This drop is not present if the load is applied as one phase and it takes little fantasy to interpolate the end of phase one and step 9 of the second phase.

The two lines which rise and then gradually drop again belong to an overtopping simulation split up into three phases. Also here the numerical instability is visible in both lines at two points, $t = 11.5$ and $t = 13.5$. Thus the beginning and ending of the overtopping phase.

An easy solution would obviously be that everything is done in one phase rather than two. This is however not desirable for the overtopping scenario as the step size for the two days of overtopping needs to be reduced manually (see next chapter) and it would be unnecessary to do so for the water level rise and drop parts of the simulation. Hence phase splitting within one scenario without a transitional pressure drop is a necessity for limiting simulation times.

For now, even after speaking to some experienced people, the cause of the drop remains unknown. It might have to be accepted as an numerical instability of the program. Taking a more practical point of view, the pressure drops have the order of magnitude of 5 centimeters. Considering all other uncertainties created in the process such as parameter settings, the phenomenon is a relative minor problem. Furthermore at the location of interest for inward slope macro stability (starting around point B as this is the inner crest), the drop is around 2 centimeters. In the main research the problem is somewhat handled by applying the relevant load only after some steps in the new phase and not directly.

D.4. Overtopping signal

One of the loads to be assessed is overtopping. However, other than rain and water level, the nature of this load is a series of very short random events. Each overtopping event occurs in a matter of seconds rather than hours or days. To approach this type of load for the PLAXIS model a MATLAB script is written which randomly generates an overtopping signal for each model boundary based on the input parameters given by Hydra-NL.

There was a problem where PLAXIS did not pick up the load signal. This was caused by the fact that PLAXIS automatically generates its optimal calculation time step to obtain an optimum between calculation time and accuracy. In order to do this PLAXIS looks at the flow inside the model and soil parameters. However, it does not consider the load files when checking the optimal step. So if the subsurface flow allows a larger time step of for example 10 minutes, the program applies that step duration. Thus skipping part of the overtopping load file and interpolating values of the file by taking the begin and end value of that 10 minute span. Especially the inner slope suffers, as loads are rare there.

The problem is solved by reducing the maximum time step to 20 seconds so the input file is checked every 20 seconds. An ever shorter maximum time step would be desirable since river waves have a rather short wave period of 2.6 seconds on average during a storm. A 20 second step would mean that 5 to 10 waves hit the dike and these loads thus need to be aggregated in a representative way.

Why not make the maximum time step shorter? Because the maximum number of steps that can be calculated per phase in PLAXIS is only 10,000 steps. So for 48h-storm minimal time step is around 20 seconds. This produces around 8,000 steps on average which takes 25 min to calculate under the coarse grid as used for this appendix but up to 4 hours for the grid of the final model.

Why not split the 48 hour storm in even more phases? Since the maximum of 10,000 steps is set per phase, the storm could be split in 8 phases. Each phase lasting 6 hours and harnessing 8151 waves/time steps. Calculation time however would naturally rise to 16 hours, which is rather long for one simulation. Furthermore the aforementioned problem of numerical instability between the phases would be even more problematic and would need to be solved first. Finally both the input program and output program of PLAXIS become extremely slow due to the enormous amount of data generated.

The results of the overtopping scenario with $k = 0.1 m/day$ gives the following results directly after the storm:

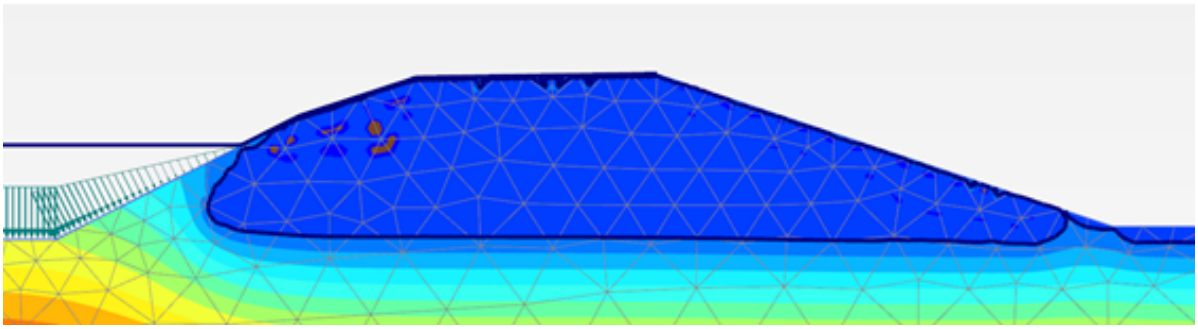

Figure D.14: $p_{active}(t = 13.5)$, k=0.1 m/day, (Red = -55 to -60 kN/m2, Blue is 10 to 5 kN/m2, Brown is >10 kN/m2)

In this case a small layer of water infiltrates at all boundaries. The infiltrated water also heightens the surface at the sides of the dike. When the hydraulic conductivity is heightened to $k = 1m/day$ the water pressures for the same overtopping load.

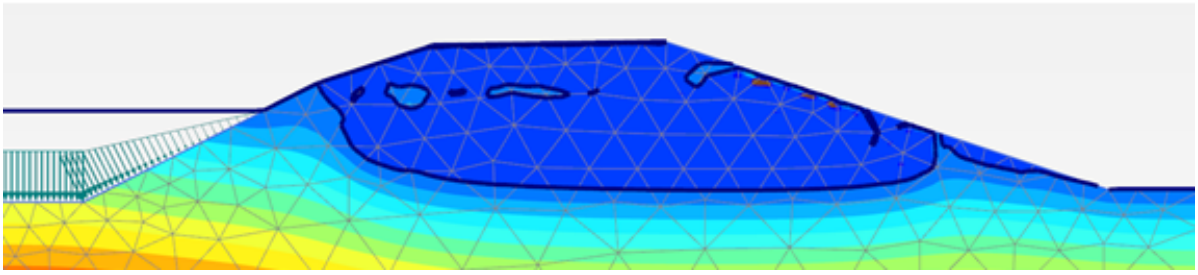

Figure D.15: $p_{active}(t = 13.5)$, k=10 m/day, (Red = -55 to -60 kN/m2, Blue is 10 to 5 kN/m2, Brown is >10 kN/m2)

The difference between the two permeabilities is quite large. The lower run-up boundary is entirely saturated. The phreatic surface is higher over the entire dike. Also some nests of water pressure form inside the dike, interpretation of this is treated later on. Right now it is of importance that the overtopping loading file works.

The final load file consists out of a list of hydraulic heads for each 20 seconds. The file in the end looks like this (this is for the lower run-up boundary, 5b):

Time (days)	Head (m)
0,000000	-0,001000
11,500000	-0,001000
11,500046	-0,001000
11,500046	0,018540
11,500278	0,018540
11,500278	0,022390
11,500509	0,022390
....	....

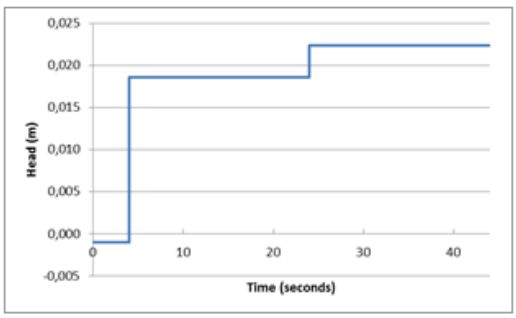

Figure D.16: Aggregated head signal.

Every 20 seconds or 0.000231 days the load is updated with the average head of 5 drawn waves of $T = 4s$ each. First two waves are shown in the table and Figure. In order to check the validity of the aggregation two runs have been performed for a 9.6 hour storm. The same wave set and soil settings were used for both runs. Only difference is that for the first run the load of 5 waves was averaged and applied for 20 seconds (as will be done in the rest of the simulations) and for the second run the individual waves, each lasting 4 seconds, were applied on the surface.

The figures below give different saturation patterns after the 9.6 hour storm. In general it is clear that the infiltration is slightly higher when individual waves are applied. The saturation pattern for the individual

waves is rather remarkable and seems to be subjected to some numerical instabilities as the saturation is high along the lines between two nodes but remain small within the elements. For the aggregated waves the saturation is more dissipated and seems to be more natural. Especially the slopes have different saturation distributions. The crest of the dike is roughly the same although the water seems to have infiltrated somewhat more in the non-aggregated scenario.

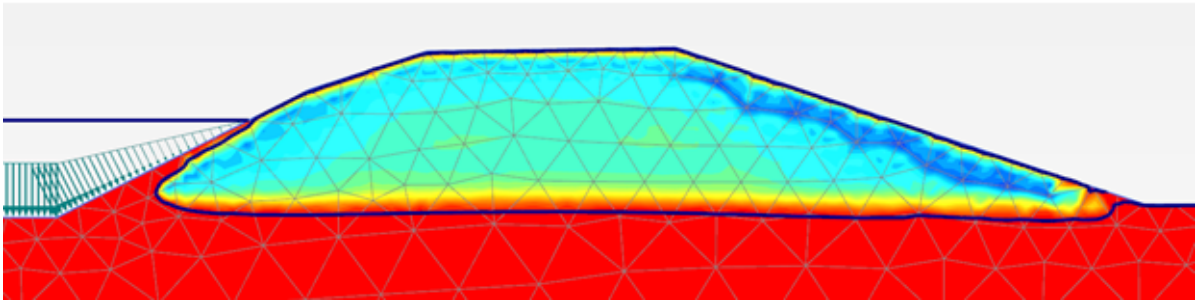

Figure D.17: $S_{eff}(t = 11.9)$, k= 1m/d Aggregated waves, average load over 20 seconds.

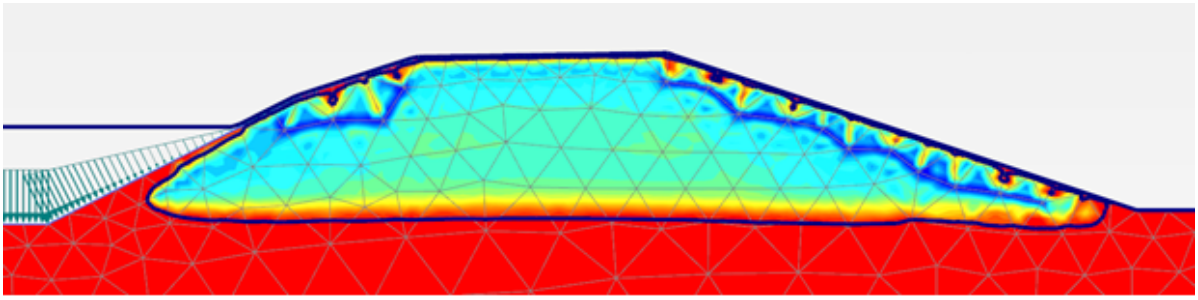

Figure D.18: $S_{eff}(t = 11.9)$, k= 1m/d Non-aggregated individual waves.

The most obvious differences between the two figures is not caused by the aggregation process but rather by a numerical stability cause by the coarseness of the grid. Therefore to check the validity of the wave load aggregation a smaller model, with very fine grid is constructed. Only boundary six (upper outer slope) is modelled. The results are below in Figure D.19 although spotting differences is really had with the naked eye.

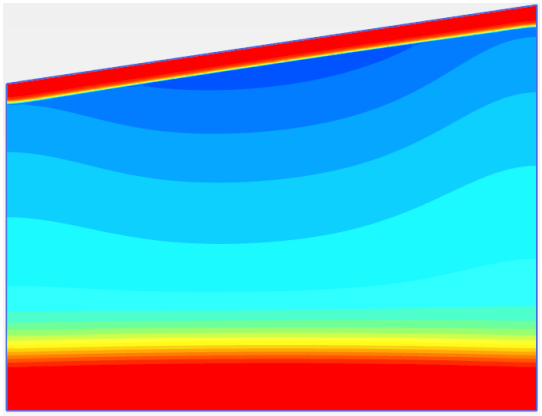

(a) $S_{eff}(t = 11.9)$, k= 1m/d Aggregated waves, average load over 20 seconds.

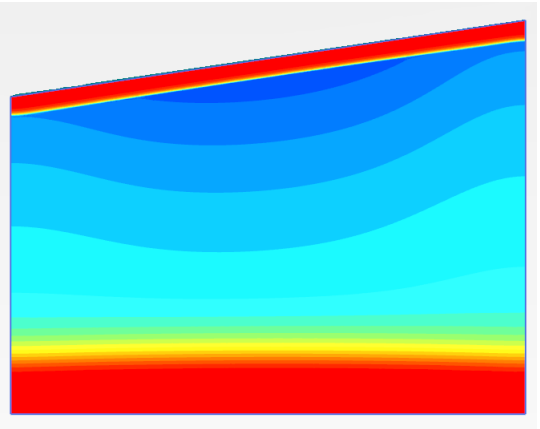

(b) $S_{eff}(t = 11.9)$, k= 1m/d Non-aggregated waves, load each 4 seconds.

Figure D.19: Theoretical inner slope sliding and an example; Breitenhagen, Elbe river, June 2013

When measured the infiltration of the aggregated wave load was $3mm$ more; 0.301 to 0.304 meter. This experiment was done for 9.6 hours (0.4 days) only, meaning that the differences for a total overtopping run

are around $1.5cm$ which is a fair trade-off as the simulation time for overtopping simulations is being reduced with 80%.

D.5. 'Van Genuchten'-parameter settings

Besides variability in loads and hydraulic conductivity of the soil, the behavior above the phreatic surface is also important. For $k_y = 0.1m/day$ and the uniform rain pattern five runs have been performed with different soil behaviour to check the influence of the van Genuchten model on the flow and saturation the phreatic surface.

The parameters are of extreme importance for the infiltration of rain and overtopping. Sources for the right parameter settings come from both literature as well as PLAXIS proposed settings. And there are large differences between the two types. First some definitions are given to make interpretation of the parameters and the model possible. The void ratio, saturation, and water content are defined as:

$$e = \frac{\text{Volume of pores}}{\text{Volume of solids}}$$

$$S = \frac{\text{Volume of water}}{\text{Volume of pores}}$$

$$\theta = \frac{\text{Volume of water}}{\text{Total volume of wet material}} = \frac{\text{Volume of water}}{\text{Volume of solids + Volume of pores}}$$

So,

$$S = \frac{\theta(1+e)}{e} \quad \text{and} \quad \theta = \frac{S \cdot e}{(1+e)}$$

These parameters are both (inconsistently) used in PLAXIS, therefore one needs to be careful. The predefined soil types are all given in terms of θ, while the user defined model requires the input of S. Five combinations of parameter settings are tested to check parameter influence, see Table D.1. 'Staring B11' is the qualification for heavy clay in the topsoil while 'Staring O12' is the qualification for heavy clay in the subsoil. 'Hypres (fine)' is the qualification for a fine topsoil type of soil.

The parameter set of Dario is from another master student at the TU Delft who talked with a PhD'er (J.Zhou) about the right settings for clay. The Yang parameter settings are from a paper of 2013 about methodologies for finding the right parameter values for the 'Van Genuchten'-model, [21]. The Dario and Yang parameters sets are referred to as the expert settings while the other three are mentioned as PLAXIS.

Soil type	$k_y[m/d]$	S_{res}	S_{sat}	θ_{res}	θ_{sat}	$g_a[1/m]$	g_l	g_n	e
Staring B11	0.1	0.017	1.00	0.01	0.59	1.95	-5.901	1.109	1.439
Hypres Fine	0.1	0.019	1.00	0.01	0.52	3.67	-1.98	1.10	1.085
Dario	0.1	0.12	1	0.0555	0.462	2.286	0.50	2.24	0.86
Staring O12	0.1	0.018	1.00	0.01	0.56	0.95	-4.295	-1.158	1.275
Yang (2013)	0.1	0.30	1.	0.18	0.60	0.96	0.5	2.60	1.50

Table D.1: Parameter values for different soil types.

The void ratio is calculated such that the saturated saturation is equal to 1 for all settings. The model for the saturation and thus the water retention curve is as follows:

$$S(p_{water}) = S_{res} + \frac{S_{sat} - S_{res}}{\left[1 + (g_a|\frac{p_{water}}{\gamma_w}|)^{g_n}\right]^{1-(1/g_n)}} \tag{D.1}$$

Or:

$$\theta(p_{water}) = \theta_{res} + \frac{\theta_{sat} - \theta_{res}}{\left[1 + (g_a|\frac{p_{water}}{\gamma_w}|)^{g_n}\right]^{1-(1/g_n)}} \tag{D.2}$$

The difference between the saturation, S, and the soil water content, θ, is that in the water content the pore space is included. So, water content is maximized at the relative pore volume, which would be consistent with a saturation degree of 1. The hydraulic conductivity function is calculated as:

$$k_r(S_{eff}) = \max\left[(S_{eff})^{g_l}\left(1-\left[1-S_{eff}^{\left(\frac{g_n}{g_n-1}\right)}\right]^{\left(\frac{g_n-1}{g_n}\right)}\right)^2, 10^{-4}\right] \tag{D.3}$$

Below, for each scenario the resulting WRC and HCF are shown. When looking at the graphs there is a clear difference between the PLAXIS automatically generated functions and the one proposed by experts.

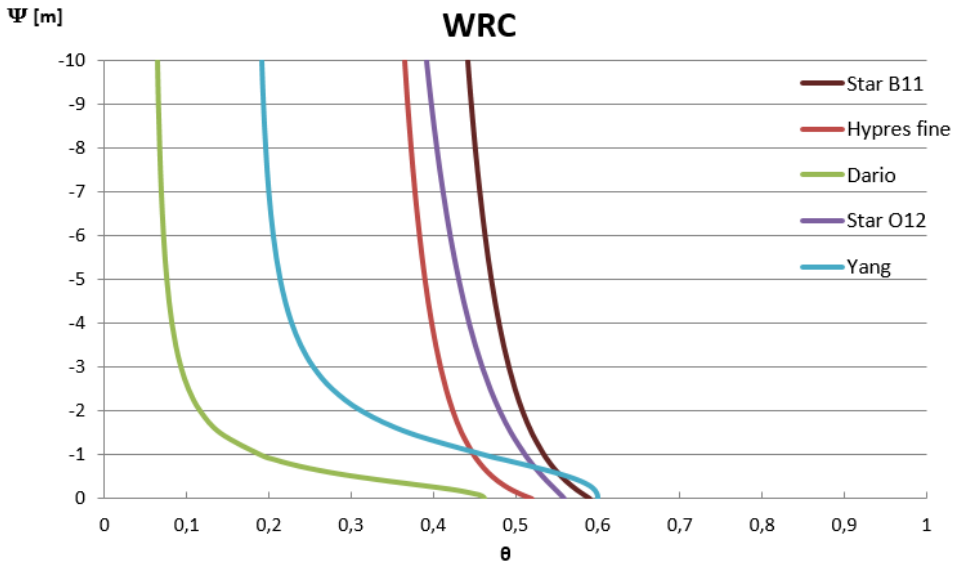

Figure D.20: Water retention curves.

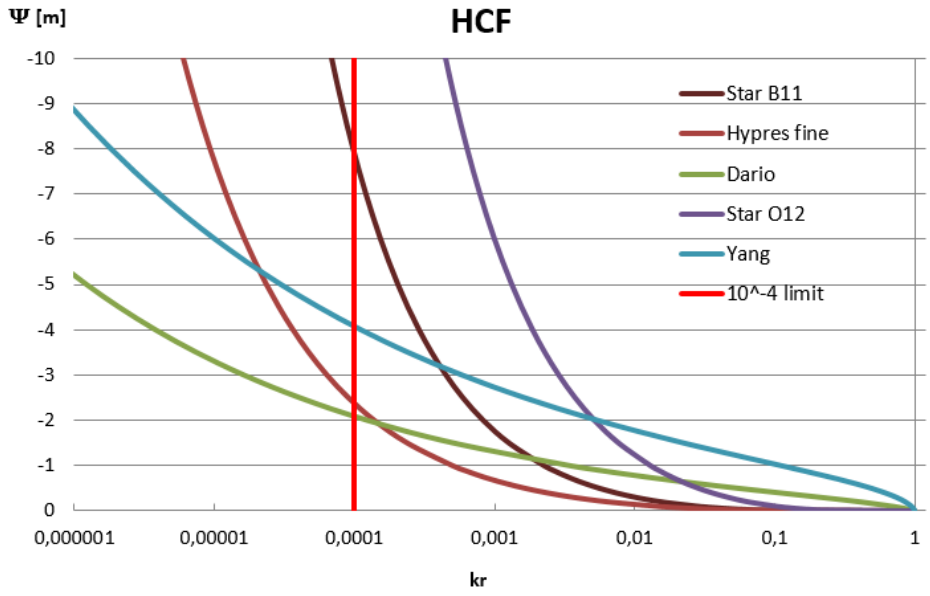

Figure D.21: Hydraulic conductivity functions.

As a consequence of these functions the soil will behave differently. For all three graphs it is important to realize that with in the model suctions higher than $-6.24+0.85=-5.39m$ do not occur on a large scale

(maybe locally they can become higher however).

The validity of the WRC-curves is checked by looking at a saturation graph after the prewetting period. This graph thus gives the saturation and not the effective saturation. In the top of the dike [$\psi = 5.4m$], for the Dario parameter set, the water content, $\theta = 0.073$, and thus the saturation should be equal to:

$$S = \frac{\theta(1+e)}{e} = \frac{0.073(1+0.86)}{0.86} = 15.8\% \tag{D.4}$$

Which is indeed what is shown in the Figure below.

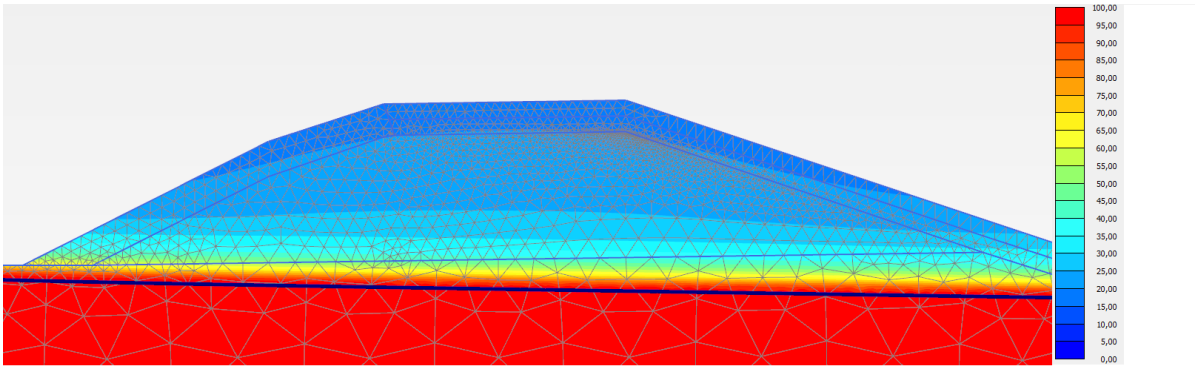

Figure D.22: Saturation degree in the dike after prewetting phase

When looking at the HCF it is clear that for rather small values of suction, the PLAXIS functions already loose a lot of their conductivity, while the expert functions remain closer to 1 for small suction. When suction becomes higher however, roles are reversed and the experts are way less permeable. The Dario-function is around two orders smaller (HCF has logarithmic x-axis!) than the PLAXIS functions, while the Yang function is around the same value for 5.39 meter. The PLAXIS program however, cuts off all relative conductivities smaller than 10^{-4} so for the higher suction values the rest of the graph does not matter in practice. Figure D.21 shows that both Staring soils are the only ones to never reach this boundary within this model.

The water retention curve shows a similar pattern where the expert functions start with higher water content for lower suction but approach to their limit rather quick, while the PLAXIS function need extreme high values of suction to reach their residual saturation. This becomes even more clear when one looks at effective saturation. Effective saturation, as depicted in the cross-sectional plots later on and used in the HCF, is defined as:

$$S_{eff} = \frac{S - S_{res}}{S_{sat} - S_{res}} \tag{D.5}$$

And is thus the saturation put on a 0 to 1 scale where 0 is equal to the S_{res} or θ_{res} and 1 to S_{sat} or θ_{sat}.

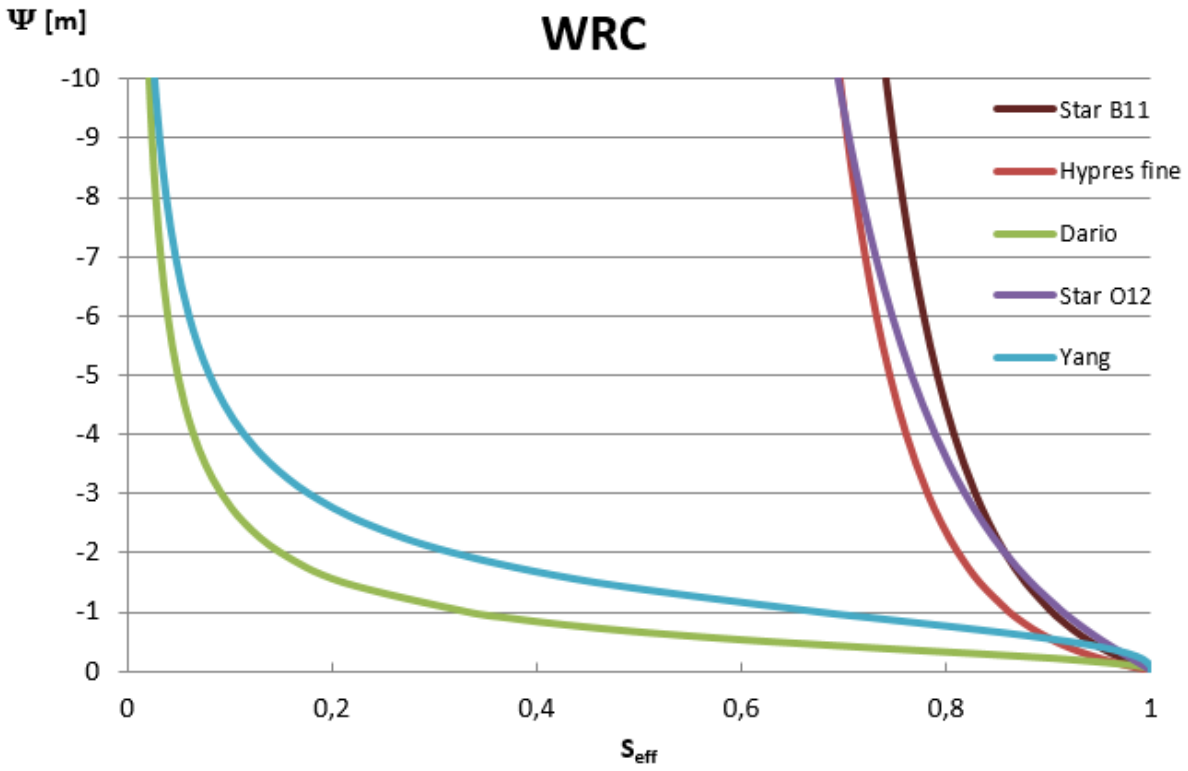

Figure D.23: Water retention curves plottet against effective saturation rather than water content.

As stated before, the saturation drop severely for lower suction if the parameter values of the experts are used, while they remain high for the PLAXIS defined soils.

The resulting effective saturation degree after 8 days of uniform rain is shown below for all 5 settings. The key for saturation is the same as in Figure D.22 and the dark blue lines is where the effective saturation has reached a value of 1. The left picture is the effective saturation directly after the 8 days of rain end, while the right depicts the effective saturation after the entire 30 days so 22 days after the rain ends. Only the parameters shown in the table before are altered all other values are kept constant. Including hydraulic conductivity which is set to $0.1 m/day$ in a vertical sense and $0.05 m/day$ in horizontal direction.

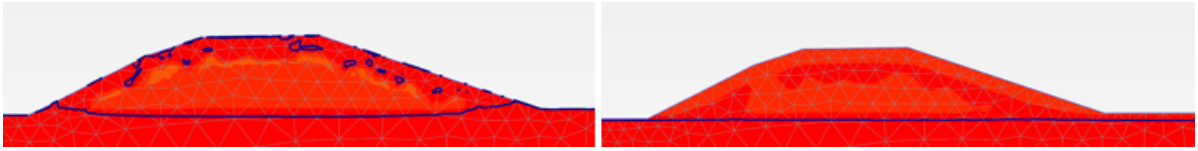

Figure D.24: S_{eff} Staring B11. Directly after rain (left) and 22 days after the rain stopped (right). (Red =100% saturated, Blue =0%)

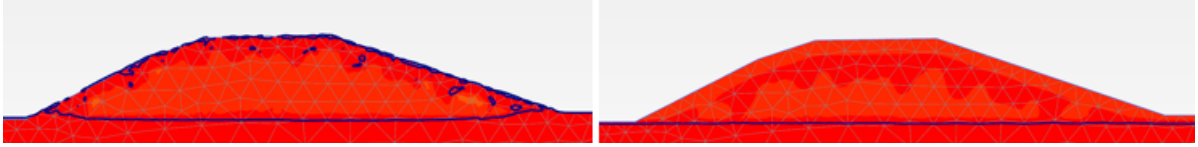

Figure D.25: S_{eff} Hypres fine. Directly after rain (left) and 22 days after the rain stopped (right). (Red =100% saturated, Blue =0%)

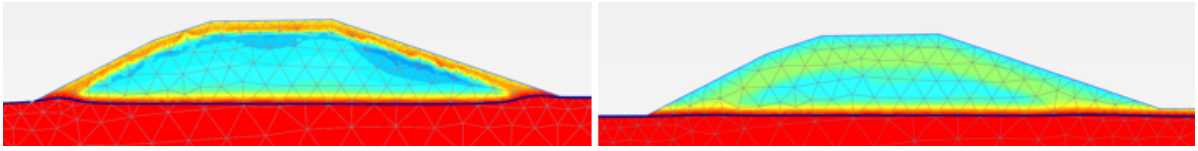

Figure D.26: S_{eff} Dario. Directly after rain (left) and 22 days after the rain stopped (right). (Red =100% saturated, Blue =0%)

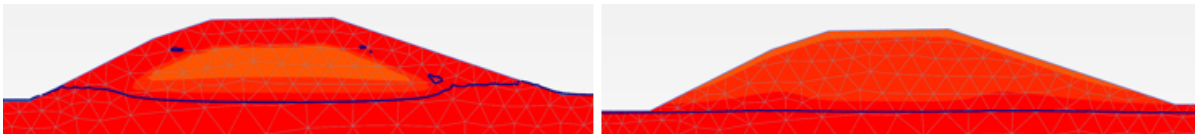

Figure D.27: S_{eff} Staring O12. Directly after rain (left) and 22 days after the rain stopped (right). (Red =100% saturated, Blue =0%)

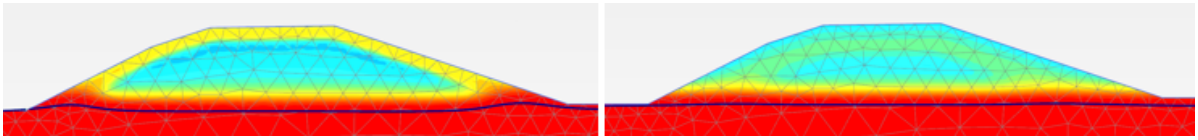

Figure D.28: S_{eff} Yang. Directly after rain (left) and 22 days after the rain stopped (right). (Red =100% saturated, Blue =0%)

The difference between the experts and the PLAXIS parameter sets becomes immediately clear. The dikes contain way less water both before and after the rainfall event as their WRC would suggest.

It is also interesting to see that the infiltration distance after the rainfall event is roughly the same for all the PLAXIS models, about 2 meters. While the expert models seem to get infiltrated much harder, only 0.75 meters. As stated above, relative hydraulic conductivity values are the lowest for the same suction levels with the Dario parameters. When looking at the phreatic surface, not much happens except some small bulging at the sides. After 30 days the phreatic surface is flat for all settings which is not strange with a k of 0.1 meter per day.

Below, the relative permeability for both expert settings is shown (same key as effective saturation). It is clear that the resulting permeability of the clay is very small at the boundary of the infiltration as is expected when combining the knowledge from the HCF and effective saturation plots. Consequences of this impermeability will be treated in the overtopping chapter further on.

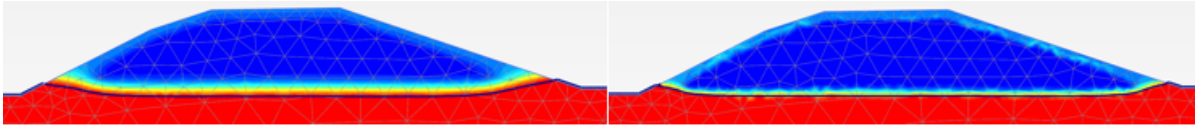

Figure D.29: k_{rel} for Yang settings (left) and Dario settings (right). (Red =100% saturated, Blue =0.01%)

D.6. Other PLAXIS soil parameters

Besides the Van Genuchten parameters some more parameters where varied to check their influence. Starting point for the following runs was the Dario parameter van Genuchten set as presented in the Table D.1, while either the void ratio, residual saturation, or maximal saturation was altered.

First the void ratio:

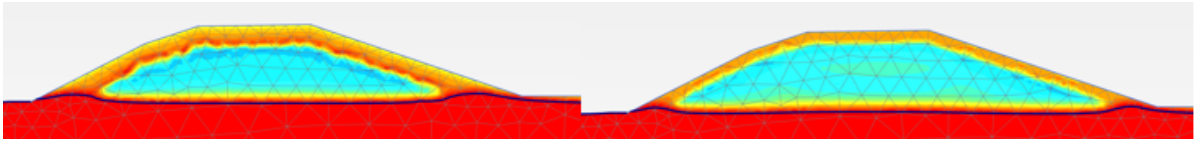

Figure D.30: Void ratio comparison for Dario settings.S_{eff} with $e = 0.3$ (left) and $e = 0.8$ (right). (Red =100% saturated, Blue =0.01%)

Since all other parameters are kept constant and the input is user defined (thus saturation boundaries as input and not water content), by altering the void ratio the water content boundaries are altered. A lower void ration means that pores get filled up more quickly with water as there are less pores to fill. So for the same hydraulic conductivity and Van Genuchten parameters the soil gets filled up quicker for lower e-numbers. For clay the e-value is usually quite high, ranging from 0.5 to 2. The first value is thus not realistic.

Residual saturation:

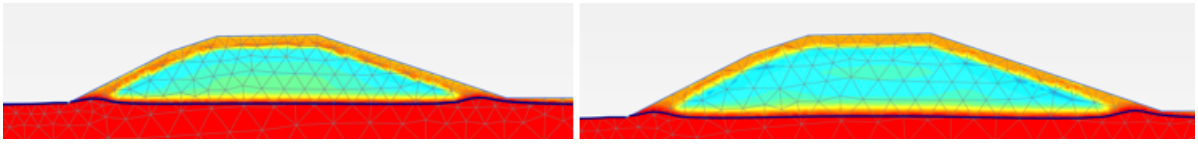

Figure D.31: Residual saturation comparison for Dario settings.S_{eff} with $S_{res} = 0.01$ (left) and $S_{res} = 0.1$ (right). (Red =100% saturated, Blue =0.01%)

No large differences seem to come up in the effective saturation. This is means that the saturation degree does change a bit, especially for the lower effective saturation values. At the beginning of the $S_{res} = 0.1$ the pores are filled with 10% more water but suction levels are the same. Apparently the residual water does not alter the infiltration speed as the same (relative) k-values are used.

Maximum saturation:

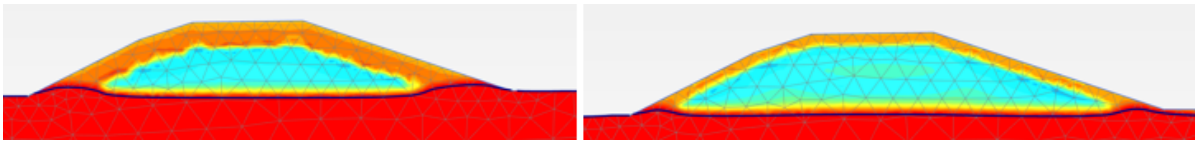

Figure D.32: Residual saturation comparison for Dario settings.S_{eff} with $S_{max} = 0.5$ (left) and $S_{max} = 1$ (right). (Red =100% saturated, Blue =0.01%)

This parameter does have a clear influence. The explanation is roughly the same as for the void ratio. The soil gets filled up sooner because with less water the max saturation is reached an the water can thus continue to fill up the lower areas. The parameters of maximum saturation and void ratio need to be treated combined and have a large influence on infiltration speed.

Based on the runs and corresponding results above the Staring parameter set is chosen for the dike in the main research. Intuitively is corresponds best to the Dutch clay used in dikes. These dikes have high saturation values throughout the year and the expert parameters seem to loose the pore water to quick in dry periods. The Hypres set is not picked because its HCF function is cut off below a possible occurring suction of 6 meter watercolumn, while the Staring sets are not. For the remainder of the Appendix, however, the Dario parameter set is continued to be used.

D.7. Runs with Variable k-values

Water level

The 1/10,000 year water level with a peak of 3.99 m +N.A.P. and a shape as presented in Chapter 5 is applied to the dike with several different hydraulic conductivities. For the ground water flow above the phreatic surface the Dario parameter set is used. Below a graph of the hydraulic head below the inner crest is shown at a depth of $-1 mN.A.P.$ Twelve runs have been executed with 6 different k-values for the dike and 2 different values for the aquifer. In the key the first number is the k-value for the dike as $k = 10^n$ and the second number that of the aquifer as $k = 10^n$. The aquifer thus has either a hydraulic conductivity of $10 m/day$ or $0.1 m/day$. The dike varies from 10 to $0.0001 m/day$. The colors for the same hydraulic conductivity for the dike are the same.

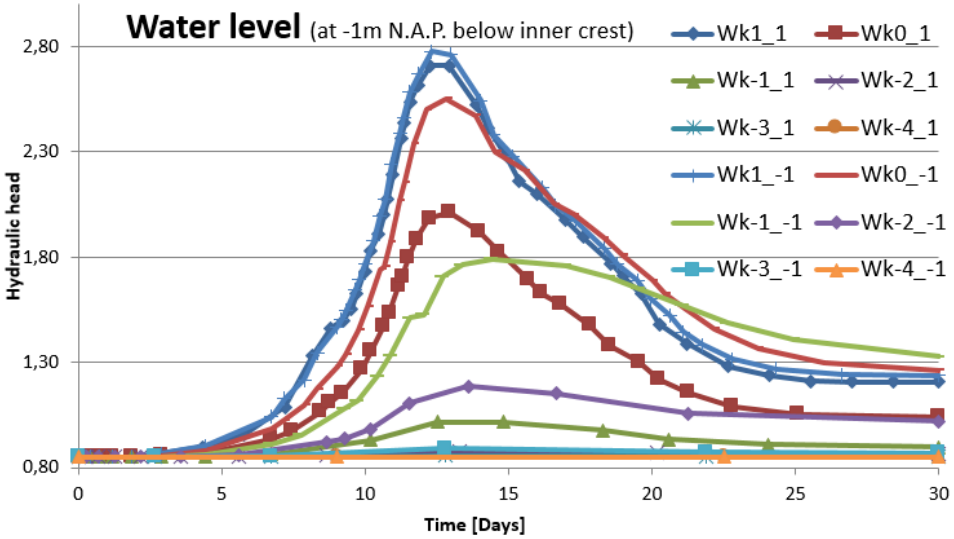

Figure D.33: Hydraulic head development in time below inner crest for different hydraulic conductivities of aquifer and clay layer and dike.

First clear observation is that for the high hydraulic conductivities the signal of the high water level is stronger and less distorted. The maximum head is reached sooner and has a higher value. For hydraulic conductivity smaller than $0.01 m/day$ no effect is noticeable within 30 days.

Secondly, when the aquifer has a low permeability the maximum hydraulic head is higher and head returns to the equilibrium slower. This is to be expected as the ground water experiences more resistance when it wants to flow into the subsoil. This difference is most noticeable with a dike of $k = 0.1 m/day$.

Figure D.34 shows the infiltration of the water into the dike at the beginning of the drawdown. Values of k_y are respectively 10, 1, 0.1, 0.01, 0.001 and $0.0001 m/day$ with k_x half of k_y. Suction values inside the dike above the phreatic surface are between 0 and $5 kN/m^2$ for all cases and are unaffected by the water level rise. It is clear that the influence of the hydraulic conductivity is rather large. The main difference is the distance for which the phreatic surface inside the dike notices the water level rise. For the more realistic clay values (the last two Figures with $k = 0.001 m/d$ and $k = 0.0001 m/d$) the influence of this high water event is negligible.

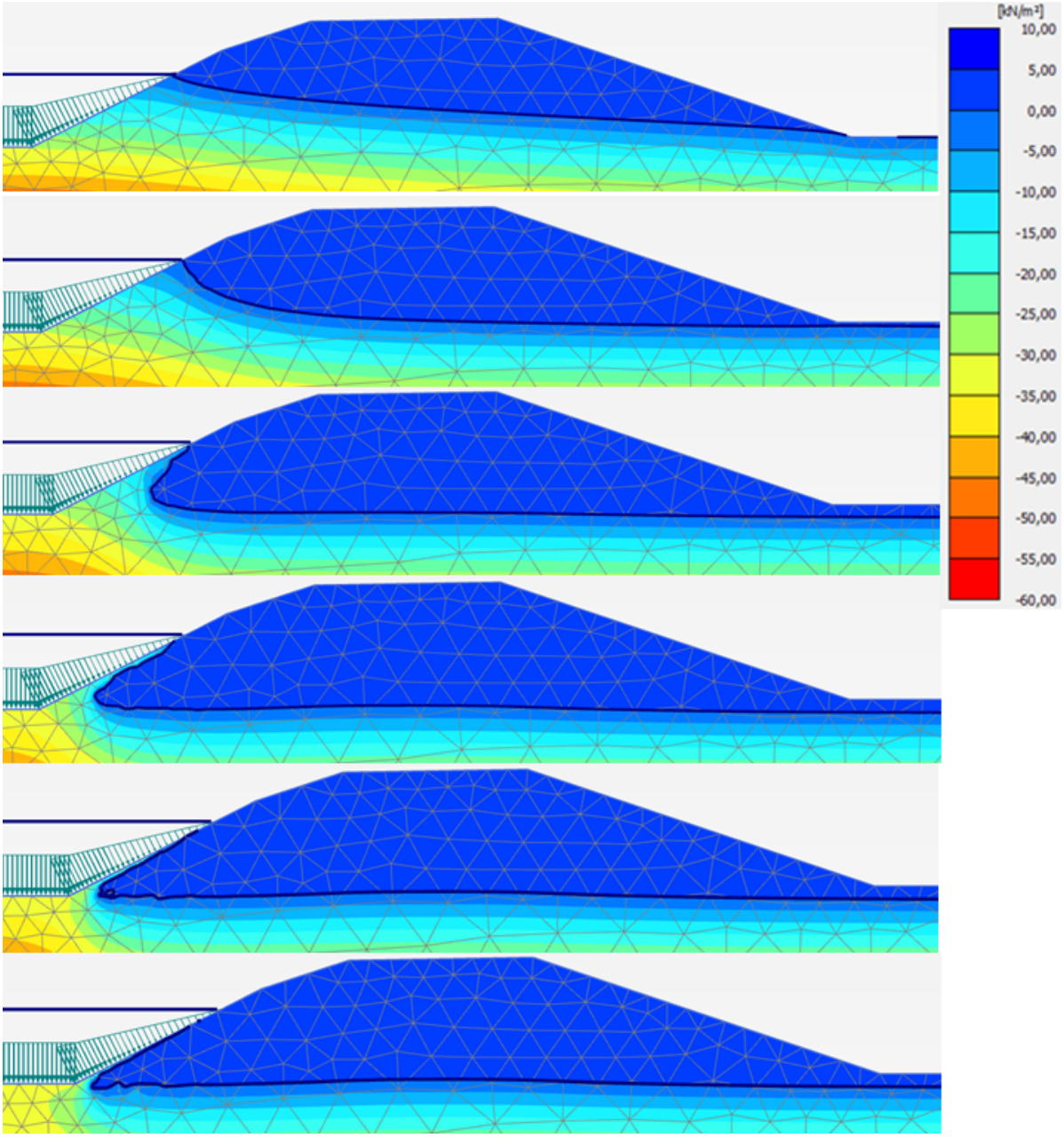

Figure D.34: p_{active} after 1/10,000 high water wave for clay dike with k_y of respectively 10, 1, 0.1, 0.01, 0.001 and 0.0001m/day.

Precipitation

To assess the influence of rain for different k-values, not all seven rain scenarios are elaborately treated. The 1/1,000 year rainfall is applied for the uniform case, scenario 1C (second highest peak), and scenario 2B, (2 peaks with 'long' time in between). These three scenarios are tested for 4 different hydraulic conductivities of the dike. The subsoil conductivity is kept constant at $10m/day$ for all scenarios. The water level in the river is kept constant and total simulation duration is 30 days. Again the Dario setting for unsaturated flow are used.

Uniform

First the situation directly after 8 days of permanent precipitation is presented for k values of 10, 1, 0.1 and $0.01m/day$ respectively. The different colors indicate effective saturation.

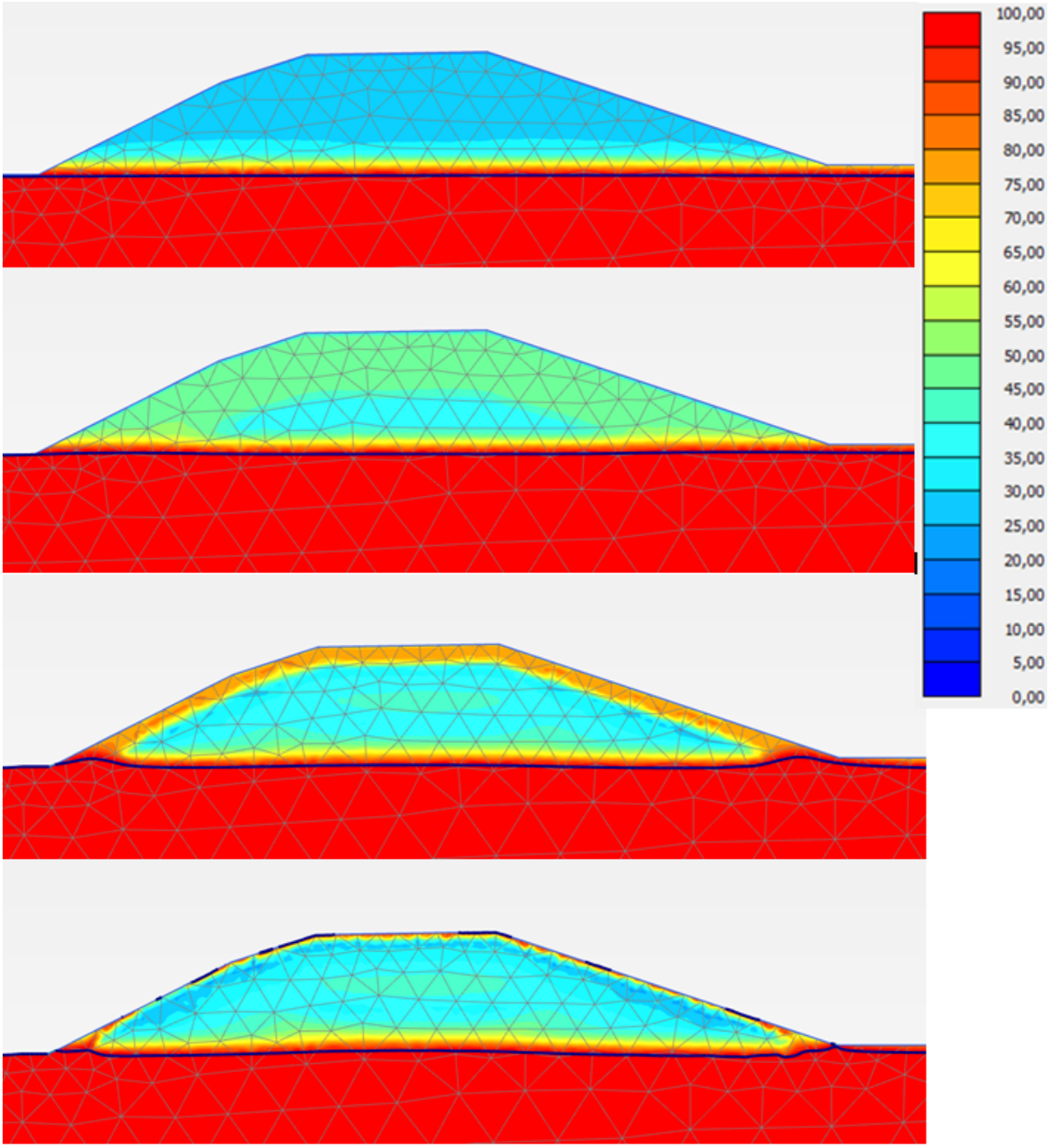

Figure D.35: Effective saturation ($t = 8days$) after 1/1,000 uniform rain for clay dike with k_y of respectively 10, 1, 0.1, and $0.01 m/day$.

For the conductivity of $10 m/day$ the entire effect of the rainfall is already disappeared some hours after the rainfall. For the $1 m/day$ the rain is still intruding into the embankment. The front of the infiltration area has not yet reached the core of the dike and since the rain has stopped the driving force behind the infiltration is gone. Further infiltration is thus only generated by gravity (suction), rather than pressure from behind. When the conductivity is lowered even further the infiltration distance naturally reduces even more. However the saturation degree of the infiltrated part seem to rise. Some kind of queuing seems to occur, as the front of the infiltrated area encounters less permeable soil due to the suction in the pores, the water can't infiltrate any faster. Behind this front, however, the permeability is higher allowing new rain to infiltrate quicker, filling up the voids in the top layer. This effect is even stronger in the last figure, where infiltration distance is smaller but saturation degrees even higher. The blue lines in the at the dikes surface even suggest that an effective saturation of 1 is reached and hydrostatic pore water pressure starts to build inside the pores.

To assess the effect of the rain after some time Figure D.36 shows the saturation pattern after 30 days, so

22 days after the end of the rain period.

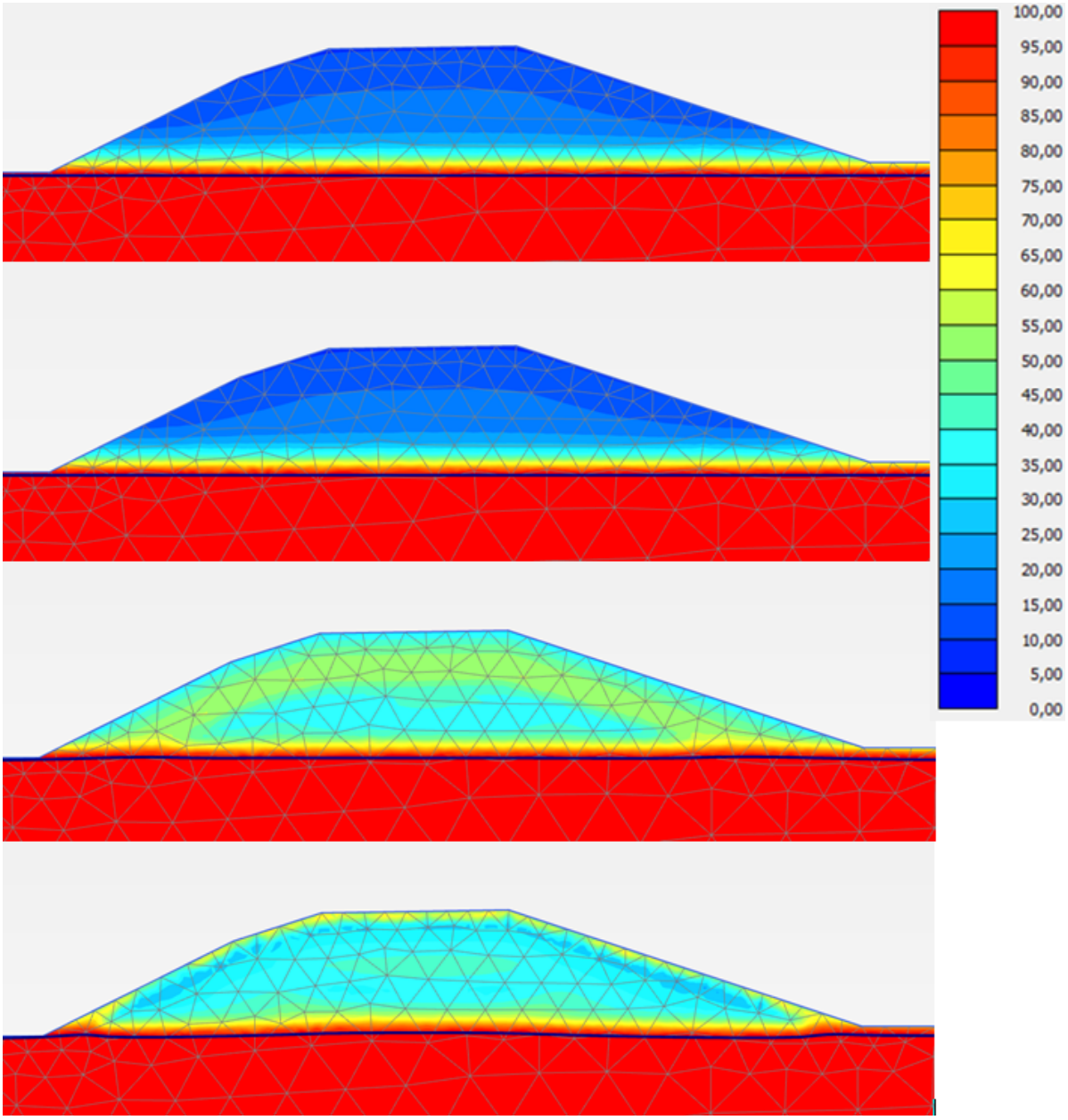

Figure D.36: Effective saturation ($t = 30 days$) after 1/1,000 uniform rain for clay dike with k_y of respectively 10, 1, 0.1, and $0.01 m/day$.

As one can see, there is quite some difference among the hydraulic conductivities. In the first two cases the ground water had enough time to reach the (obviously same) equilibrium. For the lower conductivities this is by far not the case. The large difference between $k = 1$ and $k = 0.1 m/day$ is likely to be found in the state of the infiltration when the rain stopped (besides the direct effect of k). The infiltration into the dike is driven by two forces; on the one hand gravity pulling the water down and on the other hand pressure building behind the infiltrated area due to more rain. If the rain stops one of the driving mechanisms stops leaving it all to gravity. If the infiltration front has almost reached the phreatic surface, the suction values are low and the soil behind the front has a relative high permeability. The entire bulk of infiltrated water can thus find its way to the phreatic surface rather easy once the front reached the phreatic surface. If the rain however stops when the surface is still far away, the infiltrating has to reach the bottom driven by gravity and without being supplied from behind, thus spreading the water thin and leaving saturation and permeability low.

The differences between the rainfall shapes after 30 days are entirely evened out. The plots for the 1C and

2B shapes only showed minimal differences after 30 days compared to the uniform shape and each other and are therefore not presented separately. Directly after the rainfall, differences are larger especially for lower conductivities, therefore these are presented. Below the graph is shown for the hydraulic head below the inner crest for different k-values in time.

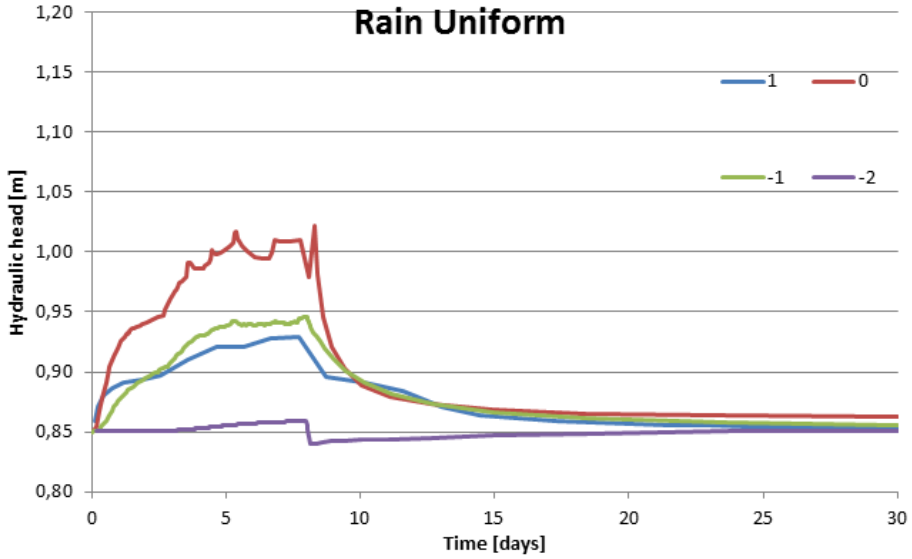

Figure D.37: Hydraulic head below inner crest during 1/1,000 uniform rain for clay dike with different k_y

A k of $1 m/day$ produces the largest phreatic surface rise but still only 15 centimeters. The more extreme k values of 10 and $0.01 m/day$ show some numerical instabilities around the time it stops raining. No explanation is found, but the instabilities are not severe.

One Peak, 1C

For the 1 peak scenario 1c, the results at rainfalls end are as follows:

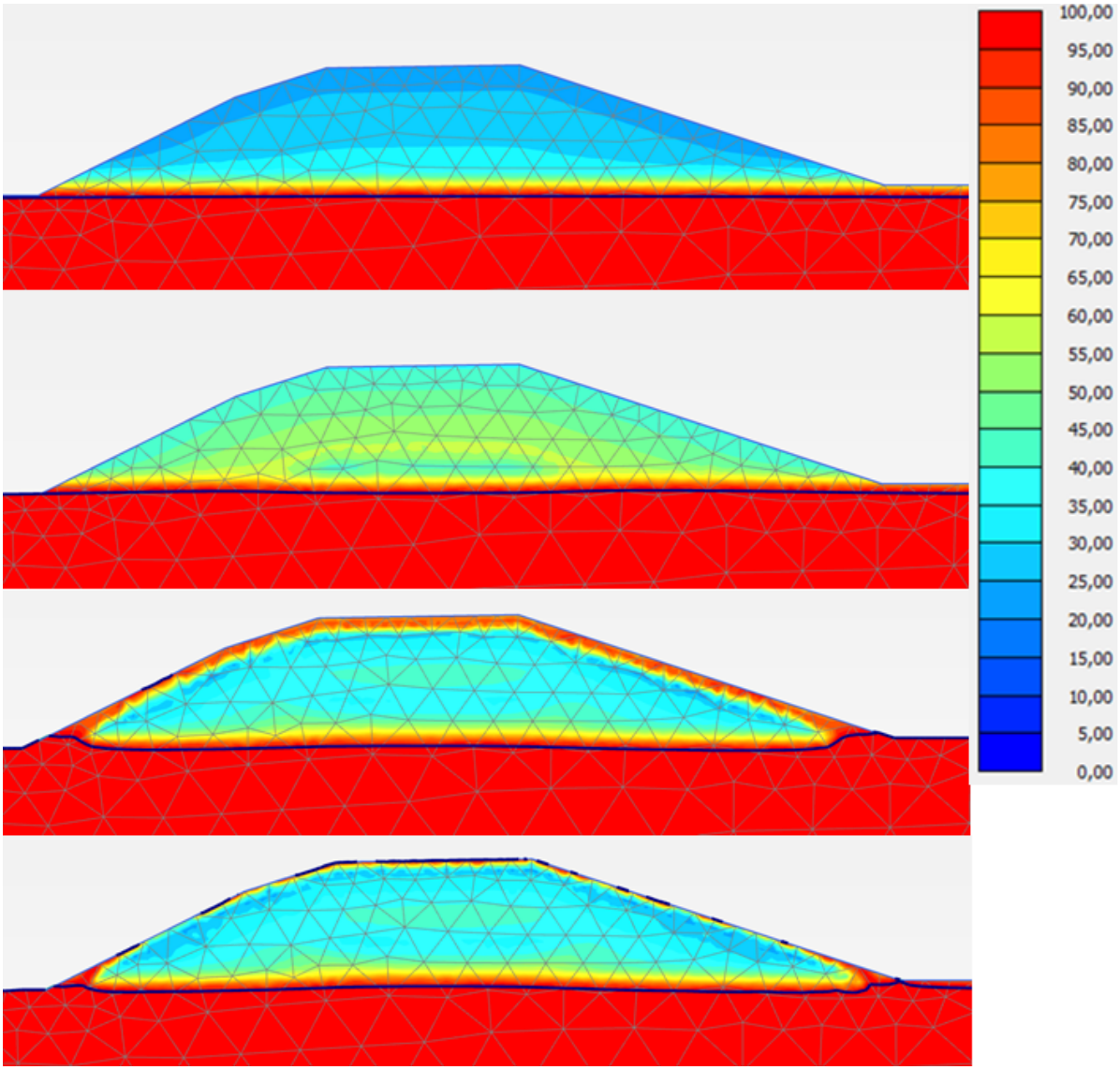

Figure D.38: Effective saturation after 1/1,000 one peaked rain for clay dike with k_y of respectively 10, 1, 0.1, and $0.01 m/day$.

It becomes immediately clear that at rains end for some k-values the distribution of water inside the soil does depend on the shape of the precipitation, especially with higher conductivities. In the first case a larger part of the rain has fallen earlier in the simulation thus giving more of the water time to infiltrate further causing lower saturation degrees inside the embankment.

When $k = 1 m/day$ the infiltration front is clearly further than with uniform precipitation. Probably because a higher volume of water could infiltrate. In the beginning of the precipitation event it is profitable if the precipitation intensity is relatively low, since less water would run of as the infiltration front needs time to infiltrate. When the peak arrives after 64 hours a layer of several meters with higher saturation and permeability has been created. The peak can thus be fully absorbed by this more saturated area with little run-off. In total less water has run off in this case than in the uniform case leading to higher infiltration driving forces inside the dike.

When $k = 0.1 m/day$ the infiltration is somewhat less or roughly the same as the uniform case. Apparently the infiltration buffer area didn't have enough time to become large enough to contain the entire peak. As a consequence still a lot of this water runs off. This phenomenon also causes that no difference is observed for the final Figure and if plots would be made for even less permeable soil. See graph below for the water pressure in time:

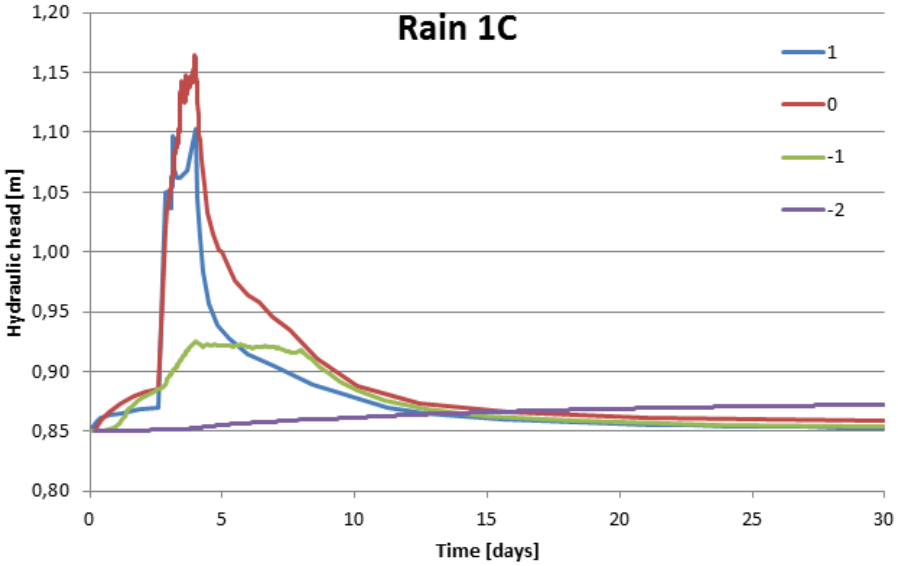

Figure D.39: Hydraulic head below inner crest during 1/1,000 one peaked rain for clay dike with different k_y

The different nature of the precipitations is quite clear for the two lower permeabilities which notice the effect of the rain almost instantly. For the case where $k = 0.1 m/day$ the shape of the hydraulic head is almost the same as with the uniform rain. The final, most impermeable, case the hydraulic head slowly rises long after the rain has fallen and is likely to fall back to $0.85 m$ long after the 30 days.

Two Peaks, 2B

Again rains' end but for an even with two peaks of which one occurs immediately and the other after 128 hours.

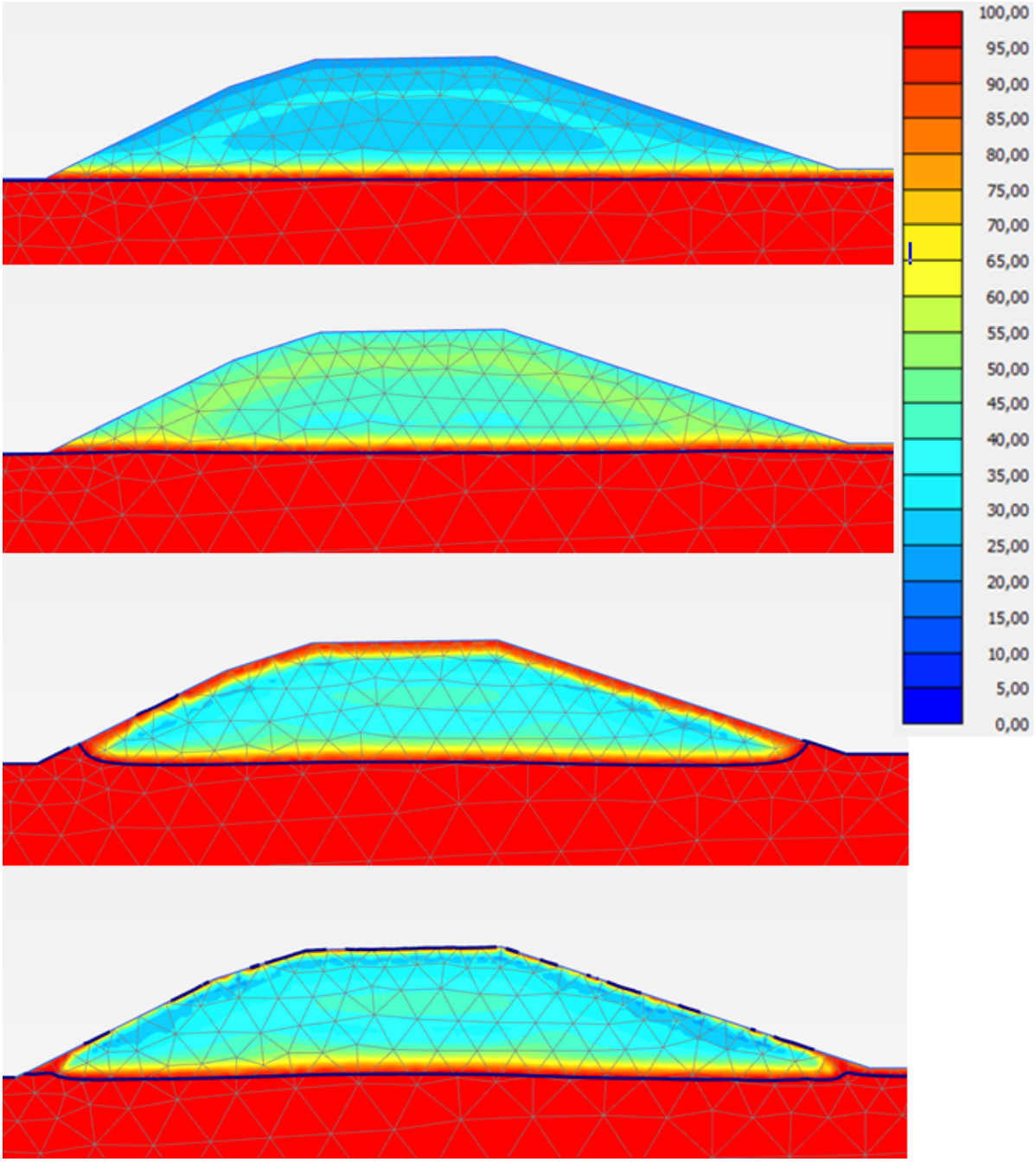

Figure D.40: Effective saturation after 1/1,000 two peaked rain for clay dike with k_y of respectively 10, 1, 0.1, and 0.01m/day.

The in the first two figures the second peak is clearly visible like tree rings telling the past. Although the first peak is not visible in any of the figures; in the first figure because it already reached the surface and thus absorbed in the ground water table. In the second figure because most of it has run off since the event started with a peak. This also explains why infiltration is less severe than in the C1 case, as a larger part of the total water amount has run off.

Overtopping

For the overtopping scenarios only two hydraulic conductivity values are compared. This is done for two different overtopping discharges a realistic one of 0.243 l/m/s and a theoretical allowed maximum of 10 l/m/s.

$q = 0.243 l/m/s$

This discharge is the value for the 1/10,000 year event as computed by HYDRA-NL and is applied for 48-hours straight.. The effective saturation and active pore water pressure for both $k = 0.1 m/d$ and $k = 1 m/d$ directly after the end of the storm are respectively.

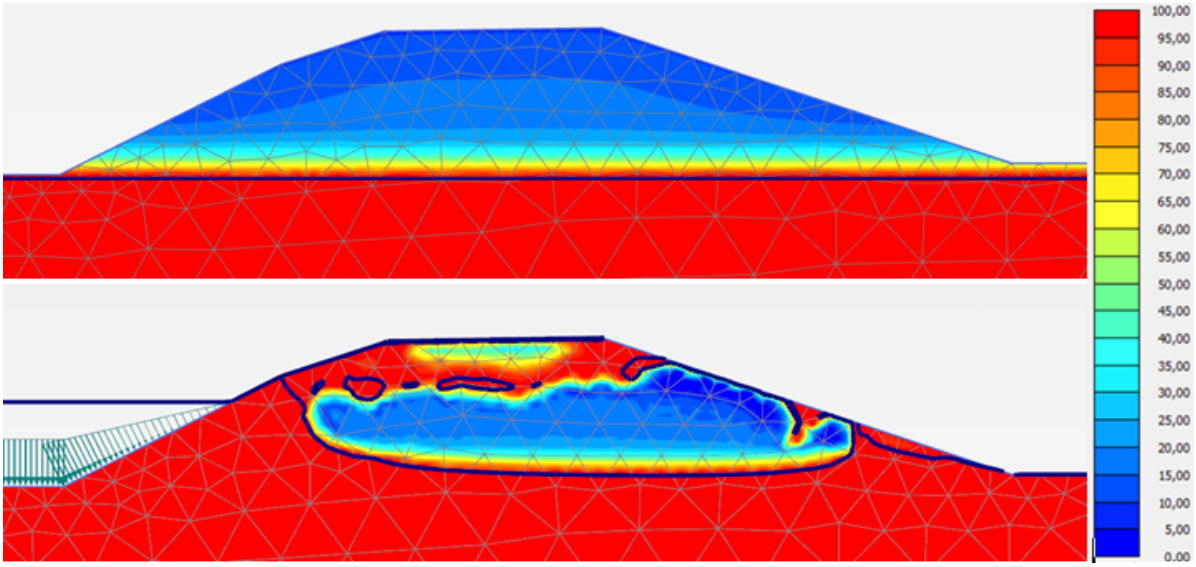

Figure D.41: Effective saturation before and after 1/10,000 overtopping event with $k = 1 m/d$.

First thing that stands out is the large difference between the saturation after two days of overtopping versus 8 days of precipitation. First of all the infiltration is not symmetric, as was expected since the outer slope is wetted more often. Next thing that catches the eye is that the saturation less dissipated and more concentrated. The behind the infiltration front the saturation is much higher. Water is even piling up behind the infiltration front, so much so, that pore water pressures become positive locally. The infiltration distance for the crest in two days' time is only slightly less than after 8 days of uniform rain. So due to more water and hydrostatic pressure on the boundaries the water presses forward quicker. However it seems there is a strange phenomenon. Right in front of the infiltration front the saturation seems to drop, compared to the initial condition. As a results the permeability also drops by quite a lot creating a 'wall' of very impermeable soil in front of the infiltration front, severely slowing down the infiltration process. This phenomenon is treated in Section D.8 and is thus not analyzed any further in the coming overtopping results. First look at the other conductivities and loads.

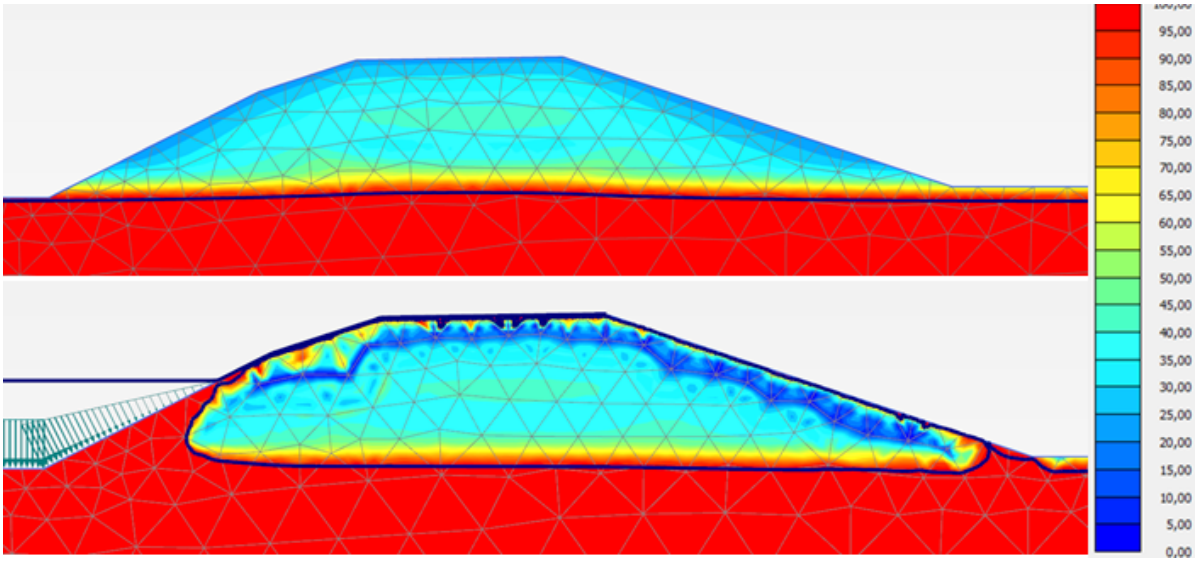

Figure D.42: Effective saturation before and after 1/10,000 overtopping event with $k = 0.1 m/d$.

When the hydraulic conductivity is lowered with a factor 10 the water barely infiltrates after a 2 day storm. Saturation is slightly higher right under surface level, but the core of the dike is not affected at all. Lowering the hydraulic conductivity of the clay to more realistic values would yield even less effects with respect to phreatic surface rise.

q* = 10*l*/*m*/*s

Hydra-NL calculates the expected overtopping discharged based on return period and given winds and discharges. Trough so called illustration points the conditions for higher discharges can be calculated. The maximum overtopping discharge engineers calculate with is $10 l/m/s$ and with Hydra-NL the corresponding significant wave height and wave period are calculated. For this dike profile such overtopping discharges have a negligible probability of occurrence but for the sake of the research the scenario is evaluated nonetheless. The effective saturation and active pore water pressure for both $k = 1 m/d$ and $k = 0.1 m/d$ respectively.

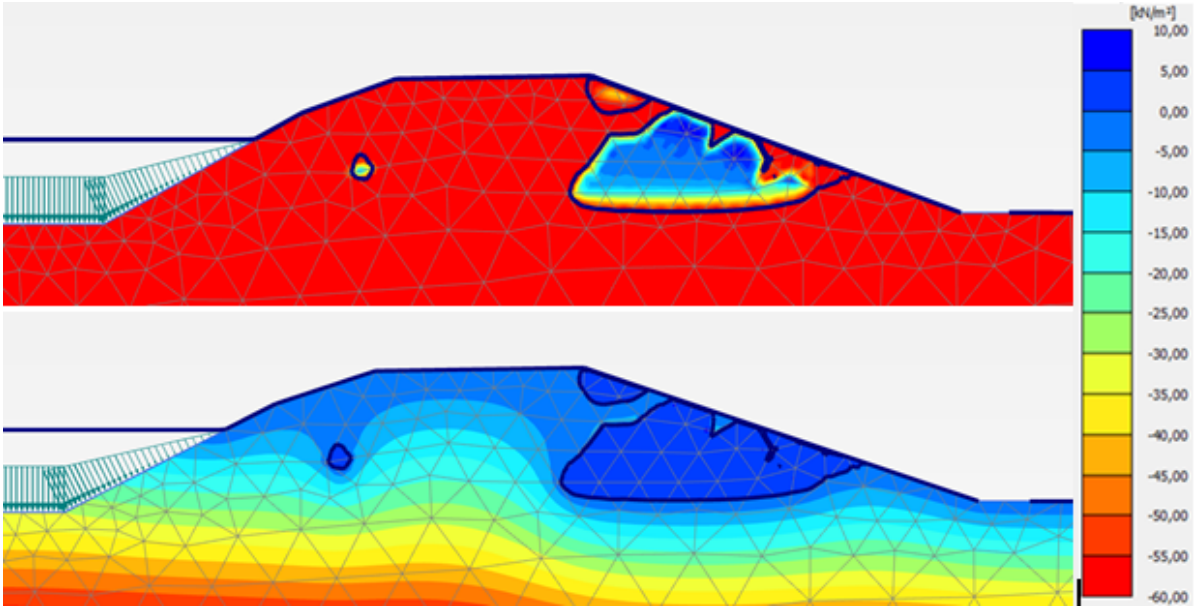

Figure D.43: Effective saturation before and after $q = 10 l/m/s$ overtopping event with $k = 1 m/d$.

Same starting conditions and soil properties apply as for the low overtopping discharge. With an average of 10 liters per meter per second the infiltration pattern is clearly different than for the lower discharge. With

this combination of extreme high permeability and extreme overtopping discharges the phreatic surface finally rises. Even so that the dike gets filled up to the crest. It is interesting to notice that even for the extreme conditions, the inner slope remains relatively dry. Which is positive with respect to inward macro-stability.

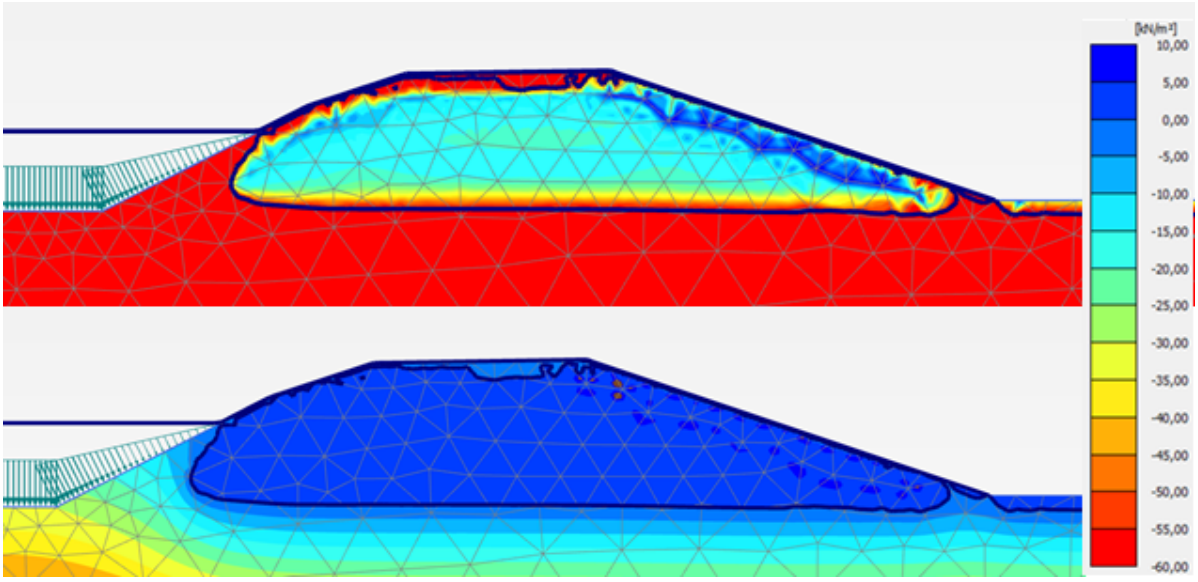

Figure D.44: Effective saturation before and after $q = 10 l/m/s$ overtopping event with $k = 0.1 m/d$.

For this lower conductivity the infiltration is again lower and has a strong resemblance with the lower discharge figures. Due to the higher head the infiltration distance is much larger, up to half a meter after the two day storm. But general conclusion remains that if the hydraulic conductivities were to be lowered to more realistic values the effects of infiltrating overtopping waves would be next to none.

D.8. Grid size and numerical instabilities

Previous sections several figures have been presented and some of them exhibited some strange saturation patterns; D.17, D.18, D.41, D.42, D.43, and D.44 especially. The sudden low saturation values just below surface level are some type of numerical instability induced by the coarse grid. More precise it is caused by the high 'load frequency/grid size'-ratio. The reason to believe that is that the phenomenon does not occur during the precipitation and water level runs.

For the model to work properly an optimal balance between grid size and simulation duration need to be found. Thus the grid needs to be as coarse as possible without inducing these numerical instabilities. In order to find this optimum, several runs have been performed for the overtopping file (new load every 20 seconds) in combination with different grids. Figures D.45 and D.46 show these four grids tested for the overtopping file and the differences are clear. For the first two the low saturation occurs creating a barrier of low saturation and thus low hydraulic conductivity which slows down any further infiltration significantly. For the second two the grid is fine enough to allow for normal infiltration speeds. About the same saturation pattern is visible for both grids.

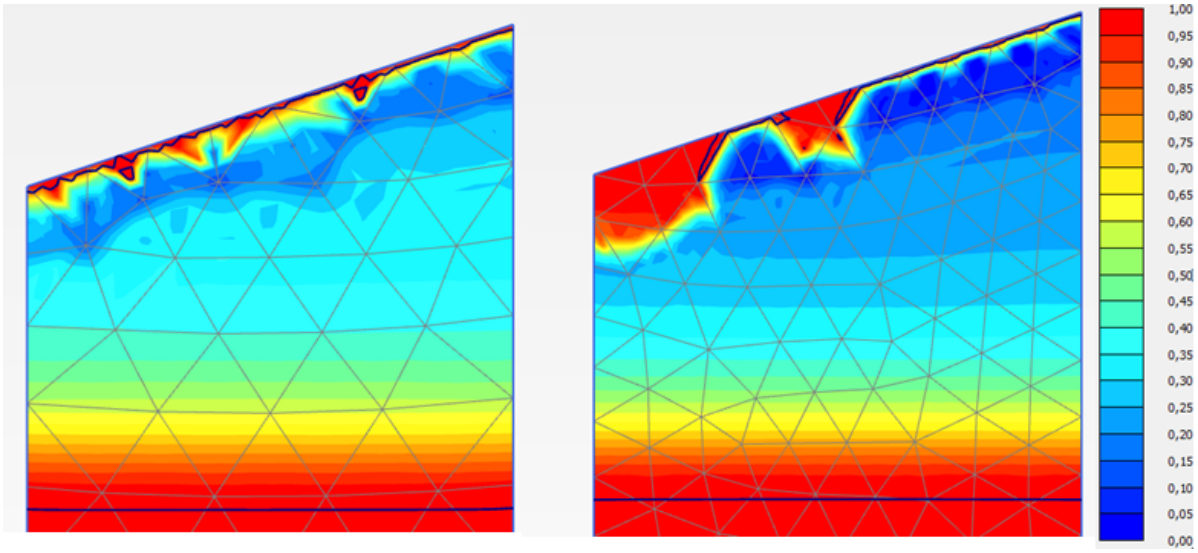

Figure D.45: Effective saturation. Effect of the grid size on numerical stability; unstable grid coarseness.

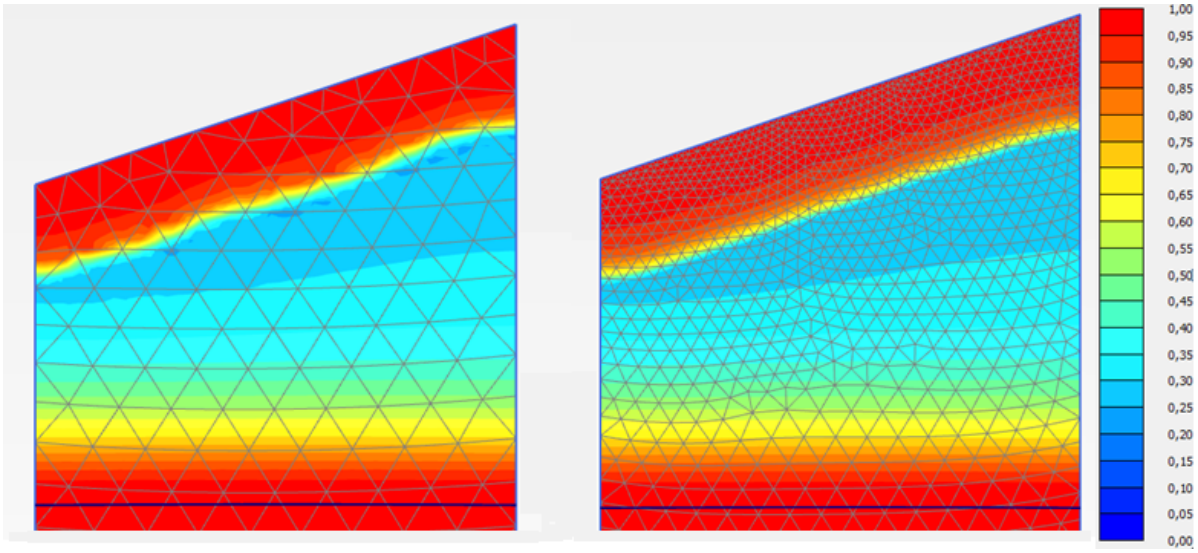

Figure D.46: Effective saturation. Effect of the grid size on numerical stability; stable grid coarseness.

The left grid in Figure D.46 however still shows some spots where the saturation is unexpectedly lower. The influence of these points one the entire pattern is negligible. The third grid coarseness is chosen as it is fine enough to show only small numerical instabilities, while computation times are kept within reasonable bounds. This grid has a node distance of about 0.1 meter.